



저작자표시-비영리-변경금지 2.0 대한민국

이용자는 아래의 조건을 따르는 경우에 한하여 자유롭게

- 이 저작물을 복제, 배포, 전송, 전시, 공연 및 방송할 수 있습니다.

다음과 같은 조건을 따라야 합니다:



저작자표시. 귀하는 원저작자를 표시하여야 합니다.



비영리. 귀하는 이 저작물을 영리 목적으로 이용할 수 없습니다.



변경금지. 귀하는 이 저작물을 개작, 변형 또는 가공할 수 없습니다.

- 귀하는, 이 저작물의 재이용이나 배포의 경우, 이 저작물에 적용된 이용허락조건을 명확하게 나타내어야 합니다.
- 저작권자로부터 별도의 허가를 받으면 이러한 조건들은 적용되지 않습니다.

저작권법에 따른 이용자의 권리는 위의 내용에 의하여 영향을 받지 않습니다.

이것은 [이용허락규약\(Legal Code\)](#)을 이해하기 쉽게 요약한 것입니다.

[Disclaimer](#)

Doctoral Dissertation

**MECHANICAL AND MICROSTRUCTURAL  
CHARACTERISTICS OF MODIFIED SULFUR  
POLYMER COMPOSITES**

Seongwoo Gwon

Department of Urban and Environmental Engineering  
(Urban Infrastructure Engineering)

Graduate School of UNIST

2018

# MECHANICAL AND MICROSTRUCTURAL CHARACTERISTICS OF MODIFIED SULFUR POLYMER COMPOSITES

Seongwoo Gwon

Department of Urban and Environmental Engineering  
(Urban Infrastructure Engineering)

Graduate School of UNIST

# Mechanical and Microstructural Characteristics of Modified Sulfur Polymer Composites

A dissertation  
submitted to the Graduate School of UNIST  
in partial fulfillment of the  
requirements for the degree of  
Doctor of Philosophy

Seongwoo Gwon

June 7, 2018

Approved by



Advisor

Myoungsu Shin

# Mechanical and Microstructural Characteristics of Modified Sulfur Polymer Composites

Seongwoo Gwon

This certifies that the dissertation of Seongwoo Gwon is approved.

June 7, 2018

(signature)



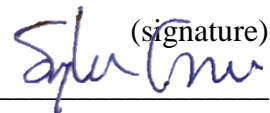
Committee Chair: Myoungsu Shin

(signature)



Committee Member: Jae Eun Oh

(signature)



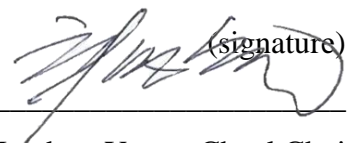
Committee Member: Sung-Han Sim

(signature)



Committee Member: Soowon Cha

(signature)



Committee Member: Young Cheol Choi

## ABSTRACT

# Mechanical and Microstructural Characteristics of Modified Sulfur Polymer Composites

by

Seongwoo Gwon

Doctor of Philosophy in Engineering

Ulsan National Institute of Science and Technology

Modified sulfur polymer composite has been developed to replace hydraulic cement concrete in specific applications. Because it has superior properties including the rapid development of high compressive strength, resistance to water environments, and resistance to strong acid and saline attack compared with the hydraulic cement concrete. Most of all, the fabrication of modified sulfur composites excludes water due to the thermoplastic properties of modified sulfur. Thus, all the raw materials such as aggregate and micro-fillers can be easily mixed with plastic modified sulfur to produce the modified sulfur composite. Early in the development of sulfur composites, however, elemental sulfur mostly from the distillation of crude oil in petroleum refineries was used as a binder. The composites made of elemental sulfur presented not only severe curing contraction but also inferior durability in weathering and chemical environments. Considering the aforesaid problems, many researchers developed modified sulfur polymers by reacting the elemental sulfur with a variety of chemical additives at a certain reaction temperature and time. The modified sulfur polymers had alternating compositions according to the reaction conditions such as the types of chemical additive, reaction temperature, and reaction time. Through a modification process, the composition of modified sulfur mixture was composed of abundant polysulfide products along with a reduced free elemental sulfur such as orthorhombic, monoclinic, and amorphous sulfur chains. Such a converted composition considerably enhanced the mechanical and durability properties of sulfur composites. The term, modified sulfur polymer, indicates the final reaction product from a mixture of elemental sulfur and chemical additive. If a certain micro-filler accounts for a part of the modified sulfur polymer, the mixture is usually called as sulfur polymer cement.

Among various modified sulfur polymers, this study employed a dicyclopentadiene (DCPD)-modified sulfur polymer as a binder, which is one of the commercially available products. Based on this modified sulfur polymer, total five research topics were carried out step by step in this study.

First, different proportions of modified sulfur composites were developed by replacing a portion of the modified sulfur polymer by fly ash and rubber powder. Both the fly ash and the rubber powder were employed to be a substitute for fine aggregate and to enhance the mechanical properties of modified sulfur composites by reducing thermal curing shrinkage. An increasing portion of the fly ash of up to 50 vol.% resulted in a continuous rise of compressive strengths with a given portion of rubber powder. Moreover, the rubber powder also significantly reduced the unit weight of modified sulfur composites without sacrificing the compressive strength. Finally, a series of microstructural analysis suggested the rationales for the enhanced mechanical properties in terms of crystalline phase transition, morphological transition, and porosity.

Second, in a similar way as the first research topic, modified sulfur composites included rubber powder, and a blend of Portland cement and fly ash as the binary cement that rendered the different particle characteristics (i.e., particle shape, particle size distribution) of micro-fillers as compared with sole fly ash or Portland cement. An increasing portion of the binary cement generally induced the higher compressive strengths of the modified sulfur composites than those with only fly ash. This was likely due to the larger indentation modulus of Portland cement than fly ash. In addition, the use of rubber powder contributed to a reduced unit weight of sulfur composites without a severe strength reduction. Most of all, because all the crystalline phases from the binary cement remained intact in hardened sulfur composites, the feasibility of using the binary cement as a self-healing material for cracked sulfur composites was confirmed empirically.

Third, considering the brittleness of modified sulfur composites except those containing rubber powder identified in the first and second research topics, a series of fiber-reinforced sulfur composites were developed and examined to convert the brittleness of modified sulfur composites into a more ductile manner, and to acquire multiple micro-cracks especially under flexures. Two micro fibers including steel and electrical chemical resistant (ECR) glass fiber were incorporated in the mixtures. By varying the total fraction of micro fibers and adjusting the relative volumetric ratios between steel and glass fiber, the flexural stress-strain responses of modified sulfur composites were greatly modified, which was supported by the change of porosity and the uniform strain distribution revealed by a digital image correlation (DIC).

Fourth, the combined effect of particle characteristics of micro-fillers and temperature on the rheological properties of fresh sulfur composites was examined through a rheometer test. Because both the portion of micro-filler and mixing temperature have been critical in determining the workability of modified sulfur composites, the author adjusted the surface areas of a given portion of binary cement and set the temperature at 120°C or 140°C. Overall, both the yield stress and plastic viscosity of the

modified sulfur composites were higher in 140°C than 120°C. Especially, the result of mini slump flow of fresh modified sulfur composites was compared with the rheology test results at 140°C. Thus, the results from the rheology and the mini slump test were deemed to suggest an optimal temperature range favorable for placement.

Finally, considering the feasibility of using cementitious materials as self-healing materials in the sulfur composites, total eight mix proportions of self-healing modified sulfur composites were developed and examined. The modified sulfur composites were comprised of a binary cement of calcium sulfoaluminate (CSA) expansive agent and Portland cement, superabsorbent polymer (SAP) powder, and fine aggregate. After through crack was made on each sample, all the samples were exposed to two wet environments: one was water curing, and the other was water permeability test. Each of them was dedicated to building different self-healing conditions. While the water curing gave a stable self-healing condition to the cracked samples, the water permeability test without any water curing was analogous to a real water intrusion through the cracks of a certain structure. For each sample, the extent of self-healing was monitored and evaluated by the optical microscope images of surface crack and elastic wave tests, respectively at specified ages. Moreover, computed tomography was used to confirm the recovery of inner crack width after 7 days of water curing. Through a series of tests, it was revealed that a higher ratio of CSA expansive agent than Portland cement in a binary cement promoted the self-healing of through cracks further with the swelling of SAP particles on crack surfaces.





## TABLE OF CONTENTS

<b>ABSTRACT.....</b>	<b>I</b>
<b>TABLE OF CONTENTS.....</b>	<b>V</b>
<b>LIST OF FIGURES .....</b>	<b>IX</b>
<b>LIST OF TABLES .....</b>	<b>XIV</b>
<b>LIST OF ABBREVIATIONS.....</b>	<b>XV</b>
<b>1. Introduction.....</b>	<b>1</b>
1.1. Problem Statement and Motivation.....	1
1.2. Academic Backgrounds for Modified Sulfur Concrete .....	4
1.3. Objectives of This Work .....	7
1.4. Outline of This Work .....	7
<b>2. Overview of Sulfur Polymer and Experimental Techniques .....</b>	<b>9</b>
2.1. Modified Sulfur Polymer .....	9
2.1.1. Mechanism.....	9
2.1.2. Types.....	10
2.1.3. Modification conditions .....	11
2.2. Dicyclopentadiene-Modified Sulfur Polymer .....	12
2.2.1. Chemical composition.....	12
2.2.2. Viscosity .....	14
2.2.3. Limitations .....	14
2.3. Experimental Techniques.....	15
2.3.1. Compression test.....	15
2.3.2. Powder X-ray diffraction .....	15
2.3.3. Mercury intrusion porosimetry .....	15
2.3.4. Scanning electron microscopy .....	16
2.3.5. Fourier-transform infrared spectroscopy.....	16
<b>3. Sustainable Sulfur Composites with Enhanced Strength and Lightweightness Using Waste Rubber and Fly Ash .....</b>	<b>17</b>
3.1. Introduction.....	17
3.2. Experimental Program .....	18
3.2.1. Materials .....	19
3.2.2. Mix proportions .....	19
3.2.3. Test methods .....	21
3.3. Results and Discussion .....	22

3.3.1. Characterization of raw materials .....	22
3.3.2. Compressive strength .....	26
3.3.3. Density .....	28
3.3.4. Crystalline phase transition (XRD).....	29
3.3.5. Morphological transition (SEM BSE/EDS).....	31
3.3.6. Porosity (MIP) .....	40
3.4. Conclusions.....	41
<b>4. Strength and Microstructural Characteristics of Sulfur Polymer Composites Containing Binary Cement and Waste Rubber.....</b>	<b>43</b>
4.1. Introduction.....	43
4.2. Experimental Program .....	44
4.2.1. Materials .....	44
4.2.2. Mix proportions .....	45
4.2.3. Production of specimens .....	46
4.2.4. Test methods .....	46
4.3. Results and Discussions .....	47
4.3.1. Characterization of raw materials .....	47
4.3.2. Compressive strength.....	51
4.3.3. Crystalline phase transition (XRD).....	53
4.3.4. Morphological transition (SEM BSE/EDS).....	54
4.3.5. Chemical bond (FT-IR).....	59
4.4. Conclusions.....	60
<b>5. Flexural Stress-Strain Responses of Micro Fiber-Reinforced Sulfur Polymer Composites.</b>	<b>62</b>
5.1. Introduction.....	62
5.2. Experimental Program .....	63
5.2.1. Materials .....	63
5.2.2. Mix proportions .....	65
5.2.3. Test methods .....	66
5.3. Results and Discussion .....	68
5.3.1. Compressive strength.....	68
5.3.2. Flexural stress-strain responses.....	70
5.3.3. Porosity (MIP) .....	76
5.3.4. Visualization of crack propagation (DIC).....	79
5.4. Conclusions.....	80
<b>6. Rheological Properties of Fresh Modified Sulfur Polymer Composites Containing Binary</b>	

<b>Cement at Different Temperatures.....</b>	<b>82</b>
6.1. Introduction.....	82
6.2. Experimental Program .....	84
6.2.1. Raw materials.....	84
6.2.2. Mix proportions .....	84
6.2.3. Test methods .....	85
6.3. Results and Discussions .....	88
6.3.1. Particle-size distributions of cement/fly ash blends.....	88
6.3.2. Compressive strength.....	90
6.3.3. Rheology .....	91
6.3.4. Mini slump flow.....	101
6.4. Conclusions.....	102
<b>7. Self-Healing Properties of Modified Sulfur Polymer Composites Containing Binary Cement and Superabsorbent Polymer .....</b>	<b>103</b>
7.1. Introduction.....	103
7.2. Experimental Program .....	104
7.2.1. Materials .....	105
7.2.2. Mix proportions .....	108
7.2.3. Sample preparation .....	109
7.2.4. Test methods .....	110
7.3. Results and Discussions .....	114
7.3.1. Compressive strength.....	114
7.3.2. Water curing.....	115
7.3.2.1. Surface crack monitoring .....	115
7.3.2.2. Self-healing evaluation using elastic wave .....	121
7.3.2.3. Monitoring of through crack using computed tomography .....	125
7.3.3. Water permeability test .....	126
7.3.3.1. Surface crack monitoring .....	128
7.3.3.2. Self-healing evaluation using elastic wave .....	131
7.4. Conclusions.....	133
<b>8. Concluding Remarks .....</b>	<b>135</b>
8.1. Overall Conclusions.....	135
8.2. Path Forward.....	137
<b>REFERENCES.....</b>	<b>138</b>

**ACKNOWLEDGEMENT..... 146**

## LIST OF FIGURES

Figure 1-1: World sulfur production and the change in prices of sulfur from 1990 to 2008 [3].....	2
Figure 1-2: Total world sulfur production in 2008 [3]. .....	2
Figure 1-3: Worldwide sulfur trade in 2000 [4]. .....	3
Figure 1-4: Classifications of the possible sources of sulfur and possible end-use categories [3]. .....	3
Figure 1-5: Strength development of elemental sulfur concrete and cement concrete [7].....	5
Figure 1-6: Alternative mix proportions of modified sulfur concrete [3]. .....	6
Figure 2-1: Effects of various modifiers on the compositions of modified sulfur [18]. .....	10
Figure 2-2: Effect of DCPD concentration on the composition of sulfur mixture at a reaction temperature of 140°C for 3 hours [18]. .....	12
Figure 2-3: Effect of heating time on the composition of sulfur mixture modified by 25 wt.% DCPD at 140°C [18]. .....	13
Figure 2-4: Reaction I between sulfur and cyclopentadiene dimer [25]. .....	14
Figure 2-5: Reaction II between cyclopentadiene dimer and polysulfide-cyclopentadiene [25]. .....	14
Figure 3-1: Raw materials: (a) modified sulfur, (b) fly ash, and (c) rubber powder. ....	19
Figure 3-2: XRD patterns of raw materials: (a) hardened modified sulfur (Mixture 0-0), (b) fly ash, and (c) rubber powder. ....	24
Figure 3-3: Particle size distributions of fly ash, rubber powder, and sand. ....	25
Figure 3-4: SE images for saw-cut surfaces of hardened modified sulfur (Mixture 0-0): (a) 500X; (b) magnified image (1,000X) of A in (a); (c) magnified image (3,000X) of B in (b); (d) magnified image (10,000X) of C in (c). The number with “X” means a magnification ratio.....	25
Figure 3-5: TGA results of rubber powder. ....	26
Figure 3-6: Compressive strengths of sulfur composites and mortars. ....	27
Figure 3-7: Densities of sulfur composites and mortars. ....	29
Figure 3-8: Integrated XRD pattern for Mixture 15-0. ....	30
Figure 3-9: XRD patterns for sulfur composites with varied ratios of rubber powder and fly ash: (a) Mixtures 0-10, 0-15, 0-40, 0-45, 0-50; (b) Mixtures 5-50, 10-50, 15-50.....	31
Figure 3-10: BSE images for microstructures of fly ash: (a) raw fly ash (700X); (b) heated fly ash (1,000X). .....	32
Figure 3-11: Microstructures of Mixture 0-0 in BSE images with EDS analyses: (a) 1,000X; (b) interfacial zone between points 1 and 2 (10,000X). Note that thin-sectioned and polished samples were used for these BSE images. ....	33
Figure 3-12: Microstructures of Mixture 15-0 in BSE images with EDS analyses: (a) 2,000X; (b) 2,500X; (c) EDS spectrum for point 1 in (b); (d) EDS spectrum for point 2 in (b). .....	34
Figure 3-13: : Microstructures of Mixture 0-15 in BSE images with EDS analyses: (a) 400X; (b) magnified image (1,500X) of A in (a); (c) 500X; (d) magnified image (2,000X) of B in (c); (e)	

magnified image (7,000X) of C in (d). .....	35
Figure 3-14: Microstructures of Mixture 0-50 in BSE images with EDS analyses: (a) 400X; (b) 3,500X; (c) 2,000X; (d) magnified image (8,000X) of A in (c).....	36
Figure 3-15: Microstructures of Mixture 5-50 in BSE images with EDS analyses: (a) 400X; (b) magnified image (3,000X) of A in (a); (c) 2,000X; (d) 400X; (e) magnified image (1,500X) of B in (d); (f) magnified image (2,000X) of C in (d).....	37
Figure 3-16: Microstructures of Mixture 10-50 in BSE images with EDS analyses: (a) 400X; (b) magnified image (1,500X) of A in (a); (c) 1,000X; (d) 1,000X; (e) 400X; (f) magnified image (1,000X) of B in (e). .....	39
Figure 3-17: Microstructures of Mixture 15-45 in BSE images with EDS analyses: (a) 400X; (b) magnified image (1,500X) of A in (a); (c) magnified image (6,000X) of B in (b); (d) 1,500X; (e) 1,000X; (f) magnified image (5,000X) of C in (e).....	40
Figure 3-18: Pore size distributions of three sulfur composites with no rubber powder (Mixtures 0-0, 0-15, 0-50): (a) log differential intrusion; (b) cumulative intrusion (units: mL/g).....	41
Figure 4-1: Raw materials: (a) modified sulfur polymer, (b) binary cement (a blend of fly ash and Portland cement), and (c) rubber powder. ....	44
Figure 4-2: XRD patterns of raw materials: (a) modified sulfur polymer, (b) binary cement, and (c) rubber powder. ....	49
Figure 4-3: Particle size distributions of binary cement, and rubber powder. ....	50
Figure 4-4: SE images for saw-cut surfaces of hardened modified sulfur polymer (Mixture C0-0): (a) 500X, (b) magnified image (1,000X) of A in (a), (c) magnified image (3,000X) of B in (b), (d) magnified image (10,000X) of C in (c).....	51
Figure 4-5: Compressive strengths of the tested sulfur polymer composites. ....	52
Figure 4-6: Integrated XRD patterns of Mixtures: (a) C15-0, and (b) C5-40, C10-40, and C15-40. ...	54
Figure 4-7: Microstructures of Mixture C0-0 in BSE images with EDS analyses for thin-sectioned and polished samples: (a) 1000 $\times$ , (b) 10000 $\times$ . ....	55
Figure 4-8: Microstructures of Mixture C15-0 in BSE images with EDS analyses for thin-sectioned and polished samples: (a) 2500 $\times$ , (b) 4000 $\times$ . ....	55
Figure 4-9: Microstructures of Mixture C0-15 in BSE images with EDS analyses for bulk-sectioned and polished samples: (a) 800 $\times$ , (b) 1300 $\times$ . ....	56
Figure 4-10: Microstructures of Mixture C0-40 in BSE images with EDS analyses for bulk-sectioned and polished samples: (a) 300 $\times$ , (b) 500 $\times$ .....	57
Figure 4-11: Microstructures of Mixture C0-50 in BSE images with EDS analyses for bulk-sectioned and polished samples: (a) 300 $\times$ , (b) 1800 $\times$ .....	57
Figure 4-12: Microstructures of Mixture C5-15 in BSE images with EDS analyses for bulk-sectioned and polished samples: (a) 300 $\times$ , (b) 300 $\times$ , (c) 1100 $\times$ (magnified image of [1] in (a)).....	58

Figure 4-13: Microstructures of Mixture C5-40 in BSE images with EDS analyses for bulk-sectioned and polished samples: (a) 300×, (b) 900×.....	59
Figure 4-14: Microstructures of Mixture C5-50 in BSE images with EDS analyses for bulk-sectioned and polished samples: (a) 300×, (b) 900×.....	59
Figure 4-15: FT-IR spectra of Mixture C15-0, modified sulfur polymer, and rubber powder.....	60
Figure 5-1: Micro fibers: (a) steel fiber, and (b) ECR glass fiber.....	64
Figure 5-2: Thermogravimetric analysis (TGA) of ECR glass fiber.....	65
Figure 5-3: Third-point bending test setup.....	67
Figure 5-4: Test setup for digital image correlation (DIC) in flexural tests.....	68
Figure 5-5: Compressive strengths of micro fiber-reinforced sulfur polymer composites.....	69
Figure 5-6: Flexural strengths of the tested composites.....	71
Figure 5-7: Flexural deflections at maximum stress of the tested composites.....	71
Figure 5-8: Flexural stress-deflection responses of the tested composites: (a) 35-0-0, (b) 35-0-1, (C) 35-0-2, and (d) 35-0-3.....	72
Figure 5-9: Flexural stress-deflection responses of the tested composites: (a) 35-1-0, (b) 35-1-0.5, (C) 35-1-1, and (d) 35-1-2.....	73
Figure 5-10: Flexural failure mode at the bottom surface of Mixture 35-1-0.5.....	73
Figure 5-11: Flexural stress-deflection responses of the tested composites: (a) 35-2-0, (b) 35-2-0.5, (C) 35-2-1, and (d) 35-2-2.....	74
Figure 5-12: Flexural stress-deflection responses of the tested composites: (a) 35-3-0, (b) 35-3-0.5, and (C) 35-3-1.....	75
Figure 5-13: Flexural failure mode at the bottom surface of Mixture 35-3-0.5.....	75
Figure 5-14: Flexural failure mode at the bottom surface of Mixture 35-3-1.....	76
Figure 5-15: Pore size distributions of Mixtures 35-0-0, 35-0-2, and 35-0-3: (a) cumulative intrusion, (b) log differential intrusion (unit: mL/g).....	77
Figure 5-16: Pore size distributions of Mixtures 35-1-1, and 35-1-2: (a) cumulative intrusion, (b) log differential intrusion (unit: mL/g).....	78
Figure 5-17: Pore size distributions of Mixtures 35-2-1, and 35-2-2: (a) cumulative intrusion, (b) log differential intrusion (unit: mL/g).....	78
Figure 5-18: Pore size distributions of Mixtures 35-3-0.5, and 35-3-1: (a) cumulative intrusion, (b) log differential intrusion (unit: mL/g).....	78
Figure 5-19: Flexural strain distributions of Mixture 35-1-0.5 at the maximum stress: (a) specimen 1, (b) specimen 2.....	80
Figure 6-1: Rheology test setup: (a) rheometer with controlled test chamber (CTC), and (b) parallel plate with sample.....	87
Figure 6-2: Shearing protocol for the rheology test.....	87



Figure 6-3: Mini slump test: (a) test apparatus, and (b) specimen geometry. ....	88
Figure 6-4: Particle size distributions of cement/fly ash blends: (a) cumulative, (b) density. ....	89
Figure 6-5: Compressive strengths of tested sulfur composites. ....	91
Figure 6-6: Shear stress-strain rate responses of fresh sulfur mixtures during first shearing cycle at 120°C: (a) up-curve, (b) down-curve. ....	92
Figure 6-7: Shear stress-strain rate responses of fresh sulfur mixtures during second shearing cycle at 120°C: (a) up-curve, (b) down-curve. ....	93
Figure 6-8: Average yield stress of fresh sulfur mixtures with varying total surface area of micro-filler at 120°C. ....	95
Figure 6-9: Average plastic viscosity of fresh sulfur mixtures with varying total surface area of micro- filler at 120°C. ....	95
Figure 6-10: Shear stress-strain rate responses of fresh sulfur mixtures during first shearing cycle at 140°C: (a) up-curve, (b) down-curve. ....	97
Figure 6-11: Shear stress-strain rate responses of fresh sulfur mixtures during second shearing cycle at 140°C: (a) up-curve, (b) down-curve. ....	98
Figure 6-12: Average yield stress of fresh sulfur mixtures with varying total surface area of micro-filler at 140°C. ....	100
Figure 6-13: Average plastic viscosity of fresh sulfur mixtures with varying total surface area of micro- filler at 140°C. ....	100
Figure 6-14: Average spreading diameter versus total micro-filler responses of fresh sulfur mixtures with varying cement/fly ash ratios. ....	101
Figure 7-1: XRD patterns of raw materials: (a) modified sulfur, (b) Portland cement, and (c) CSA expansive agent. ....	106
Figure 7-2: Microscopy images of SAP powders: (a) dry, (b) wet (exposed to tap water for 10 min). .....	107
Figure 7-3: Particle size distributions of Portland cement, dry SAP powders, wet SAP powders, and CSA expansive agent: (a) cumulative, (b) density. ....	108
Figure 7-4: Through crack sample preparation: (a) split tension test setup, (b) insertion of silicon pad and tightening. ....	110
Figure 7-5: Constant head water permeability test: (a) mounted sample, (b) entire test setup. ....	112
Figure 7-6: Transmission of elastic wave in a through crack sample. ....	113
Figure 7-7: X-ray CT test setup: (a) test device, (b) specimen mounted on CT scanner. ....	114
Figure 7-8: Compressive strengths of tested sulfur composites. ....	115
Figure 7-9: An example of measuring surface crack area: (a) 2.5D image, (b) 2D image, (c) measured crack area. ....	116
Figure 7-10: Microscopy images of samples (one sheet of silicon pad) according to water curing: (a)	

S0-25, (b) S0-15, (c) S0-10, (d) S0-0.....	117
Figure 7-11: Microscopy images of samples (one sheet of silicon pad) according to water curing: (a) S5-25, (b) S5-15, (c) S5-10, (d) S5-0.....	118
Figure 7-12: Microscopy images of samples (two sheets of silicon pad) according to water curing: (a) S0-25, (b) S0-15, (c) S0-10, (d) S0-0.....	119
Figure 7-13: Microscopy images of samples (two sheets of silicon pad) according to water curing: (a) S5-25, (b) S5-15, (c) S5-10, (d) S5-0.....	120
Figure 7-14: Signal transmission ratios of samples (one sheet of silicon pad) according to water curing: (a) Mixture S0-0, (b) Mixture S5-25.....	123
Figure 7-15: Calculated spectral energy transmission ratios of samples (one sheet of silicon pad) according to water curing.....	123
Figure 7-16: Signal transmission ratios of samples (two sheets of silicon pad) according to water curing: (a) Mixture S0-0, (b) Mixture S5-25.....	124
Figure 7-17: Calculated spectral energy transmission ratios of samples (two sheets of silicon pad) according to water curing.....	125
Figure 7-18: Tomographic images of Mixture S0-0 at mid-height: (a) before curing, (b) after 7 days of water curing. ....	126
Figure 7-19: Tomographic images of Mixture S5-10 at mid-height: (a) before curing, (b) after 7 days of water curing. ....	126
Figure 7-20: Variation of water flow rate with time for different samples: (a) “S0” series, (b) “S5” series. ....	128
Figure 7-21: Microscopy images of samples (one sheet of silicon pad) according to water permeability test: (a) S0-25, (b) S0-15, (c) S0-10, (d) S0-0.....	130
Figure 7-22: Microscopy images of samples (one sheet of silicon pad) according to water permeability test: (a) S5-25, (b) S5-15, (c) S5-10, (d) S5-0.....	131
Figure 7-23: Signal transmission ratios of samples (one sheet of silicon pad) according to water permeability test: (a) Mixture S0-0, (b) Mixture S5-25.....	132
Figure 7-24: Calculated spectral energy transmission ratios of samples (one sheet of silicon pad) according to water permeability test. ....	133

## LIST OF TABLES

Table 2-1: Compressive strength of sulfur mortar prepared at different reaction temperatures for 3 hours [20].	11
Table 3-1: Mix proportions of tested sulfur composites.	20
Table 3-2: Elemental analysis (EA) results of modified sulfur and rubber powder (unit: wt.%).	22
Table 3-3: Chemical oxide compositions of modified sulfur and fly ash from XRF.	22
Table 3-4: Elemental spot analysis on BSE image for Mixture 15-0 (Fig. 3-12(b)).	34
Table 4-1: Mix proportions of the tested sulfur polymer composites.	45
Table 4-2: Chemical oxide compositions of binary cement and modified sulfur polymer from XRF.	47
Table 5-1: Physical properties of micro fibers.	64
Table 5-2: Chemical composition of ECR glass fiber.	64
Table 5-3: Mix proportions of micro fiber-reinforced sulfur polymer composites.	65
Table 5-4: Compressive strengths and flexural test results of the tested composites.	69
Table 5-5: Total porosities and average pore diameters of various composites.	77
Table 6-1: Chemical oxide compositions of modified sulfur, Portland cement, and fly ash.	84
Table 6-2: Mix proportions of tested fresh sulfur mixtures.	85
Table 6-3: Measured particle characteristics of cement/fly ash blends.	90
Table 6-4: Average yield stress and plastic viscosity of fresh sulfur mixtures at 120°C.	94
Table 6-5: Average yield stress and plastic viscosity of fresh sulfur mixtures during 1 <sup>st</sup> shearing cycle at 140°C.	99
Table 7-1: Chemical oxide compositions of modified sulfur, Portland cement, and CSA expansive agent.	105
Table 7-2: Mix proportions of tested sulfur polymer composites.	109
Table 7-3: Compressive strengths of the tested composites.	114
Table 7-4: Average crack widths of samples (one sheet of silicon pad) at each curing age.	118
Table 7-5: Average crack widths of samples (two sheets of silicon pad) at each curing age.	120
Table 7-6: Average crack widths of samples (one sheet of silicon pad) according to water permeability test.	131

**LIST OF ABBREVIATIONS**

<b>ACI</b>	American Concrete Institute
<b>ASTM</b>	American Society for Testing and Materials
<b>BSE</b>	Backscattered electrons
<b>CCD</b>	Charge-coupled device
<b>CSA</b>	Calcium sulfoaluminate
<b>CT</b>	Computed tomography
<b>CTC</b>	Controlled test chamber
<b>DCPD</b>	Dicyclopentadiene
<b>DIC</b>	Digital image correlation
<b>EA</b>	Elemental analysis
<b>ECC</b>	Engineered cementitious composites
<b>ECR</b>	Electrical chemical resistant
<b>EDS</b>	Energy dispersive spectroscopy
<b>FRC</b>	Fiber-reinforced concrete
<b>FT-IR</b>	Fourier-transform infrared
<b>ICDD</b>	International Center for Diffraction Data
<b>ITZ</b>	Interfacial transition zone
<b>LVDT</b>	Linear variable differential transformer
<b>MIP</b>	Mercury intrusion porosimetry
<b>PMA</b>	Polymer modified asphalt
<b>PSD</b>	Particle size distribution
<b>SAP</b>	Superabsorbent polymer
<b>SE</b>	Secondary electrons
<b>SEM</b>	Scanning electron microscopy
<b>SPC</b>	Sulfur polymer concrete
<b>TGA</b>	Thermogravimetric analysis
<b>UHPFRC</b>	Ultra-high performance fiber-reinforced concrete
<b>XRD</b>	X-ray diffraction
<b>XRF</b>	X-ray fluorescence

## 1. Introduction

### 1.1. Problem Statement and Motivation

Among various minerals, sulfur is unique in terms of its mining and supply issues. Since petroleum industry has emerged, the sufficient supplies of necessary sulfur became possible in the world. Since global sulfur demand could be satisfied using the byproducts from natural gas processing plants and petroleum refineries, sulfur mining has declined. As of now, the production amount of sulfur is larger than the demand for sulfur worldwide [1]. However, many environmental regulations continued to be established with little increase in sulfur uses [2]. Thus, it is necessary to expand sulfur consumption in various markets and to find the efficient methods to dispose of surplus sulfur without environmental issues.

In general, elemental sulfur is mined from surface or underground deposits, and it is recycled from many industrial processes. For example, during the early stages at petroleum refineries, the refining process of crude oil involved a simple distillation. The crude oil is a complex mix of various hydrocarbon compounds containing sulfur. An average sulfur content of crude oil is approximately 3%. According to the increased demand for lighter fuels (e.g., jet fuel, gasoline), more advanced distillation processes were developed to produce lower density compounds. These processes often generated H<sub>2</sub>S from the organic compounds. The produced H<sub>2</sub>S from the refining was mostly burned with the other hydrocarbons, which led to the emission of noxious SO<sub>2</sub> into the atmosphere.

As shown in Fig. 1-1, sulfur production has increased since 1990. Due to the increased amount of recovered sulfur, total sulfur production continued to rise until 2008 [3]. In spite of the formation of huge global sulfur market, the sulfur production always exceeded total sulfur consumption worldwide. Consequently, the price of sulfur continued to decrease. Although the regional constraints on sulfur trade resulted in a sudden increase of the sulfur price in 2008, the sulfur price during past few decades exhibited a descending trend. In 2008, 22 countries produced a total of 69 million tons of sulfur worldwide due to the increase of oil production (Fig. 1-2). Among them, the amount of sulfur from Korea also accounted for a part of world total sulfur production. Likewise, Korea was also one of the sixteen dominant sulfur producers exporting about 21 million tons in 2000 (Fig. 1-3) [4]. Therefore, it is deemed that the domestic sulfur production of Korea will continue to increase.

As the scale of sulfur market became enlarged, a number of sulfur uses have emerged in the world. Fig. 1-4 shows the categories of numerous sulfur sources and many industries that utilize the sulfur. As one of the possible industries, construction industry used the elemental sulfur as an alternative construction material to existing construction materials, especially in specific applications. For example, sulfur construction materials have been used in sulfur-modified asphalt pavements, sulfur concrete, and

precast concrete structural elements. Considering the aforesaid issues from the construction industry, this study is dedicated to the development and microstructural characterizations of sustainable sulfur composites.

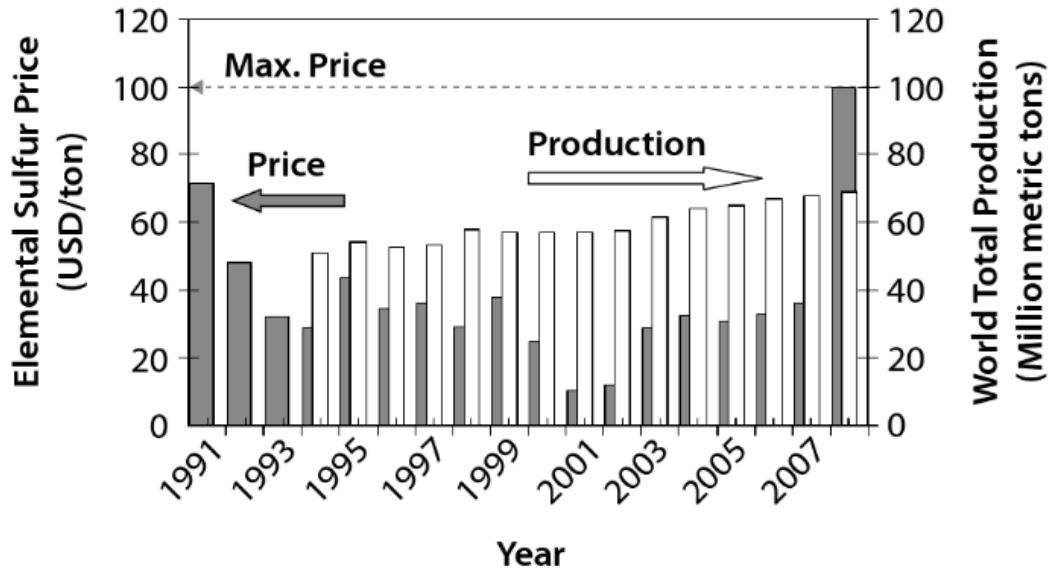


Figure 1-1: World sulfur production and the change in prices of sulfur from 1990 to 2008 [3].

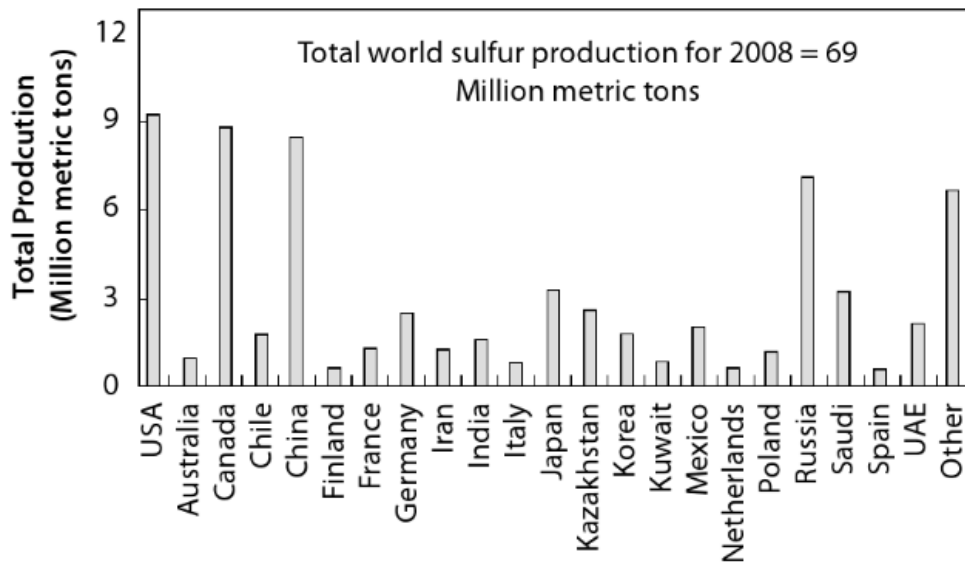


Figure 1-2: Total world sulfur production in 2008 [3].

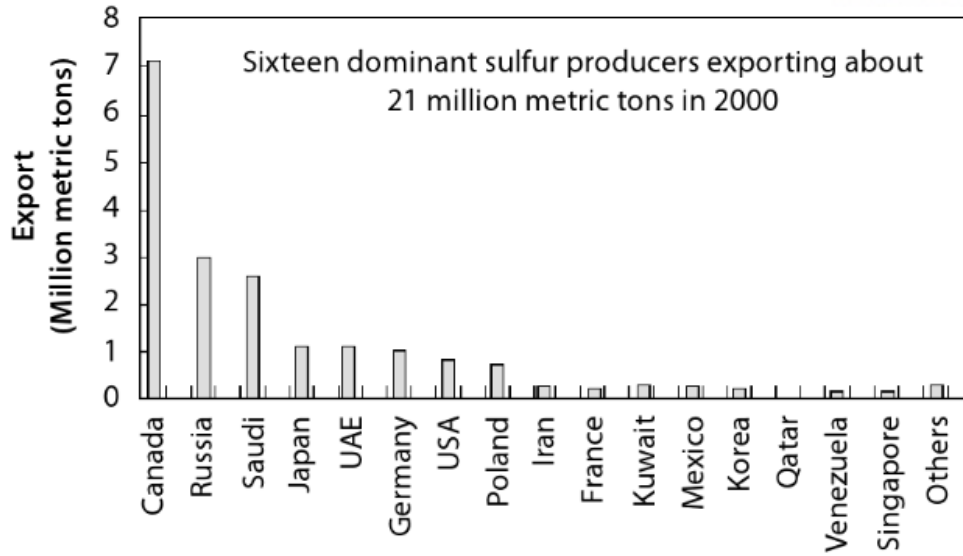


Figure 1-3: Worldwide sulfur trade in 2000 [4].

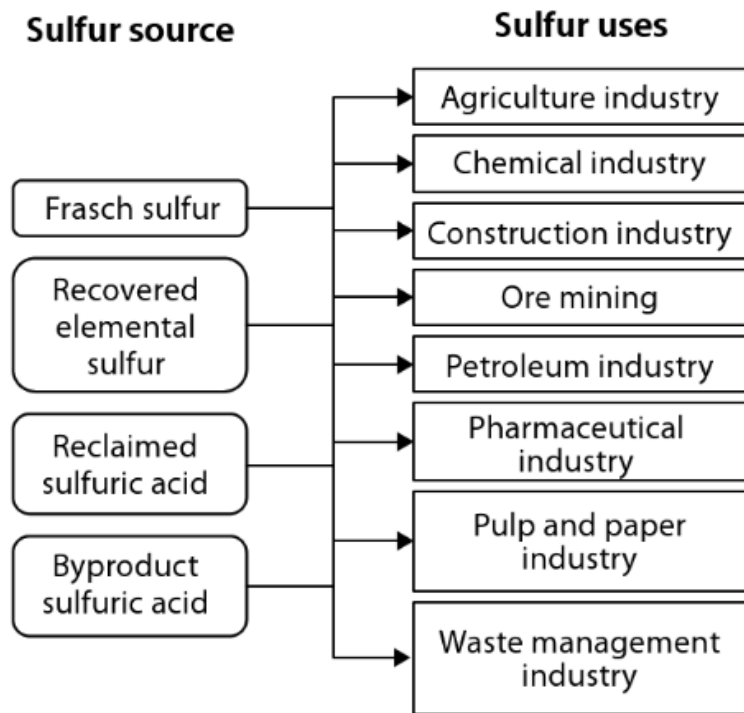


Figure 1-4: Classifications of the possible sources of sulfur and possible end-use categories [3].

## 1.2. Academic Backgrounds for Modified Sulfur Concrete

The relatively low cost of elemental sulfur and its easy availability have made a construction industry utilize the sulfur particularly as the alternative to hydraulic cement or asphalt-extended cement. The use of elemental sulfur with aggregates has been tried to produce sulfur concrete for many years. The term sulfur concrete indicates the hardened mixture of molten elemental sulfur as a binder, and various aggregates. As the mixing of molten sulfur with preheated aggregates and subsequent cooling at room temperature produces the sulfur concrete with fast setting, high strength, corrosion resistance, and low permeability, many researchers have been interested in the sulfur concrete. The feasibility of using elemental sulfur as the alternative binder was reported by Bacon and Davis in 1921 [5]; it was revealed that a mixture of 40% elemental sulfur and 60% sand made a sulfur concrete that developed an excellent strength with an acid-resistance. The same mixture was further examined by Duecker who found the volume expansion as well as the reduction of flexural strength of the sulfur concrete under thermal cycling [6]. Above all, elemental sulfur concrete rapidly developed a high compressive strength as compared to Portland cement concrete. Fig. 1-5 illustrates the strength development of sulfur concrete and cement concrete with respect to curing age and moisture supply [7]; Although cement concrete usually acquires 90% of ultimate compressive strength after 28 days of curing, the elemental sulfur concrete develops its ultimate strength within a few hours. Moreover, the strength development of the sulfur concrete is not affected by both moisture supply and temperature, whereas the cement concrete is greatly dependent on them.

Lin et al. reported that, in spite of the superior properties of elemental sulfur concrete, it suffered severe durability problem under immersion in water or the repeated cycles of freezing and thawing [8]. Moreover, during the cooling, the molten elemental sulfur underwent a volume contraction of about 7% at 114°C, at which the liquid sulfur crystallized as monoclinic sulfur ( $S_{\beta}$ ) and finally started to transform into orthorhombic sulfur ( $S_{\alpha}$ ) at below 96°C. This transformation generally occurred within 24 h. Although the orthorhombic sulfur is stable due to its larger density than that of monoclinic sulfur, the conversion (i.e., allotropic transition) of sulfur can induce a high stress in the matrix, which will lead to the premature failure of sulfur binder.



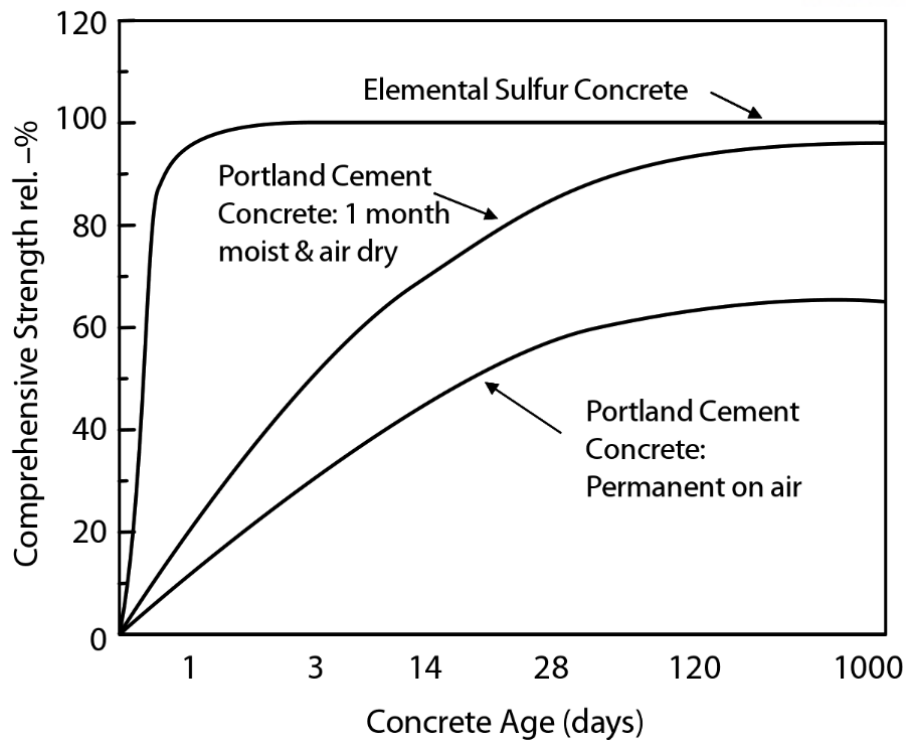


**Figure 1-5: Strength development of elemental sulfur concrete and cement concrete [7]**

Considering the severe durability problems of elemental sulfur, the need to modify the elemental sulfur was recognized by many researchers, who applied a number of chemicals to the elemental sulfur. In this manner, sulfur polymer cement (SPC) was invented by reacting ~95 wt.% of elemental sulfur with ~5 wt.% organic modifier to acquire long-term durability as well as mechanical properties. In 1972, United States Bureau of Mines originally developed SPC to utilize waste sulfur or byproduct as a substitute for hydraulic cement in construction field. Many types of SPC were invented. However, currently only a few are available commercially. Using the SPC as a binder, modified sulfur concrete was developed to replace ordinary cement concrete in specific applications. Typical composition of the modified sulfur concrete is completely different from that of Portland cement concrete. The raw materials of modified sulfur concrete encompass sulfur, chemical modifiers, aggregates, and mineral fillers. Fig. 1-6 shows the several alternative mix proportions of modified sulfur concrete [3]. For the fabrication of sulfur concrete, the prepared modified sulfur is molten in a controlled mixing chamber at 130°C. Then, the preheated aggregates at 155°C are poured and blended along with the plastic modified sulfur. Finally, the homogenized mixture of sulfur concrete is placed. As shown in Fig. 1-6, modified sulfur concrete usually consists of 75-85% of aggregate and 15-25% of modified sulfur by weight. In addition, several industrial byproducts such as furnace slag, fly ash, and cement kiln dust are used as potential aggregate in the sulfur concrete.

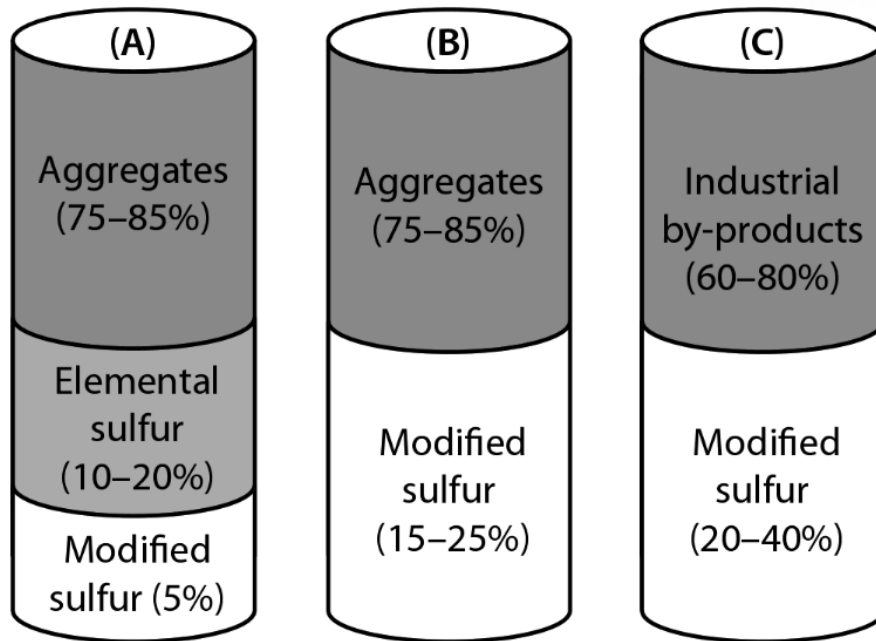


**Figure 1-6: Alternative mix proportions of modified sulfur concrete [3].**

The main advantage of modified sulfur concrete is an excellent long-term durability as compared to Portland cement concrete. Thus, it has been widely used in industrial plants or other facilities in which aggressive chemical environments caused the premature deterioration of Portland cement concrete. Generally, the characteristics of the modified sulfur concrete are summarized as follows:

- ✓ Low porosity and permeability; properties that give a impervious matrix.
- ✓ Mechanical properties such as compressive, flexural, and tensile strengths, and fatigue life were greater than those of Portland cement concrete. High compressive strength of sulfur concrete was obtained within a few hours of curing and it developed ultimate compressive strength within one day [9].
- ✓ Equivalent density of modified sulfur to that of Portland cement.
- ✓ Excellent resistance to the attacks from various acid and salt solutions at high concentrations, and to corrosive electrolyte attack [9,10,11].
- ✓ Can be cast year-round at below-zero temperatures.
- ✓ Failed sulfur concrete can be recycled and reused.
- ✓ No water in the fabrication of sulfur concrete.
- ✓ Modified sulfur concrete can be used in road pavement and bridge decks exposed to salt corrosion [12].

### 1.3. Objectives of This Work

The overall objectives of this study are to investigate the effects of micro-fillers and micro fibers on the mechanical properties of modified sulfur composites especially in compression and flexure, and to evaluate the fresh and hardened properties of the modified sulfur composites using a series of characterization analyses. Ultimately, this study aims at developing the self-healing modified sulfur composite which can heal cracks by itself. More detailed objectives of this study are as follows:

- ✓ To propose a new sustainable method for producing modified sulfur composites with two hazardous industrial wastes: rubber powder and fly ash, so as to enhance the properties of sulfur composites, and to reduce the unit weight of sulfur composites without sacrificing the compressive strength.
- ✓ To explore the effects of binary cement (blend of Portland cement and fly ash) and rubber powder on the strength and microstructural characteristics of modified sulfur composites, and to examine the feasibility of using the binary cement as a self-healing material.
- ✓ To develop the optimum mix proportions of fiber-reinforced modified sulfur composites employing fly ash and two micro fibers including steel and glass fiber to achieve multiple micro-cracks as well as an increased deflection under flexure.
- ✓ To investigate and assess the coupled effects of temperature and particle characteristics of micro-fillers on the rheological properties of fresh modified sulfur mixtures.
- ✓ To develop self-healing sulfur composites, of which cracks can be recovered naturally through water penetration, and to assess their self-healing performances using a series of analysis techniques.

### 1.4. Outline of This Work

This thesis is composed of a total of eight chapters. Chapter 1, 2, and 8 are the introduction, the overview of sulfur polymer and experimental techniques, and summary, respectively. Major research achievements and discussions are presented in Chapter 3, 4, 5, 6, and 7. Among them, Chapters 3 (Construction and Building Materials 135 (2017) 650-664) and 4 (Construction and Building Materials 181 (2018) 276-286) were already published in the journal.

Chapter 3 introduced rubber powder and fly ash as the effective components of sulfur polymer composites to replace aggregate and enhance the properties of modified sulfur composites. This chapter also aimed to reduce the unit weight of the sulfur composites without sacrificing compressive strength. In this chapter, mechanical and microstructural tests were conducted to investigate the effects of rubber powder and fly ash on the strength, density, and the microstructure of the sulfur composites. Various analytical techniques were employed for microstructural characterizations.

Chapter 4 investigated the effects of binary cement (blend of Portland cement and fly ash) and rubber powder on the strength and microstructural characteristics of modified sulfur composites. In this chapter, the binary cement was employed as the micro-filler enhancing the compressive strength of sulfur composites as well as a potential crack-healing agent. To characterize the properties of modified sulfur composites acquired from the binary cement and rubber powder, a series of macro- and micro-structural analyses were conducted.

Chapter 5 investigated the effect of micro fiber doses on the compressive strength and flexural performances of modified sulfur composites. Apart from the direct measurement of flexural stress-deflection responses, digital image correlation (DIC) as a non-contact displacement measurement was conducted simultaneously along with third-point bending tests. To evaluate the porosity of modified sulfur composites including micro fibers, mercury intrusion porosimetry (MIP) was also performed.

Chapter 6 investigated the coupled effects of temperature and the particle characteristics of micro-fillers on the rheological properties of fresh modified sulfur mixtures using a commercial rheometer. The micro-fillers were prepared as binary cements (Portland cement/fly ash blends) by varying the composition ratios between Portland cement and fly ash to allocate different particle characteristics to the fresh modified sulfur mixtures. In addition, mini slump tests were conducted to understand a correlation between the rheological properties and flowability.

Chapter 7 investigated the self-healing properties of modified sulfur composites containing fine aggregate, Portland cement, calcium sulfoaluminate (CSA) expansive agent, and superabsorbent polymer (SAP) powder. Except the fine aggregate, the others were employed as self-healing agents. Among them, Portland cement and CSA expansive agent were prepared as the binary cement by varying the relative ratios of them, which offered the different levels of self-healing capacity to the modified sulfur composites. In addition, the use of SAP powder was intended to rapidly seal cracks on absorbing water. Thus, the binary cement around swollen SAP particles likely reacted with water stably. Finally, the self-healing performances of sulfur composites were evaluated using a series of analysis techniques.

## 2. Overview of Sulfur Polymer and Experimental Techniques

### 2.1. Modified Sulfur Polymer

#### 2.1.1. Mechanism

As introduced in Section 1.2, if pristine elemental sulfur is heated to 140°C followed by cooling to ambient temperature, monoclinic sulfur is spontaneously formed and almost returns to orthorhombic sulfur completely within about 20 hours. In addition, elemental sulfur concrete exhibits a large expansion and contraction under thermal cycling, so that the changes in hydromechanical-thermal properties are expected. Thus, in order to solve this problem, it is required to modify the elemental sulfur using chemical additives.

Many researchers have tried to stabilize or plasticize the elemental sulfur as a polymeric form. Pryor noted that only carbon-sulfur (C-S) bond was formed though the sulfur-olefin reaction and there was no new carbon-carbon (C-C) bond [13]. Therefore, in this copolymerization reaction, it was expected to obtain a definitely alternating structure. The research showed that the elemental sulfur reacted with liquid olefins at 90-160°C to form several polysulfide products. Though this reaction, new molecules of cyclic polysulfides were attained, which were distinguished by the number of sulfur atoms bonded. It was assumed that two weak bonds sulfur-sulfur (S-S) were decomposed during this reaction. Both a new bond (S-S) and two fairly strong C-S bonds were formed [14]. Various chemical additives have been used to produce modified sulfur. The added chemicals can react with the elemental sulfur to give polymeric polysulfides. The extra sulfur in the mixture is not polymerized or kept in an amorphous state by the sulfur polymer.

Meanwhile, the polymer deters the growth of macro-sulfur crystals. When a certain portion of polymer accounted for ten parts of liquid sulfur by weight followed by cooling, the length of sulfur crystals was generally smaller than one micron [15,16]; this was critical concern, as sulfur had a low thermal conductivity of 6.1 kcal/cm<sup>2</sup>/sec ( $\Delta t = 1^\circ\text{C}$ ) and a rather high linear coefficient of thermal expansion of  $7.4 \times 10^{-5}/^\circ\text{C}$  both at 40°C. When a material with the macro-crystals of sulfur is exposed to a temperature change, a continuous movement between these macro-crystals will happen due to relative expansion or contraction between themselves. This movement will progressively destroy the bonds with other crystals, which induces microcracks as well as the severe weakening of the microstructure. Other similar mechanisms may be responsible for the deterioration of certain types of commercial elemental sulfur. A scanning electron microscopy study graphically exhibited how the sulfur polymers impart durability by controlling the growth of macro-crystals [17].

### 2.1.2. Types

Depending on the type of chemical additives, the percentage of polysulfide products and unreacted sulfur is expected to vary. Blight et al. applied many additives and quantitatively compared their effects on delaying the crystallization of elemental sulfur [18]. The used additives were a variety of olefins and Thiokols (polymeric polysulfides). Fig. 2-1 shows the effectiveness of each modifier; all the modifiers were added at 25 wt.% of elemental sulfur and heated at 140°C for 3 hours. They had a substantial effect on controlling the formation of orthorhombic sulfur, and the olefins except styrene were principally effective since the orthorhombic sulfur was not detected even after 18 months.

The preceding emphasizes the main purpose of adding the chemical additives in the elemental sulfur, which prevents the conversion to orthorhombic sulfur ( $\alpha$ -sulfur). Thus, a monoclinic sulfur ( $\beta$ -sulfur) should be formed after cooling.

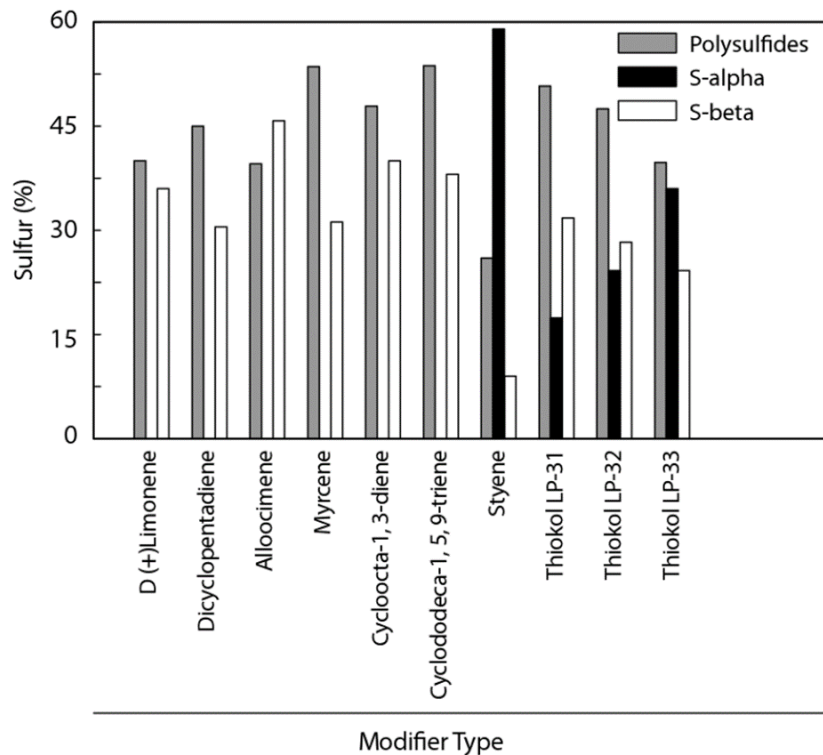


**Figure 2-1: Effects of various modifiers on the compositions of modified sulfur [18].**

Sulfur cement may be an unmodified sulfur or a plasticized sulfur. The plasticized sulfur indicates a reaction product of elemental sulfur and modifier (plasticizer). When a modifier is used, the required amount of modifier will vary depending upon the types of modifier and the required properties for a certain sulfur cement. The sulfur cement usually contains a modifier from 0.1 to 10%, and typically from about 2 to 7%, based on the total amount of free and reacted sulfur in the composition.

The term, sulfur modifier, indicates a substance or a mixture of substances that lower melting point and increases the crystallization time when added to the elemental sulfur [19]. Inorganic modifiers encompass arsenic, sulfides of iron, and phosphorus. However, an organic compound is generally preferred to the inorganic compound as the modifier, since it produces a sulfur-containing material. The preferred sulfur modifiers include styrene, acrylic acid, dicyclopentadiene (DCPD), dioctylphthalate, epoxidized soybean oil, triglycerides, aliphatic polysulfides, and aromatic polysulfides [19].

### 2.1.3. Modification conditions

The modification of sulfur has been formulated by incorporating modifier additives in elemental sulfur. Three methods were tested so as to optimize the modifications. In the first method, the elemental sulfur was added to an oil bath, then the melted elemental sulfur was blended with an olefinic additive at 130-140°C; Temperature was set at 130-140°C during the mixing process for about 3 hours [18]. In the second method, an modifier was added at 150-160°C and then the mixing continued for approximately 3 hours at the same temperature. In the third method, after an olefin additive was added to the elemental sulfur at 130-140°C, the heating lasted for 0.5, 1, 2 and 3 hours.

Reaction temperature and heating time are important factors in the modification of elemental sulfur. Tables 2-1 shows that the compression strength of sulfur mortars prepared at 140°C was larger than that prepared at 160°C [20]. At 90-160°C, the elemental sulfur reacts with olefins in a liquid phase followed by the formation of various polysulfide products [13]. According to a continuous temperature increase from 90°C, the S<sub>8</sub> rings gradually decompose into reactive bi-radicals. Without the olefins, they attain an enough concentration to be readily transformed into  $\mu$ -sulfur chains at around 160°C [21]. As these chains have a lower affinity than other compounds, the affinity of sulfur with a modifier is deemed lowered at 160°C rather than 140°C.

**Table 2-1: Compressive strength of sulfur mortar prepared at different reaction temperatures for 3 hours [20].**

Sample	Reaction temperature (°C)	Compressive strength (MPa)
1	160	10.19
2		10.98
3		8.04
4		12.36
5	140	19.91
6		20.40
7		14.32

8	36.48
9	31.38

## 2.2. Dicyclopentadiene-Modified Sulfur Polymer

### 2.2.1. Chemical composition

The advantage of using DCPD as a modifier has been examined by many researchers [22,23,24]. Currell et al. reported that the reaction between DCPD and elemental sulfur at 140°C produced a mixture of polysulfides and the free elemental sulfur that was composed of orthorhombic, monoclinic, and amorphous sulfur [24].

Fig. 2-2 shows the efficiency of using DCPD to deter the formation of orthorhombic sulfur [18]. It was observed that the orthorhombic sulfur just occurred with only 5% concentration of DCPD and not with more than 10%. This phenomenon was in parallel with the test result that the minimum loading concentration of DCPD to stop the brittleness of the elemental sulfur was 13% at the reaction temperature of 140°C, or 6% at the reaction temperature above 140°C [23].

The amount of polysulfides generally increases with a more adding of DCPD at 140°C. Fig.2-3 shows the increased polysulfide formed as the reaction time progressed [18]. After one hour of reaction using 25% of DCPD, the final reaction product included the unreacted olefin still; After 3 hours, 57.7% of the final reaction product corresponded to polysulfides; After 20 hours, 68.7% was polysulfide. Also, the molecular weight of the polysulfides increased as the reaction time progressed.

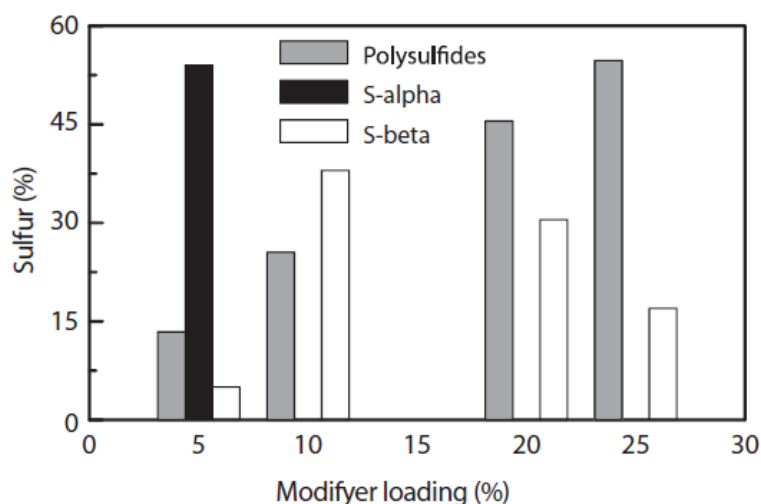


**Figure 2-2: Effect of DCPD concentration on the composition of sulfur mixture at a reaction temperature of 140°C for 3 hours [18].**



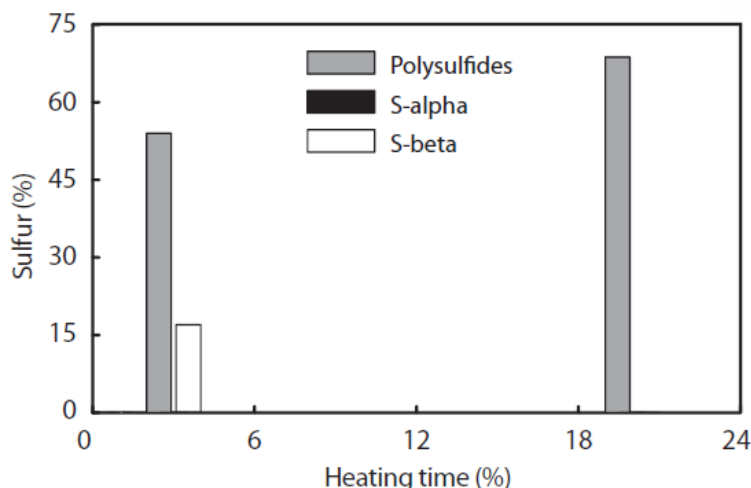


**Figure 2-3: Effect of heating time on the composition of sulfur mixture modified by 25 wt.% DCPD at 140°C [18].**

In general, the reaction between the elemental sulfur and the modifier is conducted without a solvent. However, hydrocarbon materials such as styrene or vinyl-toluene may be used as the solvents. To modify the elemental sulfur, it is required to control the reaction between the elemental sulfur and cyclopentadiene dimer carefully considering the exothermic reaction between the elemental sulfur and DCPD. The cyclopentadiene is commercially available in its dimer form. Liquid cyclopentadiene dimer will decompose spontaneously into monomers at room temperature. This depolymerization reaction will be substantially accelerated in the presence of sulfur at temperature of 120-140°C, as was suggested by the chemical scheme through the reaction number I and II, respectively in Figs. 2-4 and 2-5 [25]. Due to the exothermic characteristic of reaction I (Fig. 2-4), it is difficult to control the reaction precisely. Consecutively, when the dimer is present in reaction II, it reacts with the polysulfide products from reaction I (Fig. 2-5).

Reaction II between the cyclopentadiene dimer and polysulfide-cyclopentadiene product is less exothermic than reaction I. Thus, the cumulative exothermicity of the reactions I and II causes the serious problems of reaction control. If the reaction is not well controlled, a highly viscous sulfur polymer is formed. On the contrary, if the reaction is well controlled, it induces the formation of a linear polymeric polysulfides that are greatly associated with the durability of modified sulfur polymer [26].

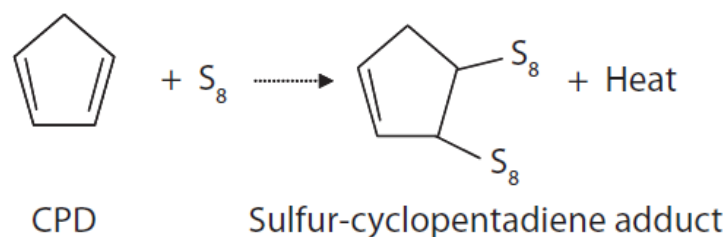


**Figure 2-4: Reaction I between sulfur and cyclopentadiene dimer [25].**

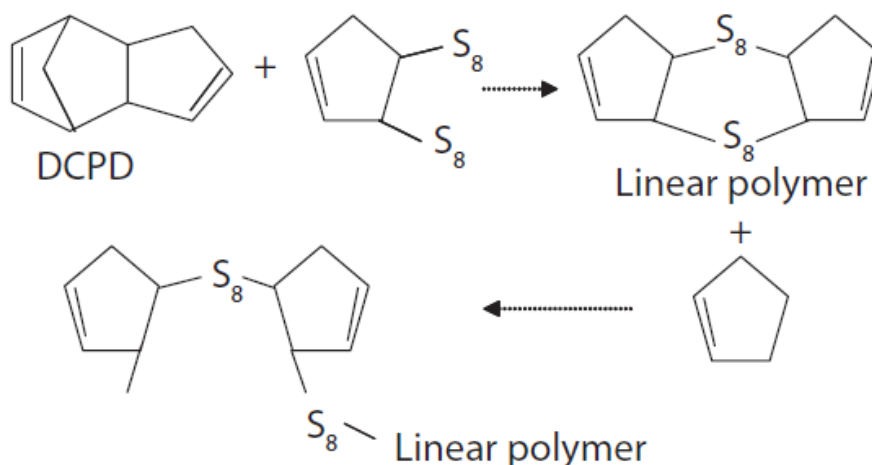


**Figure 2-5: Reaction II between cyclopentadiene dimer and polysulfide-cyclopentadiene [25].**

### 2.2.2. Viscosity

Blight et al. [18] confirmed the research results of Sullivan et al. [23] that the reaction between elemental sulfur and DCPD was exothermic. If the reaction temperature is larger than 150°C, excessive viscosity growth causes the mixture to be almost solid, making it difficult to control the reaction. Diehl [22] and Bordoloi and Pearce [27] quantitatively examined these viscosity changes. They revealed that a large increase of viscosity was induced as the concentration of DCPD, reaction time, and reaction temperature increased. Blight et al. showed that the formation of high molecular weight polysulfides resulted in the increase of viscosity [18].

### 2.2.3. Limitations

The modifications of sulfur using DCPD have been studied extensively [28,29,30]. However, because the reaction between elemental sulfur and DCPD is exothermic and needs accurate control, and it is unstable when exposed to the high temperature above 140°C, at which point unstable sulfur products

start to develop, its practical applications have been restricted. McBee and Sullivan [29] solved this problem through a process making modified sulfur be stable and insensitive to the mixing temperature of the sulfur concrete. This process involves the reaction control of cyclopentadiene.

## 2.3. Experimental Techniques

### 2.3.1. Compression test

The compressive strengths of the samples were measured using at least three cubic samples with each side 50 mm long for each mixture at each specified curing age. The compression test was performed under a displacement-control at a loading rate of 0.5 mm/min according to ASTM C109 [31]. A hydraulic universal testing machine (1500HDX, Instron, USA) with a load capacity of 1500 kN was used. During the test, an integrated software (Bluehill 2, Instron, USA) was used to control the test and acquire test data.

### 2.3.2. Powder X-ray diffraction

The X-ray diffraction (XRD) patterns of raw materials and sulfur composites were acquired to confirm constituent phases and identify possible new reaction products and crystalline phase transitions. The XRD tests were performed on powdered samples using a high-power X-ray diffractometer (Rigaku, Tokyo, Japan) emitting an incident Cu-K $\alpha$  radiation beam ( $\lambda = 1.5418 \text{ \AA}$ ) with a  $2\theta$  scanning range of  $5^\circ$ – $70^\circ$  at room temperature. All powdered samples were milled by hand using a pestle. Because the powdered samples were sifted through a 80  $\mu\text{m}$  sieve before each test, the maximum particle size was about 80  $\mu\text{m}$ . All the powdered samples were not solvent-exchanged since no water was present in the mixtures.

### 2.3.3. Mercury intrusion porosimetry

The pore size distributions and total porosities (i.e., total pore volumes) of the samples were measured using a MIP (Auto Pore IV 9500, Micromeritics, USA). The MIP tests were conducted using multiple 5-mm cubic samples for each mix type. The cumulative pore volume was determined by measuring the amount of intruded mercury for incremental pore sizes between 360 and 0.003  $\mu\text{m}$ . Thus, the pressure of the mercury intrusion varied from 0 to 60,000 psi. The density, surface tension, and contact angle of the mercury were 13.534 g/mL, 485 dynes/cm, and  $130^\circ$ , respectively.

#### 2.3.4. Scanning electron microscopy

The morphologies of raw materials and sulfur composites were investigated using an ultra-high resolution field emission scanning electron microscope (SEM) (Hitachi S-4800, Hitachi, Japan) with EDS. For each mix type, at least three sliced samples were prepared. An epoxy resin was applied to each sliced sample without solvent-exchange. Then, the epoxy-mounted sample was ground to remove about 1-mm thickness of the top surface covered with no epoxy, and the sample's ground surface was polished using 6-, 3-, and 0.25- $\mu\text{m}$  diamond suspensions successively. Prior to the SEM tests, all the polished samples were coated with an osmium film to reduce or eliminate charging, and to enhance the contrast of analysis images.

#### 2.3.5. Fourier-transform infrared spectroscopy

In Chapter 4, in order to identify the chemical bonding between the modified sulfur and rubber powder, a Fourier transform infrared (FT-IR) spectrometer (Varian 670-IR, Varian Inc., USA) coupled with a microscope (Varian 620-IR, Varian Inc., USA) was used to acquire IR absorbance or reflectance spectrum. FT-IR measurements were performed on each of the modified sulfur and rubber in powder, and on hardened samples 3 mm thick made of both the modified sulfur and rubber powder with an aperture size of  $250 \times 250 \mu\text{m}^2$  in a single point mode. Spectral resolution was  $4 \text{ cm}^{-1}$ , and the measured spectra contained the wave numbers of  $650 \text{ cm}^{-1}$  to  $4000 \text{ cm}^{-1}$ .

### **3. Sustainable Sulfur Composites with Enhanced Strength and Lightweightness Using Waste Rubber and Fly Ash**

#### 3.1. Introduction

The recycling of industrial wastes and byproducts is a common practice in the construction field today. The main materials used in this study, such as sulfur from petroleum refineries, rubber from waste tires, and coal-fired fly ash, fall into this category.

Large amounts of elemental sulfur have recently been generated from mining or as a byproduct of petroleum refining processes around the world. Due to its thermoplastic characteristics, sulfur can be mixed with aggregates or fillers at a high temperature, and they can be bound in hardened sulfur concrete at room temperature.

As for fly ash, it is reported that more than 750 million tons are produced annually worldwide. Despite various attempts to recycle fly ash in the construction industry, almost one-half of all fly ash is deposited in landfills [32]. Fly ash contains a considerable amount of leachable toxic trace elements (e.g., As, Cd), which may cause serious environmental issues if air, water, and soil are directly exposed to them. Thus, suitable utilization methods for fly ash should be developed to avoid such problems.

Also, about 1.4 billion automobile tires are traded worldwide every year, and subsequently, most of them turn into wastes after their lives [33]. Increasing amounts of waste tires are generally piled in landfills [34]; they are usually not buried in landfills due to their low density and poor biodegradation even after long periods. Therefore, reutilization methods are needed. Earlier attempts [34,35,36,37,38,39] were made to apply tire rubber in the production of Portland cement concrete. The researchers investigated using sliced rubber particles of various sizes and shapes, and they reported that the rubber particles could be utilized as lightweight aggregates while enhancing the properties of concrete (e.g., toughness, plastic energy absorption).

Many countries involved in the petroleum and natural gas industries have been aware of the environmental harms of sulfur and have enacted necessary regulations on the related industries. China is an exemplary country that recently mandated compulsory desulfurization at all petroleum refineries [2]. Canada also set the allowable quantities of sulfur in gasoline and diesel and limited the emissions of SO<sub>2</sub> from petroleum refineries. These actions have led to a considerable increase of surplus sulfur in solid form around the world. Currently, the global generation of sulfur is approximately 10–20% larger than the worldwide demand, which is about 57 million tons per year [1]. The oversupply of sulfur has dramatically reduced the market price of sulfur. Therefore, the current situation can be an attractive opportunity for other industrial fields to utilize sulfur at a cheaper price. On the other hand, the disposal of excess sulfur has emerged as a serious problem due to the shortage of temporary storage spaces at

petroleum refineries. Therefore, new recycling methods of surplus sulfur should be developed.

Global warming is a critical issue that may jeopardize the entire human society unless it is properly addressed. Cement production in the world yields about 7% of the total CO<sub>2</sub> emissions [40]. Several previous studies on sulfur polymer concrete (SPC) were conducted in past decades [3,11,26,41,42]. These studies suggested sulfur as an innovative material in civil engineering. In particular, it was confirmed that sulfur can replace entire cement paste in concrete as a binder. Molten thermoplastic sulfur binds aggregates and fillers together and forms hardened concrete within a very short time. Therefore, a sulfur polymer binder may be a promising sustainable construction material as a substitute for Portland cement.

However, the early sulfur concrete with elemental sulfur had limits for practical use due to its poorer resistance to freezing and thawing and its higher brittleness compared to Portland cement concrete [16]. To overcome such drawbacks, a more stable modified sulfur was developed by reacting elemental sulfur with chemical modifiers, such as dicyclopentadiene (DCPD), to form long-chain polymeric polysulfides [3,43]. As in Portland cement concrete, modified sulfur can be mixed with various types of aggregates or fillers, which may affect the mechanical and durability characteristics of SPC [3,41].

The main objective of this study was to propose a new sustainable method for producing sulfur composites with two hazardous industrial wastes: rubber powder and fly ash. This study introduced rubber powder and fly ash as effective components of SPC to replace aggregate and enhance the properties of sulfur composites. This study also aimed to reduce the unit weight of sulfur composites without sacrificing the compressive strength; the low specific gravity of rubber powder may decrease the unit weight of sulfur composites. The proposed method may have several major advantages compared to using cement-based concrete as well as traditional SPC: less CO<sub>2</sub> emissions, lower life-cycle cost, and superior durability.

In this study, mechanical and microstructural tests were conducted to investigate the effects of rubber powder and fly ash on the strength, density, and microstructure of sulfur composites. A variety of analytical techniques were employed for microstructural characterizations: laser diffraction particle size analysis, elemental analysis (EA), X-ray fluorescence (XRF), thermo-gravimetric analysis (TGA), powder X-ray diffraction (XRD), scanning electron microscopy (SEM) with backscattered electron image (BSE) and elemental energy dispersive spectroscopy (EDS), and mercury intrusion porosimetry (MIP).

### 3.2. Experimental Program

### 3.2.1. Materials

In this study, only industrial wastes were used to develop sustainable sulfur composites, which were sulfur, fly ash, and rubber powder (Fig. 3-1); no mineral aggregate was used. The binder used for sulfur composites was the dicyclopentadiene (DCPD)-modified sulfur polymer obtained from Micro Powder, Inc. in Ulsan, Korea, of which the specific gravity is 1.91. Recycled rubber powder with a maximum particle size of 600  $\mu\text{m}$  was used, which was produced using waste tires by One Powder, Inc. in Yeongwol, Korea. The specific gravity of the rubber powder is 1.12. The fly ash used belongs to Class F according to ASTM C 618 [44] with a specific gravity of 2.22.



**Figure 3-1: Raw materials: (a) modified sulfur, (b) fly ash, and (c) rubber powder.**

Detailed characterizations for individual raw materials were performed using various analysis techniques: laser diffraction particle size analysis, EA, XRD, XRF, and TGA.

### 3.2.2. Mix proportions

A total of 27 mix proportions were investigated as shown in Table 3-1: (1) 24 mixtures of sulfur composites with rubber powder and fly ash, and (2) three mixtures of sulfur mortars with sand. The main test variables were the relative amounts of rubber powder and fly ash. The mix proportions were designed in a volumetric ratio because this is the preferred proportioning method for sulfur composites [45]. In the mixing process, the quantity of each component was measured with a weight scale before mixing (see Table 3-1). The portions of rubber powder and fly ash varied from 0 to 15% and from 0 to 50% of the total volume of each mixture, respectively. In the label of a sulfur composite mixture, the first and second numbers stand for the volumetric ratios of rubber powder and fly ash, respectively. In the label of a sulfur mortar mixture, the letter “S” stands for sand and the following number indicates

the volumetric ratio of fine aggregate (sand). The rest portion except the rubber powder and fly ash corresponds to the modified sulfur.

**Table 3-1: Mix proportions of tested sulfur composites.**

Mixture Label	Binder precursors						Sand	
	Modified sulfur (5% DCPD)		Fly ash		Rubber powder			
	Vol.%	kg/m <sup>3</sup>	Vol.%	kg/m <sup>3</sup>	Vol.%	kg/m <sup>3</sup>	Vol.%	kg/m <sup>3</sup>
0-0	100	1910	-	-	-	-	-	-
0-10	90	1719	10	222	-	-	-	-
0-15	85	1624	15	333	-	-	-	-
0-40	60	1146	40	888	-	-	-	-
0-45	55	1051	45	999	-	-	-	-
0-50	50	955	50	1110	-	-	-	-
5-0	95	1815	-	-	-	-	-	-
5-10	85	1624	10	222	-	-	-	-
5-15	80	1528	15	333	5	56	-	-
5-40	55	1051	40	888	-	-	-	-
5-45	50	955	45	999	-	-	-	-
5-50	45	860	50	1110	-	-	-	-
10-0	90	1719	-	-	-	-	-	-
10-10	80	1528	10	222	-	-	-	-
10-15	75	1433	15	333	10	112	-	-
10-40	50	955	40	888	-	-	-	-
10-45	45	860	45	999	-	-	-	-
10-50	40	764	50	1110	-	-	-	-
15-0	85	1624	-	-	-	-	-	-
15-10	75	1433	10	222	-	-	-	-
15-15	70	1337	15	333	15	168	-	-
15-40	45	860	40	888	-	-	-	-
15-45	40	764	45	999	-	-	-	-
15-50	35	669	50	1110	-	-	-	-
S5	95	1815	-	-	-	-	5	133
S10	90	1719	-	-	-	-	10	265
S15	85	1624	-	-	-	-	15	398



### 3.2.3. Test methods

Rubber powder is recycled from waste tires that are usually made of a vulcanized rubber with a cross-linked polymer [49]. Modified sulfur is known to be well impregnated around rubber particles when the mixing temperature is around 140°C [24,50]. Thus, the mixing temperature in this study was set to 140°C.

At first, modified sulfur and rubber powder were mixed together in a bowl that was continually heated on a heating jacket at 140°C. After the complete liquefaction of modified sulfur, fly ash or sand that had been preheated in an oven at 180°C for about 6 hours was poured into the bowl. Then, the mixing operation continued for 15 minutes, with the mix temperature kept at 140°C. Finally, the mixed plastic sulfur composite was placed in specimen molds and compacted using a shaking table.

All specimens were cured for only three days before testing or sample preparation, due to the characteristics of fast hardening and rapid strength development of modified sulfur polymer [6], at room temperature (20–25°C) with a relative humidity of 60±5%. The hardened specimens were de-molded after 6 hours of curing. It is assumed that there was little effect of relative humidity on curing because water was not involved in the hardening process [45].

Compressive strength and density were determined for each mixture in Table 3-1. At least three cubic specimens with each side 50 mm long were prepared for each mixture. The density of each specimen was measured according to ASTM 642 [49] before the compression test. The exact compression test methods conform to Section 2.3.1. Also, a series of microstructural analyses were performed to investigate the characteristics of the tested sulfur composites and mortars in both quantitative and qualitative manners.

The microstructures of raw materials and hardened composites were investigated using an ultra-high resolution field emission SEM (Hitachi S-4800, Japan) with EDS. For each mixture in Table 3-1, at least three sliced samples were prepared. Bulk-sectioned samples were used for most mixtures of this study, while thin-sectioned samples were used for only two cases (Mixtures 0-0, 15-0). The detailed preparation and test conditions are given in Section 2.3.4. To examine the effect of high mixing temperature on the morphology of fly ash particles, a comparison was made between the BSE images taken for unheated fly ash and heated fly ash exposed to 140°C for an hour. Secondary electron (SE) images were captured on unpolished saw-cut surfaces of Mixture 0-0 only.

The XRD patterns of raw materials and hardened composites were measured to investigate constituent elements and to identify possible new reaction products following the test methods in Section 2.3.2. The oxide compositions of raw materials were assessed using XRF (Bruker S8 Tiger,

USA). The percentage weights of carbon, hydrogen, sulfur, and oxygen of modified sulfur and rubber powder were determined using EA (Flash 2000, USA).

The particle size distributions of fly ash and rubber powder were determined using a laser diffraction particle size analyzer (Sympatec HELOS, Germany). The particle size distribution of sand was determined using various sizes of sieves with a mechanical shaker.

The pore size distributions and total pore volumes of hardened composites were evaluated using mercury intrusion porosimetry (MIP) (Auto Pore IV 9500, Micromeritics, USA) following the test conditions in Section 2.3.3.

### 3.3. Results and Discussion

#### 3.3.1. Characterization of raw materials

The elemental compositions of modified sulfur and rubber powder from the EA analysis are shown in Table 3-2. Based on the XRF results, the chemical oxide compositions of fly ash and modified sulfur are presented in Table 3-3. The EA results show that about 98.3% of the modified sulfur was elemental sulfur. This is consistent with the XRF results indicating about 99.8% of elemental sulfur. Thus, the modified sulfur polymer used in this study mostly consisted of elemental sulfur with a minor quantity of elements from the chemical modifier (DCPD). The EA results of rubber powder display that it was dominated by 77.5% of carbon on average, and the rest portions were composed of hydrogen, nitrogen, and sulfur.

**Table 3-2: Elemental analysis (EA) results of modified sulfur and rubber powder (unit: wt.%).**

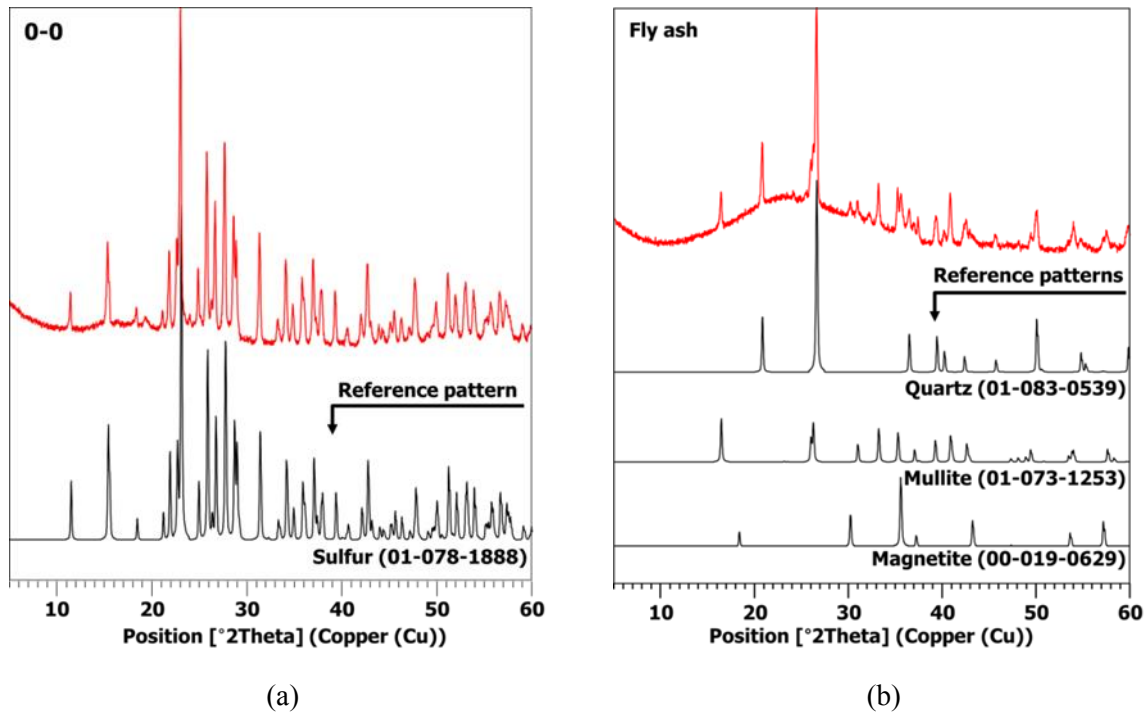
Element	Modified sulfur	Rubber powder
Carbon (%)	1.9	77.5
Hydrogen (%)	0.2	7
Sulfur (%)	98.3	0.7
Nitrogen (%)	-	0.2

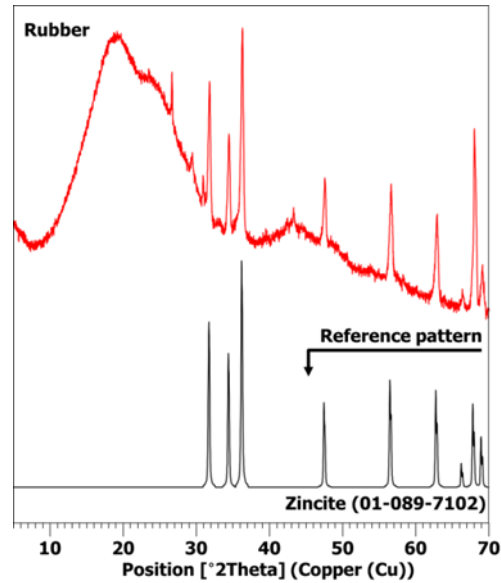
**Table 3-3: Chemical oxide compositions of modified sulfur and fly ash from XRF.**

Oxide (wt.%)	Fly ash	Modified sulfur
SiO <sub>2</sub>	52.3	-
Al <sub>2</sub> O <sub>3</sub>	22.6	-
Fe <sub>2</sub> O <sub>3</sub>	9.1	-
CaO	6.2	-

MgO	1.8	-
K <sub>2</sub> O	1.8	-
Na <sub>2</sub> O	1.8	-
TiO <sub>2</sub>	1.3	-
P <sub>2</sub> O <sub>5</sub>	1.2	-
SO <sub>3</sub>	-	99.8
Others	1.9	0.2

The measured XRD patterns of modified sulfur, fly ash, and rubber powder are shown in Fig. 3-2. The XRD pattern of hardened modified sulfur (i.e., Mixture 0-0) confirms that it contained elemental sulfur with the orthorhombic structure [3] (ICDD PDF no. 01-078-1888). Currell et al. [24] reported that the interaction between DCPD and elemental sulfur at 140°C produced a mixture of polysulfides and free elemental sulfur that was a mixture of monoclinic, orthorhombic sulfur crystal, and non-crystalline sulfur; free elemental sulfur is unreacted sulfur containing amorphous S<sub>8</sub>. Note that a slight amorphous hump was seen at about 10–30° in the XRD pattern (Fig. 3-2). The fly ash had several minerals, such as quartz (ICDD PDF no. 01-083-0539), mullite (ICDD PDF no. 01-073-1253), and magnetite (ICDD PDF no. 00-019-0629). The rubber powder consisted mostly of an amorphous carbon phase [46], manifested as a large hump from about 10° to 30°, and contained only zincite (ICDD PDF no. 01-089-7102) as a crystalline phase, which was included in the manufacturing of tire rubbers.

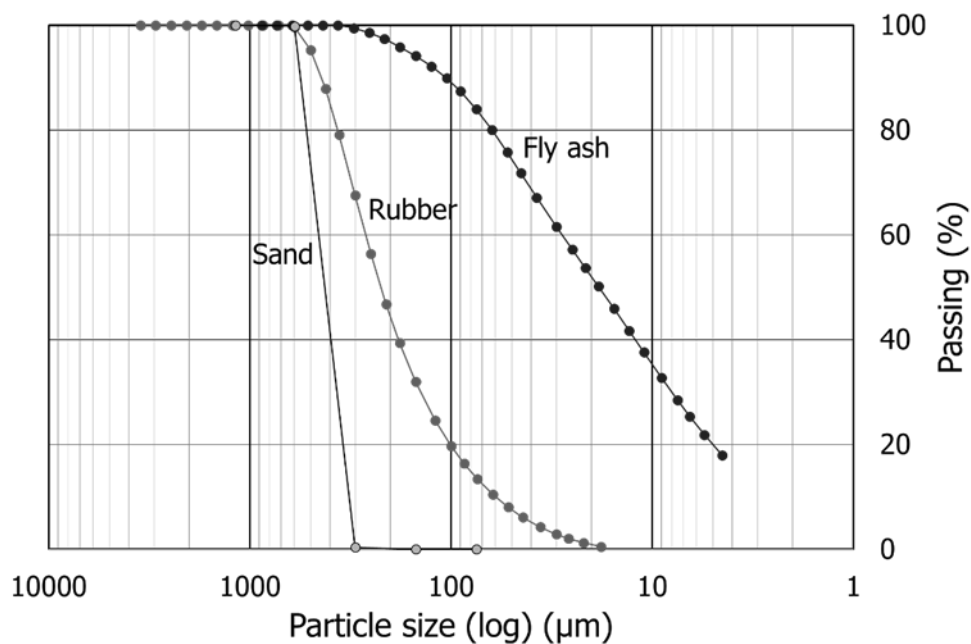




(c)

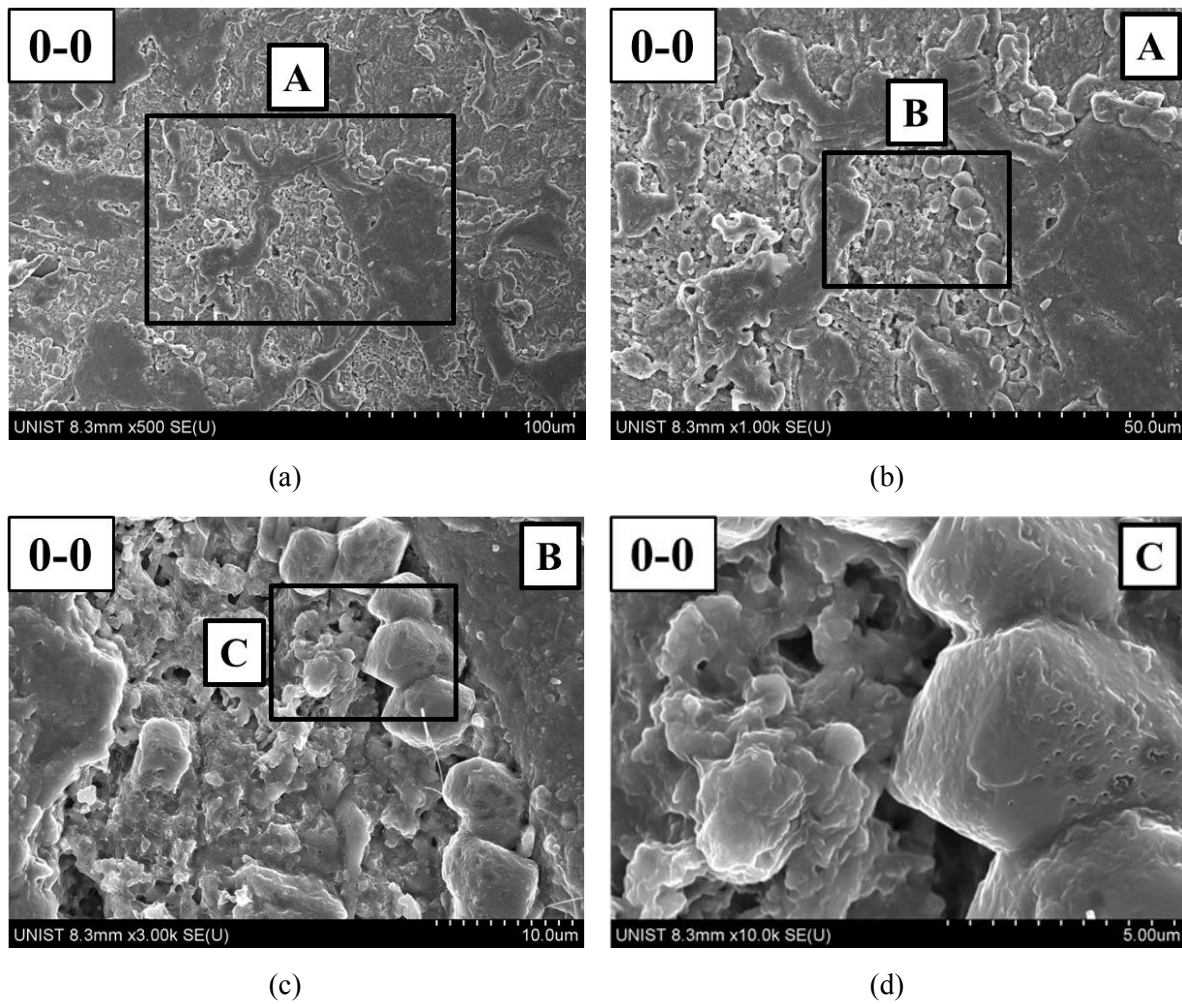
**Figure 3-2: XRD patterns of raw materials: (a) hardened modified sulfur (Mixture 0-0), (b) fly ash, and (c) rubber powder.**

Fig. 3-3 presents the particle size distributions of fly ash, rubber powder, and sand. The particle size distributions show that the maximum size of fly ash was about 300  $\mu\text{m}$ , which was smaller than those of recycled rubber powder (about 600  $\mu\text{m}$ ) and sand (about 600  $\mu\text{m}$ ). Also, the particle size of fly ash was better distributed over a wide range [50,51] and was much finer than those of rubber powder and sand.



**Figure 3-3: Particle size distributions of fly ash, rubber powder, and sand.**

Fig. 3-4 displays SE images for the unpolished saw-cut surfaces of hardened modified sulfur, which were captured using SEM. In the figure caption, the number followed by “X” means a magnification ratio, which is used throughout this paper. The SE images revealed an irregular microstructure, with porous regions separate from dense areas. More details on the microstructure of hardened modified sulfur are discussed using BSE images in Section 3.3.5.



**Figure 3-4: SE images for saw-cut surfaces of hardened modified sulfur (Mixture 0-0): (a) 500X; (b) magnified image (1,000X) of A in (a); (c) magnified image (3,000X) of B in (b); (d) magnified image (10,000X) of C in (c). The number with “X” means a magnification ratio.**

Fig. 3-5 shows the temperature-weight relationship of rubber powder acquired from TGA. The TGA results indicate that the rubber started to be decomposed from about 219.6°C, which is much

higher than the mixing temperature (near 140°C) used in this study. Thus, it is deemed that the rubber was not decomposed in the mixing process.

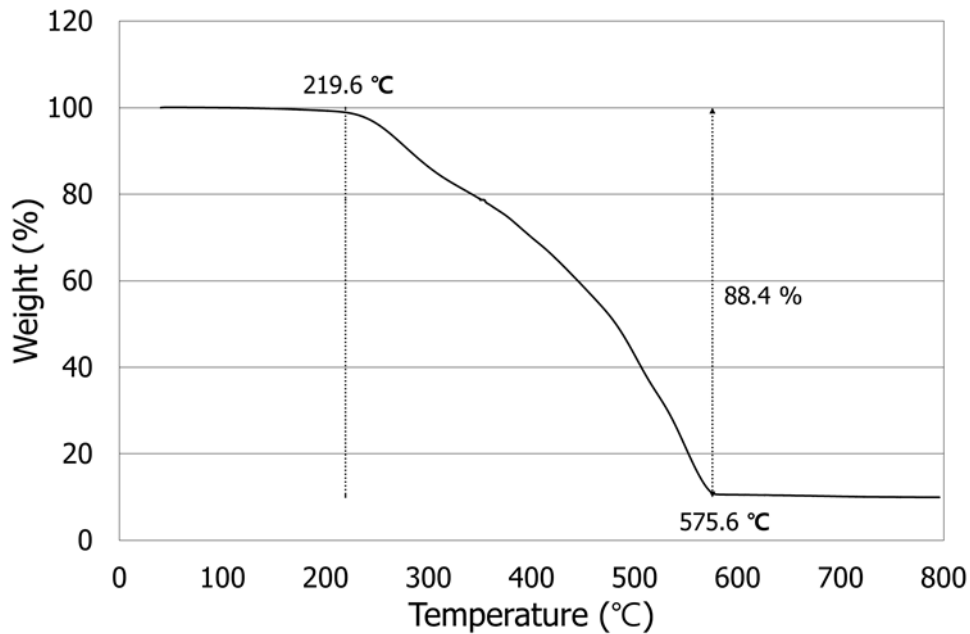


**Figure 3-5: TGA results of rubber powder.**

### 3.3.2. Compressive strength

Fig. 3-6 compares the compressive strengths of all sulfur composites and mortars in Table 3-1. The strength of hardened modified sulfur with no other materials (Mixture 0-0) was approximately 27.0 MPa on average. Most mixtures with rubber powder and/or fly ash achieved higher compressive strengths than did Mixture 0-0. The low strength of Mixture 0-0 was likely due to the volumetric contraction of plastic modified sulfur during the hardening process; a severe contraction was visually observed in Mixture 0-0. Detrimental thermal stress might occur in the sulfur matrix due to the contraction (i.e., thermal shrinkage). Mohamed and El-Gamal [3] reported that a DCPD-modified sulfur polymer might undergo expansion or contraction due to the allotropic transition of sulfur during a temperature change; the higher the concentration of the chemical modifier, the less the volumetric change. In this study, the concentration of DCPD was 5% by weight. Although the precise degree of sample contraction during hardening was not quantified in this study, it was visibly noted that more fly ash caused less contraction. This will be discussed in more detail later. Although Yue et al. [51] investigated the properties of sulfur-rubber concrete, all absolute strength values were much smaller even than the smallest one of the current study.

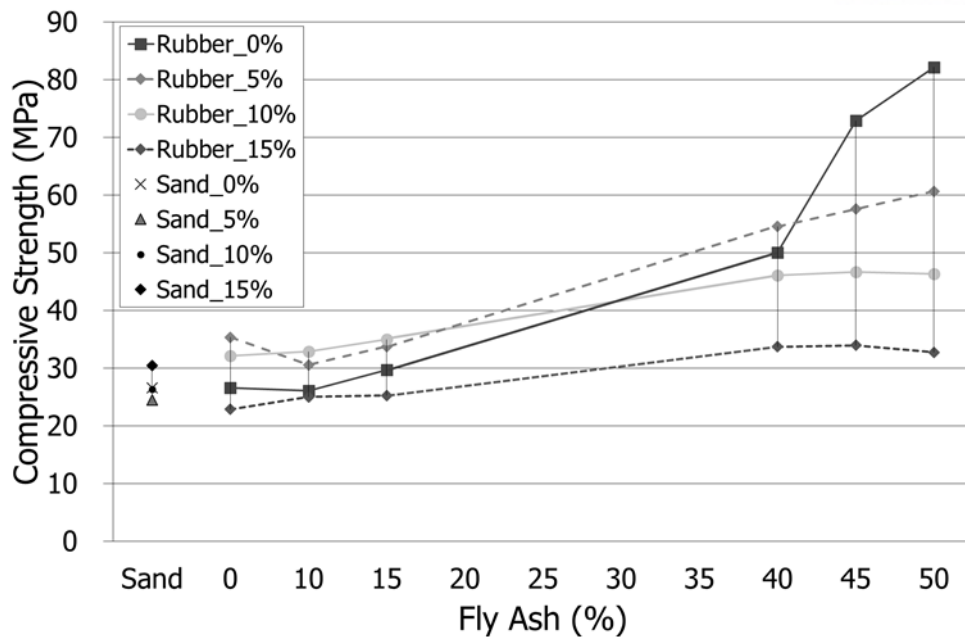


**Figure 3-6: Compressive strengths of sulfur composites and mortars.**

The larger ratio of fly ash from 10 to 45% constantly resulted in the higher compressive strength, regardless of the amount of rubber powder (Fig. 3-6). In the series of 0 or 5% rubber powder, the strength also improved when the ratio of fly ash increased from 45 to 50%. However, in the series of 10 or 15% rubber powder, the mixture with 50% fly ash showed a lower strength than that with 45% fly ash. When rubber powder was not used (“Rubber\_0%” series in Fig. 3-6), the strength significantly improved by replacing 45 or 50% modified sulfur by fly ash. The highest compressive strength of about 83.0 MPa was achieved with 50% fly ash and no rubber powder (Mixture 0-50) among all of the mixtures in Table 3-1. Yue et al. [51] reported a similar result that the addition of fly ash or Portland cement as micro-fillers in sulfur-rubber concrete led to about 30% higher compressive strength than those with no micro-filler. They found that using fly ash as a micro-filler was more effective than cement. In their tests, both micro-fillers and rubber particles were used as a partial replacement of sand, with the same amount of sulfur.

The optimal content of rubber powder for the compressive strength was highly dependent on the content of fly ash. When 15% or less fly ash was included, the mixtures with 5 or 10% rubber powder displayed at least 13.1% higher strengths than did the mixtures with no rubber powder for a given ratio of fly ash. However, when the fly ash content was 45% or more, the mixture with a smaller ratio of rubber powder constantly had a higher strength. The mixture with 15% rubber powder produced the lowest strength at every given ratio of fly ash. Also, the influence of fly ash on the strength was the least in the sulfur composites with 15% rubber powder; with a higher ratio of rubber powder, the strength development was less affected by the variation of fly ash content in general. According to Yue

et al. [51], the inclusion of rubber particles of 5.8% by volume as a partial replacement of sand, when mixed with 5.8% fly ash, 46.4% sand, and 42.0% sulfur, caused a roughly 30% reduction of compressive strength. Raising the volume of rubber particles up to 29.0% using 23.2% sand resulted in a drastic strength reduction of 76%. On the other hand, the current study observed that the mixture with 15% rubber powder, 45% fly ash, and 40% sulfur had a roughly 33 MPa of compressive strength, which was a roughly 2.75 times that of Yue et al. [51] mixture with similar amount of rubber particles and sulfur as the previously referred mixture, 17.4% and 42%, respectively, with 34.8% sand and 5.8% fly ash. Note that the specimens of Yue et al. [51] included a considerable ratio of sand and tested rubber particles as a partial replacement of the sand, while the specimens of the current study did not contain mineral aggregate. Thus, the above comparisons would rather be interpreted qualitatively than quantitatively.

Fig. 3-6 also presents the results of sulfur mortars with three different amounts of sand and no fly ash (Mixtures S5, S10, and S15); “Sand\_0%” in the legend stands for hardened modified sulfur itself (Mixture 0-0). The compressive strengths of the sulfur mortars ranged from about 24.5 to 30.5 MPa. The sulfur mortars with 5 or 10% sand showed lower compressive strengths than did the sulfur composites with 5 or 10% rubber powder and even no fly ash (Mixture 5-0 or 10-0). This suggests that rubber powder may effectively replace a portion of fine aggregate in sulfur composites without sacrificing the resulting strength.

### 3.3.3. Density

Fig. 3-7 plots the measured densities of all sulfur composites and mortars in Table 3-1. The density of hardened modified sulfur was approximately  $1,915 \text{ kg/m}^3$ . However, the densities of the sulfur composites with rubber powder were smaller than  $1,900 \text{ kg/m}^3$  except for three cases with large fly ash contents (Mixtures 5-40, 5-45, and 5-50). ACI 213R-03 [52] defines the density of structural lightweight concrete as being below  $1,920 \text{ kg/m}^3$ . The density of sulfur composites decreased as the rubber powder ratio increased (Fig. 3-7) because of the lower specific gravity of rubber (about 1.12) compared with modified sulfur (about 1.91). For a given rubber content, a larger ratio of fly ash generally resulted in a higher density.

The densities of the sulfur mortars with 5–15% sand (Mixtures S5, S10, and S15) ranged from about  $1,947$  to  $2,021 \text{ kg/m}^3$ . Of them, the highest density was obtained from Mixture S15 with 15% of sand since the specific gravity of sand (about 2.65) was higher than that of modified sulfur. The density of Mixture 5-0 with 5% rubber powder was 95.0% of that of Mixture S5, 87.8% of S10 for Mixture 10-0, and 82.7% of S15 for Mixture 15-0. This demonstrates that the use of rubber powder as a replacement of sand can feature the advantage of reducing the self-weight of sulfur composites.



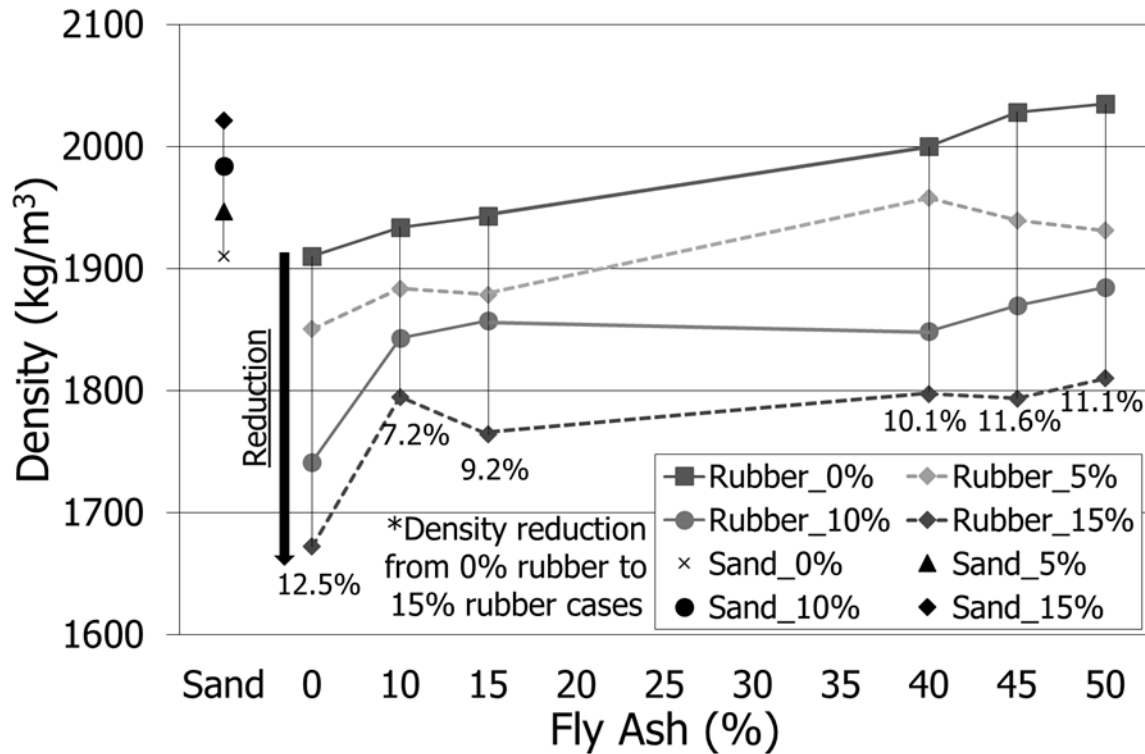
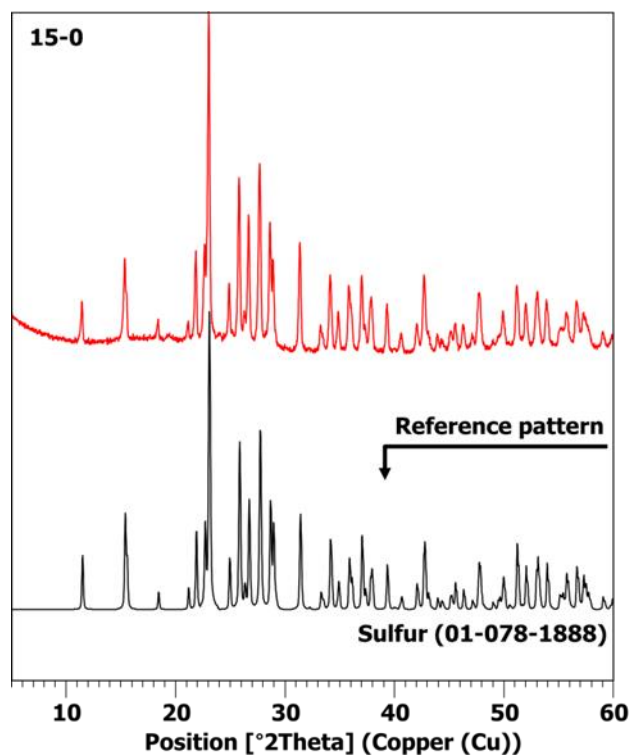


Figure 3-7: Densities of sulfur composites and mortars.

#### 3.3.4. Crystalline phase transition (XRD)

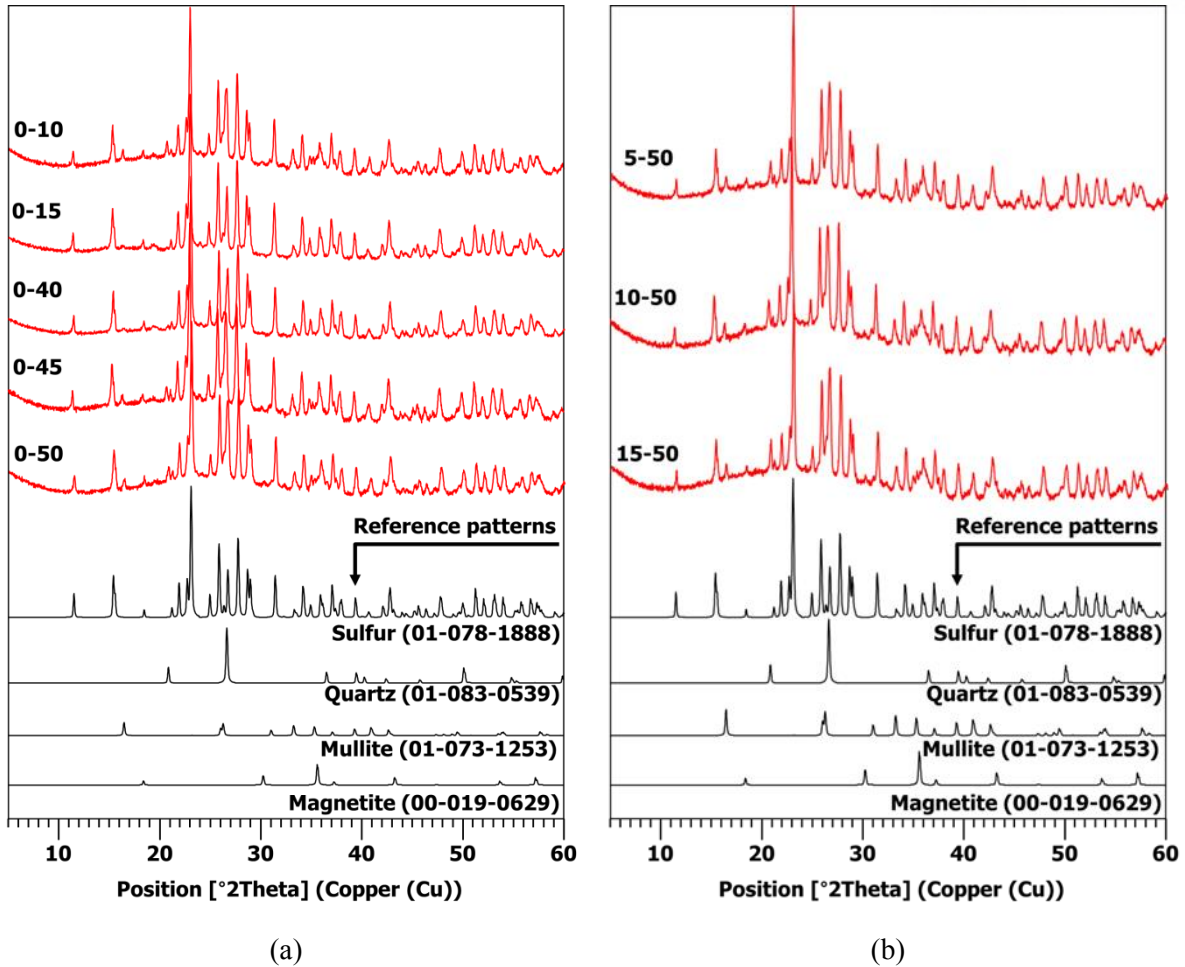
The purpose of the XRD tests was to investigate the effects of rubber powder and fly ash on the reaction products of sulfur composites. In Fig. 3-8, the XRD pattern of Mixture 15-0 showed mostly the reflections of modified sulfur. Despite the presence of 15% rubber powder, the amorphous carbon hump and peaks of zincite were hardly visible in the XRD pattern because the peak intensities of modified sulfur were significantly stronger than those of rubber powder. Most of all, there were no other reflections that might indicate the formation of new reaction products between modified sulfur and rubber powder during the mixing and hardening processes.



**Figure 3-8: Integrated XRD pattern for Mixture 15-0.**

Fig. 3-9(a) shows the influence of varying the fly ash ratio on the XRD patterns of the five sulfur composites with no rubber powder (Mixtures 0-10, 0-15, 0-40, 0-45, and 0-50). The mixtures with low fly ash ratios (Mixtures 0-10, 0-15) weakly showed the reflections of fly ash, while those with high fly ash ratios (Mixtures 0-40, 0-45, 0-50) clearly showed the characteristics of fly ash (i.e., amorphous hump and peaks). As the amount of fly ash increased, the XRD peaks of fly ash became more apparent and stronger. On the other hand, there was no evidence for the formation of any new reaction products between modified sulfur and fly ash.

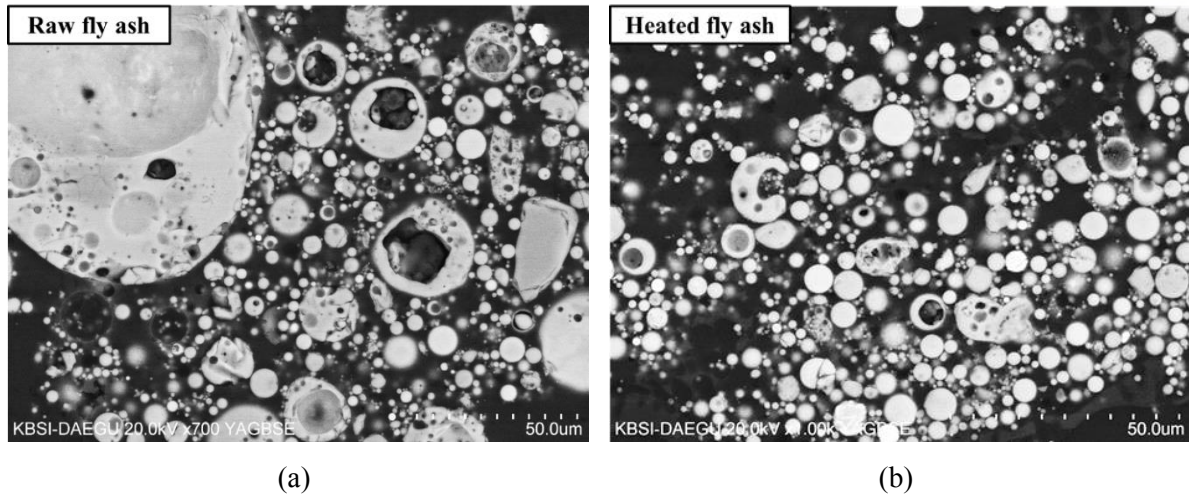
The three mixtures with different rubber ratios and 50% of fly ash (Mixtures 5-50, 10-50, 15-50) were examined by XRD to investigate the effect of varying the rubber powder ratio (Fig. 3-9(b)); as in Mixture 15-0 (Fig. 3-8), the amorphous hump of carbon in rubber powder was barely seen in the XRD patterns of these composites. The three composites with different rubber ratios exhibited similar XRD patterns, and the formation of any new reaction products between modified sulfur, fly ash, and/or rubber was not detected.



**Figure 3-9: XRD patterns for sulfur composites with varied ratios of rubber powder and fly ash: (a) Mixtures 0-10, 0-15, 0-40, 0-45, 0-50; (b) Mixtures 5-50, 10-50, 15-50.**

### 3.3.5. Morphological transition (SEM BSE/EDS)

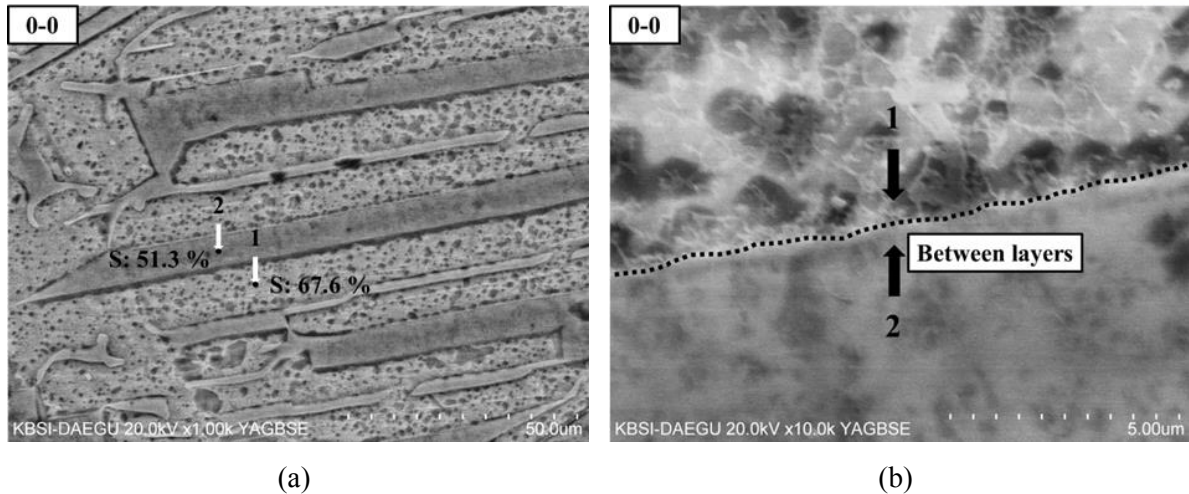
The purpose of the SEM tests was to examine the possible morphological transition of sulfur composites with varying ratios of mix components. The BSE images of raw and heated fly ashes are presented in Fig. 3-10; the images were obtained from polished samples. Both samples had very similar morphologies consisting of solid, partially broken, and plero-spheres with various diameters ranging from 0.5 to 300  $\mu\text{m}$ . No difference was found between the two samples despite the different temperature conditions. Therefore, it is deemed that there was no morphological transition of fly ash in the tested sulfur composites due to the high temperature mixing process [45].



**Figure 3-10: BSE images for microstructures of fly ash: (a) raw fly ash (700X); (b) heated fly ash (1,000X).**

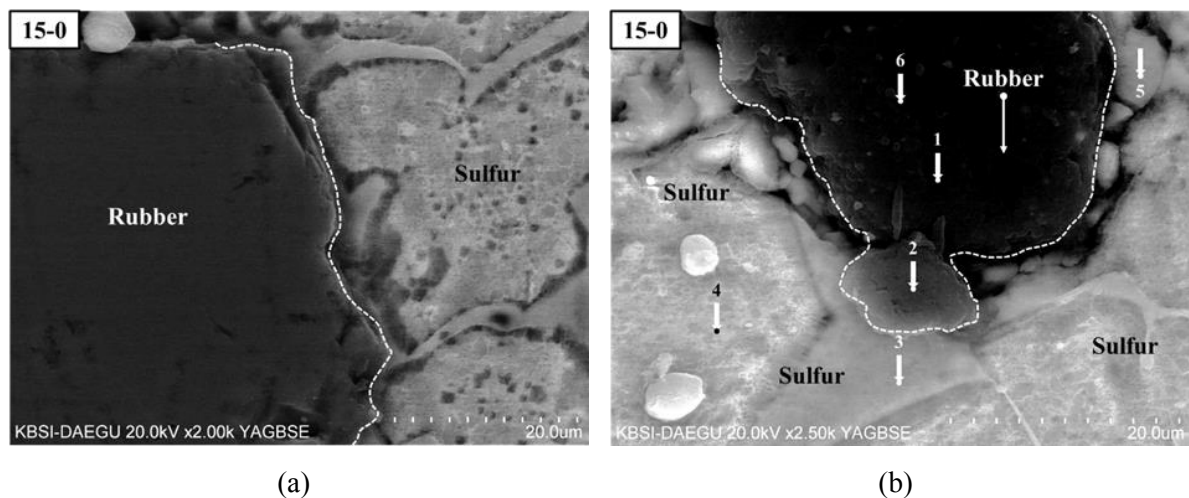
The BSE images of hardened modified sulfur with no other substitutes (Mixture 0-0) were taken at several different locations with different magnifications, as shown in Fig. 3-11. Unlike the SE images on the saw-cut surfaces of Mixture 0-0 in Fig. 3-4, the BSE images were obtained from polished sections.

Fig. 3-11(a) displays a layered structure that consists of multiple different layers aligned parallel to one another. This layered microstructure was likely formed through a heterogeneous allotropic transition during the hardening process [3]. In particular, the regions of points 1 and 2 exhibited very different microstructures even though both regions were composed of modified sulfur only. In general, regions with lower density appear darker (e.g., pores) than those with higher density in BSE images. Thus, it is supposed that the region at point 1 contained more pores but had a higher density compared with the region at point 2 (Fig. 3-11(b)). This layered microstructure may be an indicator that different regions underwent different degrees of thermal shrinkage in different orientations during hardening, resulting in detrimental thermal stress in the sulfur matrices, as discussed in Section 3.3.2. It is expected that some agents (e.g., mineral fillers, such as fly ash) may prevent the formation of the layered morphologies in sulfur composites by reducing the degree of differential thermal shrinkage of modified sulfur.



**Figure 3-11: Microstructures of Mixture 0-0 in BSE images with EDS analyses: (a) 1,000X; (b) interfacial zone between points 1 and 2 (10,000X). Note that thin-sectioned and polished samples were used for these BSE images.**

The BSE images of Mixture 15-0 were taken at several different locations; Fig. 3-12 shows two images on the interfacial zones between modified sulfur and rubber, along with EDS analysis results for two selected spots. Table 3-4 presents the results of EDS analysis for the spots marked in Fig. 3-12(b). The EDS results indicate that the dark region had a rubber particle, and the bright regions around the rubber particle were occupied by modified sulfur; note that the bright regions present a similar brightness to that of hardened modified sulfur itself in Fig. 3-11. The layered microstructure of hardened modified sulfur itself (Fig. 3-11) remained even in the matrix of the sulfur-rubber composite (Mixture 15-0). It is also worth noting that the gray area near point 2 was a transition zone for sulfur and rubber; the brightness around point 2 became darker toward the rubber side.



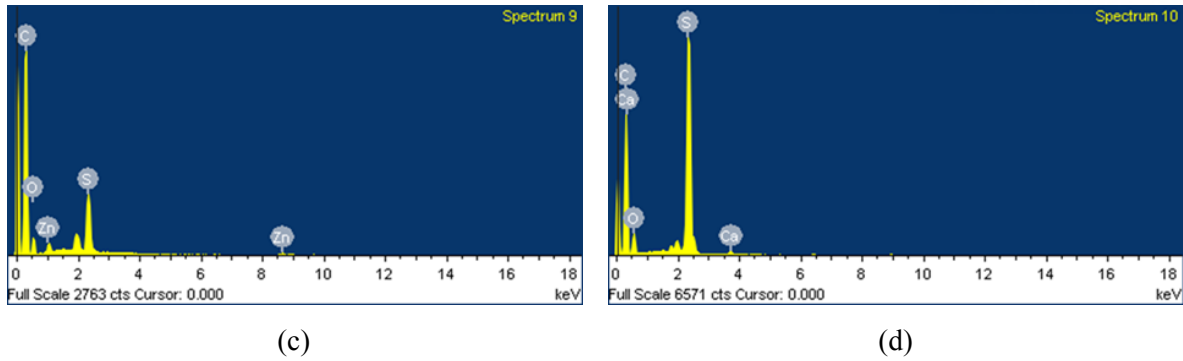


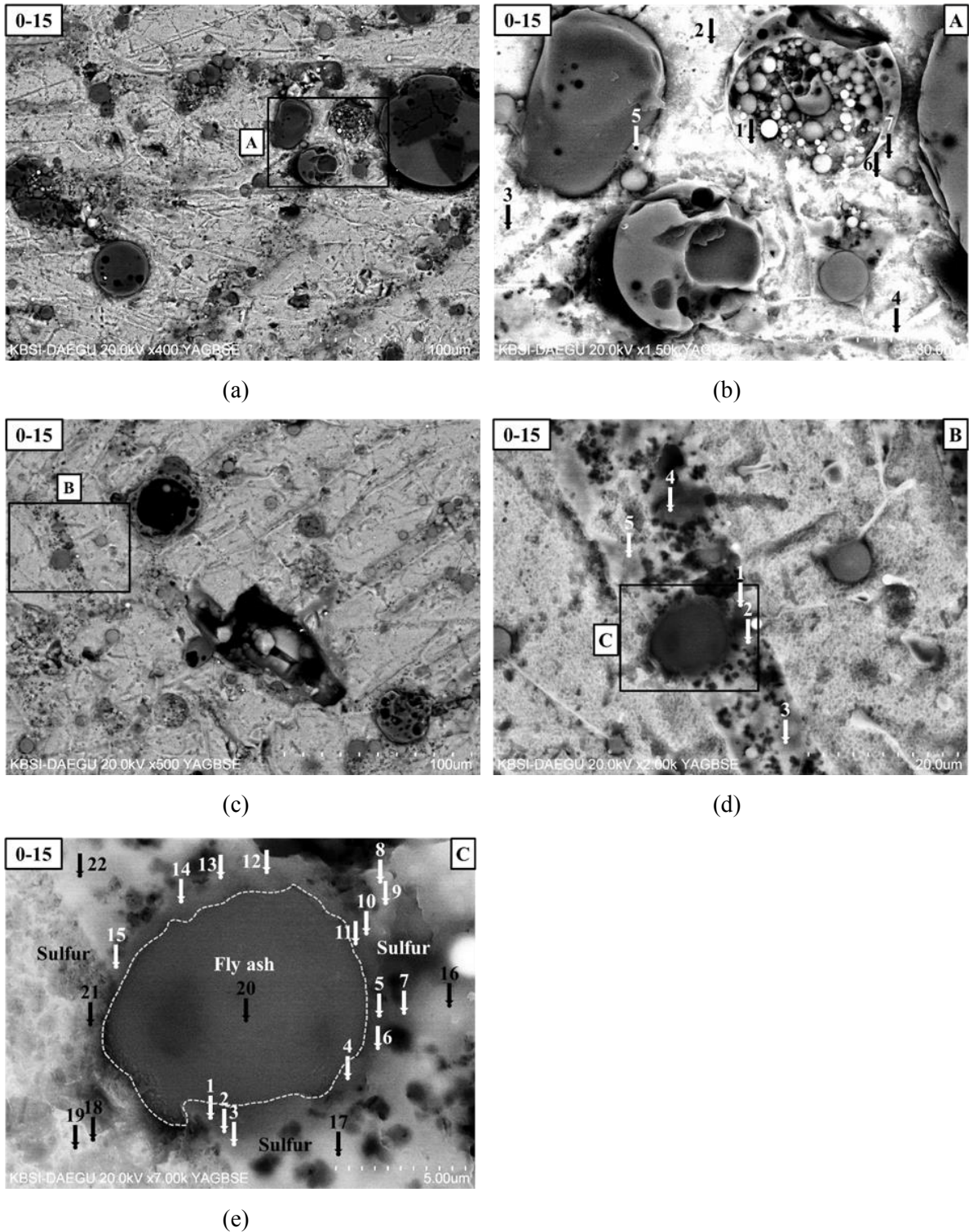
**Figure 3-12: Microstructures of Mixture 15-0 in BSE images with EDS analyses: (a) 2,000X; (b) 2,500X; (c) EDS spectrum for point 1 in (b); (d) EDS spectrum for point 2 in (b).**

**Table 3-4: Elemental spot analysis on BSE image for Mixture 15-0 (Fig. 3-12(b)).**

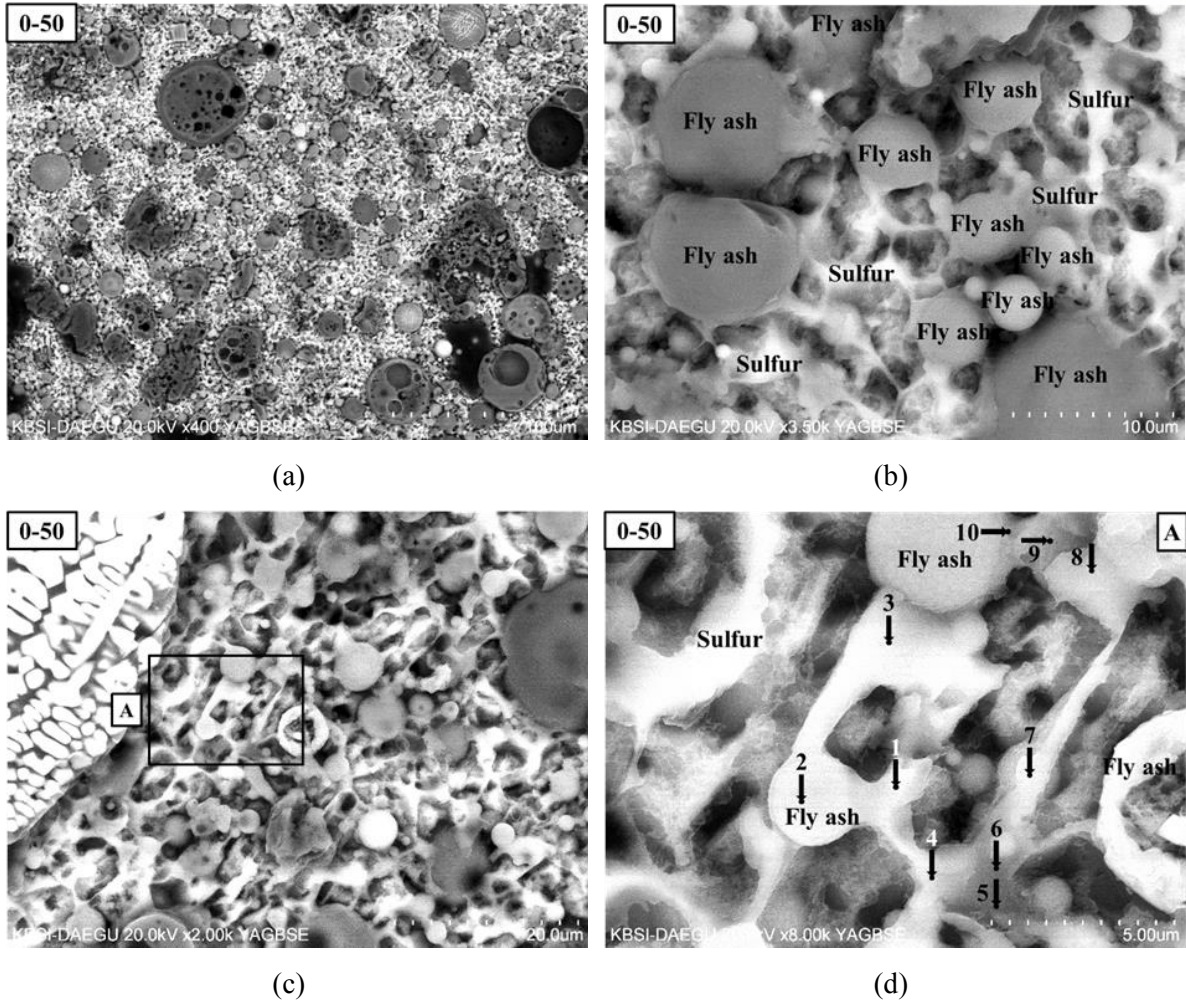
Spot	Elemental content (atomic %)					Total (%)
	C	O	S	Ca	Zn	
1	85.6	12.1	2.0	0.0	0.3	100
2	83.1	11.2	5.6	0.1	0.0	100
3	65.2	5.5	29.3	0.0	0.0	100
4	67.4	3.8	28.8	0.0	0.0	100
5	66.3	7.9	25.9	0.0	0.0	100
6	83.8	14.2	1.7	0.0	0.2	100

Fig. 3-13 presents the BSE images of Mixture 0-15 with a small quantity (i.e., 15%) of fly ash. The sulfur matrix and fly ash particles were clearly distinguishable from each other in the composite. The morphology of the sulfur matrix in Mixture 0-15 was similar to that of the hardened modified sulfur itself (Fig. 3-11).

However, as fly ash was used at a higher ratio, the microstructure (or morphology) of sulfur matrix was entirely changed; Mixture 0-50 with 50% fly ash in Fig. 3-14 showed not only many more fly ash particles, but also a completely different microstructure of sulfur matrix, compared to that of Mixture 0-15 (Fig. 3-13). In Mixture 0-50, fly ash particles were well distributed in a honeycomb-shaped sulfur matrix. Although this distinctive microstructure looked as if it possessed a large volume of micro-sized pores, the compressive strength of this mixture was the highest among those of the tested sulfur composites in this study. It seems that this morphological evolution had a substantial influence on the strength development of sulfur composites. This will be discussed more using the results of MIP in Section 3.3.6.



**Figure 3-13 :** Microstructures of Mixture 0-15 in BSE images with EDS analyses: (a) 400X; (b) magnified image (1,500X) of A in (a); (c) 500X; (d) magnified image (2,000X) of B in (c); (e) magnified image (7,000X) of C in (d).

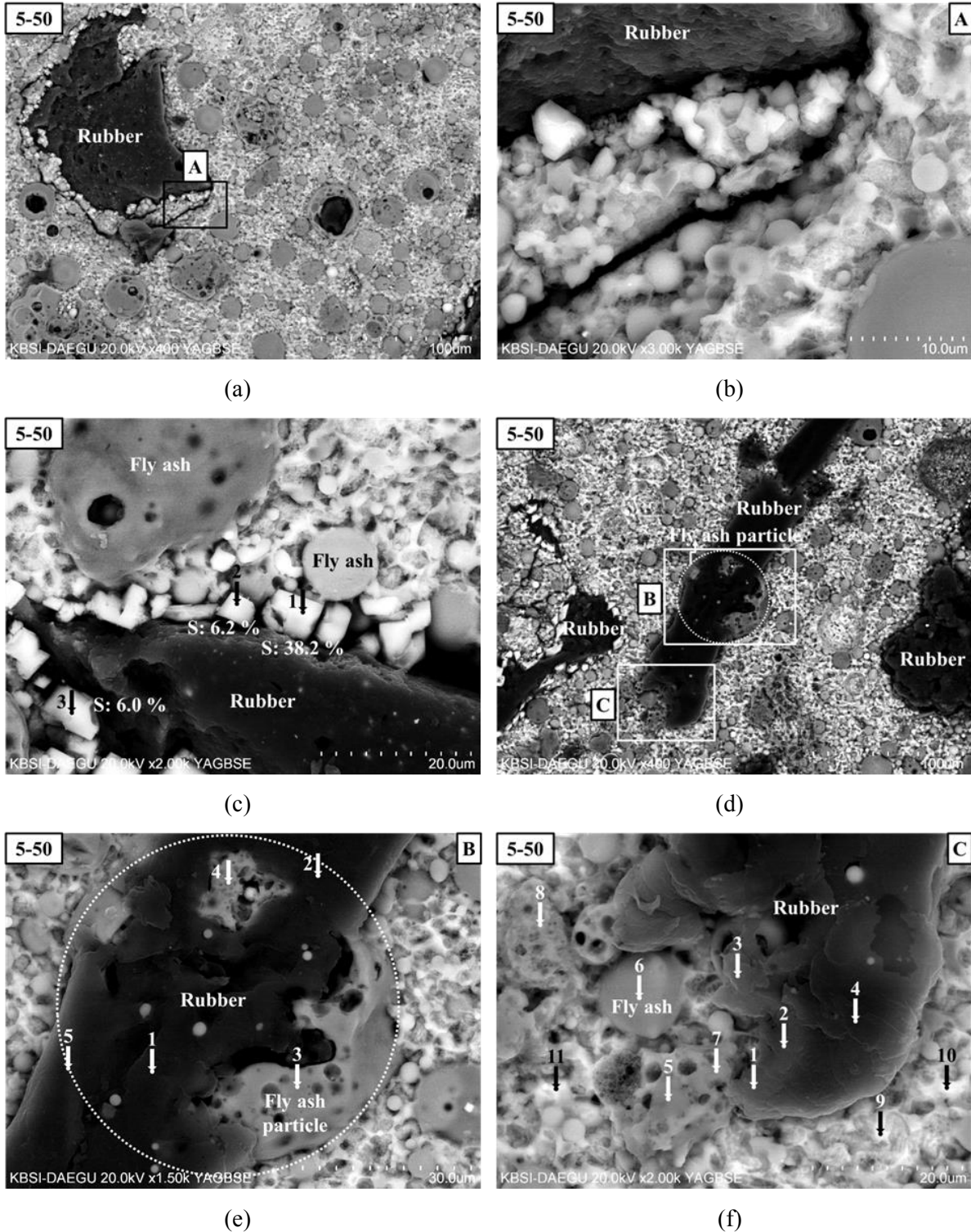


**Figure 3-14: Microstructures of Mixture 0-50 in BSE images with EDS analyses: (a) 400X; (b) 3,500X; (c) 2,000X; (d) magnified image (8,000X) of A in (c).**

The BSE images of Mixture 5-50 in Fig. 3-15 display a similar microstructure to that of Mixture 0-50, except that rubber particles were well distributed and surrounded by the sulfur-fly ash composite. The rubber particles were detected in various sizes and irregular shapes. Most rubber particles were separated with clear boundaries from the modified sulfur matrix or fly ash particles, but some rubber particles were diffused into the voids of hollow fly ash particles (Fig. 3-15(e)).

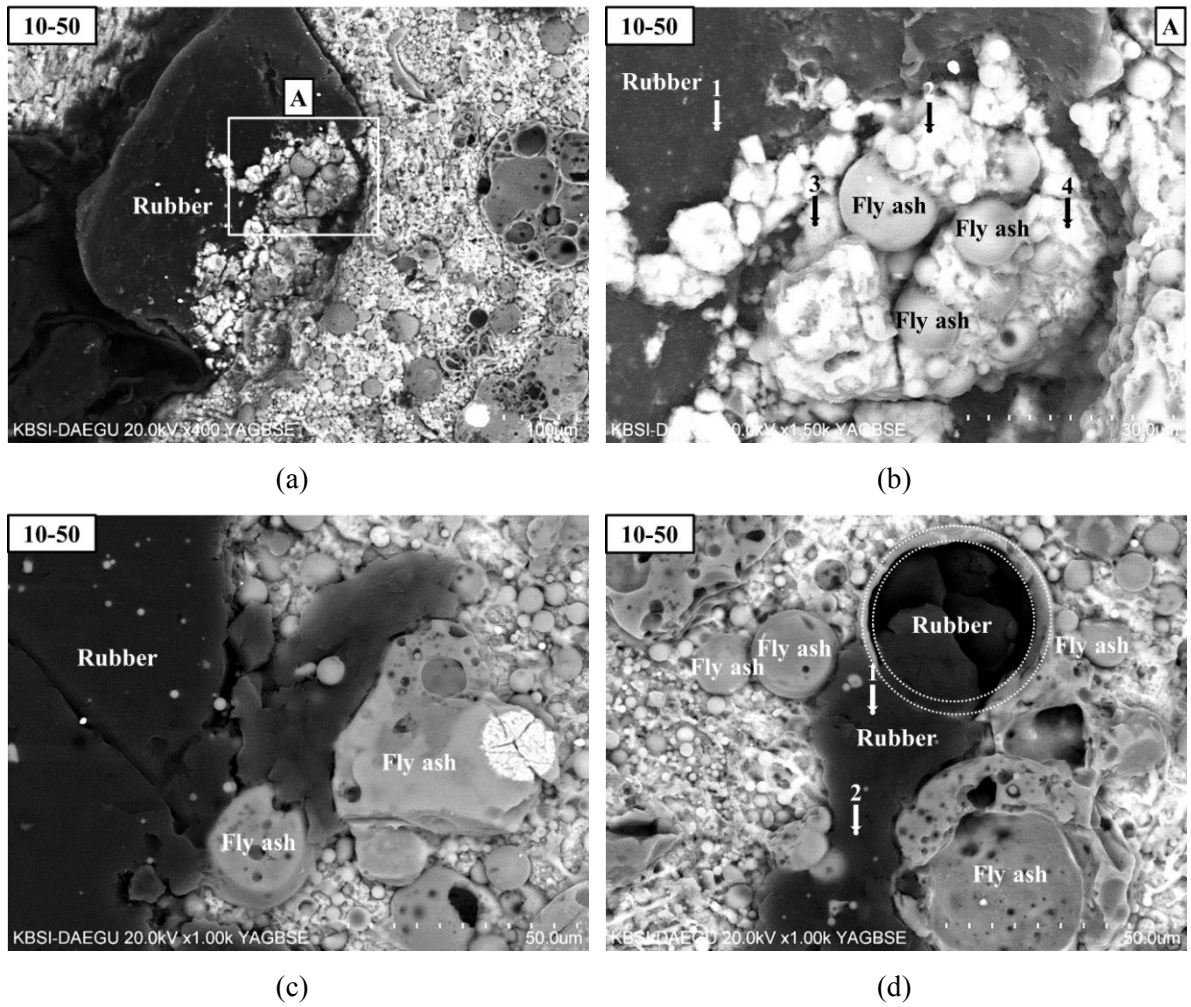
One interesting feature was observed in the matrices of the sulfur composites with rubber (Figs. 3-15 through 3-17), different from those with no rubber. Small sizes of polyhedral sulfur particles were often found at the perimeters of rubber particles.





**Figure 3-15: Microstructures of Mixture 5-50 in BSE images with EDS analyses: (a) 400X; (b) magnified image (3,000X) of A in (a); (c) 2,000X; (d) 400X; (e) magnified image (1,500X) of B in (d); (f) magnified image (2,000X) of C in (d).**

According to the BSE images in Fig. 3-16, Mixture 10-50 exhibited a similar microstructural morphology to that of Mixture 5-50; fly ash and rubber particles were well distributed in a honeycomb-shaped sulfur matrix, and some rubber particles were diffused into the voids of hollow fly ash particles. The only difference was that rubber particles were more frequently detected. The BSE images of Mixture 15-45 in Fig. 3-17 also showed a similar microstructure to those of Mixtures 5-50 and 10-50 (i.e., a honeycomb-shaped sulfur matrix), and the infiltration of diffused rubber particles into the voids of hollow fly ash particles.



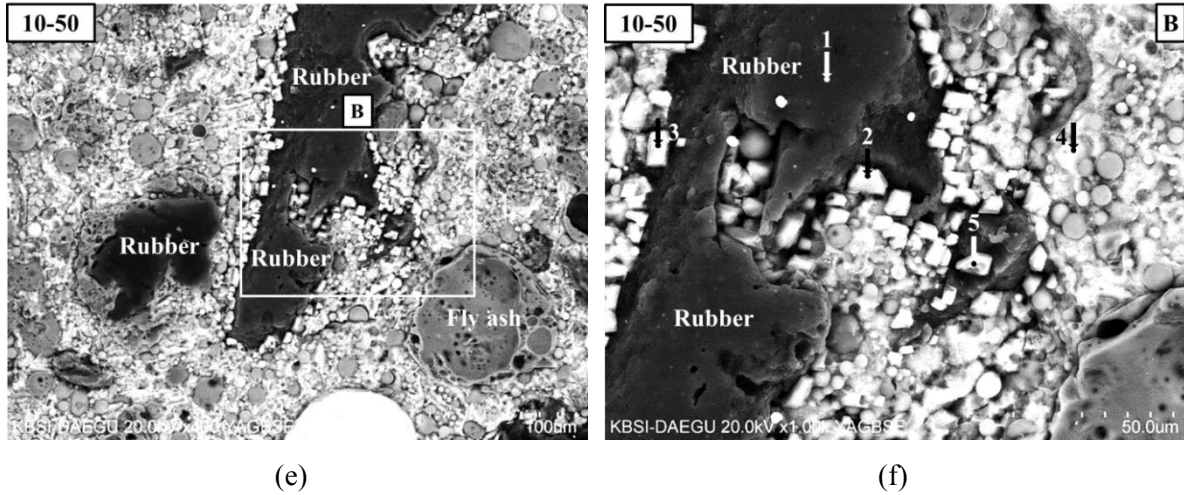
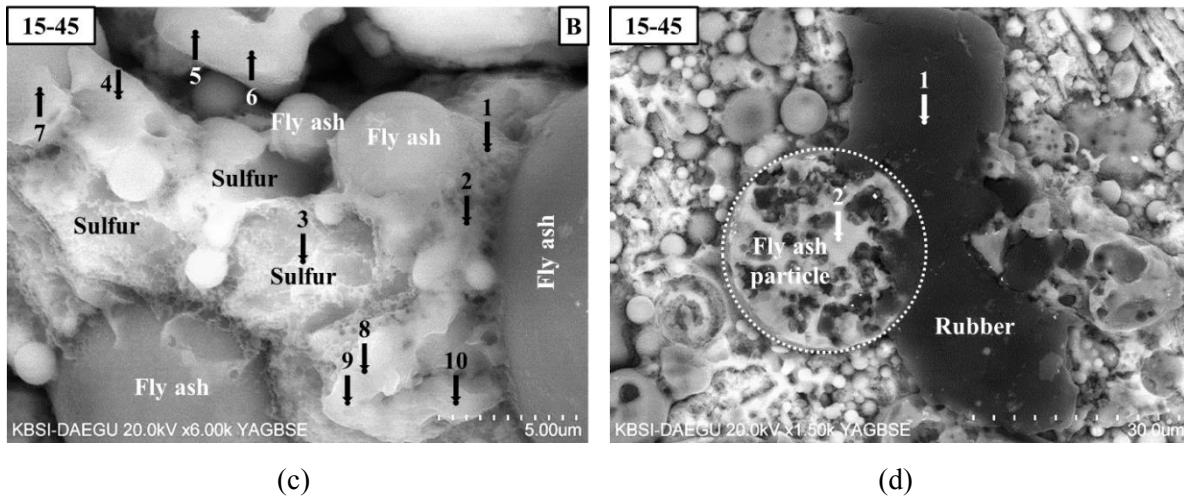
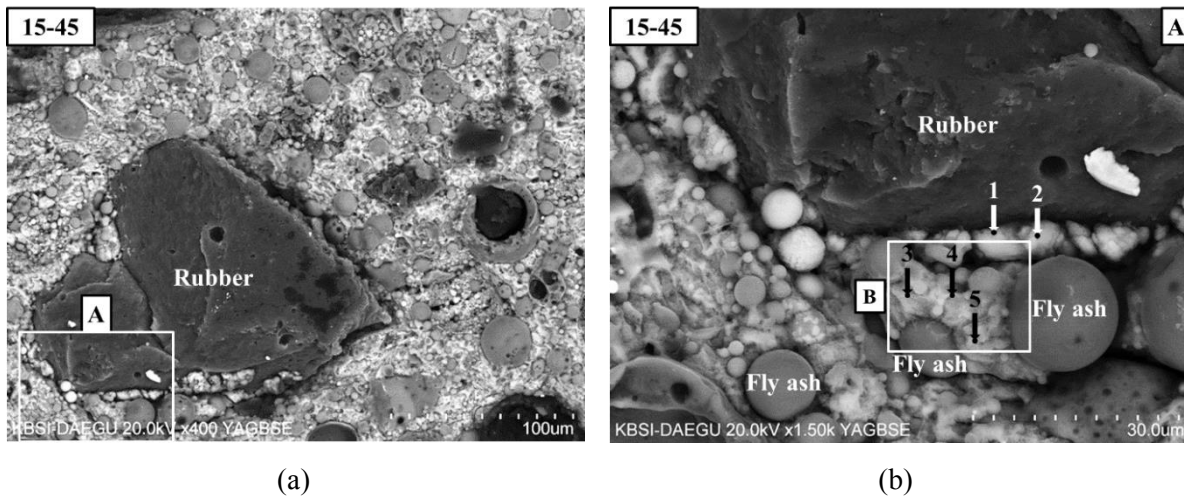
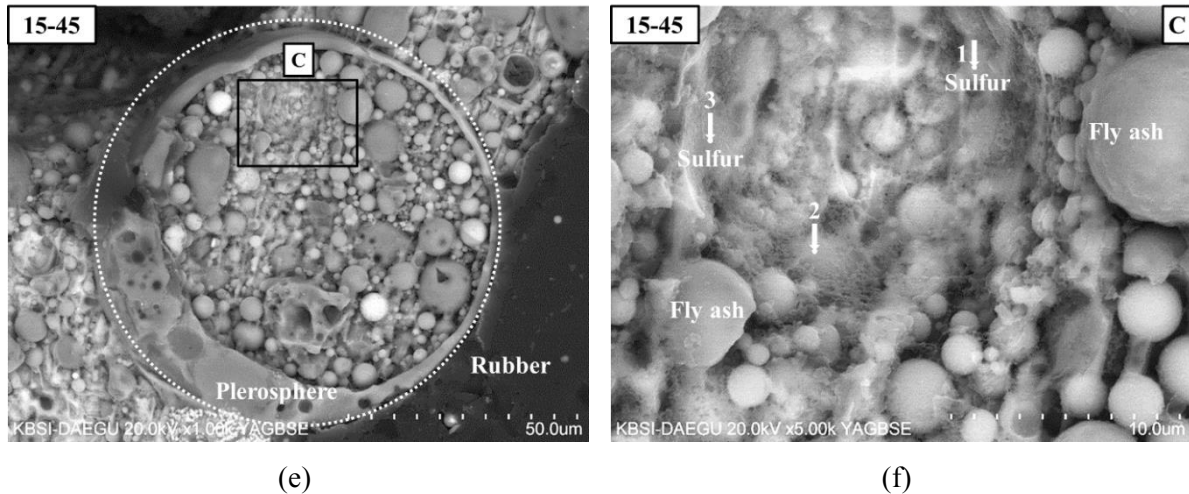


Figure 3-16: Microstructures of Mixture 10-50 in BSE images with EDS analyses: (a) 400X; (b) magnified image (1,500X) of A in (a); (c) 1,000X; (d) 1,000X; (e) 400X; (f) magnified image (1,000X) of B in (e).





**Figure 3-17: Microstructures of Mixture 15-45 in BSE images with EDS analyses: (a) 400X; (b) magnified image (1,500X) of A in (a); (c) magnified image (6,000X) of B in (b); (d) 1,500X; (e) 1,000X; (f) magnified image (5,000X) of C in (e).**

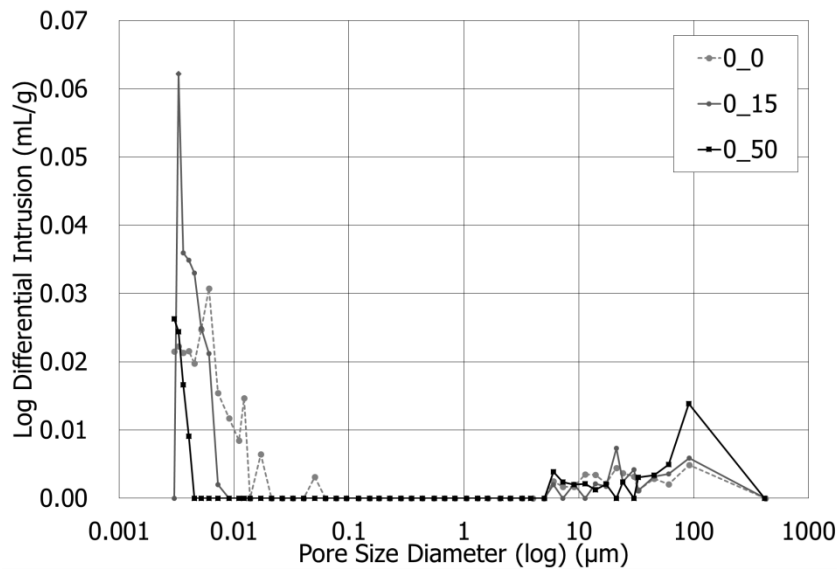
### 3.3.6. Porosity (MIP)

Three sulfur composites with no rubber powder, Mixtures 0-0, 0-15, and 0-50, were selected to investigate the pore size distribution and total pore volume through MIP analysis. Fig. 3-18 presents the intruded amount of mercury with respect to pore size diameter for the three composites. The pore size distributions of the three composites were similar in that most pores were smaller than about 0.1  $\mu\text{m}$  and bigger than about 100  $\mu\text{m}$ .

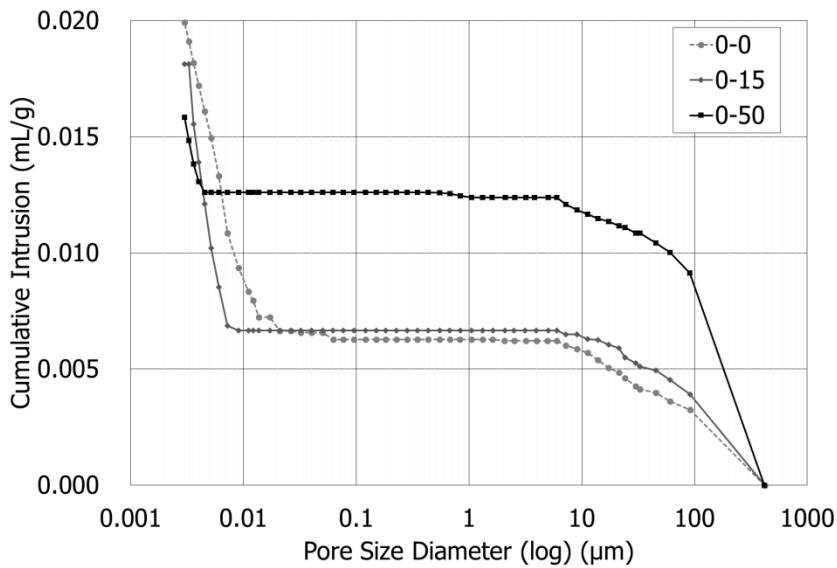
All three composites exhibited very small total volumes of mercury intrusion below 0.02 mL/g, and the measured total porosities of Mixtures 0-0, 0-15, and 0-50 were 3.8, 4.0, and 3.4%, respectively. Very low porosities can be erroneously measured for the solids that contain many disconnected pores, as mercury cannot easily intrude into interior pores in such solids [53]. However, the BSE images of Mixture 0-50 in Fig. 3-15 clearly show that pores were mostly interconnected one another. Therefore, the very low porosities acquired in this study were likely to be the actual pore characteristics of sulfur composites [54].

The MIP results indicate that the use of fly ash generally reduced the total porosity of sulfur composites. As the ratio of fly ash increased, the volume of small pores ( $<$  about 0.1  $\mu\text{m}$ ) decreased, while the volume of big pores ( $>$  about 100  $\mu\text{m}$ ) increased. For instance, the volume of small pores was the least in Mixture 0-50, but the volume of big pores was the greatest. As the total pore volume decreased with increasing the amount of fly ash, the compressive strength increased. This is in accordance with the general solid-porosity relationship [53]. More importantly, it was likely that the strength increase by the use of fly ash originated from the reduction of small pores, and the presence of

big pores appeared not to affect the compressive strength of the sulfur composites [53,55,56].



(a)



(b)

**Figure 3-18: Pore size distributions of three sulfur composites with no rubber powder (Mixtures 0-0, 0-15, 0-50): (a) log differential intrusion; (b) cumulative intrusion (units: mL/g).**

### 3.4. Conclusions

In this study, 24 mixtures of sulfur composites and three mixtures of sulfur mortars were tested to investigate the effects of rubber powder and fly ash on the strength and microstructure of sulfur composites. Overall, the use of rubber powder and fly ash proved to be an effective method for replacing

mineral aggregate and enhancing the mechanical properties of sulfur composites. The findings and conclusions of this study are summarized as follows:

- ✓ Most mixtures with rubber powder and/or fly ash exhibited higher strengths than did hardened modified sulfur itself. The observed layered microstructure of hardened modified sulfur indicated the presence of detrimental thermal stress being produced during the curing process throughout the matrix.
- ✓ As the ratio of fly ash increased, the compressive strength of sulfur composites generally increased, regardless of the amount of rubber powder. The highest strength was achieved when 50% of modified sulfur was replaced by fly ash and no rubber powder was used.
- ✓ The optimal ratio of rubber powder for the compressive strength was highly dependent on the ratio of fly ash. At low ratios of fly ash, 5–10% of rubber powder enhanced the strength of sulfur composites, while at 45% or more fly ash, a smaller ratio of rubber powder constantly resulted in a higher strength.
- ✓ Sulfur mortars with 5–10% sand showed lower compressive strengths than did sulfur composites with the same ratios of rubber powder, suggesting that rubber powder may effectively replace a portion of fine aggregate in sulfur composites without sacrificing the strength.
- ✓ The density of sulfur composites decreased much below  $1,900 \text{ kg/m}^3$  as the rubber powder ratio increased, because of the lower specific gravity of rubber.
- ✓ As fly ash was used at a higher ratio (e.g., 45%), the microstructure of sulfur matrix was entirely changed, and this morphological evolution likely provided a substantial benefit on the strength development of sulfur composites.
- ✓ The sulfur composites had very low total porosities, and the use of fly ash generally reduced the total porosity of sulfur composites. It was likely that the strength increase of sulfur composites by the use of fly ash originated from the reduction of small pores.

## **4. Strength and Microstructural Characteristics of Sulfur Polymer Composites Containing Binary Cement and Waste Rubber**

### 4.1. Introduction

A considerable amount of elemental sulfur has been generated from petroleum or gas refineries around the world, and more refineries are being equipped with desulfurization facilities to meet environmental regulations [2]. The global generation of elemental sulfur is currently 10-20% larger than the total demand worldwide, which is approximately 57 million tons per year, and it is expected to increase constantly [1]. Therefore, without proper plans for utilizing surplus sulfur, its disposal cost is supposed to rise exponentially. So far, most of the surplus sulfur has been deposited in storage spaces at the petroleum refineries.

Regarding the aforesaid environmental and economic concerns, a number of studies were conducted to utilize surplus sulfur as a sustainable material in the construction field. At the initial stages of the studies, most researchers focused on the modification of elemental sulfur by using chemical modifiers such as dicyclopentadiene (DCPD) [3,16,43], because elemental sulfur is much more vulnerable to brittle failure and freezing and thawing compared with Portland cement. Attributed to the thermoplastic characteristics of modified sulfur polymers, they may be used as an alternative binder for concrete construction, which can exclude water in the production of sulfur composites or concretes [3,16,43,57].

Some recent studies aimed at developing the mix proportions of even more sustainable sulfur polymer composites by employing various industrial wastes [41,57,58]. In particular, our research group examined the effects of rubber powder (from waste tires) and fly ash on the macro- and microstructural properties of sulfur composites [58]. One of the main findings of the foregoing studies was that fly ash significantly enhanced both the strength and durability (e.g., resistance to chemicals, freezing and thawing) of sulfur composites. In our previous study [58], the use of fly ash more than about 40% by volume produced a unique honeycomb-shaped microstructure that was deemed to cause a superior compressive strength with a reduced total porosity. In addition, the rubber powder played an effective role as a sustainable replacement of fine aggregate without causing an excessive strength reduction, and reduced the unit weight of sulfur composites.

This study especially explores the effects of binary cement (blend of Portland cement and fly ash) and rubber powder on the strength and microstructural characteristics of modified sulfur polymer composites. Binary or ternary blended cement systems are often employed in concrete construction [50,59,60], which typically include supplementary cementitious materials such as fly ash and furnace slag. In this study, the binary cement was employed as a micro-filler to enhance the compressive

strength of sulfur composites as well as a potential crack-healing agent. Because the particle size distributions of Portland cement and fly ash are different from each other, their combination, compared with the use of fly ash only in our companion study [58], was likely to refine the microstructure of the sulfur composites. With regard to the potential of crack healing, if the binary cement grains remain unreacted and are evenly embedded in the sulfur composites, water intrusion through future cracks may stimulate hydration and/or pozzolanic reactions of Portland cement and fly ash so as to heal the cracks. To characterize the properties of modified sulfur polymer composites due to the binary cement and rubber powder, a series of macro- and micro-structural analyses were conducted based on the results of compressive strength, X-ray diffraction (XRD), scanning electron microscopy (SEM) with elemental energy dispersive spectroscopy (EDS), and Fourier transform infrared (FT-IR) spectroscopy.

## 4.2. Experimental Program

### 4.2.1. Materials

In this study, several industrial wastes were employed as primary components to produce sustainable sulfur polymer composites. The used industrial wastes were sulfur, fly ash, and waste rubber. The binder for the sulfur polymer composites was a dicyclopentadiene (DCPD)-modified sulfur produced by Micro Powder, Inc. in Ulsan, Korea. The loading percentage of DCPD was 5% by weight. Waste rubber powder with a maximum particle size of 500  $\mu\text{m}$  and specific gravity of 1.12 was used, which was recycled from scrap tires by One Powder, Inc. in Yeongwol, Korea. Binary cement, a blend of fly ash (about 68 wt.% (75 vol.%)) and Portland cement (about 32 wt.% (25 vol.%)), was used as a filler in this study (Fig. 4-1(b)), which is the major difference from the previous study [58]. Portland cement was incorporated to potentially achieve the self-healing of potential cracks in the modified sulfur composites. The fly ash in the binary cement belongs to Class F according to ASTM C 618 [44].

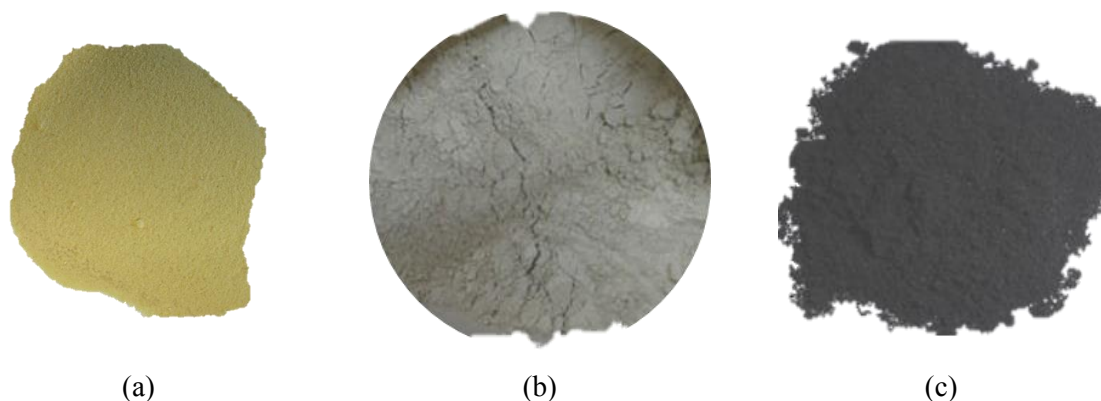


**Figure 4-1: Raw materials: (a) modified sulfur polymer, (b) binary cement (a blend of fly ash and**



**Portland cement), and (c) rubber powder.**

Individual raw materials were characterized using a series of analysis techniques: laser diffraction particle size analysis, elemental analysis (EA), X-ray diffraction (XRD), X-ray fluorescence (XRF), and thermogravimetric analysis (TGA). The raw material analysis results are presented in Section 4.3.1.

4.2.2. Mix proportions

A total of 24 mixtures containing different portions of modified sulfur, binary cement, and rubber powder were investigated as shown in Table 4-1. Major test variables were the volumetric ratios of modified sulfur, binary cement, and rubber powder. The ratios of binary cement and rubber powder in the mix proportions ranged in 0~50% and 0~15%, respectively; the ratios of fly ash and Portland cement ranged in 0~37.5% and 0~12.5%, respectively. In the mixture labels, the first and second figures stand for the volumetric ratios of binary cement and rubber powder, respectively.

**Table 4-1: Mix proportions of the tested sulfur polymer composites.**

Mixture label	Modified sulfur (5% DCPD)		Binary cement				Rubber powder	
			Portland cement		Fly ash			
	Vol.%	kg/m <sup>3</sup>	Vol.%	kg/m <sup>3</sup>	Vol.%	kg/m <sup>3</sup>	Vol.%	kg/m <sup>3</sup>
C0-0	100	1910	-	-	-	-	-	-
C0-10	90	1719	2.5	78	7.5	167	-	-
C0-15	85	1624	3.8	117	11.2	250	-	-
C0-40	60	1146	10.0	314	30.0	666	-	-
C0-45	55	1051	11.3	352	33.7	749	-	-
C0-50	50	955	12.5	392	37.5	833	-	-
C5-0	95	1815	-	-	-	-	-	-
C5-10	85	1624	2.5	78	7.5	167	-	-
C5-15	80	1528	3.8	117	11.2	250	-	-
C5-40	55	1051	10.0	314	30.0	666	5	56
C5-45	50	955	11.3	352	33.7	749	-	-
C5-50	45	860	12.5	392	37.5	833	-	-
C10-0	90	1719	-	-	-	-	-	-
C10-10	80	1528	2.5	78	7.5	167	10	112
C10-15	75	1433	3.8	117	11.2	250	-	-
C10-40	50	955	10.0	314	30.0	666	-	-

C10-45	45	860	11.3	352	33.7	749		
C10-50	40	764	12.5	392	37.5	833		
C15-0	85	1624	-	-	-	-		
C15-10	75	1433	2.5	78	7.5	167		
C15-15	70	1337	3.8	117	11.2	250		
C15-40	45	860	10.0	314	30.0	666	15	168
C15-45	40	764	11.3	352	33.7	749		
C15-50	35	669	12.5	392	37.5	833		

#### 4.2.3. Production of specimens

Rubber powder is mostly recycled from scrap tires that are produced from vulcanized rubber composed of cross-linked polymers [46]. Modified sulfur polymer is known to infiltrate well into rubber particles at about 140°C [47,48]. Although the rubber powder itself was likely vulcanized during its production, the mixing in this study was performed at a temperature about 140°C to promote further possible vulcanization that might instigate a stronger bond between the modified sulfur polymer and rubber powder.

In the specimen production procedures, firstly modified sulfur and rubber powder were stirred together in a mixing bowl wrapped by a heating jacket. After the complete liquefaction of the heated modified sulfur, binary cement preheated in an oven at 180°C for 6 hours was poured into the mixing bowl [45]. Then, the mixing was continued for approximately 15 min. Finally, the plastic sulfur composites were cast into molds, and the molds were compacted on a shaking table. It should be noted that no water was used in the mixing process.

All specimens were cured at a room temperature (20–25°C) with a relative humidity of 60±5%. The hardened specimens were demolded after 6 hours of curing and kept under the same curing condition. It is deemed that there is little influence of relative humidity on the curing of sulfur polymer composites because the specimen construction does not involve the use of water [41].

#### 4.2.4. Test methods

For compression tests, three cubic specimens with sides 50 mm long were prepared for each mixture in Table 4-1. Considering the rapid strength development characteristics of modified sulfur polymer [3], the compression tests were performed after three days of curing following the test methods in Section 2.3.1.

The XRD patterns of raw materials and hardened samples were determined by a high-power X-ray diffractometer (Rigaku, Japan) as suggested in Section 2.3.2. The XRD measurements were

conducted on powdered samples prepared using a hand pestle after three days of curing. The oxide compositions of raw materials were assessed using a XRF (Bruker S8 Tiger, USA).

The morphologies of raw materials and hardened samples were observed using an ultra-high resolution field emission SEM (Hitachi S-4800, Japan) equipped with EDS. Bulk-sectioned samples were prepared for most mixtures of this study, and thin-sectioned samples (30 μm thick) were prepared for two cases only (Mixtures C0-0 and C15-0). The exact preparation and test conditions conform to Section 2.3.4. Both types of samples were set up for backscattered electron (BSE) images.

In order to identify the chemical bonding between the modified sulfur and rubber powder, a Fourier transform infrared (FT-IR) spectrometer (Varian 670-IR, USA) coupled with a microscope (Varian 620-IR, USA) was used to measure the IR absorbance or reflectance spectrum as explained in Section 2.3.5. FT-IR measurements were conducted on each of the modified sulfur and rubber in powder, and on hardened samples 3 mm thick made of both the modified sulfur and rubber powder.

The weight percentage of carbon, hydrogen, sulfur and oxygen in the modified sulfur and rubber powder were determined using an EA (Flash 2000, USA). The particle size distributions of the binary cement and rubber powder were determined using a laser diffraction particle size analyzer (Sympatec HELOS, Germany).

### 4.3. Results and Discussions

#### 4.3.1. Characterization of raw materials

The elemental compositions of the modified sulfur polymer and rubber powder acquired from the EA analysis are given in the companion paper [58]. The chemical oxide compositions of the raw binary cement and modified sulfur polymer obtained from the XRF analysis are presented in Table 4-2. The binary cement contains a large portion (about 25.8%) of calcium oxide from Portland cement, whereas calcium oxide typically accounts for less than 10% of Class F fly ash [44]. The EA results [58] show that 98.3% of the modified sulfur polymer consists of elemental sulfur, which is consistent with the XRF results (Table 4-2). According to the EA results [58], about 77.5% of the rubber powder is composed of carbon, and the rest portion comprises hydrogen, nitrogen, and sulfur with impurities.

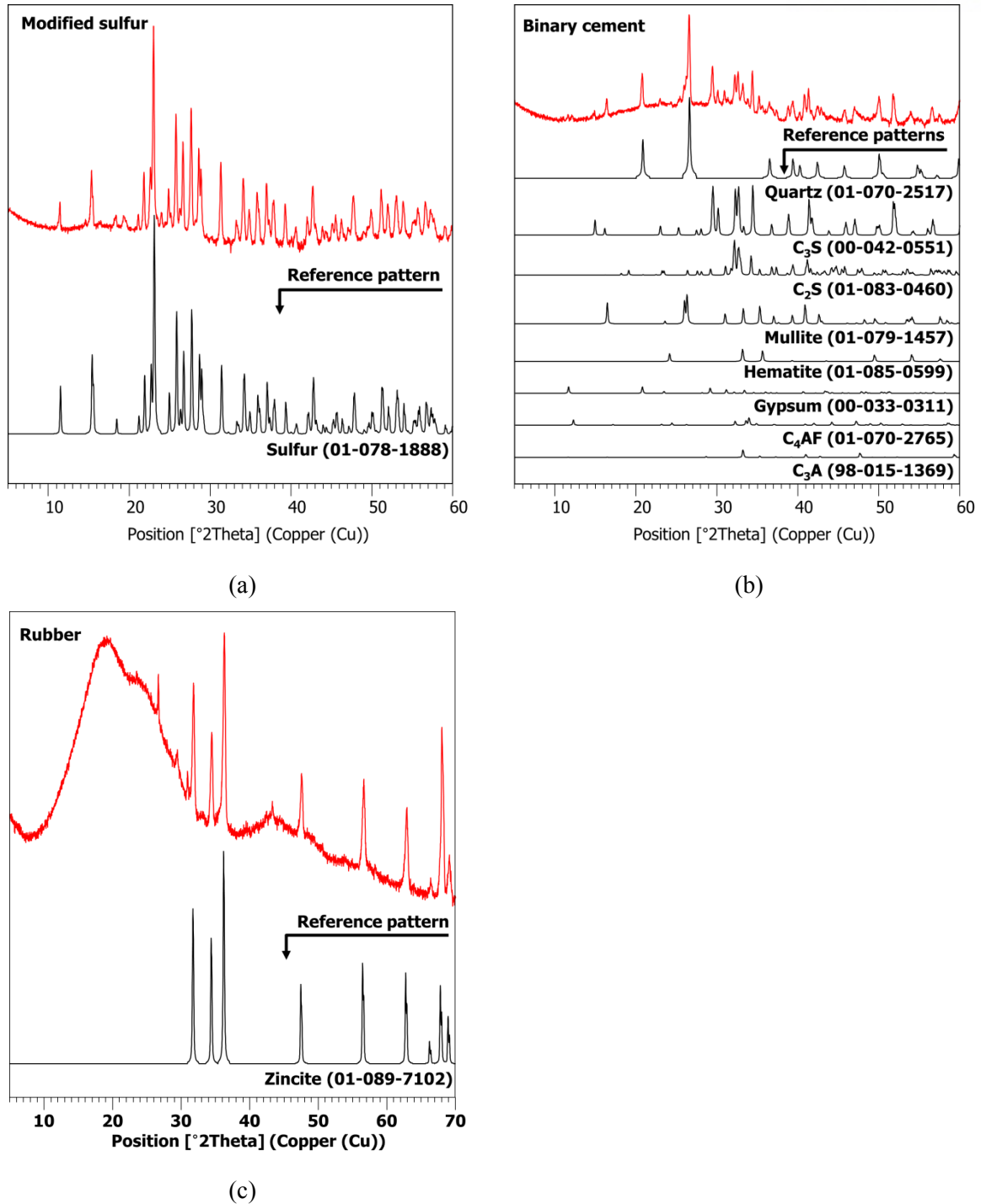
**Table 4-2: Chemical oxide compositions of binary cement and modified sulfur polymer from XRF.**

Oxide (wt.%)	Raw materials	
	Binary cement	Modified sulfur
SiO <sub>2</sub>	45.5	-
CaO	25.8	-

Al <sub>2</sub> O <sub>3</sub>	16.2	-
Fe <sub>2</sub> O <sub>3</sub>	4.8	-
MgO	2.3	-
SO <sub>3</sub>	2.0	99.8
K <sub>2</sub> O	1.2	-
TiO <sub>2</sub>	1.0	-
Na <sub>2</sub> O	0.7	-
Others	0.5	0.2

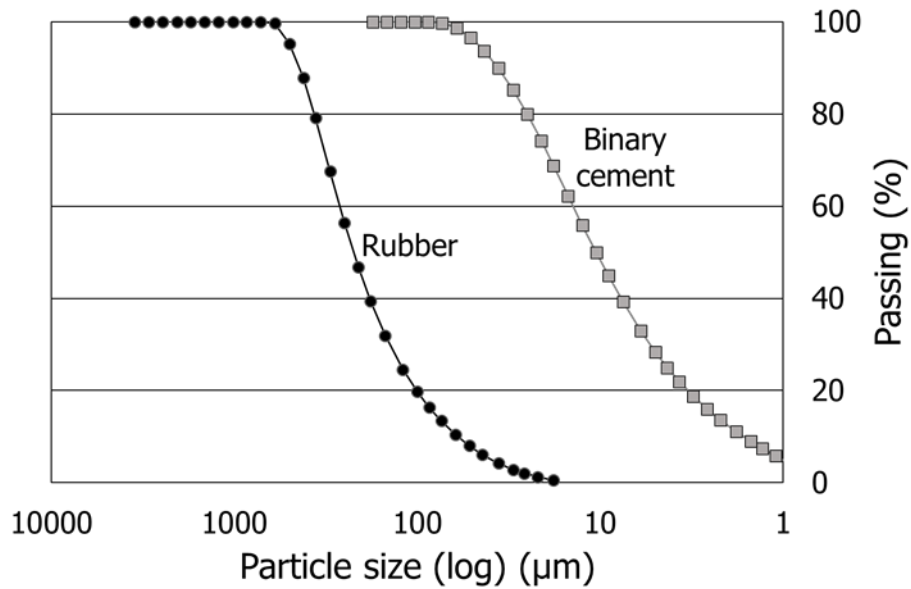
The measured XRD patterns of the raw materials (modified sulfur polymer, binary cement, and rubber powder) are shown in Fig. 4-2. The XRD pattern of the raw modified sulfur reveals that it consists of elemental sulfur with the orthorhombic structure [3] (ICDD PDF no. 01-078-1888). Currell et al. [24] reported that the polymerization of elemental sulfur using DCPD at a reaction temperature of 140°C produced a mixture of poly-sulfides and free elemental sulfur that consisted of monoclinic, orthorhombic sulfur crystals, and non-crystalline sulfur. Free elemental sulfur is unreacted sulfur containing amorphous S<sub>8</sub> reflected by an amorphous hump at about 10–30° in the XRD pattern.

The XRD results in Fig. 4-2(b) illustrate that the binary cement contains minerals from fly ash such as quartz (SiO<sub>2</sub>, ICDD PDF no. 01-070-2517), mullite (Al<sub>6</sub>Si<sub>2</sub>O<sub>13</sub>, ICDD PDF no. 01-079-1457), and hematite (Fe<sub>2</sub>O<sub>3</sub>, ICDD PDF no. 01-085-0599), and from Portland cement such as C<sub>3</sub>S (Ca<sub>3</sub>SiO<sub>5</sub>, ICDD PDF no. 00-042-0551), C<sub>2</sub>S (Ca<sub>2</sub>SiO<sub>4</sub>, ICDD PDF no. 01-083-0460), gypsum (CaSO<sub>4</sub>, ICDD PDF no. 00-033-0311), C<sub>4</sub>AF (Ca<sub>4</sub>Al<sub>2</sub>Fe<sub>2</sub>O<sub>10</sub>, ICDD PDF no. 01-070-2765), and C<sub>3</sub>A (Ca<sub>3</sub>Al<sub>2</sub>O<sub>6</sub>, ICDD PDF no. 98-015-1369). The XRD pattern of the rubber powder (Fig. 4-2(c)) indicates the dominant presence of an amorphous carbon phase [46], manifested by a large hump from about 10 to 30°, and reflects zincite (ZnO, ICDD PDF no. 01-089-7102) of a crystalline phase, which was incorporated during the manufacturing process.



**Figure 4-2: XRD patterns of raw materials: (a) modified sulfur polymer, (b) binary cement, and (c) rubber powder.**

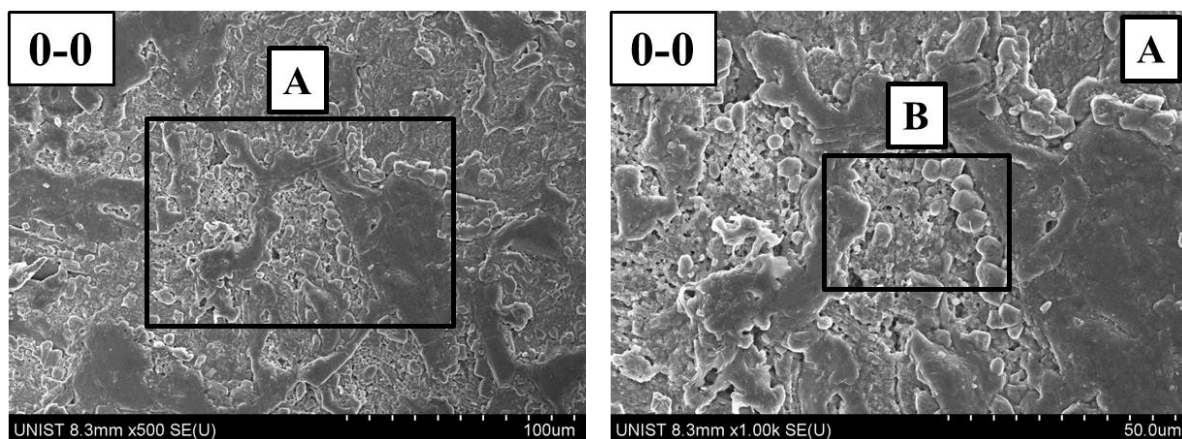
Fig. 4-3 presents the particle size distributions of the binary cement, and rubber powder. The maximum particle size of the binary cement is about 90  $\mu\text{m}$ , which is smaller than the majority of the rubber powder. It is notable that the average particle size of the binary cement is smaller than that of the fly ash only.



**Figure 4-3: Particle size distributions of binary cement, and rubber powder.**

Fig. 4-4 displays secondary electron (SE) images by SEM for the unpolished saw-cut surfaces of hardened modified sulfur polymer containing no other mix components (Mixture C0-0). The SE images in high magnifications expose an irregular morphology with unevenly distributed porous and dense matrix regions. More details on the microstructure of hardened modified sulfur polymer will be discussed using BSE images in Section 4.3.4.

The thermogravimetric response of the rubber powder acquired from the TGA analysis is presented in the companion paper [58]. The rubber powder is decomposed at about 219.6°C, which is much higher than the mixing temperature (around 140°C) for the sulfur polymer composites in this study. Thus, the rubber powder is assumed to undergo no weight loss in the mixing process.



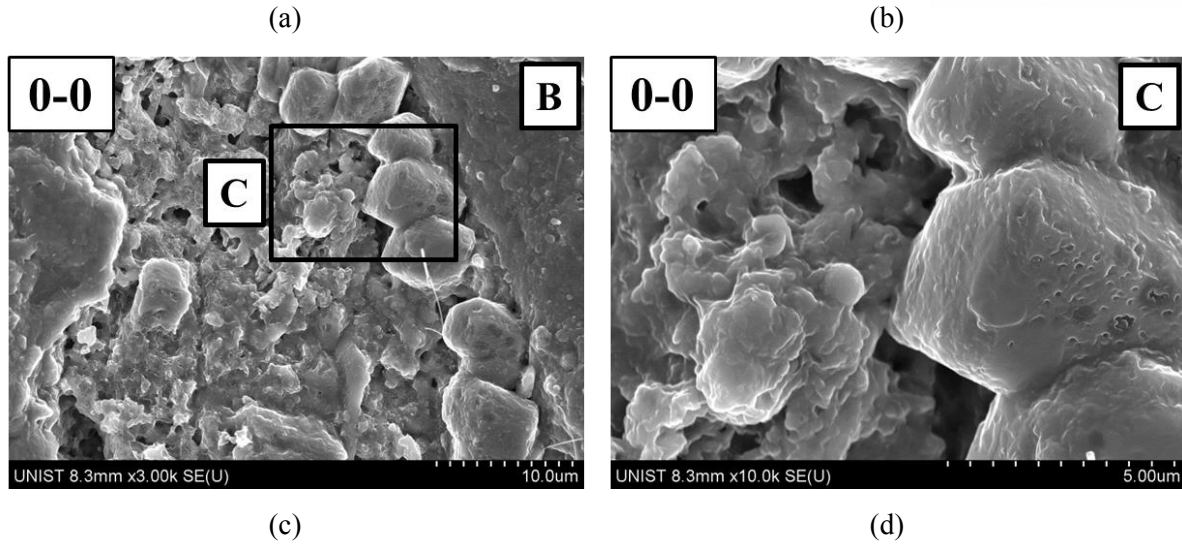


**Figure 4-4: SE images for saw-cut surfaces of hardened modified sulfur polymer (Mixture C0-0): (a) 500X, (b) magnified image (1,000X) of A in (a), (c) magnified image (3,000X) of B in (b), (d) magnified image (10,000X) of C in (c).**

#### 4.3.2. Compressive strength

Fig. 4-5 compares the compressive strengths of all twenty-four sulfur polymer composites in Table 4-1. The compressive strength of hardened modified sulfur itself (Mixture C0-0) containing no other mix components was approximately 26.6 MPa on average. Regardless of the test variables, all the mixtures showed a compressive strength larger than 20 MPa. This is similar to the previous test results for sulfur composites with fly ash instead of binary cement [58].

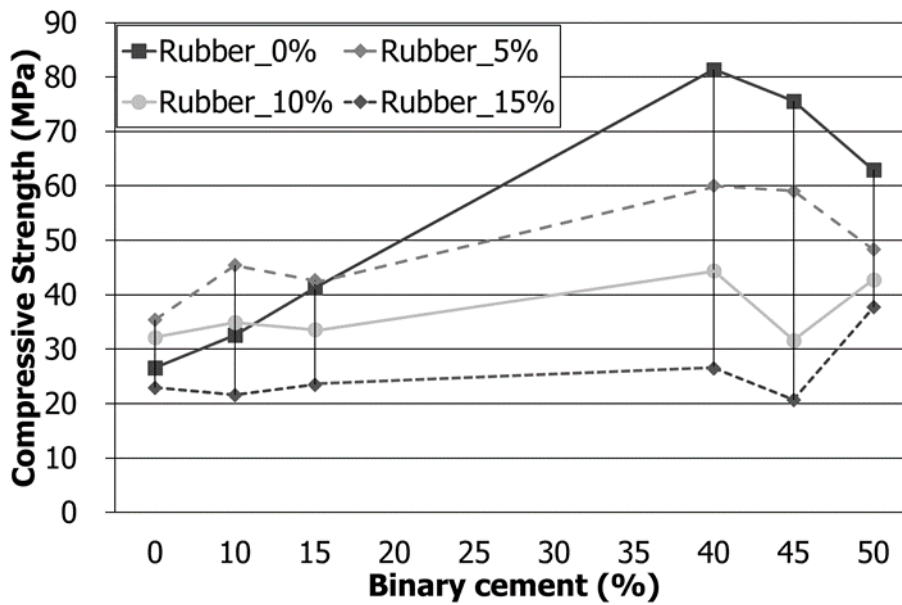


**Figure 4-5: Compressive strengths of the tested sulfur polymer composites.**

The compressive strength of the sulfur polymer composites generally increased as the binary cement ratio increased up to 40% (Fig. 4-5). The mixtures with no rubber powder showed the fastest growth of compressive strength from the increase of the binary cement ratio. Furthermore, for the cases with no or 5% rubber powder, the mixtures containing the binary cement (up to 40%) generally exhibited higher strengths than those containing the fly ash only (the same amount of fly ash as binary cement) in the companion study [58]. This was likely because Portland cement typically has a larger modulus of indentation than fly ash [61], which is approximately  $111.0 \pm 13.0$  GPa and  $66.1 \pm 14.2$  GPa for Portland cement and fly ash, respectively. In addition, the higher strength development of the mixtures with the binary cement was possibly attributed to the smaller average particle size of the binary cement compared with the fly ash only; Urabe et al. [62] noted that the use of a smaller size of fillers induced a higher strength of composite resins.

On the other hand, the beneficial effect of the binary cement on the compressive strength decreased as the rubber powder ratio increased (Fig. 4-5). The strength ratio between the mixtures with 40% and 0% binary cement was 3.06, 1.69, 1.38, or 1.16 for the series with the rubber content equal to 0, 5, 10, or 15%, respectively. The mixtures with 15% rubber powder scarcely exhibited the effect of increasing the binary cement ratio, which was similar with fly ash instead of binary cement in the companion paper [58].

The increase of the rubber powder ratio generally caused a reduction in the compressive strength of the sulfur polymer composites (Fig. 4-5). However, in the cases with 15% or less binary cement, the rubber powder ratio of up to 10% enhanced the compressive strength compared with Mixture C0-0. The low strength of Mixture C0-0 was likely attributed to severe volumetric shrinkage during the curing process [3], as discussed in the companion paper [58]. Although the length changes of the samples in curing were not measured by instruments, it was distinctly observed that the addition of the binary cement and rubber powder led to a less contraction of the sulfur composites.

The inclusion of more than 40% binary cement generally led to a decrease of the strength of the sulfur composites, although the mixtures with 10 and 15% rubber powder showed no clear trend from 40 to 50% binary cement ratio. Overall, 40% binary cement ratio induced the highest strength among the sulfur composites with an identical rubber content. Mixture C0-40 achieved the highest compressive strength equal to 81.4 MPa. It appears that the optimal binary cement ratio with respect to the compressive strength is approximately 40% by volume. In contrast, the strength of the sulfur composites constantly increased as the fly ash ratio increased up to 50% at each rubber content in the companion study [58]; the mixture with 50% fly ash presented the highest compressive strength of 83.0 MPa, which employed fly ash only instead of binary cement [58].



#### 4.3.3. Crystalline phase transition (XRD)

The purpose of the XRD analyses was to determine the effects of the binary cement and rubber powder on the formation of crystalline phases in hardened sulfur polymer composites. In Fig. 4-6(a), the XRD pattern of Mixture C15-0 is very similar to that of the raw modified sulfur only (Fig. 4-2(a)) despite the presence of 15% rubber powder. The amorphous carbon hump and footprints of zincite observed for the rubber powder itself (Fig. 4-2(c)) are only slightly seen in Mixture C15-0; the peak intensities of the modified sulfur polymer are dominant.

Fig. 4-6(b) presents the XRD patterns of the mixtures with 40% binary cement: C5-40, C10-40, and C15-40. All the three mixtures just reflected the mineral phases of the raw modified sulfur and raw (unhydrated) binary cement. The XRD pattern of Mixture C15-40 displays the peaks representing the mineral phases from the binary cement cumulative to those from Mixture 15-0. These results indicate that there were no chemical reactions between the constituent materials (i.e., modified sulfur polymer, binary cement, and rubber powder) in the curing process. Therefore, it is deemed that the unreacted Portland cement and fly ash will be available to undertake hydration and pozzolanic reactions for the sake of crack healing, if exposed to an environment of cracking damage followed by water intrusion. In addition, the mixtures with 40% binary cement but different rubber contents exhibited no apparent effects of rubber powder on the formation of minerals in the sulfur composites (Fig. 4-6(b)).

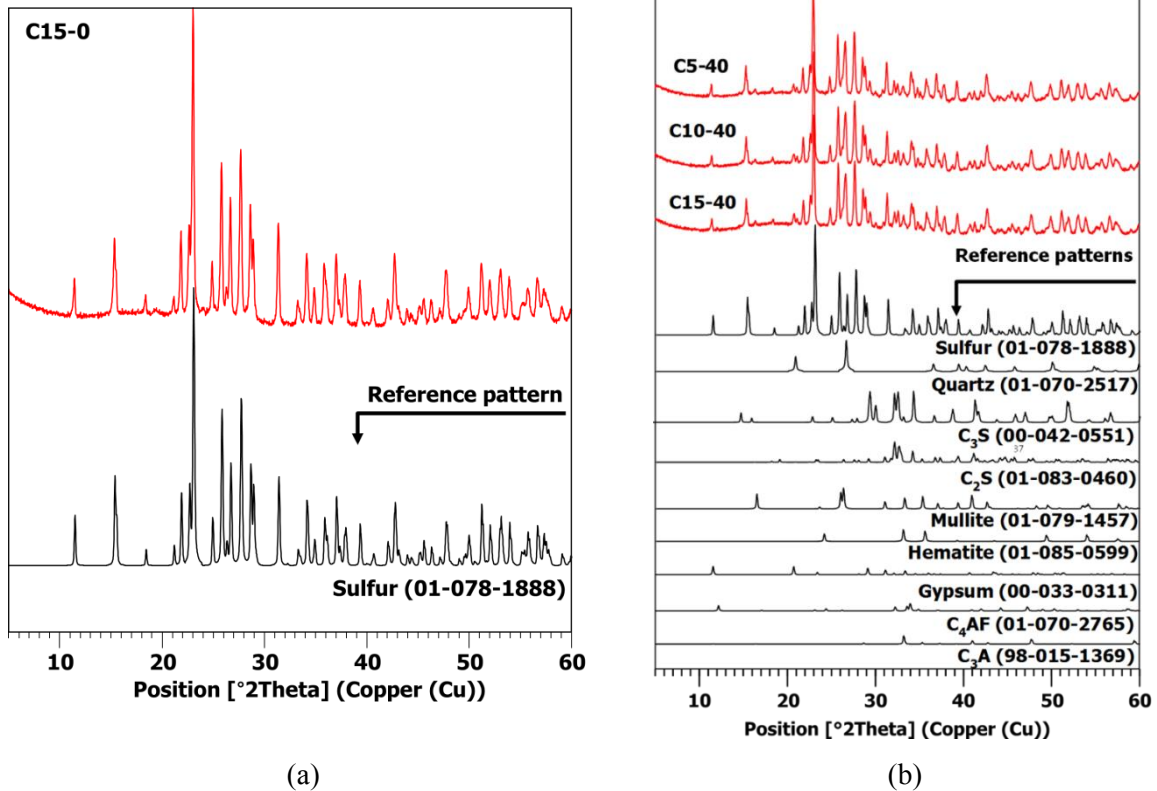
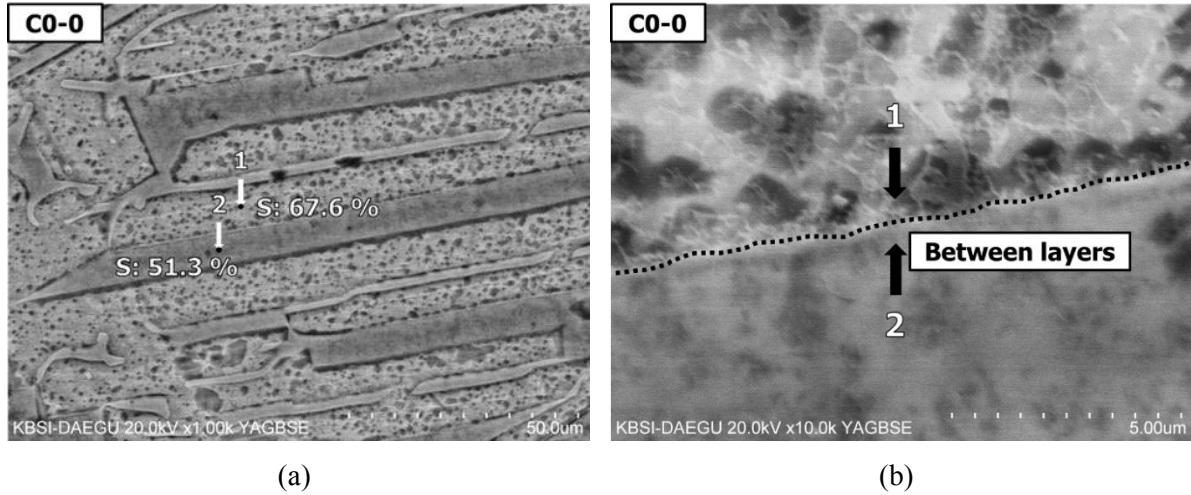


Figure 4-6: Integrated XRD patterns of Mixtures: (a) C15-0, and (b) C5-40, C10-40, and C15-40.

#### 4.3.4. Morphological transition (SEM BSE/EDS)

The BSE images of Mixture C0-0 made of the modified sulfur polymer only were taken at several different locations with various magnifications (Fig. 4-7). Fig. 4-7(a) shows an irregularly layered structure of the hardened modified sulfur, which was deemed a defective microstructure leading to the poor compressive strength (Fig. 4-5), as discussed in detail in the companion paper [58]. From the EDS analyses, both points 1 and 2 in Fig. 4-7(a) were mostly comprised of sulfur despite their different microstructures.



**Figure 4-7: Microstructures of Mixture C0-0 in BSE images with EDS analyses for thin-sectioned and polished samples: (a) 1000×, (b) 10000×.**

The BSE images of Mixture C15-0 made of the modified sulfur polymer and rubber powder were captured at different locations as shown in Fig. 4-8: two images aiming at the interfacial zones between the hardened modified sulfur and rubber particles. It is noted that a strong intensity of carbon along with sulfur existed especially at the interfacial zones between the modified sulfur and rubber powder (indicated as “Sulfur-rich rubber” in Fig. 4-8), where the brightness gets darker close to the rubber particles. This coupled morphology seems to be the primary reason for the higher compressive strengths of Mixtures C5-0 and C10-0 compared with the hardened modified sulfur itself (Mixture C0-0) as shown in Fig. 4-5; this will be discussed more with reference to their chemical bonds in Section 4.3.5.

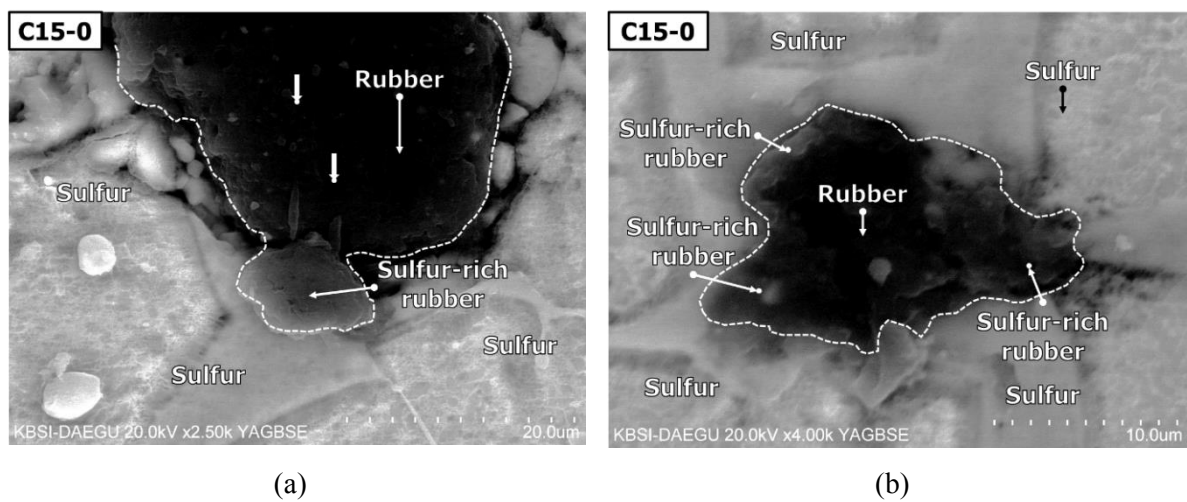


**Figure 4-8: Microstructures of Mixture C15-0 in BSE images with EDS analyses for thin-sectioned and polished samples: (a) 2500×, (b) 4000×.**

The BSE images of Mixtures C0-15, C0-40, and C0-50, containing the binary cement but no rubber powder, were presented in Figs. 4-9, 4-10, and 4-11, respectively. In Figs. 4-9 to 4-13, “G” stands for gypsum, “M” for mullite, “Q” for quartz, “A” for C<sub>3</sub>S (alite), “B” for C<sub>2</sub>S (belite), “F” for C<sub>4</sub>AF, and “H” for hematite. Overall, the mineral crystalline phases of the binary cement remained unreacted in the sulfur composites, which can undertake hydration and/or pozzolanic reactions toward crack healing in case of cracking damage followed by water intrusion (or supply).

In Fig. 4-9, the morphology of Mixture C0-15 exhibited sparsely embedded grains of the binary cement and a considerable amount of pores in the sulfur matrix. In contrast, the microstructure of Mixture C0-40 in Fig. 4-10 contained a much smaller portion of pores and densely embedded grains of the binary cement compared to Mixture C0-15. It appears that the dense embedment of the binary cement caused the enhancement of compressive strength. Similarly in the companion study [58], the volume and size of pores in the sulfur composites were greatly dependent on the portion of the filler; the use of more fly ash constantly led to a decrease of porosity and an increase of strength.

Despite the increase of the binary cement ratio from 40 to 50%, Mixture C0-50 (Fig. 4-11) displayed larger sizes of pores compared with Mixture C0-40. This is likely the main reason for the lower compressive strength of C0-50 compared with C0-40. It is noted that the use of 50% binary cement caused no microstructural change similar to that observed in the companion study [58]; the use of 50% fly ash instead of 50% binary cement caused the formation of a honeycomb-shaped microstructure [58] that was considered to improve the strength.

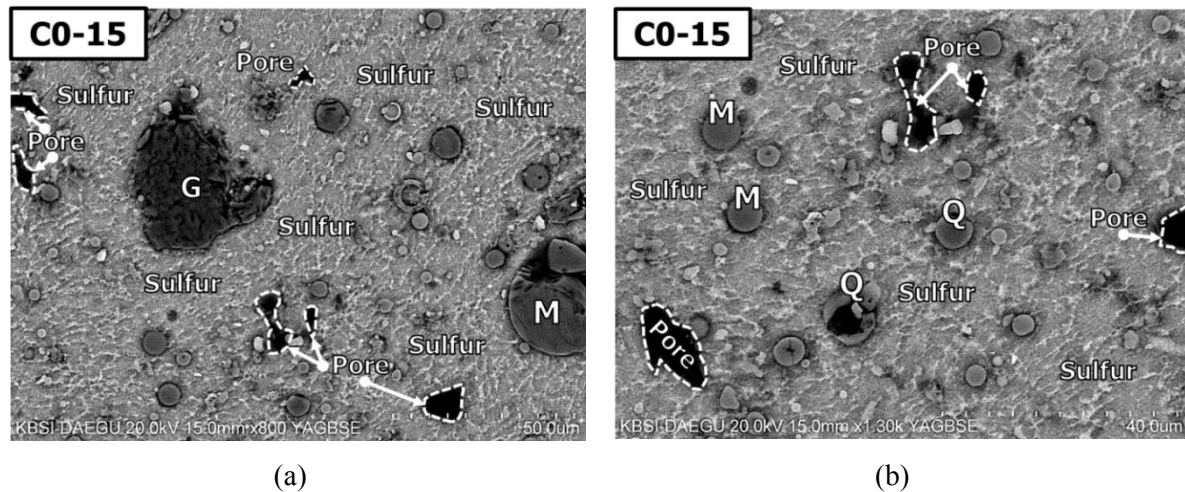


**Figure 4-9: Microstructures of Mixture C0-15 in BSE images with EDS analyses for bulk-sectioned and polished samples: (a) 800×, (b) 1300×.**

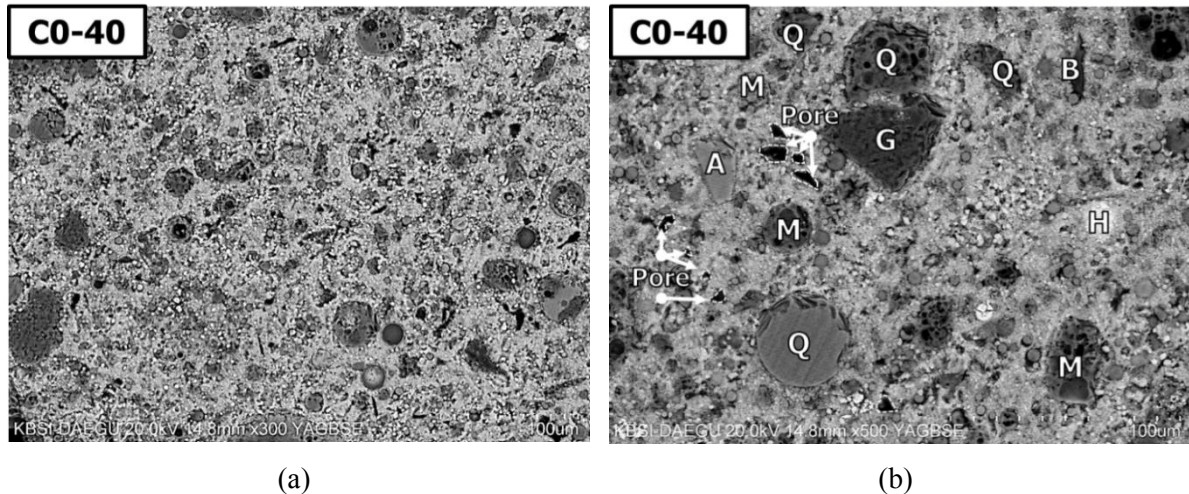


**Figure 4-10: Microstructures of Mixture C0-40 in BSE images with EDS analyses for bulk-sectioned and polished samples: (a) 300 $\times$ , (b) 500 $\times$ .**

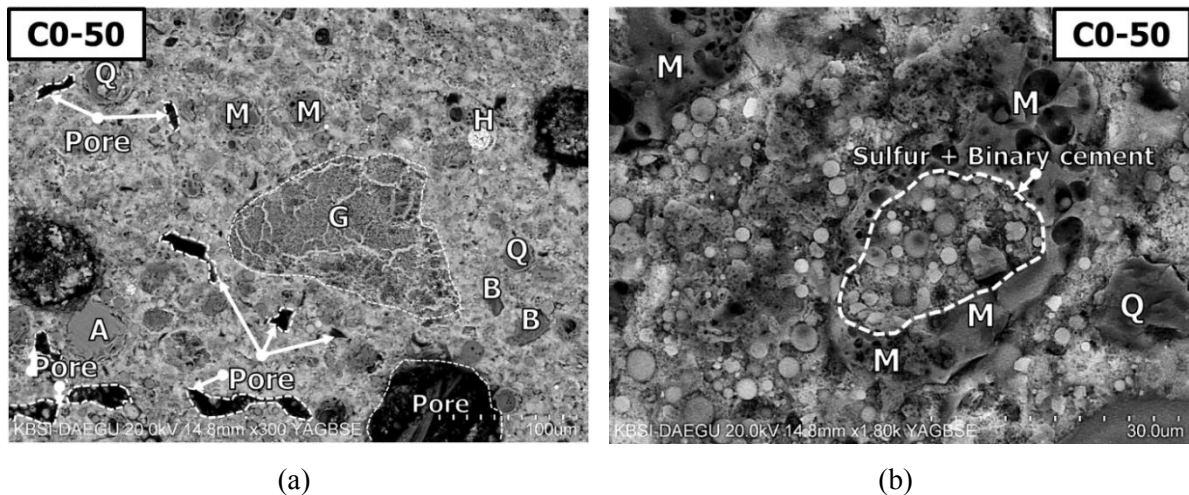


**Figure 4-11: Microstructures of Mixture C0-50 in BSE images with EDS analyses for bulk-sectioned and polished samples: (a) 300 $\times$ , (b) 1800 $\times$ .**

The microstructures of Mixtures C5-15, C5-40, and C5-50 (Figs. 4-12 to 4-14) containing 5% rubber powder were quite similar to those of Mixtures C0-15, C0-40, and C0-50 (Figs. 4-9 to 4-11) containing no rubber powder, respectively, excluding the zones around rubber particles. However, the inclusion of the rubber powder produced varying coupling conditions at the interfacial transition zones (ITZs) between the sulfur-binary cement matrix and rubber particles (marked as “Matrix-rubber ITZ” in Figs. 4-12 to 4-14).

Of the mixtures with 5% rubber powder, Mixture C5-15 (Fig. 4-12) containing 15% binary cement allowed abundant couplings of sulfur and rubber at the ITZs, which implies a close bond between the sulfur and rubber particles. This phenomenon was likely attributed to a higher probability

of contact between the sulfur and rubber powder due to a relatively small portion (i.e., 15%) of binary cement. In particular, such packed couplings of sulfur along the ITZs may partially justify that the compressive strength of C5-15 was a little higher than that of C0-15 (Fig. 4-5). In contrast, the ITZs of Mixture C5-40 (Fig. 4-13(b)) attracted more grains of binary cement compared with C5-15, which deterred couplings between the sulfur and rubber powder at the ITZs. Moreover, Mixture C5-50 (Fig. 4-14(b)), containing 10% more binary cement than Mixture C5-40, exhibited micro openings along the ITZs with much less sulfur bonded to rubber particles. This observation supports the test result that C5-50 showed a smaller compressive strength than C5-40. In addition, it is assumed that the degradation of coupling conditions at the ITZs from the use of more binary cement in 5% rubber series possibly resulted in a smaller increase of strength than in 0% rubber series according to the increase of the binary cement ratio.

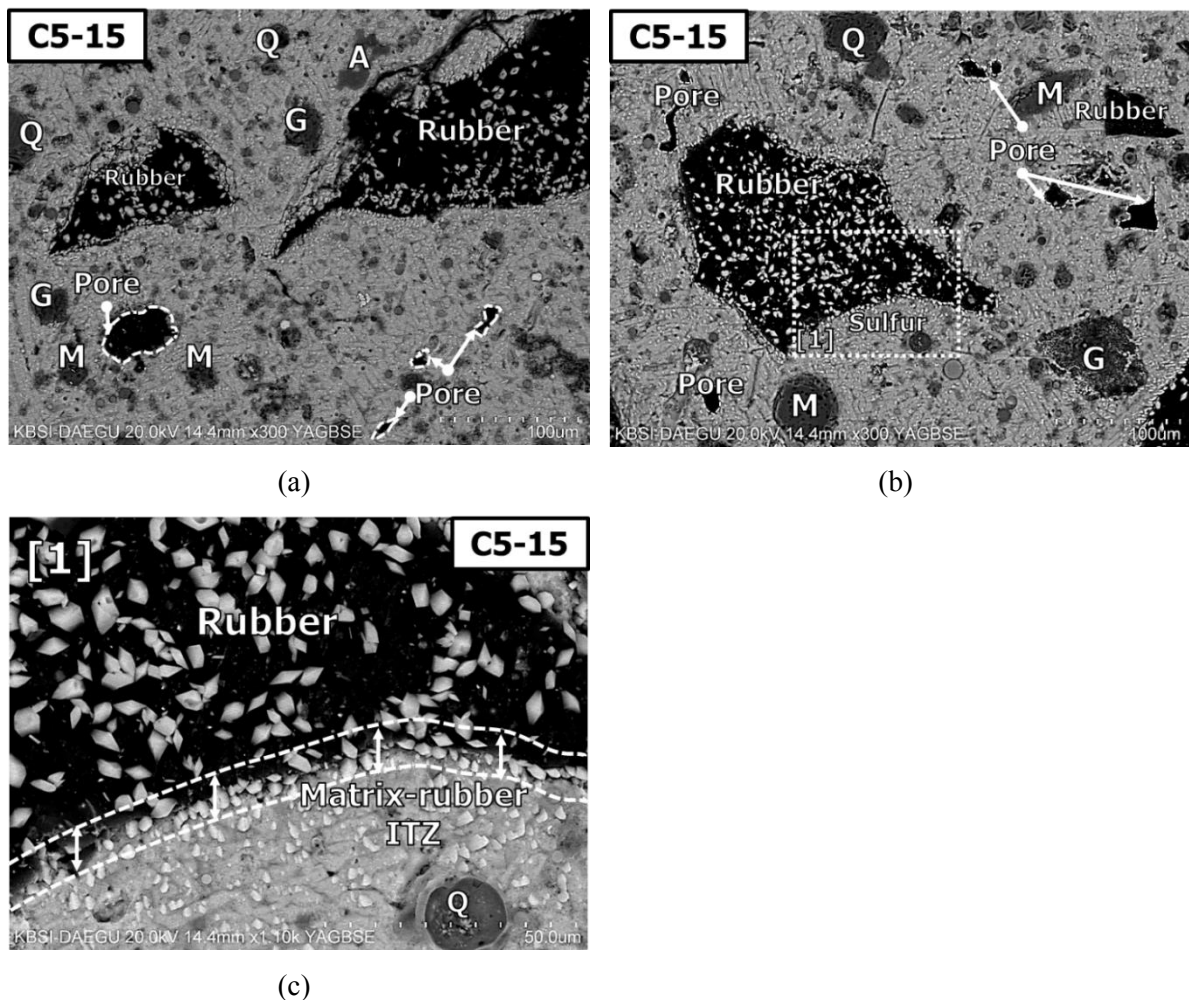


**Figure 4-12: Microstructures of Mixture C5-15 in BSE images with EDS analyses for bulk-sectioned and polished samples: (a) 300×, (b) 300×, (c) 1100× (magnified image of [1] in (a)).**

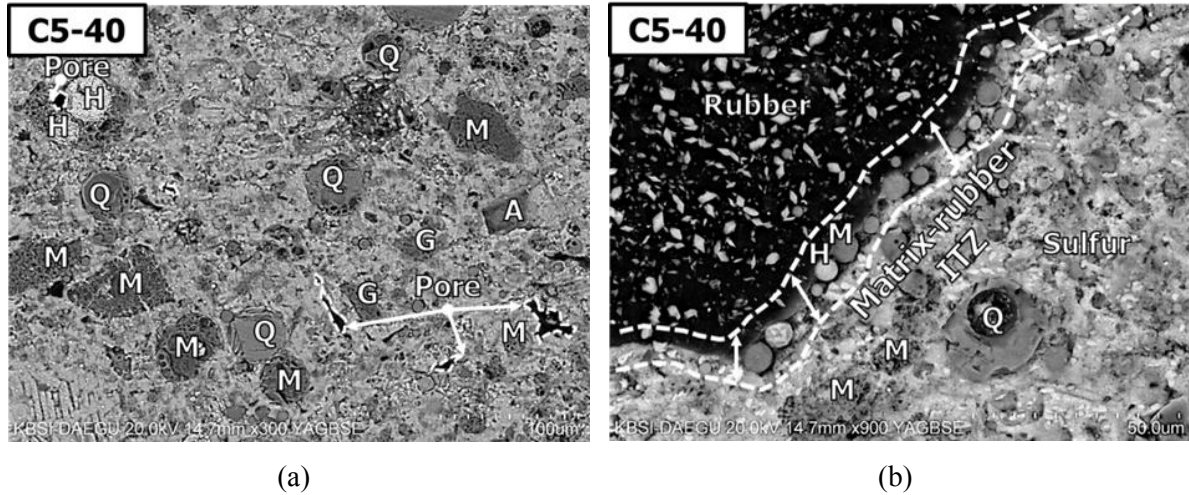


**Figure 4-13: Microstructures of Mixture C5-40 in BSE images with EDS analyses for bulk-sectioned and polished samples: (a) 300×, (b) 900×.**

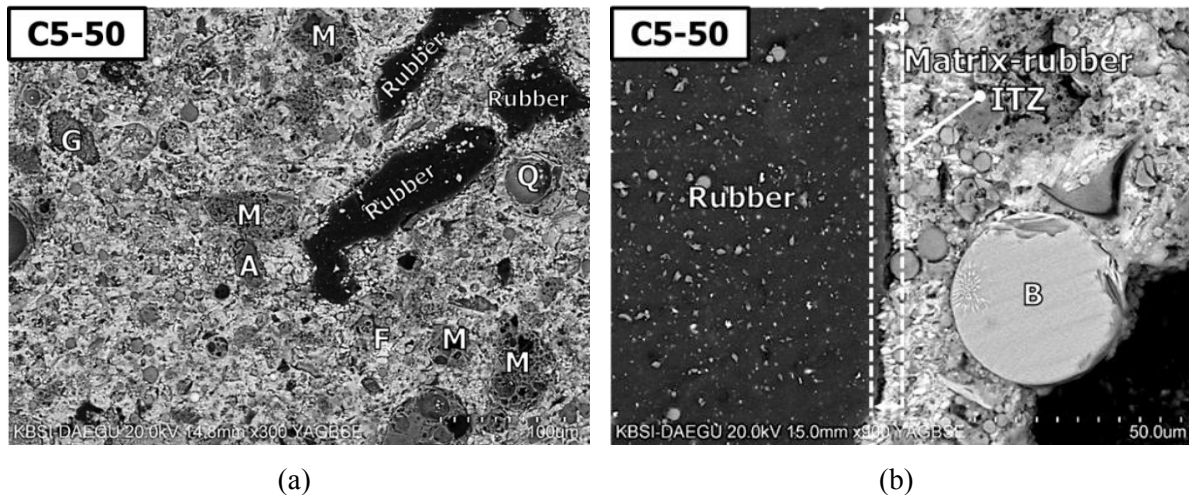


**Figure 4-14: Microstructures of Mixture C5-50 in BSE images with EDS analyses for bulk-sectioned and polished samples: (a) 300×, (b) 900×.**

#### 4.3.5. Chemical bond (FT-IR)

As discussed in the SEM results, the sulfur composites containing rubber powder developed so-called “Sulfur-rich rubber” regions as well as various coupling conditions at the ITZs between the sulfur-binary cement matrix and rubber particles. Further investigation on possible chemical bonds between the modified sulfur and rubber powder were conducted using an FT-IR spectrometer. Fig. 4-15 presents the IR absorbance test results for hardened bulk samples made of the modified sulfur and rubber powder (Mixture C15-0) as well as powder samples of both the hardened modified sulfur (Mixture C0-0) and rubber powder. To interpret the IR absorbance data for Mixture C15-0, a software

(Analyzeit) integrating an infrared spectroscopy database (KnowItAll) was utilized, by which certain wavelength bands in a measured infrared spectrum can be evaluated by functional group analysis. In the IR spectrum of Mixture C15-0, most major peaks were located at such wave numbers (equal to the inverse of wavelength) in which the IR absorbance spectra of sole rubber powder and sole modified sulfur polymer manifested themselves. However, Mixture C15-0 exhibited a distinctive IR peak at the wave number of  $1095.4\text{ cm}^{-1}$ , and this was regarded as the evidence of a double bond between the sulfur (S) and carbon (C); the wave number of their double bond is known to cover approximately  $1200$  to  $1050\text{ cm}^{-1}$  [63]. The database of NIST Chemistry WebBook also specifies that the IR absorbance of the double bond between sulfur and carbon ranges from  $1275$  to  $1030\text{ cm}^{-1}$  [64]. Therefore, it is deemed that the use of rubber powder with a smaller portion of binary cement allowing a higher probability of contact between the sulfur and rubber powder facilitated densely packed couplings at the ITZs between the sulfur-binary cement matrix and rubber particles, which was substantiated by the double bond between the sulfur and carbon.

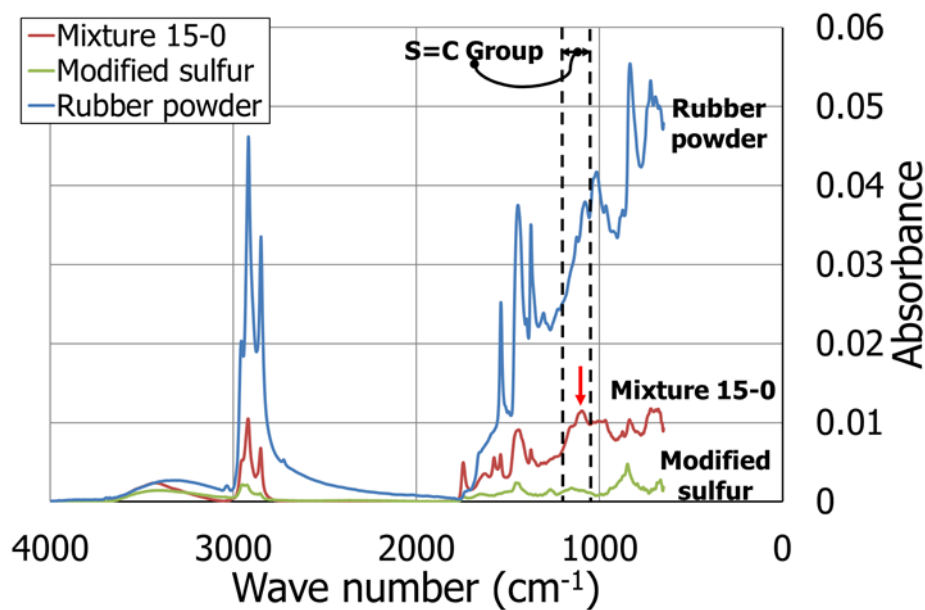


Figure 4-15: FT-IR spectra of Mixture C15-0, modified sulfur polymer, and rubber powder.

#### 4.4. Conclusions

This study primarily examined the effects of binary cement and rubber powder on the strength and microstructural development of modified sulfur polymer composites by conducting various microstructural analyses including SEM, XRD, and FT-IR spectroscopy. All the analysis results attested the favorable effect of the binary cement on the compressive strength of the sulfur composites, and supported its potential role as a crack-healing agent. Findings and conclusions from this study are



summarized in the following:

- ✓ The sulfur composites commonly developed a higher compressive strength with a higher binary cement ratio up to 40%, for a given portion of rubber powder. This complied with the SEM results that the addition of more binary cement led to a smaller portion of pores. This trend of strength development was analogous in the cases with fly ash only instead of binary cement.
- ✓ However, the use of more than 40% binary cement caused a reduction in the compressive strength of sulfur composites. This was reflected in the SEM results that the sample with 50% binary cement displayed larger sizes of pores than the one with 40% binary cement. In contrast, the use of 50% fly ash instead of 50% binary cement led to the formation of a honeycomb-shaped microstructure that was deemed to improve the strength.
- ✓ A higher rubber powder ratio generally resulted in a reduction in the strength of sulfur composites. With less than 15% binary cement, however, the use of rubber powder up to 10% produced higher compressive strengths than that of the hardened modified sulfur itself. This was supported by the development of the double bond between carbon and sulfur, shown in the FT-IR results.
- ✓ As the portion of rubber powder increased, the beneficial effect of binary cement on the compressive strength of sulfur composites generally decreased. This was evidenced by inferior coupling conditions at the ITZs between the sulfur-binary cement matrix and rubber particles with a combination of higher binary cement and rubber powder ratios.
- ✓ The sulfur composites made of binary cement generally had higher compressive strengths than those made of the same amount of fly ash only, especially in the cases with no or 5% rubber powder. This is deemed attributable to the larger modulus of indentation as well as smaller average particle size of binary cement.
- ✓ No reflections indicating new reaction products and phase transitions were observed in the XRD results of all the sulfur composites. In addition, the binary cement grains were evenly embedded in the sulfur matrix as shown in the SEM results. These imply that the binary cement grains, unreacted and evenly embedded in the sulfur matrix, will develop hydration and/or pozzolanic reactions toward crack healing in case of cracking damage followed by water intrusion.

## 5. Flexural Stress-Strain Responses of Micro Fiber-Reinforced Sulfur Polymer Composites

### 5.1. Introduction

A vast amount of elemental sulfur has been generated mostly from the mining or petroleum refineries around the world [1,3]. While the global demand for elemental sulfur has been stationary at 57 million tons per year on average during last few decades [3], the amount of surplus sulfur is expected to account for 10-20% of the global sulfur demand [1]. Due to new regulations about compulsory desulfurization or controlling sulfur content in gasoline and diesel [2,3], the projected amount of surplus sulfur is challenging for producers in that the disposal cost of sulfur can rise with a more lack of storage area. Meanwhile, the surplus sulfur is likely deemed promising to new applications such as construction field that can utilize economical and functional advantages of the elemental sulfur with reduced unit price. One of the most efficient ways to utilize the elemental sulfur was to fabricate elemental sulfur concretes in the construction [3].

Elemental sulfur concretes reveal unique properties that cannot be acquired by ordinary hydraulic cement concretes, including a rapid development of high ultimate strength, great resistance to saline and strong acid solutions, and low permeability [3,26]. However, the critical drawback of elemental sulfur concrete was that elemental sulfur itself shrank about 6 vol.% during the curing of molten elemental sulfur mixtures to an ambient temperature after casting [3]. This phenomenon usually happens due to the allotropic transition of a needle-like monoclinic ( $\beta$ -phase) sulfur to orthorhombic ( $\alpha$ -phase) sulfur at approximately 95.5°C [3]. Consequently, the induced strain and cracking of sulfur binder from the allotropic transition will remain in the matrices regardless of the countermeasure of curing shrinkage.

In principle, the most effective way to control the contraction of elemental sulfur is to stimulate the reaction between elemental sulfur and chemical modifiers such as dicyclopentadiene (DCPD), oligomer, and styrene at a certain temperature [3]. Consequently, commercial modified sulfur polymers have been invented. They exhibit greater performances over elemental sulfur primarily in terms of reduced contraction and increased resistance to water environments. Besides the modification of elemental sulfur, the incorporation of aggregates or fillers plays a key role in the mix design of robust and durable sulfur composites and concretes [41,42]. The author also confirmed that the mechanical and durability properties of sulfur concrete were influenced by the type of aggregate (natural or recycled aggregate) and the replacement of modified sulfur by micro-fillers such as Portland cement and fly ash [41,58]. It was found that the replacement of modified sulfur by micro-fillers up to certain amount was substantial in enhancing the compressive strength of sulfur composites with a conversion of the

microstructure [58].

Even though the modified sulfur composites developed higher compressive strengths from the inclusion of micro-fillers and aggregates, they still exhibit intrinsic brittleness under both compression and tension [58]. To alleviate the brittleness of modified sulfur composites, two types of micro fibers, steel and electric chemical resistant (ECR) glass fibers, are employed in this study. In the production of ultra-high performance fiber-reinforced concrete (UHPFRC), a considerable amount of micro steel fibers (length/diameter  $\geq 65$ ) up to 4% by volume has been included [65,66]. Although such a high dose of micro steel fibers is used, UHPFRC can have sufficient flowability with a required tensile performance (e.g., tensile strength and ductility) owing to its unique homogeneous microstructure [65,66]. Thus, a certain required tensile performance can be attained by adjusting the amount of micro steel fibers without a flowability reduction. As for the fiber reinforcement of hydraulic cement concrete, an alkali resistant (AR) glass fiber has been widely used considering a strong alkali condition of cement [67]. In general, an AR glass fiber has an equivalent or higher tensile strength than steel fiber. Moreover, because it has similar density as the cement concrete, it can increase both the dispersion of glass fibers and lightweightness of concrete. In this study, however, an ECR glass fiber was used rather than an AR glass fiber because of no moisture and alkali conditions in modified sulfur composites [58]. Furthermore, ECR glass fibers have higher tensile strengths and elastic moduli than AR glass fibers in general. Both steel and ECR glass micro fibers are intact at the high temperature of about 120~140°C, so that they are deemed suitable for thermoplastic sulfur matrices.

In this study, to examine the effects of micro fibers on the compressive and flexural performances (i.e., strength, ductility, toughness) of modified sulfur composites, a total of 15 mixture cases were tested by varying the volumetric ratio of each micro fiber. The replacement portion of modified sulfur by fly ash was set to 35% by volume for all mixtures, which was expected to ensure the desired flowability of micro fiber-reinforced sulfur composites. Besides the direct measurement of flexural stress-deflection responses, a non-contact displacement measurement, called digital image correlation (DIC) method, was conducted simultaneously with the third-point bending tests to read strain distributions and corresponding micro-cracks on front face at midspan of specimens. To evaluate the porosity of modified sulfur composites that might be affected by the inclusion of micro fibers especially at the interfaces between the fibers and the sulfur matrix, mercury intrusion porosimetry (MIP) was executed.

## 5.2. Experimental Program

### 5.2.1. Materials

In this study, a dicyclopentadiene (DCPD)-modified sulfur produced by Micro Powder, Inc. in Ulsan, Korea was used as the binder for making micro fiber-reinforced sulfur polymer composites. The concentration of DCPD was 3.3% by weight. All the matrices excluding the portion of fibers comprised Class F fly ash of 35% by volume, of which amount facilitated suitable flowability even with 4% volume of micro fibers. Two types of straight micro fibers were used, steel and electric chemical resistant (ECR) glass fibers, respectively, as shown in Fig. 5-1. The physical properties of two micro fibers are given in Table 5-1. The chemical composition of ECR glass fiber is presented in Table 5-2. It underwent no weight loss under a thermogravimetric analysis (TGA) of up to 900°C, as shown in Fig. 5-2. The used ECR glass fiber is boron-free, which affords a superior resistance to acid solutions.



**Figure 5-1: Micro fibers: (a) steel fiber, and (b) ECR glass fiber.**

**Table 5-1: Physical properties of micro fibers.**

Type	Length (mm)	Diameter (mm)	Tensile strength (MPa)	Modulus of elasticity (GPa)	Density (g/cm <sup>3</sup> )	Softening point (°C)	Feature
Steel	13	0.2	2,500	200	7.85	-	Copper coated
ECR glass	12	0.017	3,750	81	2.62	916	Boron free

**Table 5-2: Chemical composition of ECR glass fiber.**

Oxide (wt.%)				
SiO <sub>2</sub>	CaO	Al <sub>2</sub> O <sub>3</sub>	Fe <sub>2</sub> O <sub>3</sub>	Others
46.2	39.3	10.5	1.2	2.8

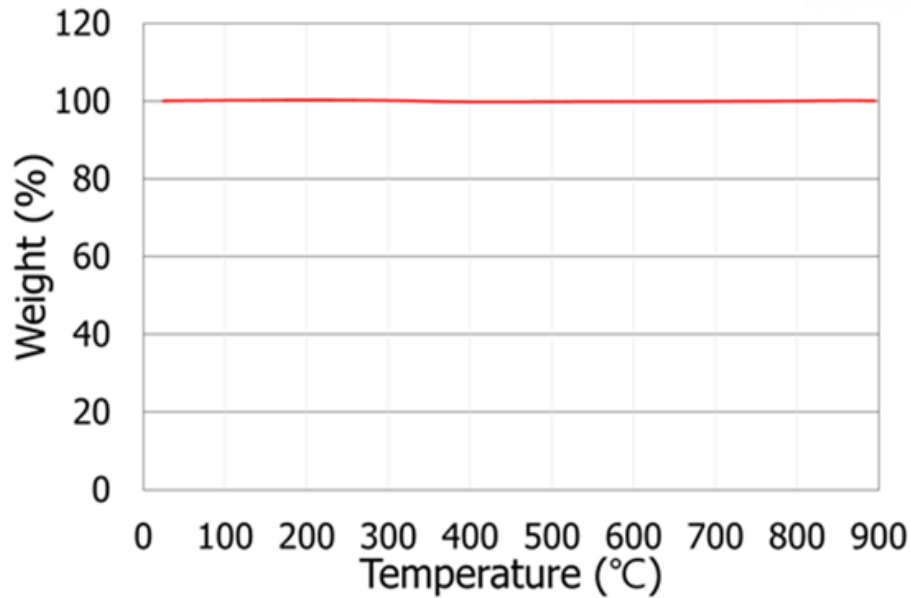


**Figure 5-2: Thermogravimetric analysis (TGA) of ECR glass fiber.**

### 5.2.2. Mix proportions

A total of 15 micro fiber-reinforced sulfur polymer composites were developed by varying the relative portion of each micro fiber, as shown in Table 5-3. The maximum dose of each micro fiber didn't exceed more than 2% by volume. Thus, the maximum fraction of micro fibers was 4%. In the mixture labels, the first, second, and third figures stand for the portion of fly ash, steel, and ECR glass fiber, respectively.

**Table 5-3: Mix proportions of micro fiber-reinforced sulfur polymer composites.**

Mixture label	Modified sulfur (3.3% DCPD)		Fly ash		Fiber fraction (vol.%)	
	vol.%	kg/m <sup>3</sup>	vol.%	kg/m <sup>3</sup>	Steel	ECR glass
35-0-0					0	0
35-0-1					0	1
35-0-2					0	2
35-0-3					0	3
35-1-0	65	1242	35	777	1	0
35-1-0.5					1	0.5
35-1-1					1	1
35-1-2					1	2

35-2-0	2	0
35-2-0.5	2	0.5
35-2-1	2	1
35-2-2	2	2
35-3-0	3	0
35-3-0.5	3	0.5
35-3-1	3	1

### 5.2.3. Test methods

For the fabrication of fresh sulfur mixtures, all the raw materials except the modified sulfur were preheated in an oven at 180°C for about 6 hours in advance. After the perfect liquefaction of modified sulfur in a mixing bowl at 140°C, the preheated fly ash and micro fibers were poured successively. Then, the mixing was continued approximately for 15 mins. Finally, the plastic mixtures were cast in the specified molds for compression, flexure, and microstructural analysis, and were compacted on a shaking table.

The compression tests were conducted using the cubic samples with each side of 50 mm. At least three samples were tested for each mixture. Considering the rapid strength development characteristic of modified sulfur, all the compression tests were conducted after three days of curing. The exact test conditions are to be in accordance with Section 2.3.1.

For flexure tests, referring to the typical test setups for engineered cementitious composites (ECC) [68,69], 535 mm-long thin plate specimens with a 25.4×128 mm<sup>2</sup> cross-section were subjected to a third-point bending. At least three specimens were tested to measure the flexural stress-strain responses. To read the vertical deflection at midspan, two linear variable differential transformers (LVDTs) were installed at both the front and rear parts of the specimens, as shown in Fig. 5-3. The tests were displacement-controlled with a loading rate of 2 mm/min.

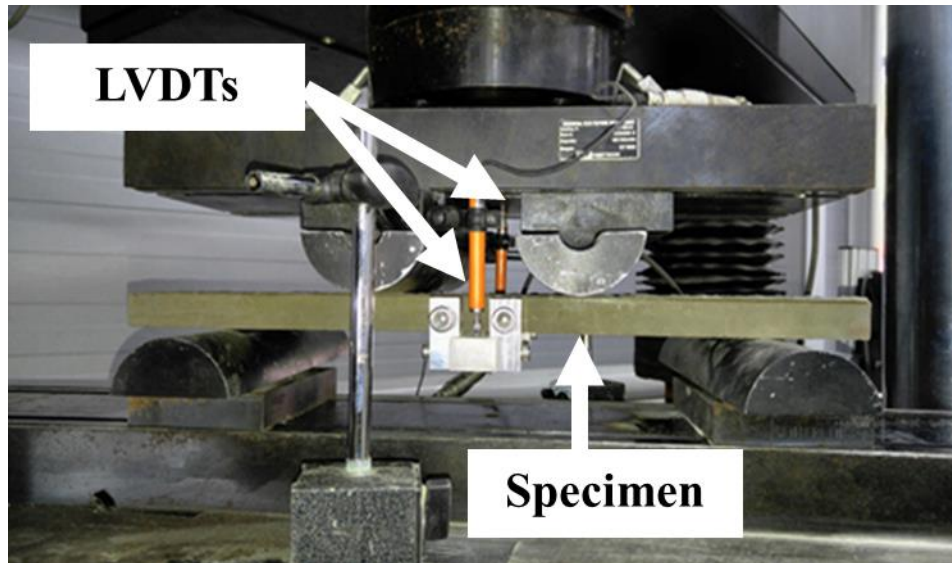


**Figure 5-3: Third-point bending test setup.**

To investigate the effect of portion of the micro fibers on porosity, the pore size distributions and total pore volumes of sulfur composites were evaluated using mercury intrusion porosimetry (MIP) (Auto Pore IV 9500, Micromeritics, USA). The detailed test conditions are explained in Section 2.3.3.

In addition to the flexural tests, a non-contact displacement measurement method, called digital image correlation (DIC), was executed using an optical 3D deformation measuring system (Aramis 3D, GOM, Germany) for the mixtures as shown in Fig. 5-4. This technique can identify the deformation of objective field due to the variation of stress field during the tests. Thus, the propagation of non-visible flexural micro-cracks can be visualized using the DIC during the flexure tests. Prior to DIC tests, the objective front face of the flexural test specimen was densely dotted with small and random speckles to calculate the correlation between the continuous captured digital images. In this study, a commercial program (GOM Inspect, Germany) was used as an analysis software.

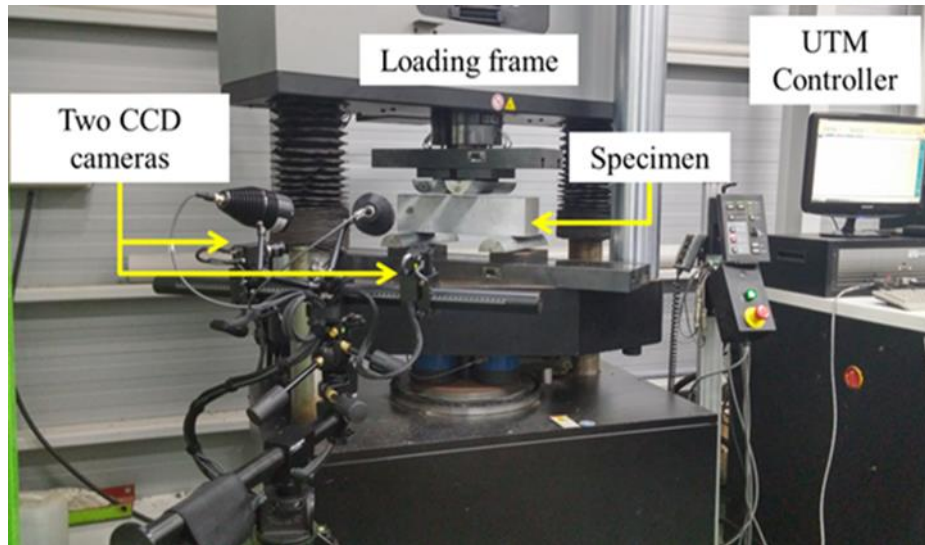


**Figure 5-4: Test setup for digital image correlation (DIC) in flexural tests.**

### 5.3. Results and Discussion

#### 5.3.1. Compressive strength

The compressive strength of sulfur composite (Mixture 35-0-0) with no fibers was 36.5 MPa on average (Fig. 5-5, Table 5-4). Regardless of the varying portions of micro fibers, all the composites developed higher compressive strengths than Mixture 35-0-0. Although the incorporation of micro fillers such as fly ash and Portland cement enhanced the compressive strengths of sulfur composites [41,58], they were vulnerable to severe brittleness largely inherited from modified sulfur itself [3]. Meanwhile, in the field of ultra-high performance fiber reinforced concrete, it was reported that the more micro steel fibers of up to 3% by volume resulted in larger compressive strength and elastic modulus [65], which was deemed attributable to the effect of fibers on delaying micro-crack formation [70]. Thus, it is expected that the micro fiber reinforcement in sulfur composites can alleviate the brittleness under both the compression and tension [65,70].

Except the “0% steel fiber” series, the more glass fibers generally induced a lower compressive strength for a given level of steel fiber. In contrast, the more steel fibers substantially enhanced the compressive strengths for a given level of glass fiber. In this regard, the micro steel fibers were considered more effective in resisting the formation of micro-crack than glass fiber under compression. Even though Mixture 35-3-1 included 1% more steel fiber than Mixture 35-2-1 containing 2% steel and 1% glass fibers, it developed smaller compressive strength than Mixture 35-2-1. The reduction in compressive strength likely originated from the inhomogeneous dispersion of fibers due to overdose of fibers [71]. Overall, all the mixtures failed abruptly and barely exhibited fragmentations due to



confinement of micro fiber.

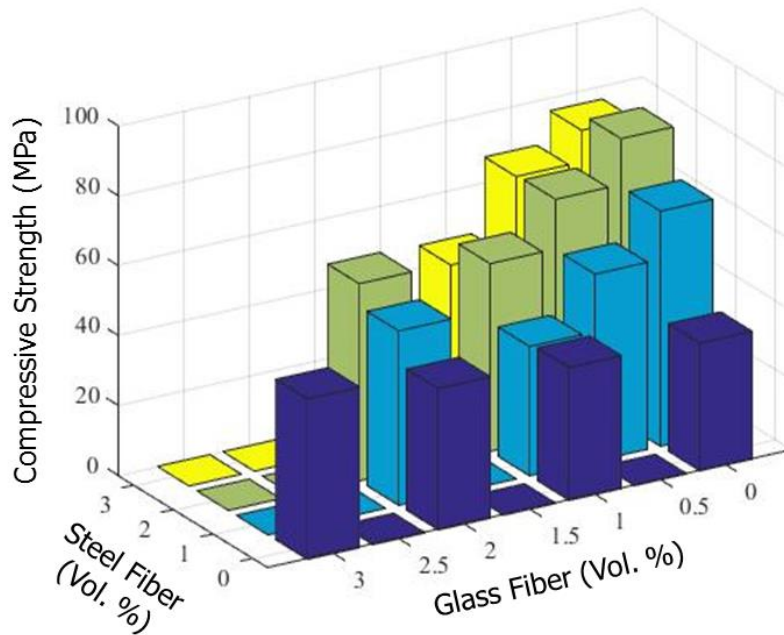


**Figure 5-5: Compressive strengths of micro fiber-reinforced sulfur polymer composites.**

**Table 5-4: Compressive strengths and flexural test results of the tested composites.**

Mixture label	Fiber fraction (vol.%)		Compressive strength (MPa)	Flexural strength (MPa)	Flexural deflection at max. stress (mm)
	Steel	ECR glass			
35-0-0	0	0	36.5	4.9	0.42
35-0-1	0	1	38.0	7.6	2.21
35-0-2	0	2	40.4	14.9	5.05
35-0-3	0	3	45.9	13.9	3.35
35-1-0	1	0	67.3	10.5	3.10
35-1-0.5	1	0.5	53.5	6.6	3.72
35-1-1	1	1	37.0	9.3	2.84
35-1-2	1	2	49.9	15.7	3.62
35-2-0	2	0	81.0	25.2	4.18
35-2-0.5	2	0.5	67.9	15.3	3.80
35-2-1	2	1	53.7	15.3	3.79
35-2-2	2	2	56.4	17.3	3.58
35-3-0	3	0	76.4	29.5	5.75

35-3-0.5	3	0.5	67.4	19.5	4.54
35-3-1	3	1	46.3	19.1	3.21

### 5.3.2. Flexural stress-strain responses

While the flexural strength of Mixture 35-0-0 without fibers was just 4.9 MPa, the others developed significantly large flexural strengths due to fiber reinforcement (Fig. 5-6). For a given level of glass fiber, the more steel fibers resulted in higher flexural strengths. This phenomenon fairly corresponds to the compressive strength result. Likewise, excluding the mixtures (Mixtures 35-1-0, 35-2-0, and 35-3-0) with only steel fibers, the more glass fibers led to higher flexural strength for a given steel fiber, whereas the trend of compressive strength development was the opposite. Thus, it is deemed that the flexural strengths of all mixtures were primarily dependent on the total fraction of fibers [72,73,74].

As indicated in Figs. 5-7, 5-8(a) and Table 5-4, Mixture 35-0-0 with no fiber suddenly failed with the smallest flexural deflection at maximum stress. However, the others showed the increased deflection capacity according to more fiber fraction. Among two types of micro fibers, the steel fibers were considered more influential than the glass fiber in terms of the flexural deflection. In Figs. 5-8, 5-9, 5-11, and 5-12, the use of more micro fibers commonly modified flexural stress-deflection responses. All the mixtures containing fibers sustained a gradual descending of flexural stress after the peak stress. In particular, Mixture 35-1-0.5 developed a relatively stable behavior of strain hardening and softening during the whole tests (Fig. 5-9(b)), which was also evidenced by the micro-cracks on tension bottom side of the specimen (Fig. 5-10). Similarly, both Mixtures 35-3-0.5 and 35-3-1 also showed a similar failure mode with micro-cracks (Figs. 5-13 and 5-14). Thus, as confirmed by Mixtures 1-0.5, 2-0.5, 2-1, 3-0.5, and 3-1 (Figs. 5-9, 5-11, and 5-12), the hybrid use of micro fibers with more steel fiber than glass fiber was deemed strategic in acquiring superior post-peak ductility, which had never been observed by non-fiber-reinforced sulfur composites or concretes.

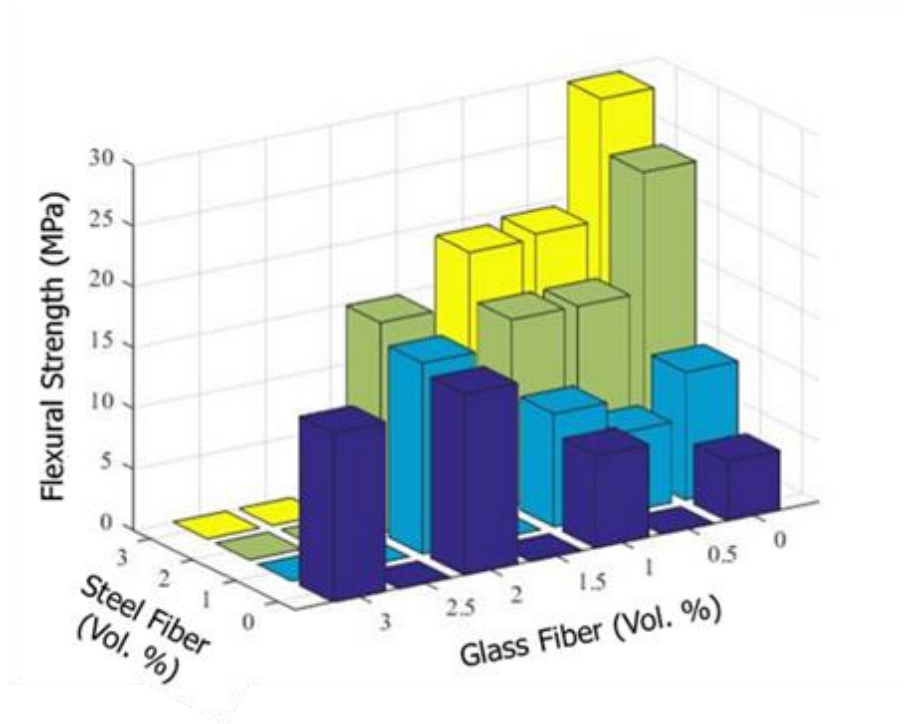


Figure 5-6: Flexural strengths of the tested composites.

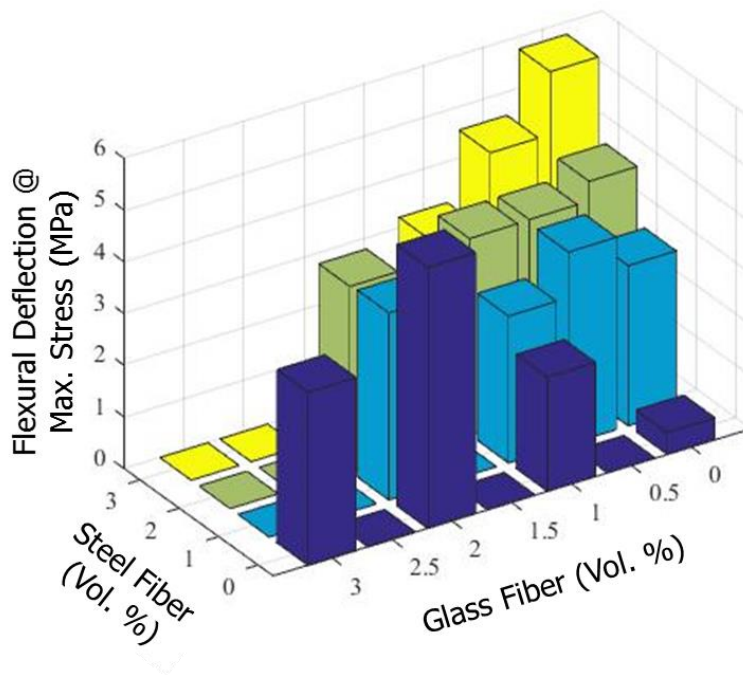
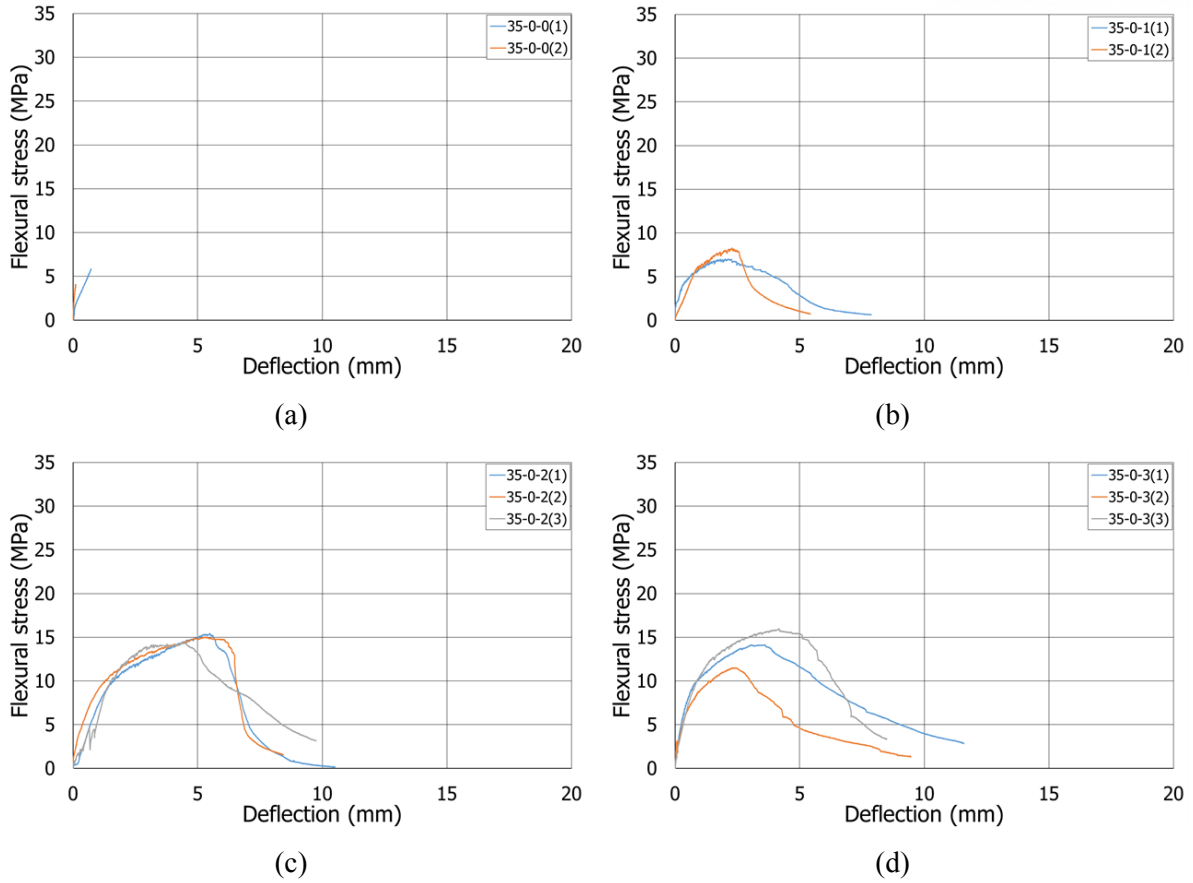
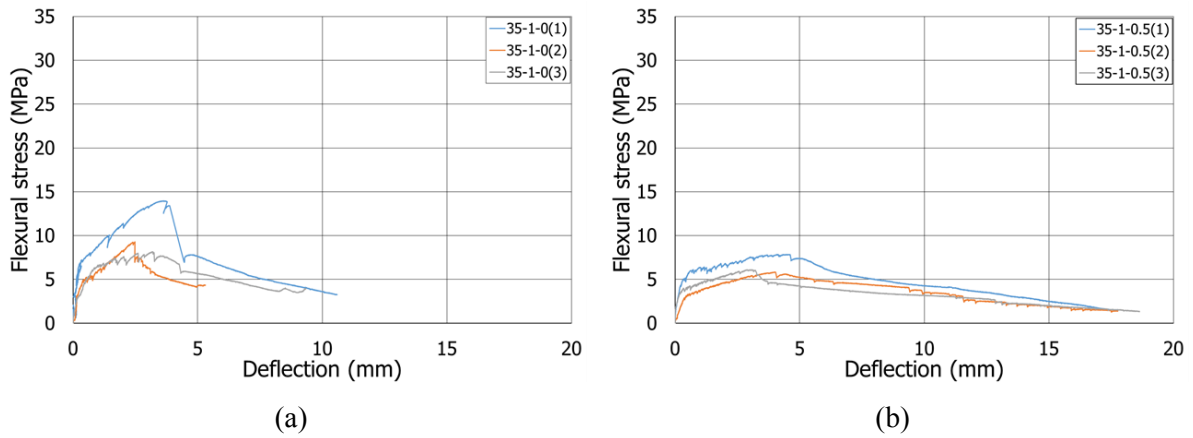


Figure 5-7: Flexural deflections at maximum stress of the tested composites.



**Figure 5-8: Flexural stress-deflection responses of the tested composites: (a) 35-0-0, (b) 35-0-1, (c) 35-0-2, and (d) 35-0-3.**



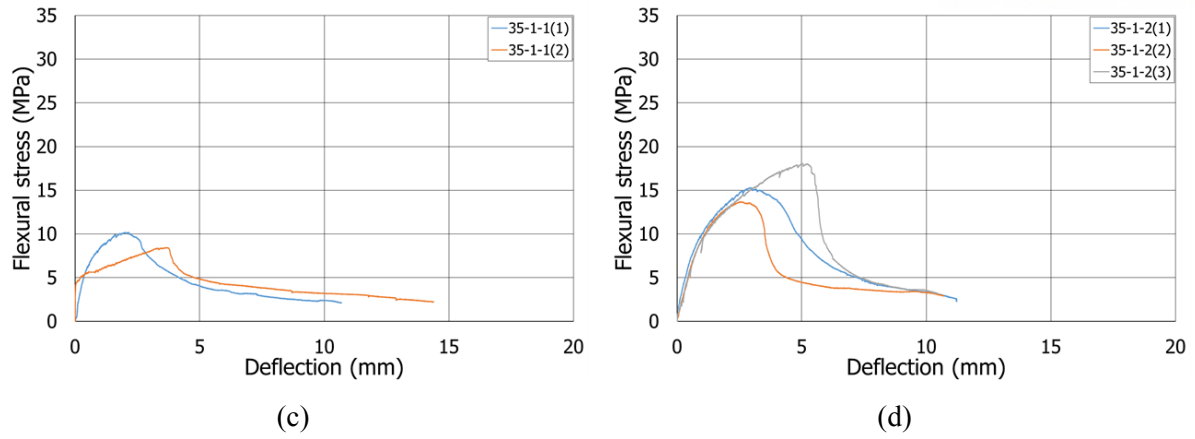


Figure 5-9: Flexural stress-deflection responses of the tested composites: (a) 35-1-0, (b) 35-1-0.5, (c) 35-1-1, and (d) 35-1-2.

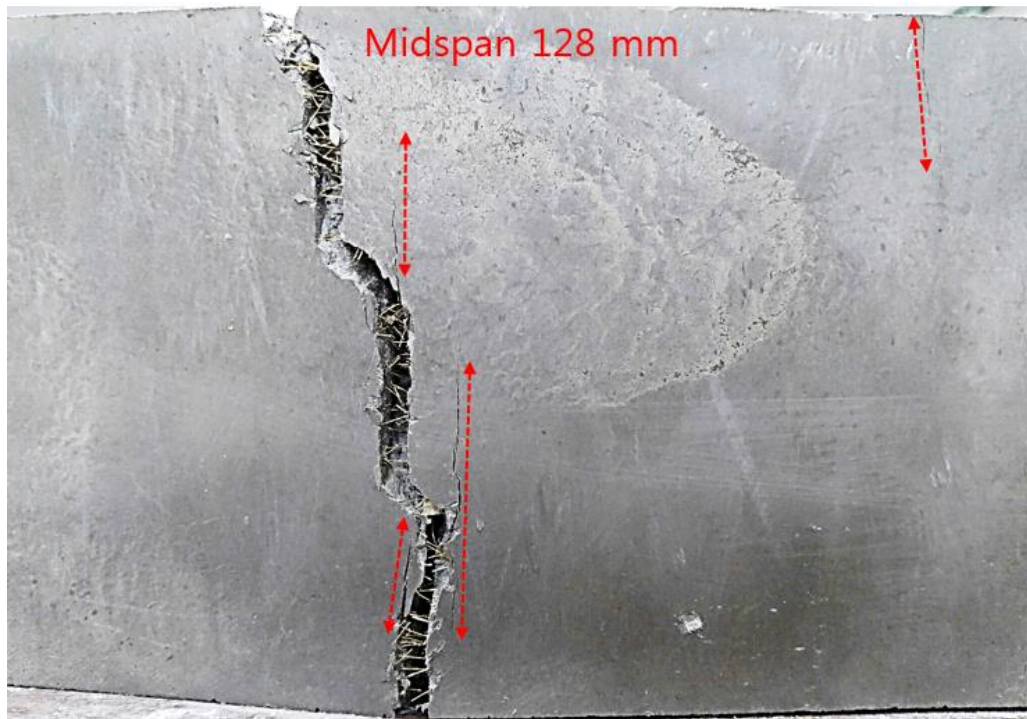
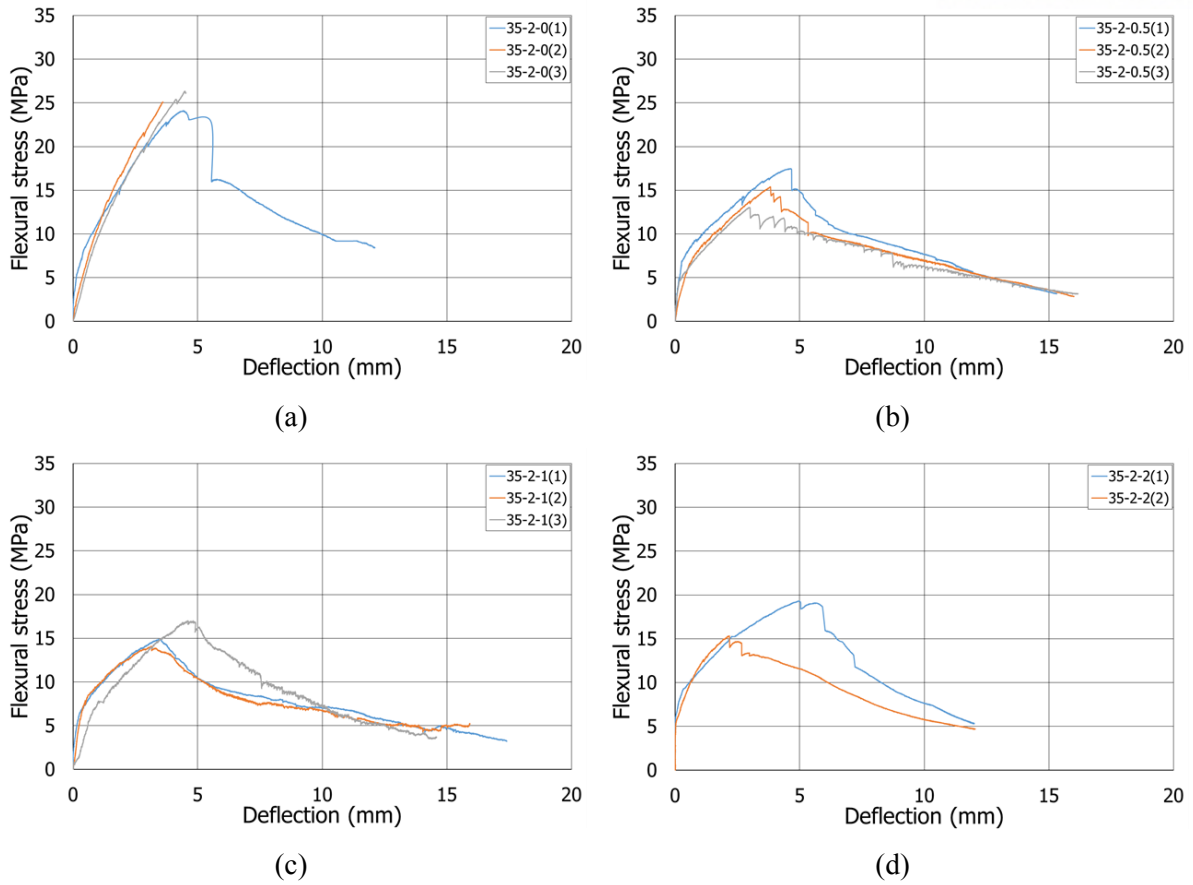
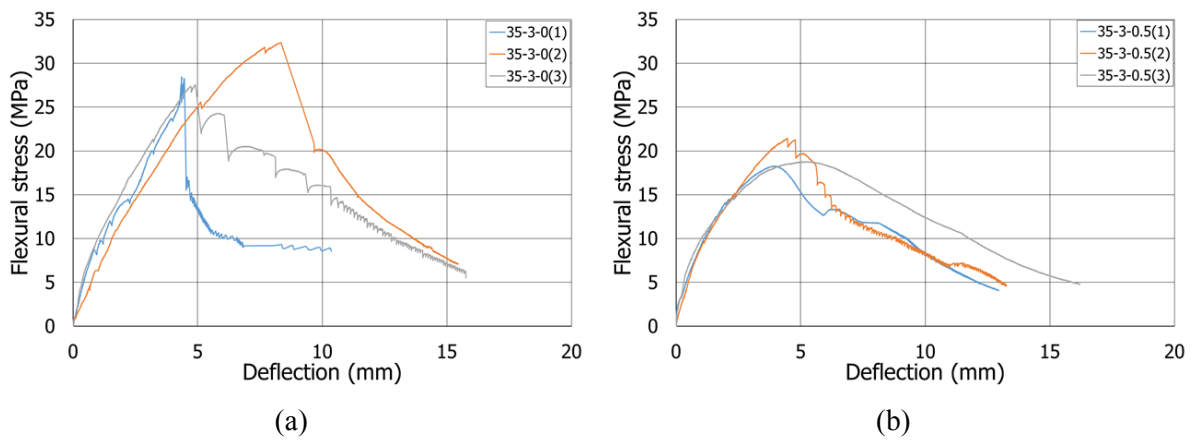
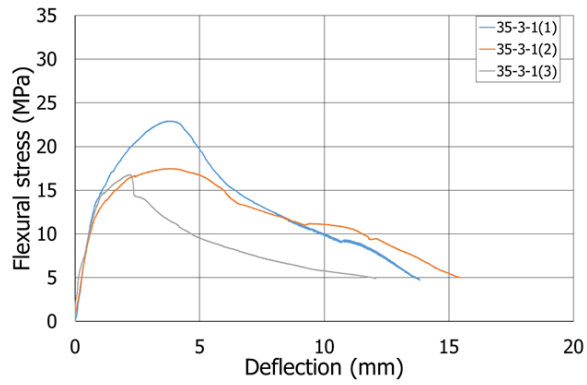


Figure 5-10: Flexural failure mode at the bottom surface of Mixture 35-1-0.5.



**Figure 5-11: Flexural stress-deflection responses of the tested composites: (a) 35-2-0, (b) 35-2-0.5, (c) 35-2-1, and (d) 35-2-2.**





(c)

Figure 5-12: Flexural stress-deflection responses of the tested composites: (a) 35-3-0, (b) 35-3-0.5, and (C) 35-3-1.

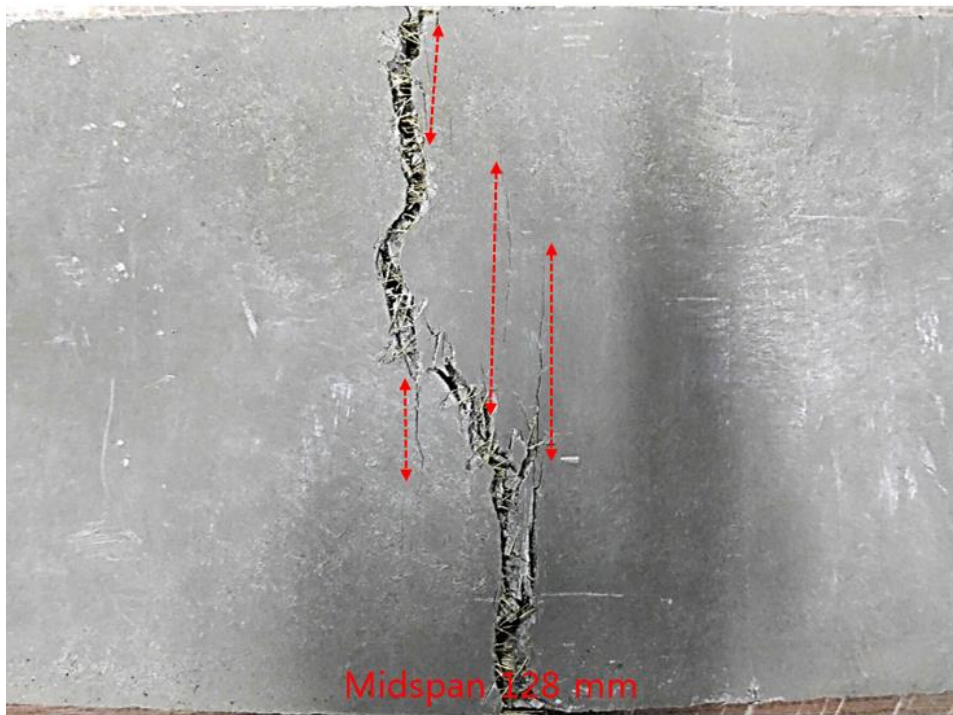
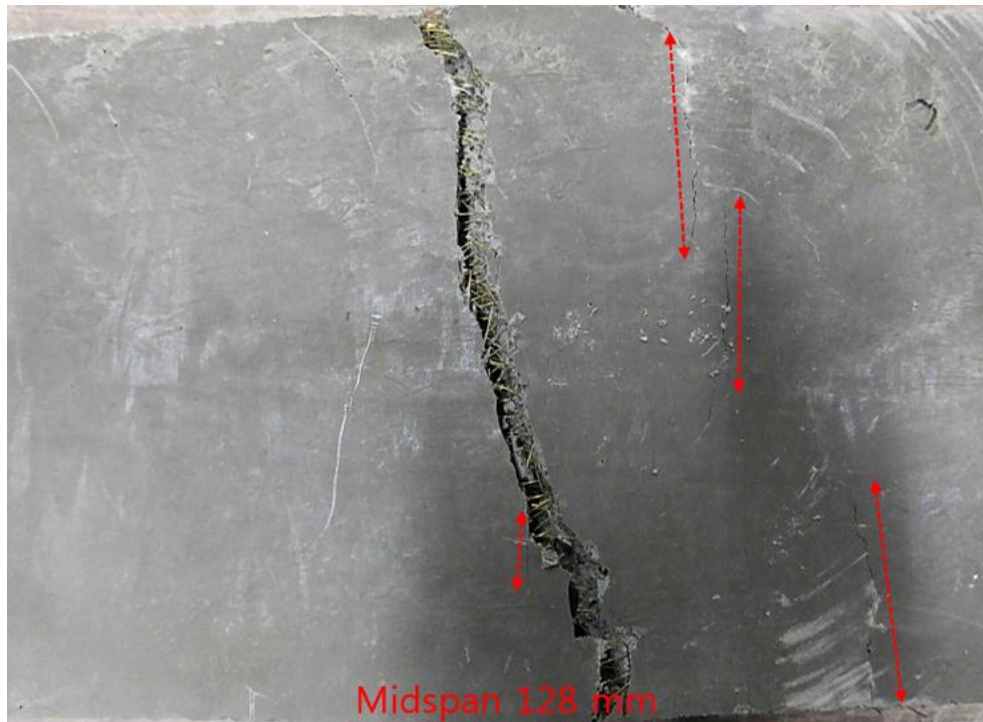


Figure 5-13: Flexural failure mode at the bottom surface of Mixture 35-3-0.5.



**Figure 5-14: Flexural failure mode at the bottom surface of Mixture 35-3-1.**

### 5.3.3. Porosity (MIP)

In order to examine the effect of fiber fraction on the porosity, a total of 9 mixtures were analyzed through MIP. The porosity of non-fiber-reinforced mixture (Mixture 35-0-0) was 7.4%. Without steel fiber, the total porosities became lowered according to the more glass fibers through 3% (Table 5-5). This phenomenon is in parallel with the test results that compressive and flexural strengths mostly increased with more glass fibers but no steel fibers (“0% steel fiber” series in Table 5-4). However, the average pore diameters of them were enlarged with the more glass fibers. This was also reflected in the formation of abundant pores bigger than 50 nm according to the more glass fibers (Fig. 5-15 and Table 5-5). As the author confirmed that sulfur composites developed smaller porosities and contained more cumulative volume of pores bigger than 100 nm according to more of a replacement of modified sulfur by the fly ash [58], it is concluded that the conversion of pore structures into relatively big pores (>50 nm) with the reduction of small pores (<50 nm) had substantial effects on both the compressive and flexural strengths of the sulfur composites.

In the same manner, as for a given level of 1% steel fiber (Fig. 5-16 and Table 5-5), the use of more glass fibers drew the less volume of small pores with the larger average pore diameters. However, there was no reduction of total porosity in spite of the addition of 1% more glass fiber. Likewise, the mixtures of “2% steel fiber” series attained similar porosities as those of “1% steel fiber” series (Fig. 5-17 and Table 5-5). They also attracted the more of the big pores as the volume of glass fiber increased.



Even though the mixtures of “3% steel fiber” series exhibited similar trend of pore structures according to the more of the glass fibers (Fig. 5-18 and Table 5-5), Mixture 35-3-1 containing 0.5% more glass fibers than Mixture 35-3-0.5 did not attain the enhanced flexural strength, as it was observed similarly in the compressive strength result. Therefore, the overdose of 3% steel and 1% glass fibers are considered inadequate for the homogeneous dispersion of micro fibers in the sulfur composites [71].

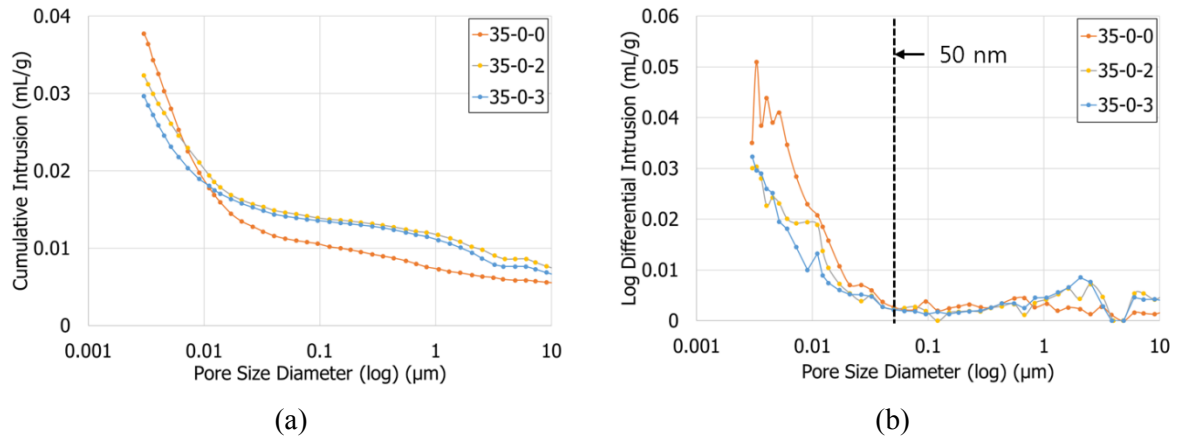
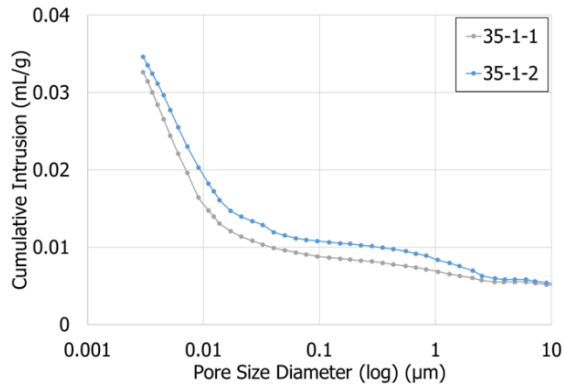


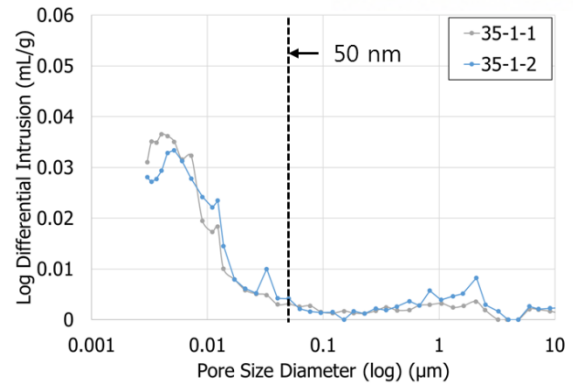
**Figure 5-15: Pore size distributions of Mixtures 35-0-0, 35-0-2, and 35-0-3: (a) cumulative intrusion, (b) log differential intrusion (unit: mL/g).**

**Table 5-5: Total porosities and average pore diameters of various composites.**

Mixture label	Cumulative pore volume (%)			Porosity (%)	Average pore diameter (nm)
	Sum (> 50nm)	Sum (< 50nm)	Total		
35-0-0	29.7	70.3	100	7.4	8.7
35-0-2	45.2	54.8	100	6.4	11.4
35-0-3	47.6	52.4	100	5.9	11.2
35-1-1	29.4	70.6	100	6.6	8.7
35-1-2	33.3	66.7	100	7.0	10.0
35-2-1	30.9	69.1	100	6.8	10.0
35-2-2	40.1	59.9	100	7.0	11.0
35-3-0.5	31.3	68.7	100	7.9	12.7
35-3-1	40.4	59.6	100	7.8	11.9

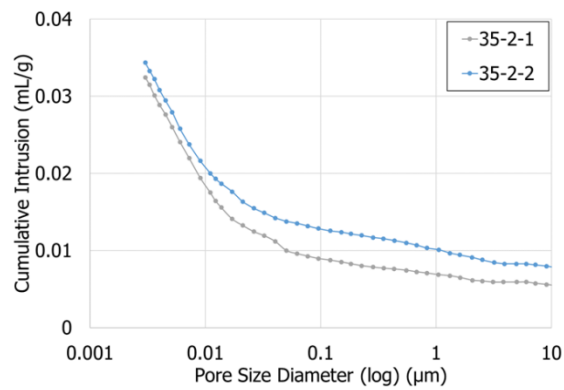


(a)

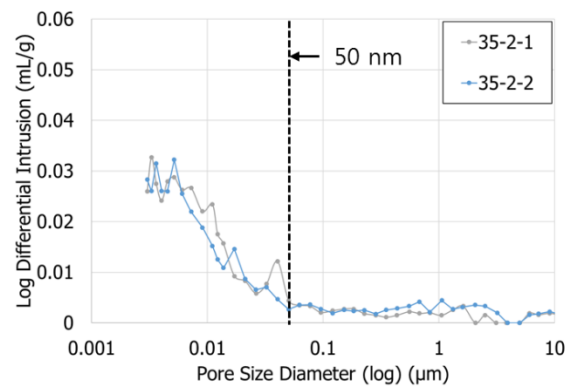


(b)

**Figure 5-16: Pore size distributions of Mixtures 35-1-1, and 35-1-2: (a) cumulative intrusion, (b) log differential intrusion (unit: mL/g).**

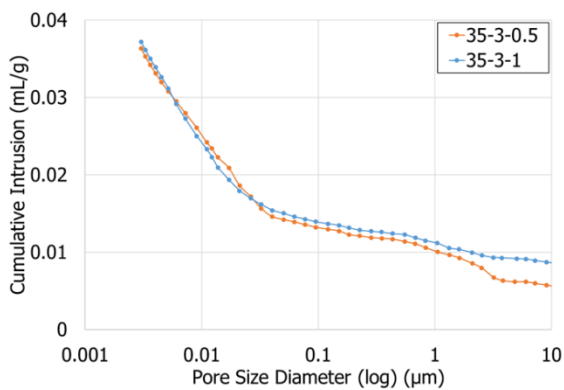


(a)

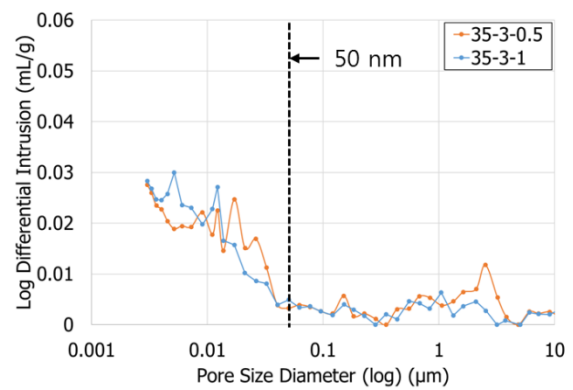


(b)

**Figure 5-17: Pore size distributions of Mixtures 35-2-1, and 35-2-2: (a) cumulative intrusion, (b) log differential intrusion (unit: mL/g).**



(a)

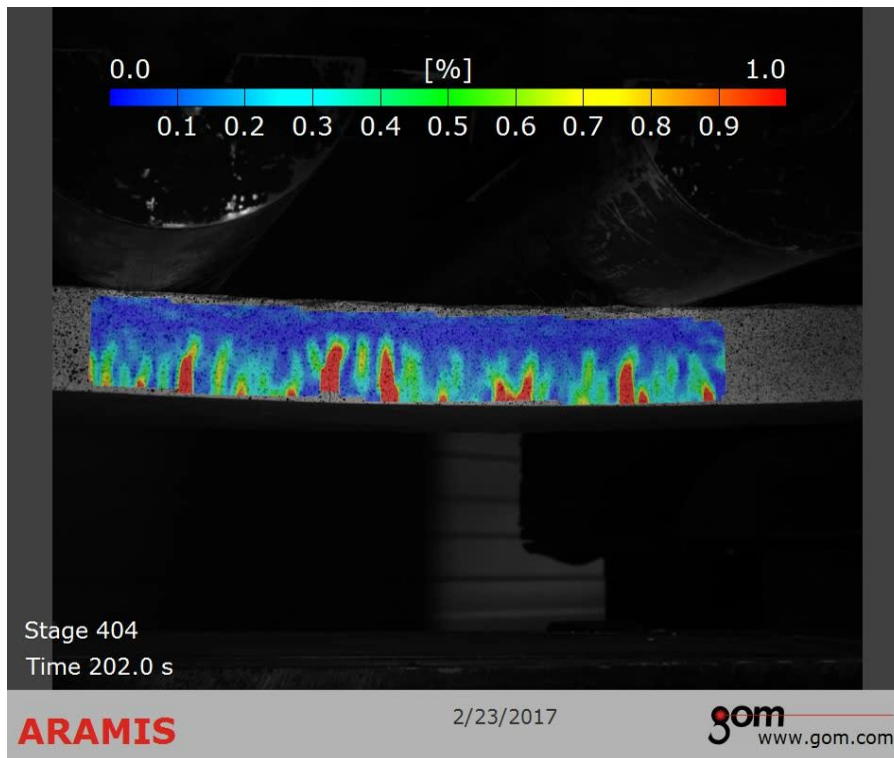


(b)

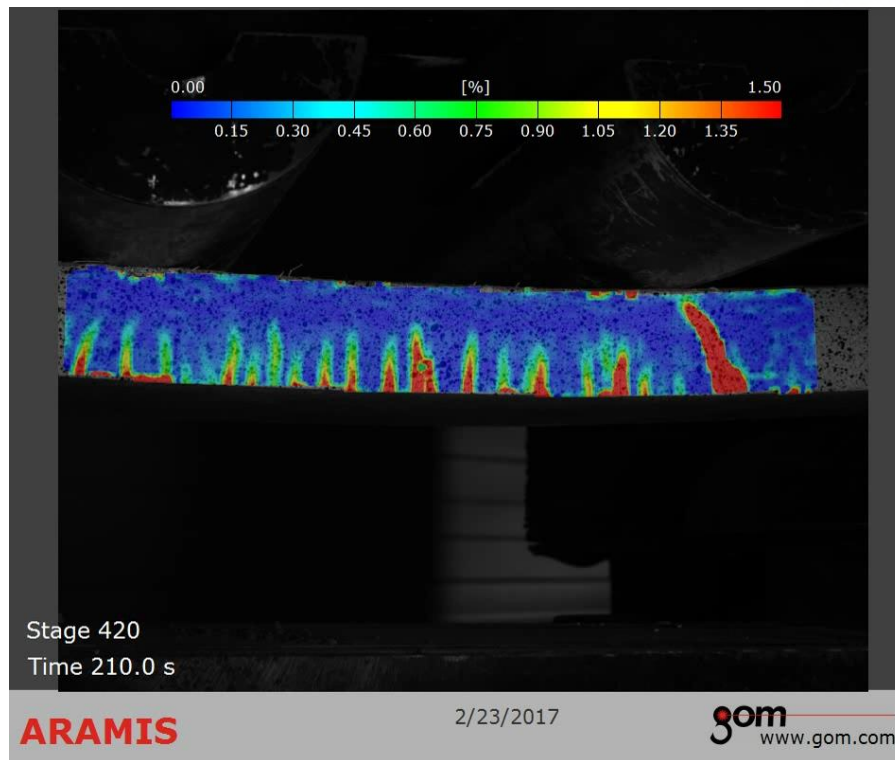
**Figure 5-18: Pore size distributions of Mixtures 35-3-0.5, and 35-3-1: (a) cumulative intrusion, (b) log differential intrusion (unit: mL/g).**

#### 5.3.4. Visualization of crack propagation (DIC)

As discussed in Section 5.3.2, the improved flexural stress-strain responses with the development of micro-cracks were obtained through the hybrid use of more steel fibers than glass fibers. Due to the closure of most micro-cracks without applied loading, it was difficult to record the exact formation of micro-cracks after each test. Among the cases showing the multiple micro-cracks, the flexural tests of Mixture 35-1-0.5 were additionally performed with DIC. Two specimens of Mixture 35-1-0.5 exhibited gradual micro-cracking as confirmed by the broad distributions of flexural strains especially at midspan. Fig. 5-19 illustrates the exact strain distributions on the front face of the midspan under the maximum flexural stress. Therefore, it is rational to conclude that the hybrid use of more steel fiber than glass fiber is promising to convert the brittleness of sulfur composites into ductile manner with multiple micro-cracks.



(a)



(b)

**Figure 5-19: Flexural strain distributions of Mixture 35-1-0.5 at the maximum stress: (a) specimen 1, (b) specimen 2.**

#### 5.4. Conclusions

In this study, 15 mixtures of micro fiber-reinforced sulfur composites were tested to investigate the effects of micro steel and electric chemical resistant (ECR) glass fibers on the compressive strength and flexural performances of sulfur composites. Overall, the hybrid use of micro fibers with more steel fiber than glass fiber was deemed effective in modifying the flexural stress-deflection responses, which was evidenced by strain hardening and softening behaviors with the development of micro-cracks. The findings and conclusions of this study are summarized as follows:

- ✓ Regardless of the volume of micro fibers, all the composites containing micro fibers developed higher compressive strength than non-fiber-reinforced sulfur composite. The compressive strength of micro fiber-reinforced sulfur composites was more dependent on the portion of micro steel fiber than ECR glass fiber. Meanwhile, total volume of both micro fibers had a considerable effect on the flexural strength development.
- ✓ Even though non-fiber-reinforced sulfur composite did not acquire post-peak ductility in flexure, all the micro fiber-reinforced sulfur composites commonly attained an enlarged post-peak ductility.

Moreover, the hybrid use of more steel fiber than glass fiber afforded the strain hardening and softening behaviors of the specimens, which showed a fine distribution of flexural strain and corresponding multiple micro-cracks. Obviously, Mixture 35-1-0.5 containing 1% steel fiber and 0.5% ECR glass fibers exhibited an even distribution of flexural strain on the front face of midspan through the digital image correlation (DIC).

- ✓ The micro fiber-reinforced sulfur composites failed abruptly at maximum compressive strengths without severe fragmentations owing to the confinement of micro fibers. Likewise, the flexural failure modes were also converted into ductile manner that had never been observed in conventional non-fiber-reinforced sulfur composites or concretes.
- ✓ Regardless of the kind of micro fibers, the more micro fibers attracted the larger cumulative volume of big pores ( $> 50$  nm) with the reduction of cumulative volume of small pores ( $< 50$  nm) in the sulfur composites. For the sulfur composites without steel fibers (“0% steel fiber” series), the increase in fraction of ECR glass fiber led to a gradual reduction of porosity accompanied by the increase in both the compressive and flexural strengths. For the other cases with steel fiber, however, the increase of glass fiber fraction usually enlarged the total porosity. At a given 3% steel fiber (“3% steel fiber” series), the more ECR glass fiber barely changed the porosity, which may suggest poor dispersion of micro fibers from an overdose of fibers.
- ✓ Overall, the sulfur composites entrained the more cumulative volume of big pores with a more total fiber. Even though this neglected the general solid-porosity relationship, it is deemed an unique characteristic of sulfur composites inherited from modified sulfur.

## 6. Rheological Properties of Fresh Modified Sulfur Polymer Composites Containing Binary Cement at Different Temperatures

### 6.1. Introduction

It was observed that the viscosity of fresh elemental sulfur decreased continuously up to approximately 0.007 Pa·s at 160°C, at which point the viscosity drastically grew to about 0.932 Pa·s at around 190°C [75]. However, it eventually fell again. This history of viscosity with respect to increasing temperature was associated with the length and concentration of amorphous sulfur chain ( $S_8$ ) formed within liquid sulfur. Thus, the steep rise in viscosity at 160°C reflects the increase of both the length and concentration of polymeric sulfur. Above around 190°C, however, the disintegration of sulfur chains prevailed.

Dicyclopentadiene (DCPD) was effective enough to compensate for the intrinsic drawbacks of elemental sulfur [3,26]. Through this modification process, the properties of modified sulfur were enhanced including its compressive and flexural strengths, resistance to water and aggressive chemical solutions [41,57]. Besides those properties, the relations between viscosity and temperature revealed that the viscosity of modified sulfur increased markedly at 150°C, at which point the mixture hardened so that further mixing was difficult to control [18]. In the modification of elemental sulfur through DCPD, the viscosity gradually increased with a more amount of DCPD, higher reaction temperature, and lengthened reaction time [27]. This phenomenon was also reflected in the formation of high molecular weight polysulfides [18]. However, excessive doses of DCPD should be avoided to allow for a workable fresh sulfur mixture as well as for economic efficiency. For example, at 140°C the reaction between elemental sulfur and 5 wt.% DCPD caused a viscosity of approximately 0.06 Pa·s after 5 h. Meanwhile, the use of 20 wt.% DCPD induced a viscosity of 1.5 Pa·s within 3 h of reaction [27]. Even though higher amounts of DCPD induced the rapid achievement of higher viscosity, more than 3 wt.% led to a decrease in the compressive strength of sulfur concrete [7]. Thus, the optimal loading of DCPD depends on modification costs, if the sulfur concretes made of modified sulfur have sufficient mechanical and durability properties.

Once most commercial modified sulfur polymers were produced with a certain dose of chemical modifier, they were often used in the construction field as an alternative binder to cement pastes or as additives to asphalt pavement [3,26,41,76]. These modified sulfur polymers exhibited a thermoplastic behavior, which could exclude water in the mixing process. Meanwhile, water is a key ingredient in cement paste; the mechanical and rheological properties of which are significantly dependent on the water-to-cement ratio [77]. Regarding the rheological properties of pristine modified

sulfur, reaction temperature is the most influential factor. In most cases, however, modified sulfur has been blended with micro-fillers such as cement and fly ash to enhance the physical properties (e.g., compressive strength, curing shrinkage) [41,57]. In a previous study, the author also observed that, when some portion of modified sulfur was replaced by micro-fillers, both the total amount and particle characteristics of the micro-fillers caused fresh modified sulfur mixtures to attain different degrees of workability [58]. Therefore, ascertaining the optimal amount of micro-filler and its particle characteristics (e.g., particle-size distributions, total surface area) was deemed critical to render a proper workability for fresh sulfur composites or concretes at about 140°C within a limited time.

As a paving material, conventional asphalt produced by a vacuum distillation process has been used as a basic binder [78]. In general, the asphalt should sustain certain degrees of both the penetration and performance grade to resist plastic deformation caused by different traffic loads [79,80]. The measured penetration depth can be empirically correlated with a binder's performance. For example, asphalt binders with high penetration values are suitable for cold climates while the others with low penetration value are suited for warm climate. Likewise, performance grade assessments take paving temperature as well as aging into account. However, the conventional asphalt binders are vulnerable to continuous rain fall, which cause severe stripping on the pavement. Accordingly, various polymer modified asphalt (PMA) binders have been invented to substitute for the conventional asphalt in pavements that are subject to severe traffic loads and harsh climate [81]. PMA binders can include mineral fillers such as quicklime and Portland cement to enhance the anti-stripping capacity of asphalt concrete by increasing viscosity [82]. In reality, however, PMA binders have been rarely used because of expensive initial cost in the field.

As a PMA binder, our research group developed sulfur modified asphalt mixture that contain DCPD-modified sulfur, and fly ash as the filler [76]. In this mixture, conventional asphalt binder is replaced by 20~50% modified sulfur. This mixture facilitated superior durability, higher resistance to aggressive chemicals, and rapid hardening. Most of all, its adhesion and water tightness were significantly enhanced by adding fly ash as the filler. Therefore, it will ultimately reduce life cycle costs. Nonetheless, there has been no quantitative approach dealing with the effect of micro-fillers on the properties of fresh modified sulfur mixtures at a given temperature.

Based on the aforementioned concern, the main objective of this study was to investigate the coupled effects of temperature and particle characteristics of micro-fillers on the rheological properties of fresh modified sulfur mixtures. The micro-fillers were prepared as binary cements (Portland cement/fly ash blends) by varying the composition ratios between Portland cement and fly ash to allocate different particle characteristics to the fresh modified sulfur mixtures. The particle-size distributions of binary cements were measured using a laser diffraction particle size analyzer. In addition, this study conducted mini slump tests, which are often used in measuring the flowability of cement

pastes [83], to identify a correlation between the rheological properties and flowability. Eventually, the established database between the rheology and mini slump flow will suggest a useful reference to design workable fresh sulfur composites or concretes with micro-fillers at certain temperatures.

## 6.2. Experimental Program

### 6.2.1. Raw materials

In this study, a DCPD-modified sulfur, provided by Micro Powder, Inc. in Ulsan, Korea was used as the binder for fresh sulfur polymer mixtures. The loading percentage of DCPD was 3.1% by weight. Ordinary Portland cement and Class F fly ash were blended together to yield binary cements. They were employed as the micro-fillers providing different particle-size distributions. Based on the XRF results, the chemical compositions of modified sulfur, Portland cement, and fly ash are presented in Table 6-1.

**Table 6-1: Chemical oxide compositions of modified sulfur, Portland cement, and fly ash.**

Oxide (wt.%)	Modified sulfur (DCPD 3.1%)	Portland cement	Fly ash
CaO	-	67.0	6.2
SiO <sub>2</sub>	-	17.3	52.3
Al <sub>2</sub> O <sub>3</sub>	-	4.3	22.6
Fe <sub>2</sub> O <sub>3</sub>	-	3.9	9.1
SO <sub>3</sub>	99.8	3.4	-
MgO	-	1.8	1.8
K <sub>2</sub> O	-	1.3	1.8
TiO <sub>2</sub>	-	0.3	1.3
Na <sub>2</sub> O	-	0.1	1.8
MnO	-	0.2	-
P <sub>2</sub> O <sub>5</sub>	-	0.2	1.2
Others	0.2	0.2	1.9

### 6.2.2. Mix proportions

The main variable of mix proportions was the replacement ratios of modified sulfur by the binary cements (Portland cement/fly ash blends). The portions of binary cement were 15%, 25%, and



35% by volume. The composition ratio of cement to fly ash was varied to assign different particle-size distributions of micro-filler to fresh sulfur mixtures. Accordingly, a total of 16 mix proportions were examined as listed in Table 6-2. In the nomenclature of the mixture labels, the first character “B” stands for binary cement. The following succeeding figures stand for total volume of binary cement, relative ratio between Portland cement and fly ash for each binary cement, respectively.

**Table 6-2: Mix proportions of tested fresh sulfur mixtures.**

Mixture label	Modified sulfur (DCPD 3.1%)		Binary cement				Total vol.%
	vol.%	kg/m <sup>3</sup>	Portland cement		Fly ash		
			vol.%	kg/m <sup>3</sup>	vol.%	kg/m <sup>3</sup>	
B0-0-0	100	1910	-	-	-	-	0
B15-1-0		1624	15	470	-	-	
B15-3-1		1624	11.25	352	3.75	83	
B15-1-1	85	1624	7.5	235	7.5	167	15
B15-1-3		1624	3.75	117	11.25	250	
B15-0-1		1624	-	-	15	333	
B25-1-0		1433	25	783	-	-	
B25-3-1		1433	18.75	587	6.25	139	
B25-1-1	75	1433	12.5	391	12.5	278	25
B25-1-3		1433	6.25	196	18.75	416	
B25-0-1		1433	-	-	25	555	
B35-1-0		1242	35	1096	-	-	
B35-3-1		1242	26.25	822	8.75	194	
B35-1-1	65	1242	17.5	548	17.5	389	35
B35-1-3		1242	8.75	274	26.25	583	
B35-0-1		1242	-	-	35	777	

### 6.2.3. Test methods

A laser diffraction particle size analyzer (Sympatec HELOS, Germany) was used to measure the particle-size distributions of cement/fly ash blends. Before the tests, all the powder samples were diluted with 1% volume fraction of isopropanol as a solvent to preclude the aggregation of particles during the measurement. The tests were performed at least three times for each cement/fly ash blend with the same amount of each sample.

For the preparation of fresh sulfur mixtures, modified sulfur was initially liquefied in a mixing

bowl at 140°C. Then, the binary cement that was preheated in an oven at 150°C over 6 hours was mixed together with plastic modified sulfur for 15 min using a mechanical hand mixer generating 100 rpm. All the instruments including steel molds and the mixing paddle were preheated as was done for the binary cement. Finally, the homogenized plastic mixtures with a surface temperature approximately of 140°C were prepared for specific tests.

After 7 days of curing, compression tests were performed using the cubic samples with sides of 50 mm. At least three samples were tested for each mixture. The main objective of the compression tests was to investigate the effects of replacement ratios of modified sulfur by binary cement and the particle-size distributions of binary cement on the strength development of hardened sulfur composites. The detailed test conditions are specified in Section 2.3.1.

To investigate the effect of temperature on the rheological properties of fresh sulfur mixtures, listed in Table 6-2, rheology tests were performed under two constant temperatures: 120°C and 140°C. As shown in Fig. 6-1, a commercial rheometer (HAAKE MARS III, Thermo Fisher Scientific, USA) was used with a controlled test chamber (CTC) radiating homogenous temperatures (30-600 °C) enclosing a parallel plate system. The diameter of the parallel plates was 35 mm. The gap between the upper and lower plate was 1 mm. Following ASTM C1749 [84], the shearing protocol was designed to determine the yield stress and the plastic viscosity of fresh sulfur mixtures based on the Bingham plastic flow. As shown in Fig. 6-2, an increasing shear strain rate from 1 s<sup>-1</sup> to 40 s<sup>-1</sup> and back to 1 s<sup>-1</sup> was imposed in 360 s. This range of shear strain rates falls into the boundary used in a concrete rheometer [85]. During one cycle of shearing history, the slopes of both increasing (up-curve) and decreasing shear strain rate (down-curve) were used to estimate the plastic viscosity. Thus, the intercept of each curve at zero shear strain rate corresponded to the yield stress. During the initial 20 s, the shear strain rate was 1 s<sup>-1</sup> to homogenize the mixtures [86]. Then, each step of 20 s commenced successively. At each step, the shear stress was measured every 1 s. Thus, the average of constant shear stresses was used to calculate the plastic viscosity and the yield stress.

In addition to the rheology tests, the spread flow was measured using a mini slump test following ASTM C1437 [87] and C230 [88]. The apparatus for the mini slump test and its dimensions are given in Fig. 6-3. Both the mini slump cone and steel plate were preheated in an oven at about 150°C to eliminate the temperature difference between the surfaces of the cone and plate and fresh mixtures. Once the mini slump cone was filled with the fresh mixtures, the cone was smoothly lifted and the diameter of the disk formed was measured in the four directions.

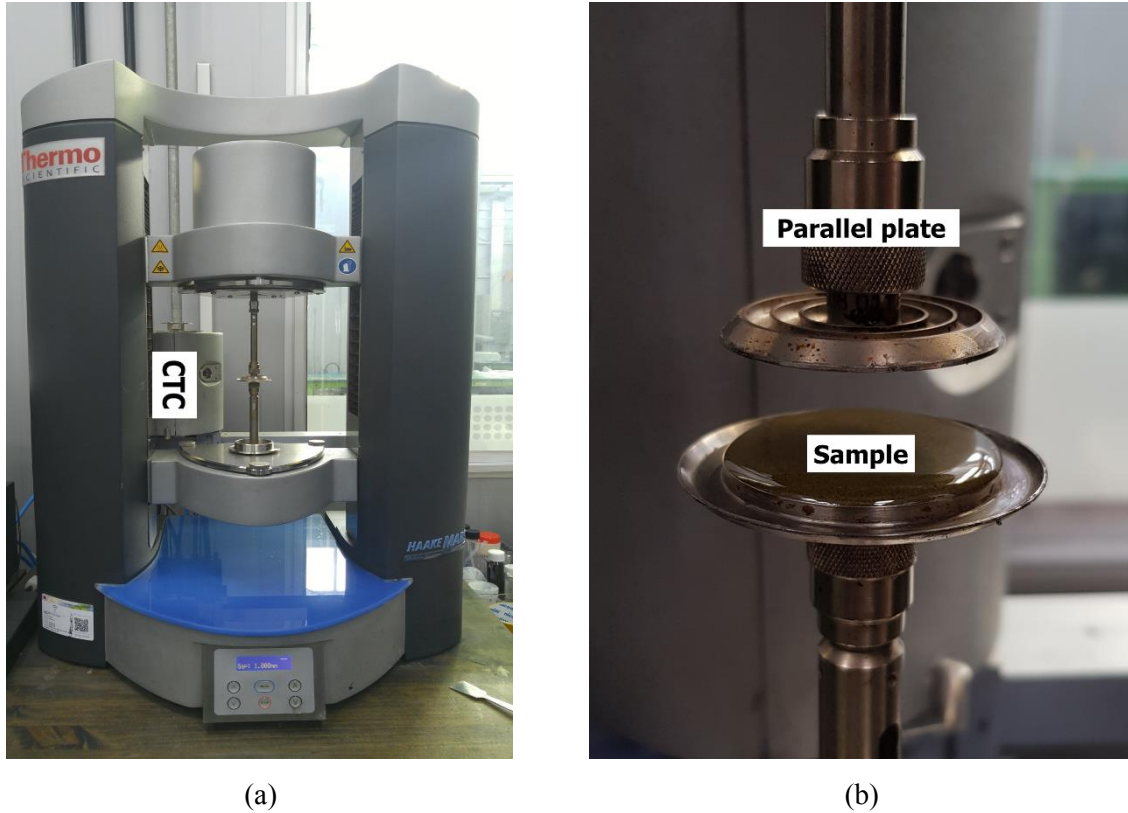


Figure 6-1: Rheology test setup: (a) rheometer with controlled test chamber (CTC), and (b) parallel plate with sample.

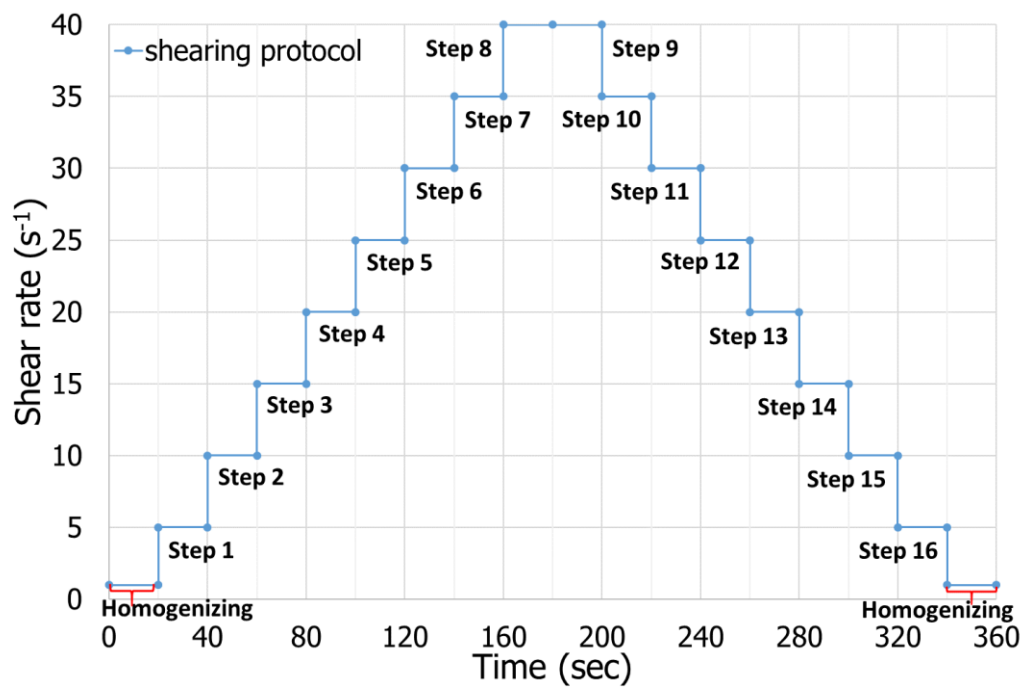
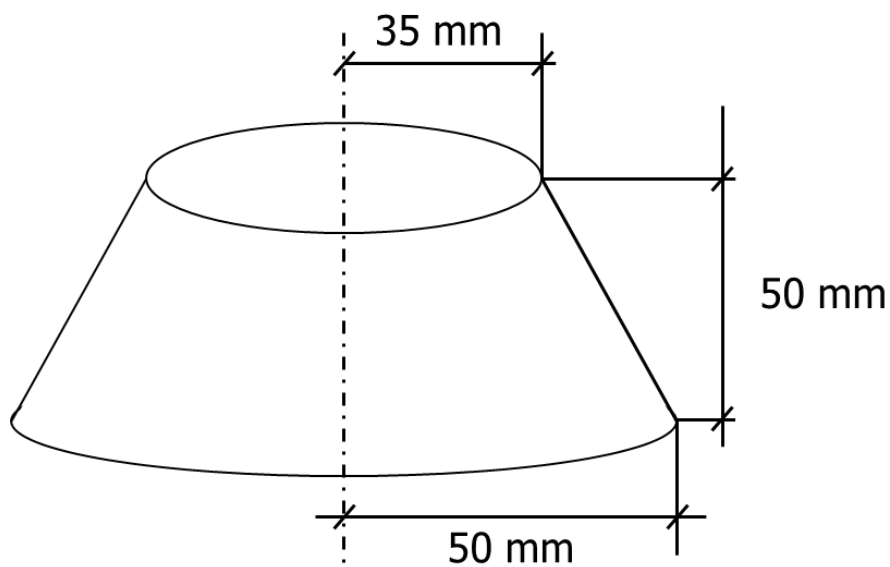


Figure 6-2: Shearing protocol for the rheology test.



(a)



(b)

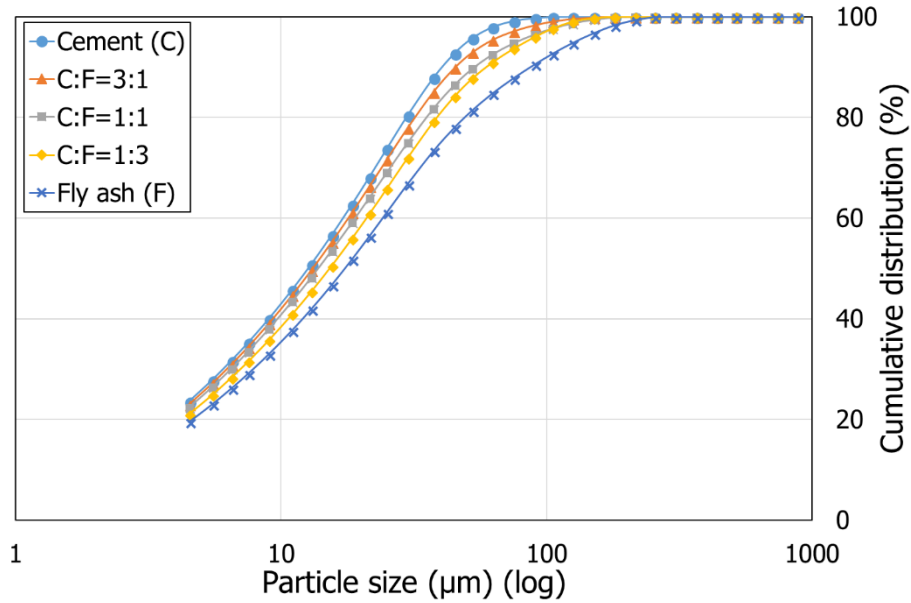
**Figure 6-3: Mini slump test: (a) test apparatus, and (b) specimen geometry.**

### 6.3. Results and Discussions

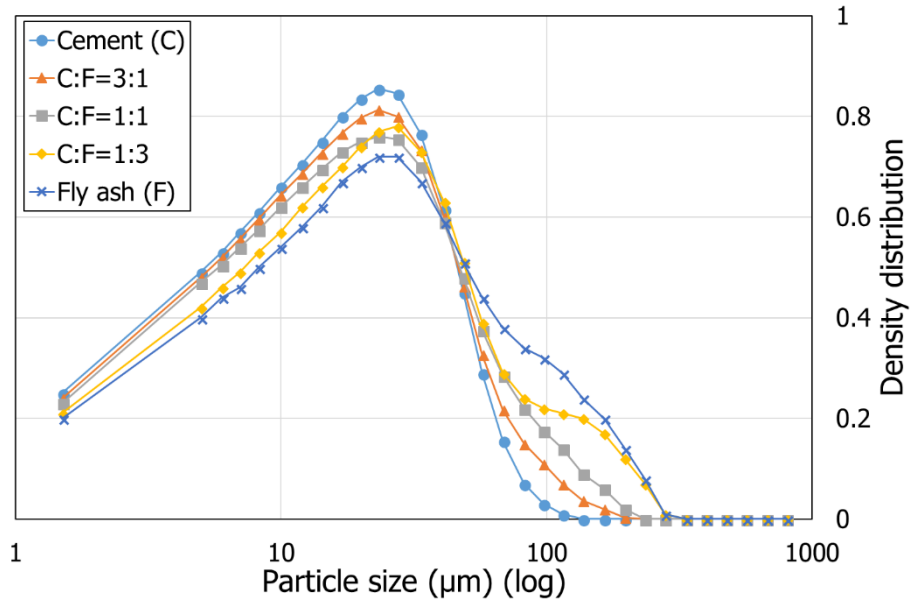
#### 6.3.1. Particle-size distributions of cement/fly ash blends

Using a laser diffraction analyzer, the particle-size distribution (PSD) of each cement/fly ash blend was measured three times and averaged as shown in Fig. 6-4. In Fig. 6-4, among five cases, the

PSD of Portland cement exhibited a higher leftward distribution density than the others. With a greater proportion of fly ash, however, the PSD of cement/fly ash blends shifted towards a bigger particle size. Likewise, sole Portland cement presented the maximum values of both the measured total surface area and specific surface area, which became smaller as the proportion of fly ash increased (Table 6-3).



(a)



(b)

**Figure 6-4: Particle size distributions of cement/fly ash blends: (a) cumulative, (b) density.**

**Table 6-3: Measured particle characteristics of cement/fly ash blends.**

Composition ratio (vol.)		Total surface area (m <sup>2</sup> /cm <sup>3</sup> )	Specific surface area (cm <sup>2</sup> /g)
Portland cement	Fly ash		
1	0	0.90	8988
3	1	0.88	8767
1	1	0.85	8533
1	3	0.81	8122
0	1	0.76	7557

### 6.3.2. Compressive strength

For a given type of cement/fly ash blend (binary cement), the compressive strength of hardened sulfur mixtures generally increased with the more of micro-filler (Fig. 6-5) (except for Mixture B35-1-0, which contained only Portland cement). Meanwhile, with the same proportion of micro-filler, the compressive strength decreased in the samples with a higher ratio of fly ash than Portland cement. Thus, the compressive strength of hardened sulfur mixtures was likely subjected to the particle-size distribution of micro-fillers. In other words, it was found that the higher ratio of Portland cement than fly ash formulated a higher contact area between the modified sulfur and micro-fillers in the sulfur mixtures. This phenomenon was due to the relatively larger total surface area of Portland cement than fly ash (Table 6-3). In addition, because the indentation modulus of raw Portland cement ( $111.0 \pm 13.0$  GPa) is generally larger than that of fly ash ( $66.1 \pm 14.2$  GPa) [61], it was deemed that the greater proportion of Portland cement afforded a higher stiffness to the hardened sulfur mixtures.

The compressive strength of Mixture B15-0-1 was 25.8 MPa on average, which was smaller than that (i.e., 30 MPa) of a modified sulfur mixture containing the same proportion (15%) of fly ash in the author's previous study [58]. The strength gap between them can likely be attributed to different concentrations of DCPD in each modified sulfur sample as well as different particle characteristics of each used fly ash. Meanwhile, it was noted that Mixture B15-1-0 containing 15% Portland cement only presented a compressive strength of 50 MPa, of which value was almost same as that of the mixture containing only 40% of fly ash in the author's previous study [58]. Based on this observation, it is reasonable to conclude that the small quantity of Portland cement contributed markedly to the enhanced compressive strength compared with much quantity of fly ash.

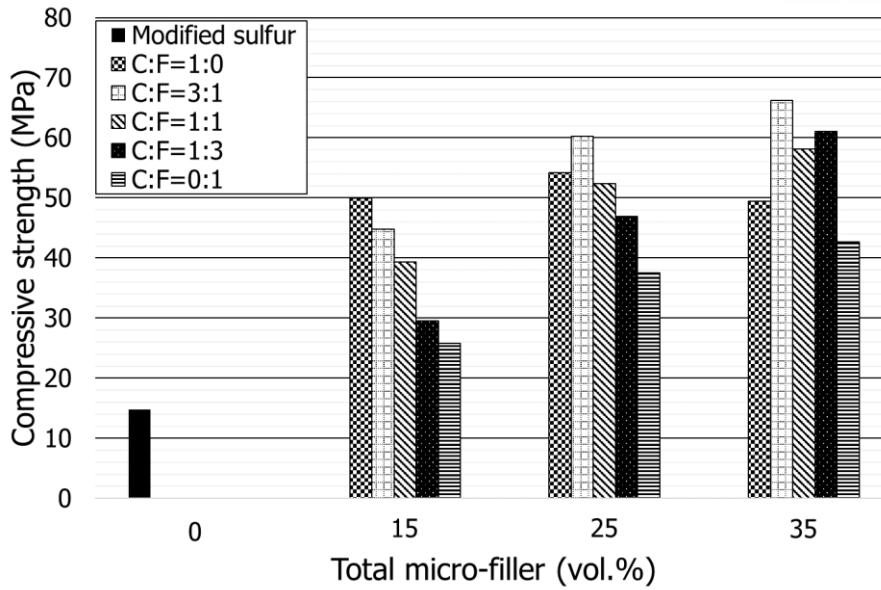
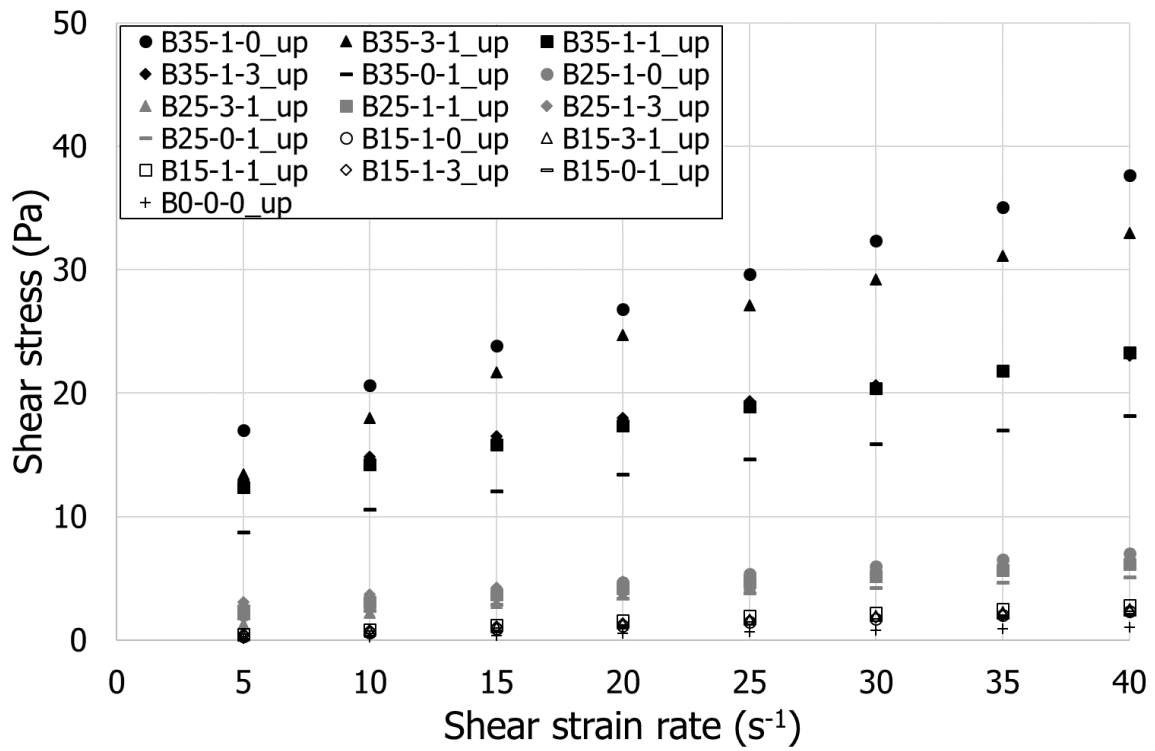


**Figure 6-5: Compressive strengths of tested sulfur composites.**

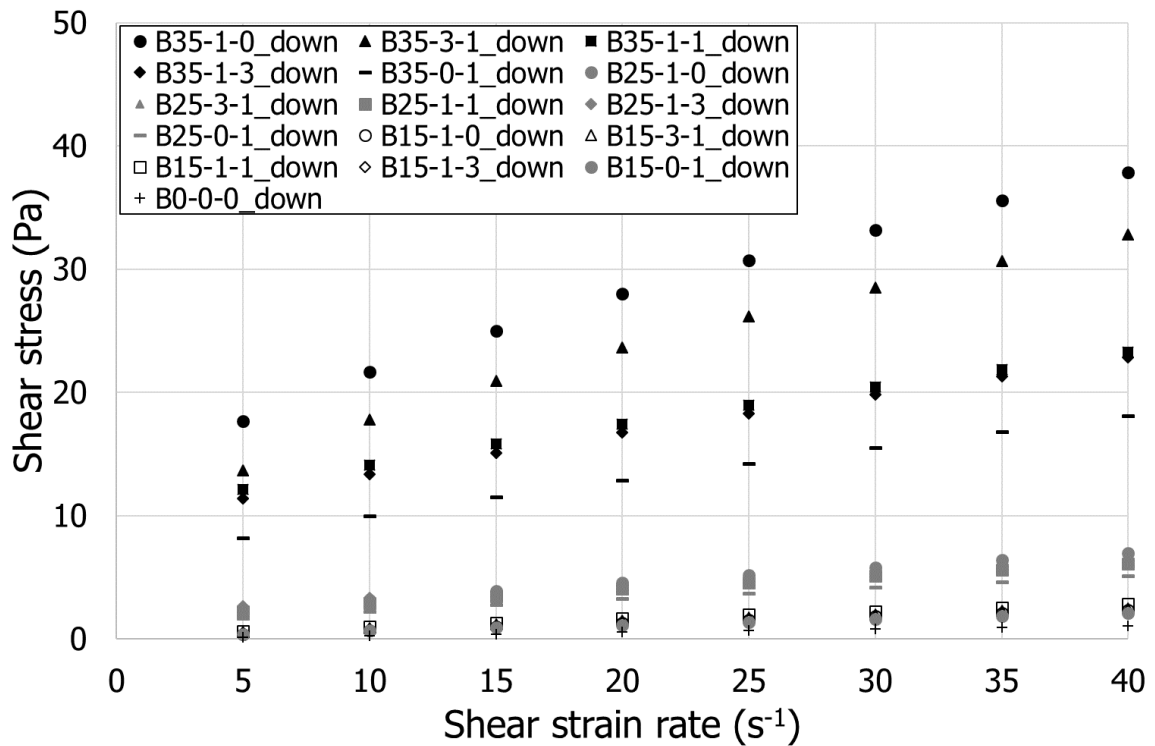
### 6.3.3. Rheology

For all tests, all the measured shear stresses at the first shear strain rate of  $1 \text{ s}^{-1}$  were excluded in the estimation of flow curve to neglect unstable development of shear stress under a low shear strain rate [89]. At  $120^\circ\text{C}$ , both the yield stress and the plastic viscosity of each fresh sulfur mixture were markedly influenced by the total fraction of micro-filler (Table 6-4). Overall, they increased with a more of micro-filler. For a given proportion of micro-filler up to 25%, however, there were barely distinct gaps between the mixtures, despite the use of different types of micro-filler with varying total surface area (Table 6-4). This phenomenon was likely attributed to relatively lower viscous mixtures compared to those containing 35% micro-filler. As shown in Fig. 6-6, both ascending and descending flow curves of each mixture traced a similar shear stress history at each shear strain rate during the first shearing cycle. Moreover, a repeated second shearing cycle also followed similar shear stress history as the first shearing cycle (Fig. 6-7), which did not render a thixotropy at  $120^\circ\text{C}$ . Thus, the average yield stress and plastic viscosity were calculated using two shearing cycles with four flow curves for each mixture.

In the series of 35% micro-filler, an increasing total surface area of micro-filler in the unit volume of sulfur mixture caused the yield stress and the plastic viscosity to rise from 7.3 to 15.2 Pa, and from 0.273 to 0.593 Pa-s, respectively (Table 6-4, Figs. 6-8 and 6-9). Mixture B35-1-0 containing only Portland cement attained both the maximum yield stress and plastic viscosity among the mixtures. Thus, it was deemed that the total surface area of micro-filler had a substantial effect on the rheological properties of fresh sulfur mixtures with the same fraction of micro-filler.



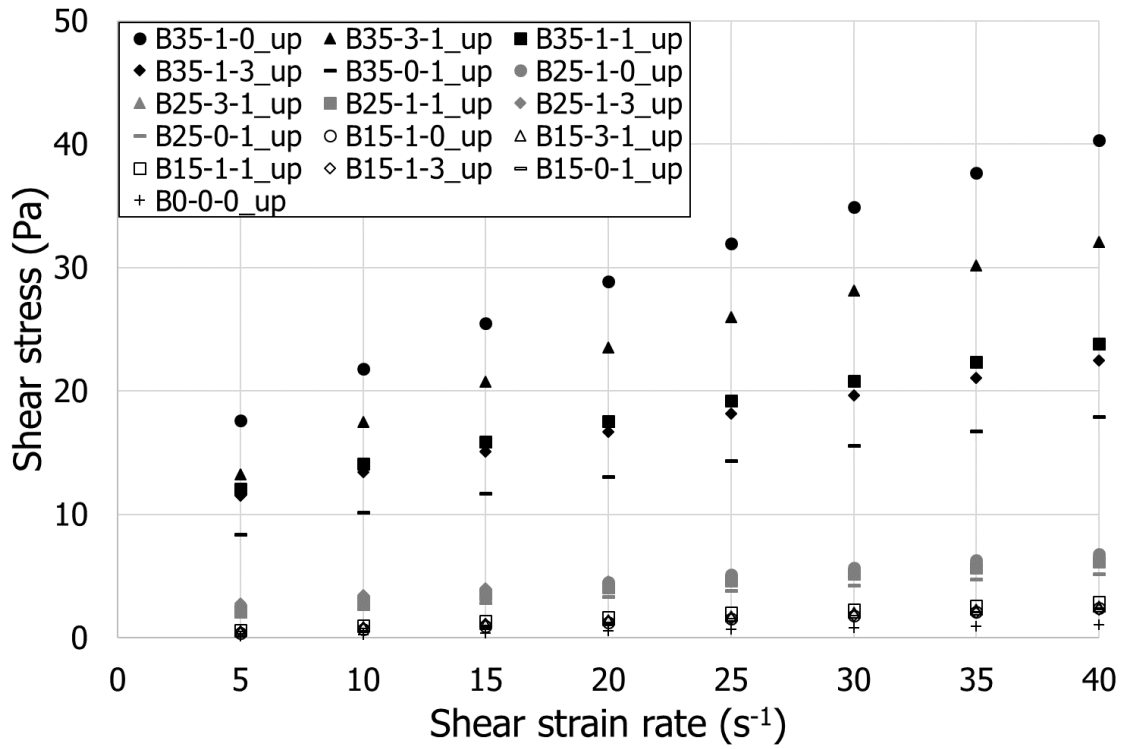
(a)



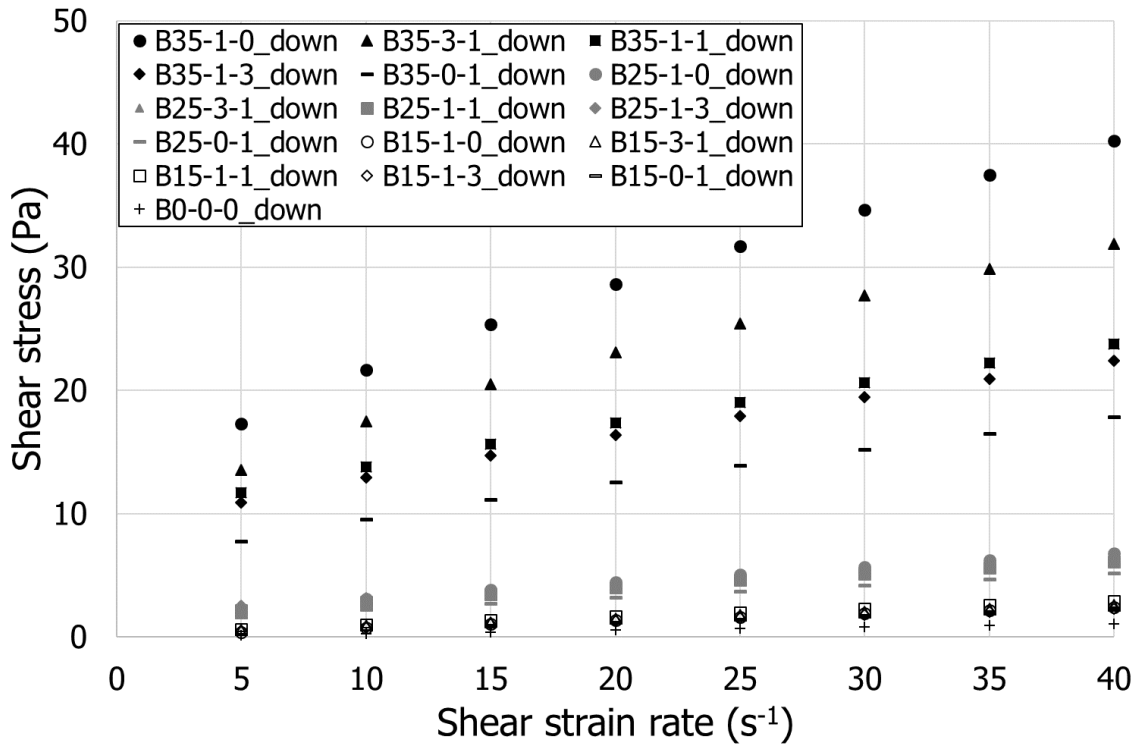
(b)

Figure 6-6: Shear stress-strain rate responses of fresh sulfur mixtures during first shearing cycle at 120°C: (a) up-curve, (b) down-curve.





(a)



(b)

Figure 6-7: Shear stress-strain rate responses of fresh sulfur mixtures during second shearing cycle at  $120^{\circ}C$ : (a) up-curve, (b) down-curve.

**Table 6-4: Average yield stress and plastic viscosity of fresh sulfur mixtures at 120°C.**

Mixture label	Total surface area of micro-filler (m <sup>2</sup> /cm <sup>3</sup> )	Yield stress (Pa), (CV*)	Plastic viscosity (Pa-s), (CV)
B0-0-0	0	0.005 (0)	0.030 (0)
B15-1-0	0.237	0.12 (0.08)	0.060 (0)
B15-3-1	0.131	0.26 (0.15)	0.060 (0)
B15-1-1	0.125	0.32 (0.10)	0.065 (0)
B15-1-3	0.123	0.29 (0.02)	0.050 (0)
B15-0-1	0.110	0.19 (0.01)	0.050 (0)
B25-1-0	0.395	1.74 (0.01)	0.133 (0.02)
B25-3-1	0.218	1.50 (0.15)	0.123 (0.02)
B25-1-1	0.208	1.83 (0.03)	0.110 (0)
B25-1-3	0.205	2.35 (0.05)	0.105 (0)
B25-0-1	0.183	1.31 (0.02)	0.098 (0.03)
B35-1-0	0.553	15.2 (0.01)	0.593 (0.03)
B35-3-1	0.305	12.3 (0.01)	0.525 (0.02)
B35-1-1	0.291	10.8 (0.02)	0.323 (0.04)
B35-1-3	0.287	9.90 (0)	0.308 (0.02)
B35-0-1	0.256	7.30 (0.03)	0.273 (0.01)

\*CV denotes coefficient of variation.

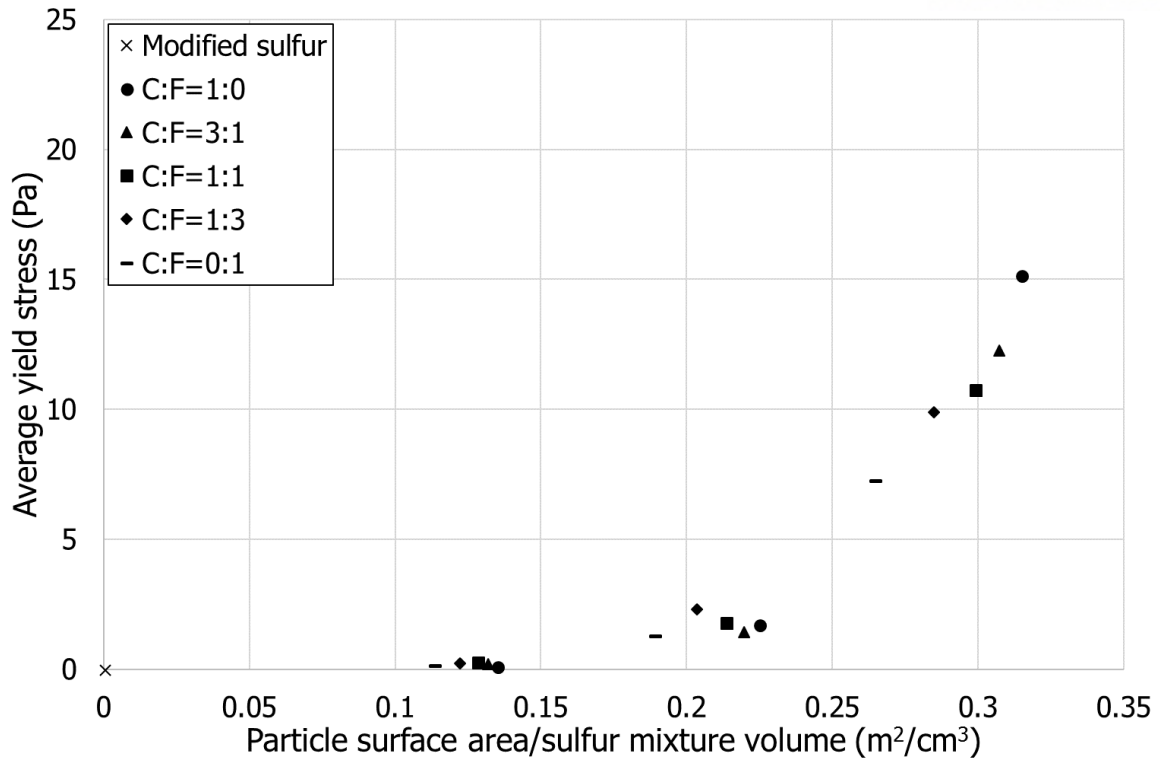


Figure 6-8: Average yield stress of fresh sulfur mixtures with varying total surface area of micro-filler at 120°C.

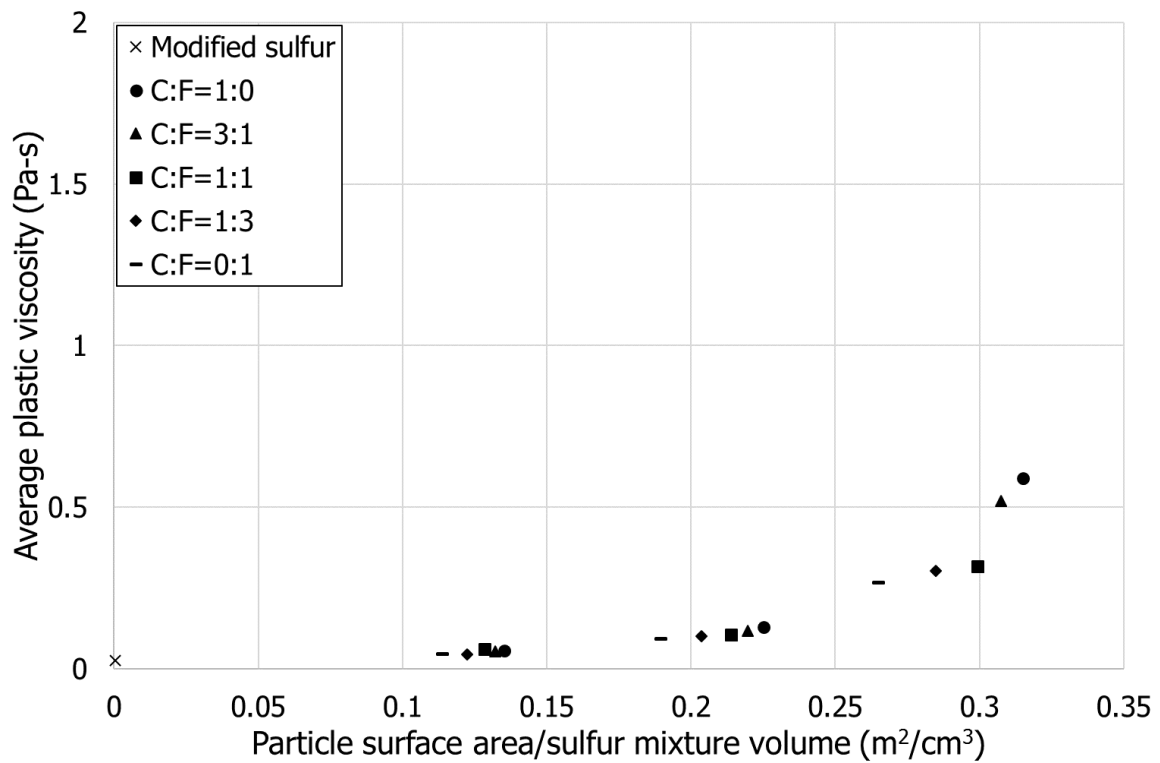
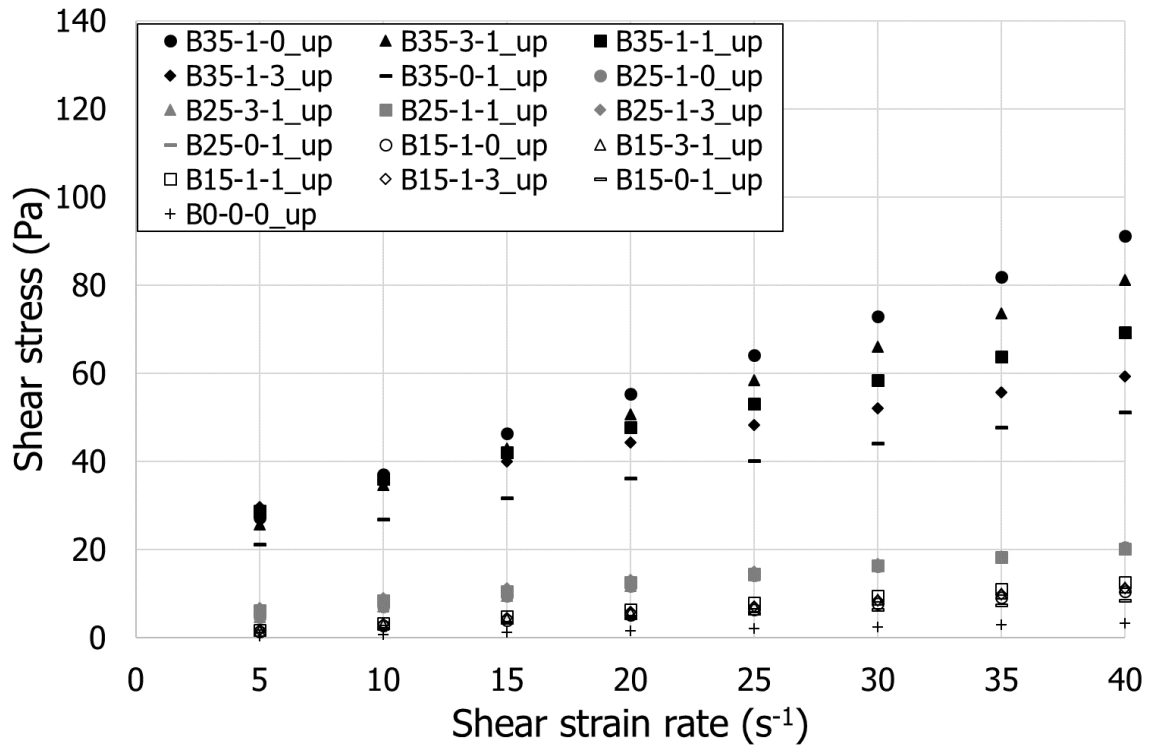


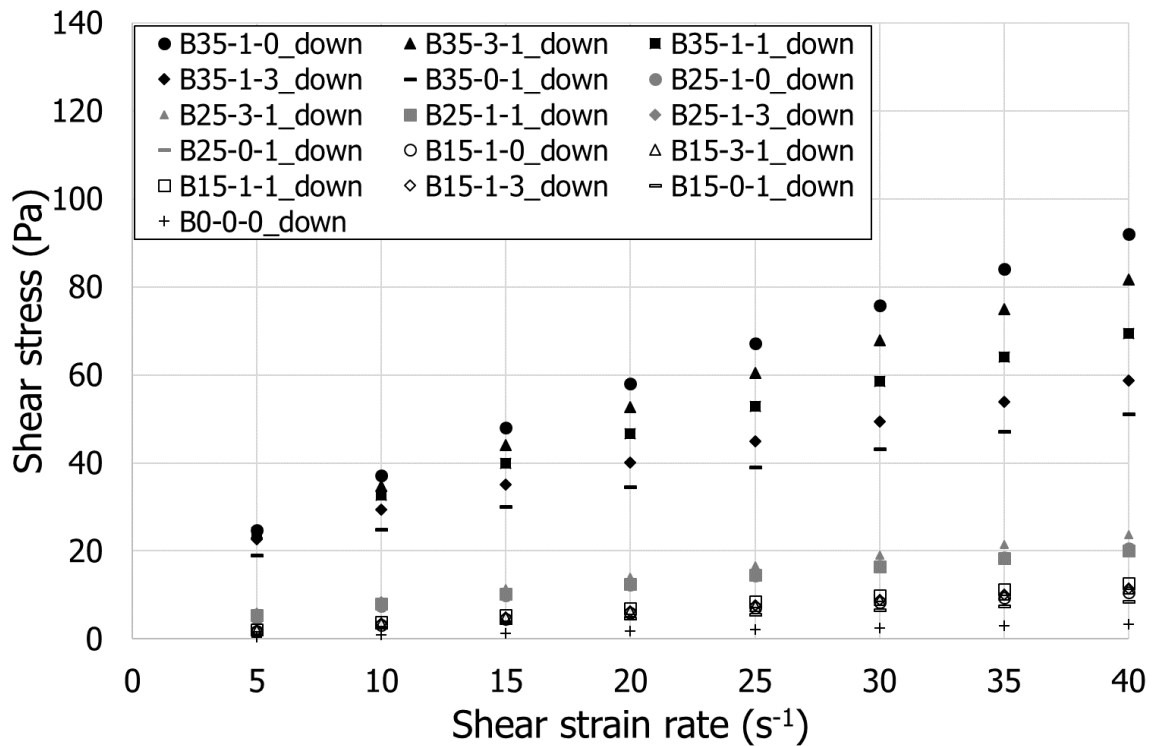
Figure 6-9: Average plastic viscosity of fresh sulfur mixtures with varying total surface area of micro-filler at 120°C.

Unlike the conditions at 120°C, the second shearing cyclic history presented a higher level of shear stress than the first shearing cycle at 140°C (Figs. 6-10 and 6-11), at which point overall viscosity of each mixture increased (Table 6-5). Because the modification between elemental sulfur and DCPD is usually promoted at 140°C, molten modified sulfur can involve a further reaction of sulfur at 140°C [3], which leads to the formation of a longer chain of amorphous sulfur ( $S_8$ ) inducing a larger viscosity. In addition, as the used modified sulfur was prepared using a relatively low concentration (3.1%) of DCPD, the molten modified sulfur might include a lower proportion of polysulfides than those modified with a higher concentration of DCPD. Thus, it was deemed that a larger portion of amorphous sulfur ( $S_8$ ) was ready to actively form longer sulfur chains in the molten modified sulfur than those with a higher dose of DCPD. Therefore, the flow curve at 140°C was estimated using only the first shearing cycle in this study.

As with the mixtures at 120°C, for a given portion of micro-filler up to 25%, the fresh sulfur mixtures barely reflected the effect of total surface area of the used micro-filler on the flow curves at 140°C (Fig. 6-10, Table 6-5). As expected, the mixtures usually exhibited a higher level of both yield stress and plastic viscosity according to a more portion of micro-filler. In the series of “35% micro-filler”, both the yield stress and the plastic viscosity increased from 15.9 to 21.7 Pa, and from 0.875 to 1.805 Pa-s, respectively. As shown in Figs. 6-12 and 6-13, in the “35% micro-filler” series, an increasing total surface area of the used micro-filler in unit volume of sulfur mixture resulted in the growth of both the yield stress and the plastic viscosity.

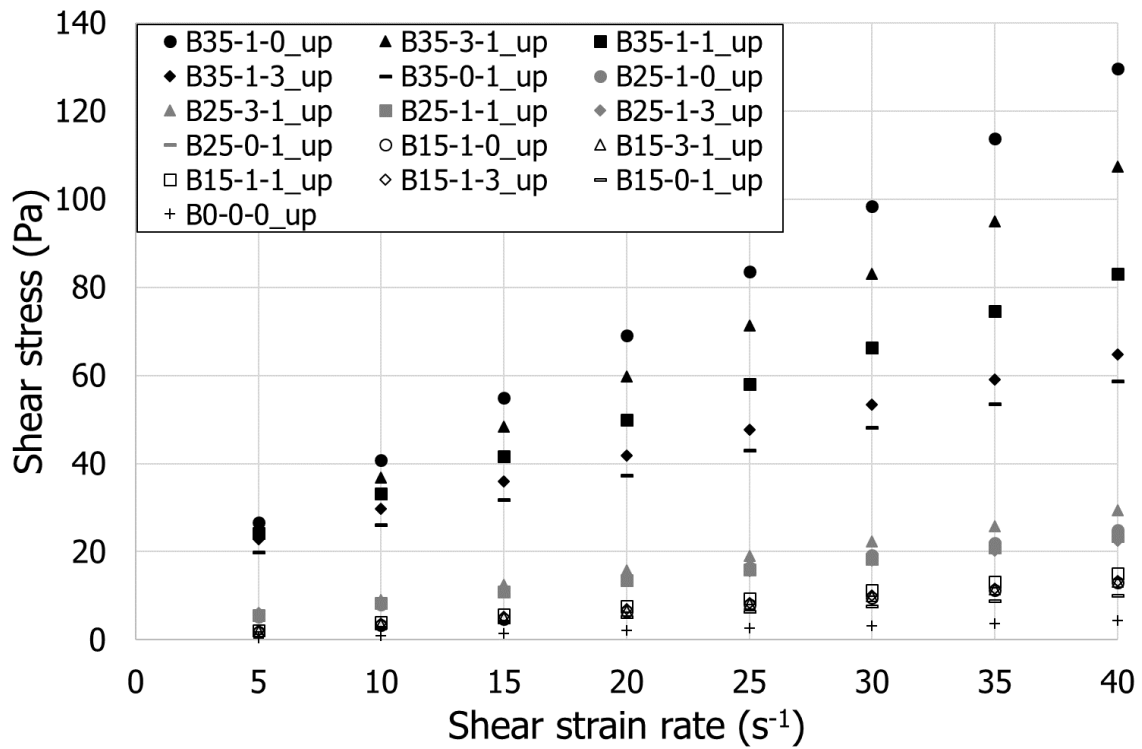


(a)

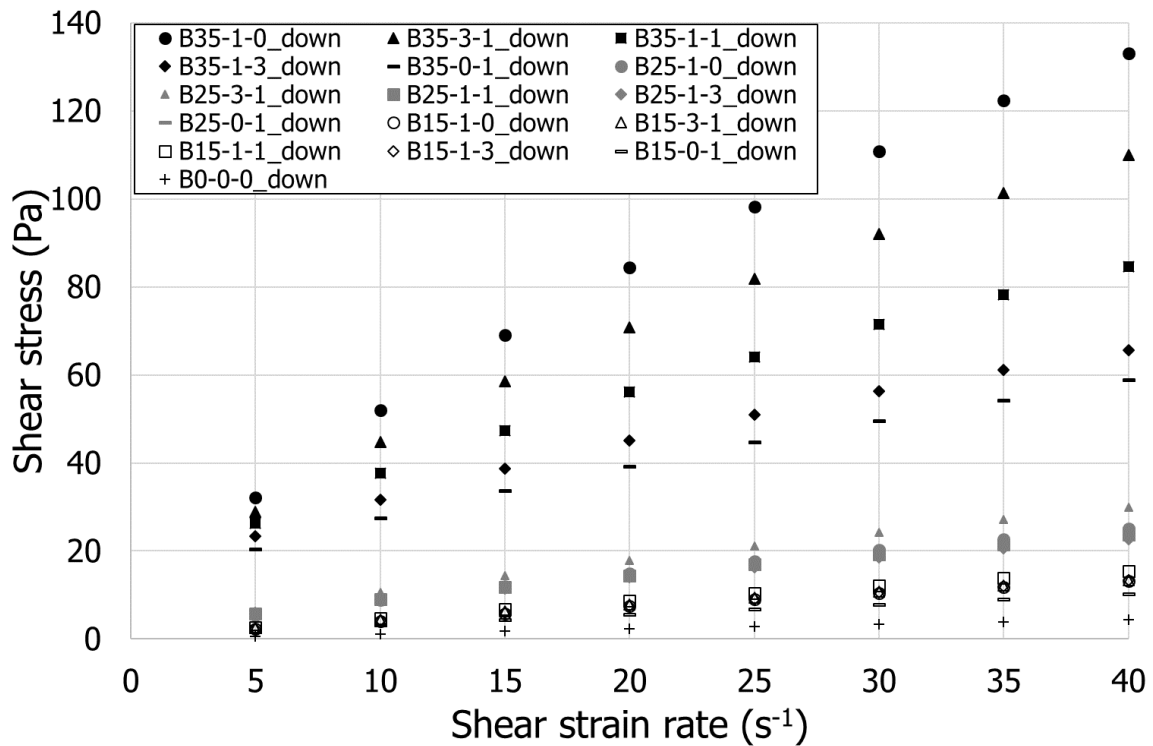


(b)

Figure 6-10: Shear stress-strain rate responses of fresh sulfur mixtures during first shearing cycle at 140°C: (a) up-curve, (b) down-curve.



(a)



(b)

**Figure 6-11: Shear stress-strain rate responses of fresh sulfur mixtures during second shearing cycle at 140°C: (a) up-curve, (b) down-curve.**

**Table 6-5: Average yield stress and plastic viscosity of fresh sulfur mixtures during 1<sup>st</sup> shearing cycle at 140°C.**

Mixture label	Total surface area of micro-filler (m <sup>2</sup> /cm <sup>3</sup> )	Yield stress (Pa), (CV*)	Plastic viscosity (Pa-s), (CV)
B0-0-0	0	0.02 (1.00)	0.080 (0.00)
B15-1-0	0.237	0.40 (0.75)	0.255 (0.02)
B15-3-1	0.131	0.44 (0.70)	0.275 (0.02)
B15-1-1	0.125	0.56 (0.59)	0.305 (0.02)
B15-1-3	0.123	0.66 (0.33)	0.270 (0.00)
B15-0-1	0.110	0.60 (0.05)	0.200 (0.00)
B25-1-0	0.395	2.82 (0.06)	0.450 (0.00)
B25-3-1	0.218	3.08 (0.07)	0.520 (0.00)
B25-1-1	0.208	4.18 (0.08)	0.405 (0.04)
B25-1-3	0.205	4.77 (0.11)	0.390 (0.03)
B25-0-1	0.183	3.67 (0.04)	0.420 (0.02)
B35-1-0	0.553	21.7 (0.04)	1.805 (0.01)
B35-3-1	0.305	20.2 (0.02)	1.545 (0.00)
B35-1-1	0.291	19.5 (0.01)	1.240 (0.03)
B35-1-3	0.287	19.1 (0.00)	0.970 (0.04)
B35-0-1	0.256	15.9 (0.00)	0.875 (0.03)

\* CV denotes coefficient of variation.

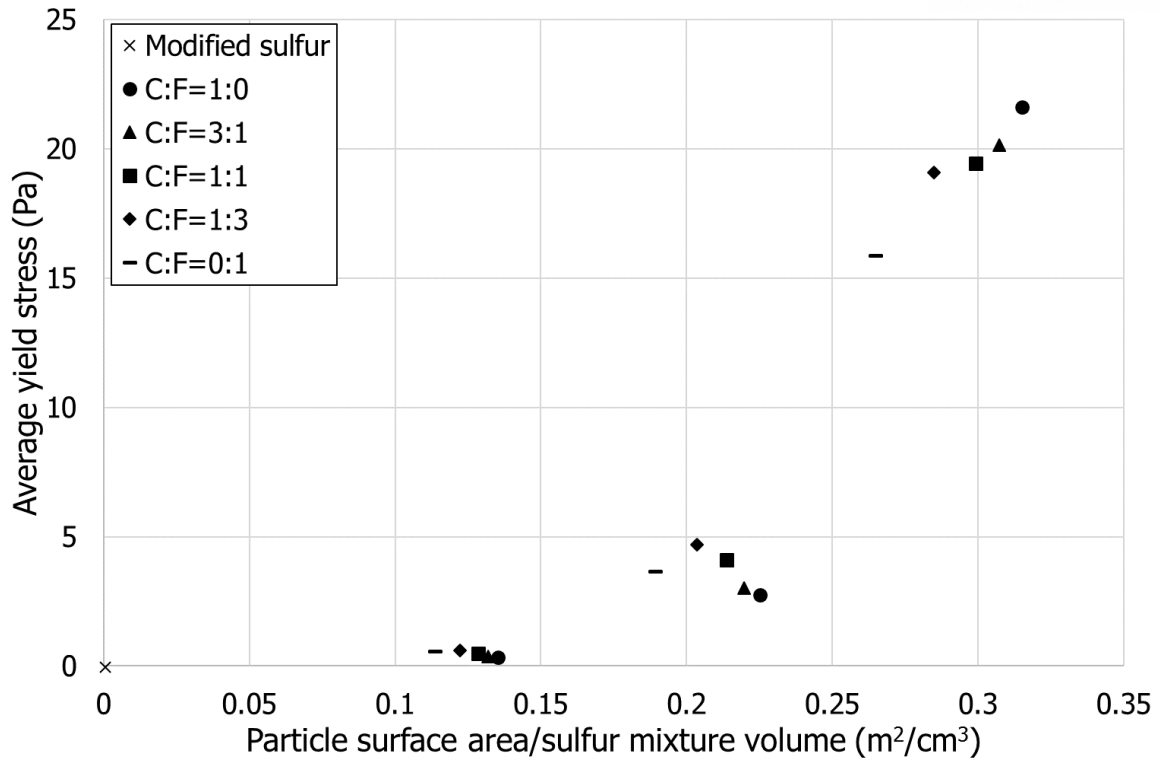


Figure 6-12: Average yield stress of fresh sulfur mixtures with varying total surface area of micro-filler at 140°C.

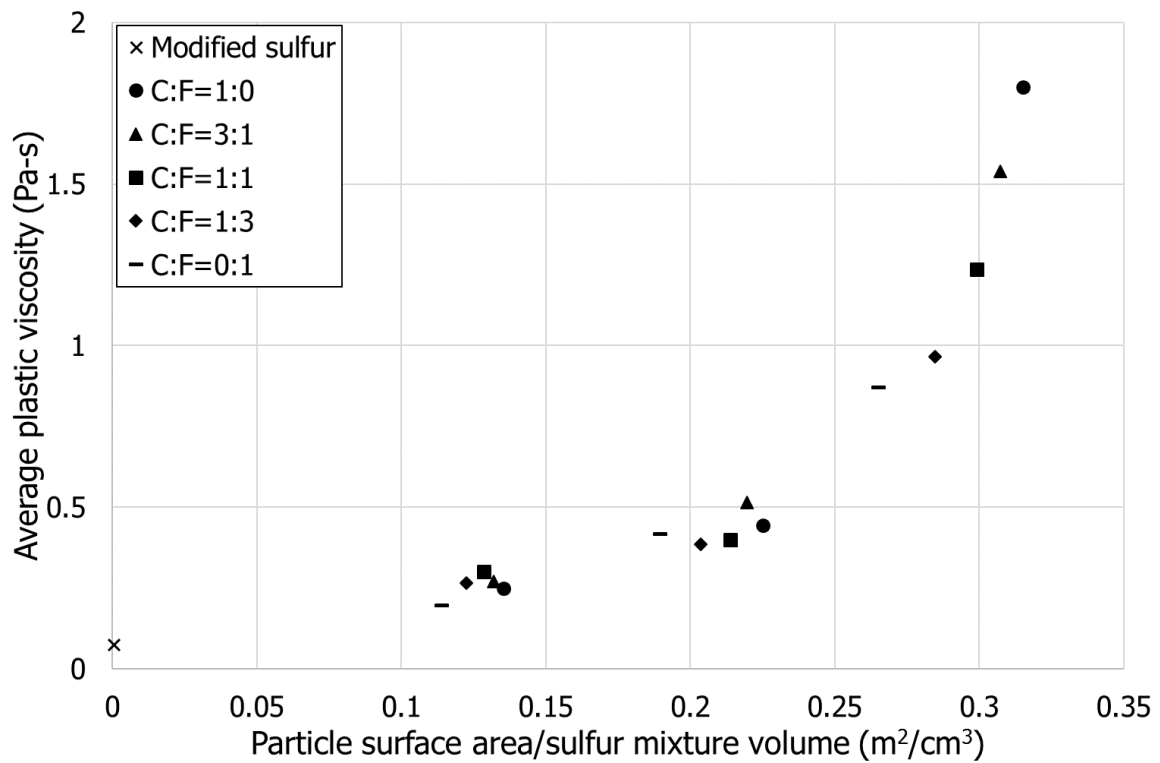


Figure 6-13: Average plastic viscosity of fresh sulfur mixtures with varying total surface area of micro-filler at 140°C.



#### 6.3.4. Mini slump flow

As soon as the fresh sulfur mixtures were ready for casting, their surface temperature were generally about 140°C so that the measured spreads could represent flow behavior at a real placement conditions. The fresh modified sulfur (Mixture B0-0-0) showed the biggest average spreading diameter (477.5 mm) as expected (Fig. 6-14). With a higher proportion of micro-filler, the average spreading diameters of fresh sulfur mixtures became smaller. This observation was also reflected in the growth of yield stress of fresh sulfur mixtures with a higher proportion of micro-filler through the rheology test at 140°C (Table 6-5). For a given total fraction of micro-filler, an increasing ratio of Portland cement as compared to fly ash resulted in a smaller spreading diameter, which was likely associated with the total surface area of Portland cement being larger than that of fly ash (Table 6-3).

Compared to the others, the mixtures with 35% micro-filler exhibited a drastic fall of average spreading diameters. Among them, Mixture B35-1-0 (with only Portland cement) presented a reduction in spreading diameter of approximately 50.7% compared to Mixture B0-0-0. This phenomenon corresponded fairly well to the rheology test result that Mixture B35-1-0 showed the highest average yield stress at 140°C. Accordingly, the correlation between the yield stress from the rheology test and mini slump flow was well understood quantitatively. Thus, it was deemed that the flow behavior of fresh sulfur mixtures was subjected to both the total portion and surface area of the used micro-filler at an operative temperature of 140°C.

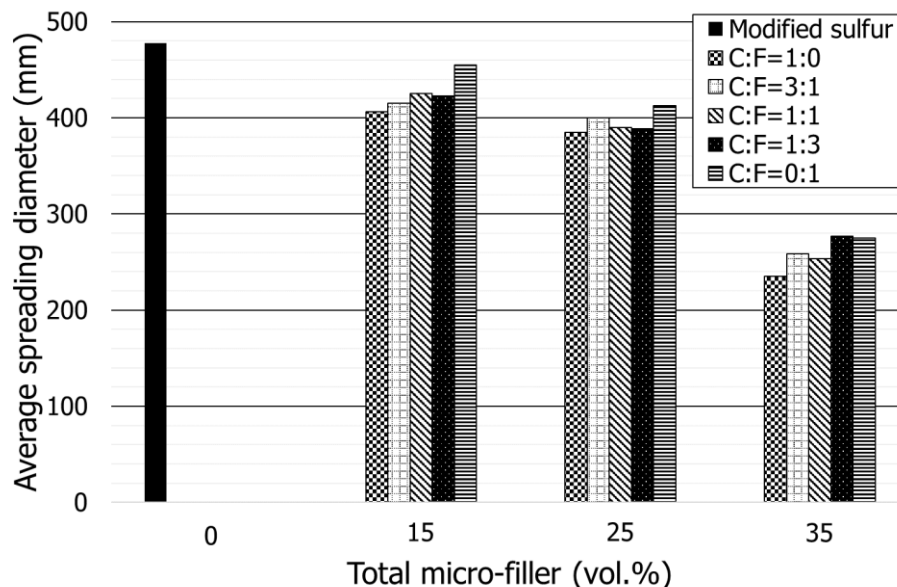


**Figure 6-14: Average spreading diameter versus total micro-filler responses of fresh sulfur mixtures with varying cement/fly ash ratios.**

#### 6.4. Conclusions

This study mainly examined the coupled effect of the particle characteristics of micro-filler and temperature on the rheological properties of fresh sulfur mixtures using a rheometer. In addition, the flow behaviors of all the fresh sulfur mixtures were empirically identified through a mini slump test. The main finding of this study was that both the total proportion and surface area of the used micro-filler had a substantial effect on the rheological properties of fresh sulfur mixtures at a certain operative temperature at 120 or 140°C. The summary and conclusions from this study are summarized as follows:

- ✓ Regardless of temperature, an increasing portion of micro-filler led to a gradual growth of the yield stress as well as the plastic viscosity of the fresh sulfur mixtures. For a given portion of micro-filler up to 25%, however, the rheological indices were not clearly distinguished between the mixtures despite the different total surface areas of the used micro-fillers at both 120 and 140°C. This phenomenon appeared to be associated with the relatively lower viscous mixtures compared to “35% micro-filler” series.
- ✓ At 120°C, the shear stress of each fresh mixture traced a similar history at each shear strain rate under the repeated shearing cycles, which barely suggested a thixotropy. All the mixtures containing 35% micro-filler showed a gradual growth in both the yield stress and the plastic viscosity according to a larger total surface area of the used micro-filler.
- ✓ At 140°C, each fresh mixture presented a higher level of shear stress in the second shearing cycle compared to the first shearing cycle. This likely originated from the further production of longer amorphous sulfur chains in the fresh modified sulfur. Thus, only the first shearing cycle was used for the estimation of flow curve. For a given 35% micro-filler, an increasing total surface area of the used micro-filler led to a progressive increase in both the yield stress and the plastic viscosity.
- ✓ Overall, the fresh sulfur mixtures with a surface temperature of about 140°C showed a smaller spreading diameter with a higher proportion of micro-filler through the mini slump flow test. This observation was in parallel with the increased yield stress due to a higher proportion of micro-filler through the rheology test at 140°C. Moreover, for each total portion of micro-filler, it was clearly seen that the spreading diameter became smaller in the fresh sulfur mixtures with a larger total surface area of micro-filler.
- ✓ The hardened sulfur composites showed a higher compressive strength as the total proportion of micro-filler that had a larger total surface area was increased. Therefore, it was deemed that both the fresh and hardened properties of modified sulfur composites were greatly governed by the particle characteristics of the micro-filler.

## 7. Self-Healing Properties of Modified Sulfur Polymer Composites Containing Binary Cement and Superabsorbent Polymer

### 7.1. Introduction

Contrary to elemental sulfur, modified sulfur polymer generally exhibits a superior resistance to water environment, consequently displaying greater durability under aggressive chemical solutions, and rapid development of ultimate compressive strength [3,41]. Above all, as the modified sulfur polymer is a thermoplastic material, it excludes water in the fabrication of sulfur composites or concretes [3,16]. Meanwhile, modified sulfur composites or concretes exhibit a severe brittleness especially under compression [42,58]. During last few decades, sulfur concrete has been utilized in the production of precast concrete structures, usually exposed to water environments, such as in sewer pipes [90]. Nowadays, artificial fishing reefs and tetrapods are also in the stage of early adaptation using sulfur concrete [91]. In spite of the superior benefits of sulfur concretes, those structures made of sulfur concrete are vulnerable to severe impact loads inducing cracks [3]. Even though sulfur concretes possess high compressive strength, they are susceptible to tensile cracks if they are not reinforced, just as in hydraulic cement concrete.

Recently, many sinkholes have been found around the world. It has been reported that they mostly happened due to the deterioration of concrete sewer pipes [92], followed by cracks leading to water leakage out of the pipes. Thus, the outflow of water eroded the surrounding soil. As with concrete tetrapods in seashores, they are known to suffer severe degradation (cracks) during their lifespan because of continuous wave [93]. Once their legs are broken, they lose their efficiency to absorb the wave's energy. As for the two examples above, the life cycle cost of existing concrete structures will rise unless there are countermeasures taken against these cracks.

Considering the aforementioned issues with concrete structures in aggressive environments, it is recommended that they are built with special concrete resistant to cracking. In order to achieve this, fiber-reinforced concrete or cement composites may be the most powerful solution. Although the fiber reinforcement of concrete converts the load transfer mechanism into a more even stress distribution followed by micro-cracks [72,73], in practice it cannot prevent the water leakage through the cracks. Thus, the lifespan of cracked concrete can be considerably extended if the cracks are recovered. As one of the concrete technologies, self-healing technology has emerged to prolong the service life of existing and future infrastructures [94]. Research on such technology has been mostly dedicated to autonomous healing (i.e., engineered healing) using bacteria [95,96], microcapsules [97,98], or organic or inorganic materials [99,100]. In addition, superabsorbent polymer has been employed as a self-healing agent to seal the crack volume on absorbing water [101,102]. However, because such self-healing agents are

usually promoted under the crack width ranging from 0.05 to 0.2 mm [103], several researchers have introduced those materials in engineered cementitious composites (ECC) or fiber-reinforced concrete (FRC) to assess the self-healing performance obviously [104,105]. Therefore, it is clear that current self-healing technology is greatly dependent on the engineered healing rather than the autogenous healing.

In a previous study, the author confirmed that the replacement of modified sulfur by micro-filler was effective in the development of compressive strength [58]. Moreover, when the micro-filler was prepared as a binary cement composed of Portland cement and fly ash, their particles remained intact in the hardened sulfur composites as discussed in Section 5. This observation revealed the feasibility of binary cement as a self-healing agent in sulfur composites. Accordingly, if cracking happens in the sulfur composites, some particles of binary cement on the crack surfaces will be exposed to the air. Eventually, they may undertake the autogenous healing due to their anhydrous phase unless water intrudes.

Provided that water can penetrate the cracks in real structures, this study investigated the self-healing properties of modified sulfur composites containing fine aggregate, Portland cement, calcium sulfoaluminate (CSA) expansive agent, and superabsorbent polymer (SAP) powder. Except the fine aggregate, all the materials were employed as self-healing agents. Among them, Portland cement and CSA expansive agent were prepared as a binary cement by varying the relative ratios between them, which offered different levels of self-healing capacity to the sulfur composites. In addition, the use of SAP powder was intended to rapidly seal the cracks on absorbing water, at which the surrounding binary cement was likely to be stuck stable to react with water.

The main purpose of this study is to develop self-healing sulfur composites and to evaluate their self-healing performances using a series of analysis techniques. In this study, all the samples were prepared using two split pieces from a cylindrical specimen with a 100-mm diameter and 50-mm height that were tightened to formulate a through crack with a certain width. To promote the self-healing of this induced crack, all the samples were subjected to a water curing or water permeability test. The former allowed the samples heal more slowly than the latter. Meanwhile, the latter was conducted to simulate real conditions in which water penetrates the cracks of damaged structures during a limited period of time. During each test, the closure of the surface crack area and width was monitored using an optical microscope. In addition, the extent of self-healing was evaluated and scanned using an elastic wave transmission and three-dimensional computed tomography (CT), respectively before and after crack healing.

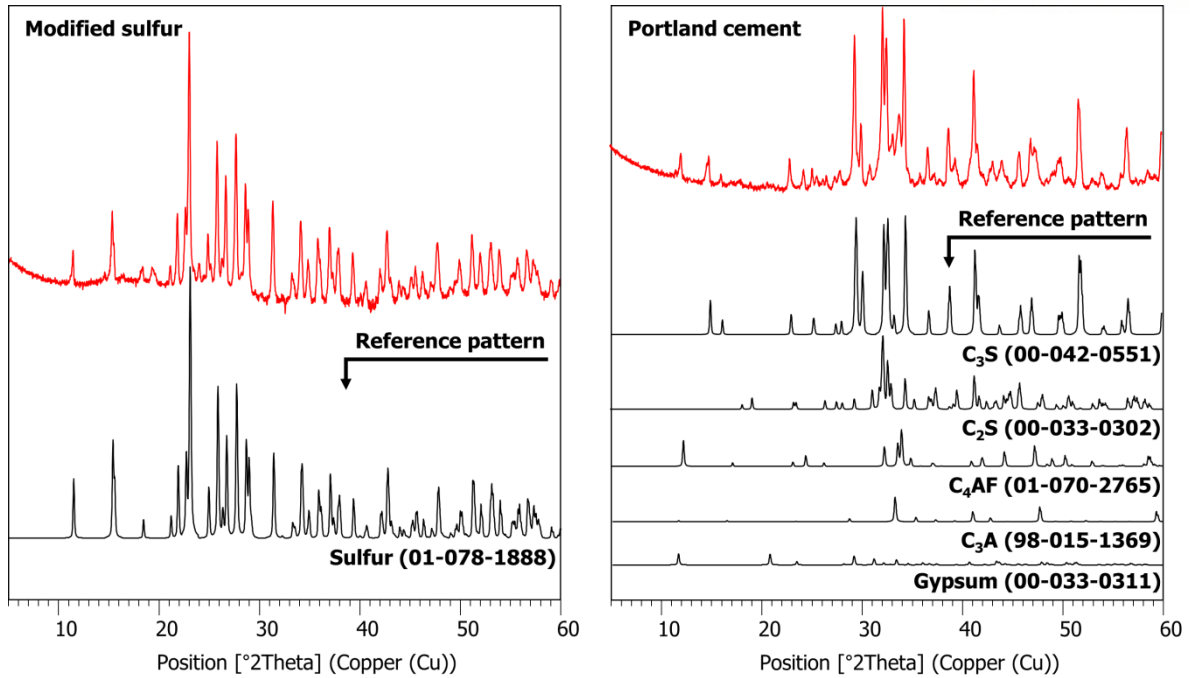
## 7.2. Experimental Program

### 7.2.1. Materials

In this study, the used modified sulfur was produced using 3.1 wt.% concentration of DCPD. As indicated in the chemical composition (Table 7-1), the measured XRD also reflected an orthorhombic sulfur (Fig. 7-1(a)). Type-I ordinary Portland cement (fineness: 3,690 cm<sup>2</sup>/g, density: 3.13 g/cm<sup>3</sup>) and fine aggregate (density: 2.61 g/cm<sup>3</sup>) with a maximum particle size of 2 mm were used. CSA expansive agent (fineness: 4,310 cm<sup>2</sup>/g, density: 2.88 g/cm<sup>3</sup>) exhibited a larger portion of aluminum oxide and sulfur oxide than Portland cement (Table 7-1), which were also reflected in the XRD result that displayed dominant peaks from anhydrite and yeelimite (Fig. 7-1(c)). SAP powders (bulk density: 0.6~0.8 g/cm<sup>3</sup>), which were irregularly-shaped as shown in Fig. 7-2(a), were used. The SAP powders (LG Chemistry) composed of sodium polyacrylate (≥92%) and water (≤8%) was produced by a bulk polymerization and subsequent pulverization. Wet SAP powders exposed to tap water for 10 min, which had swollen appearance as shown in Fig. 7-2(b), had a maximum particle size of approximately 435 μm (Fig. 7-3). From the particle size analyses using a laser diffraction, it was seen that the dry SAP powders had the largest total surface area as compared to Portland cement and CSA expansive agent (Fig. 7-3).

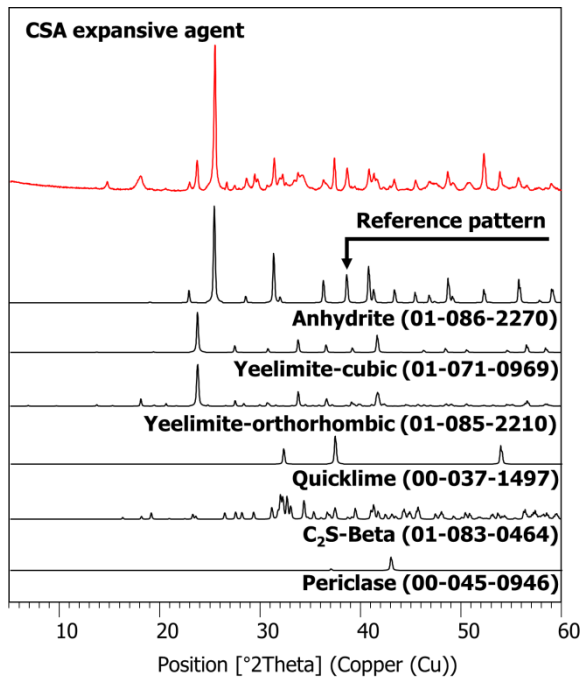
**Table 7-1: Chemical oxide compositions of modified sulfur, Portland cement, and CSA expansive agent.**

Oxide (wt.%)	Modified sulfur (DCPD 3.1%)	Portland cement	CSA expansive agent
CaO	-	67.0	56.7
SiO <sub>2</sub>	-	17.3	3.0
Al <sub>2</sub> O <sub>3</sub>	-	4.3	7.2
Fe <sub>2</sub> O <sub>3</sub>	-	3.9	0.8
SO <sub>3</sub>	99.8	3.4	30.5
MgO	-	1.8	0.9
K <sub>2</sub> O	-	1.3	0.2
TiO <sub>2</sub>	-	0.3	0.4
Na <sub>2</sub> O	-	0.1	0.1
MnO	-	0.2	-
P <sub>2</sub> O <sub>5</sub>	-	0.2	-
Others	0.2	0.2	0.2



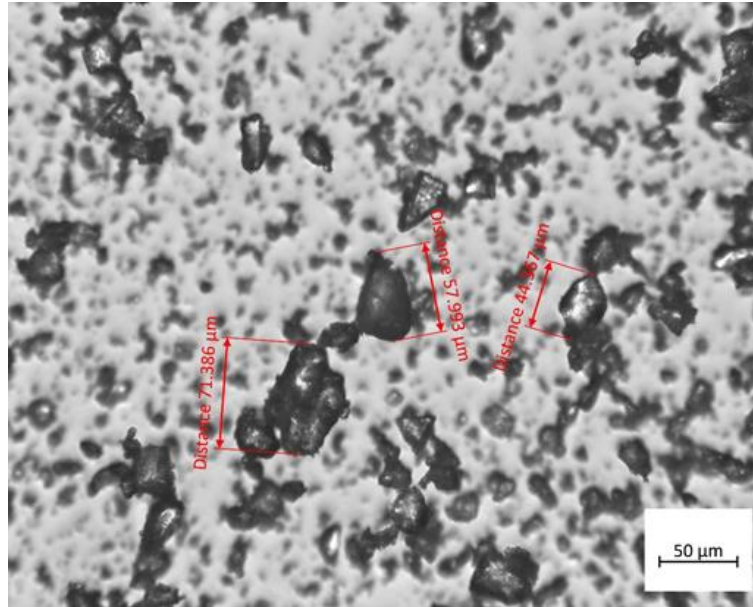
(a)

(b)

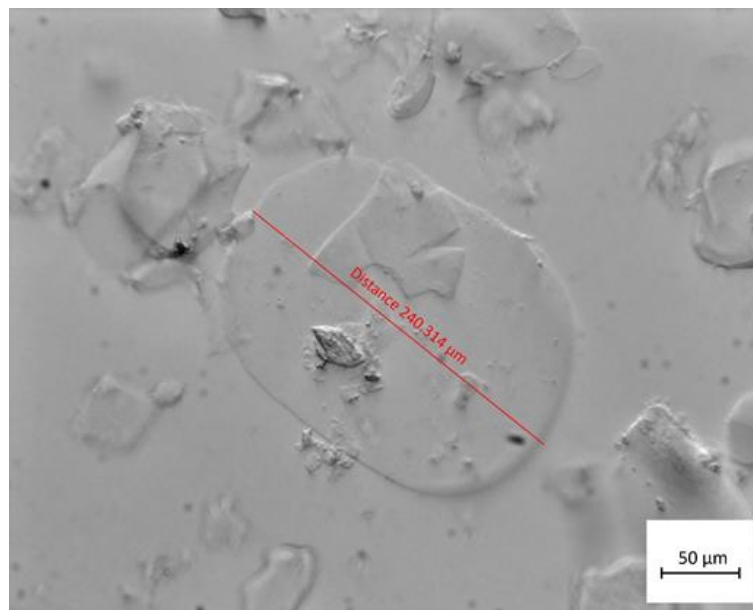


(c)

**Figure 7-1: XRD patterns of raw materials: (a) modified sulfur, (b) Portland cement, and (c) CSA expansive agent.**



(a)



(b)

**Figure 7-2: Microscopy images of SAP powders: (a) dry, (b) wet (exposed to tap water for 10 min).**

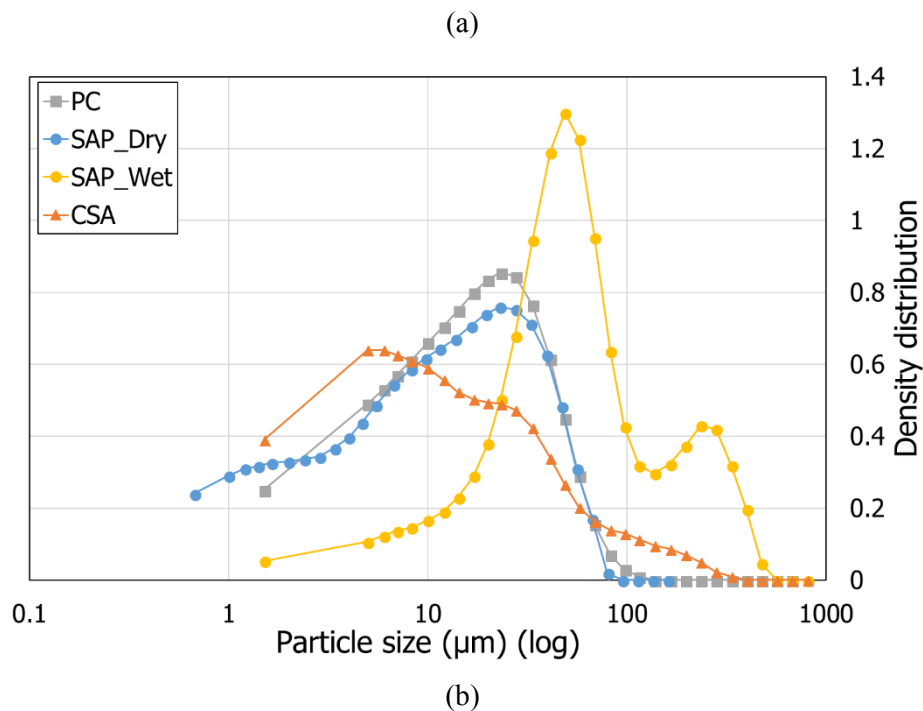
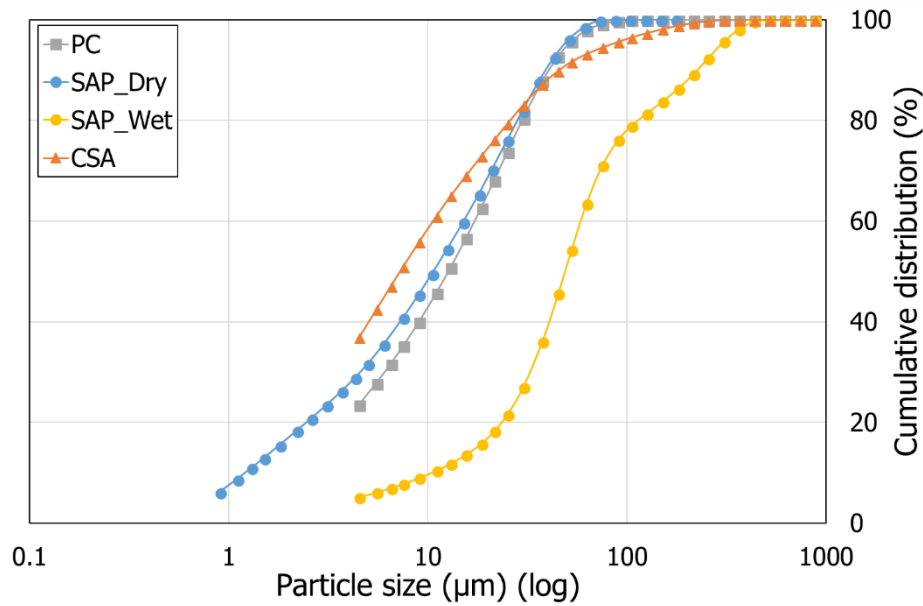


**Figure 7-3: Particle size distributions of Portland cement, dry SAP powders, wet SAP powders, and CSA expansive agent: (a) cumulative, (b) density.**

### 7.2.2. Mix proportions

In this study, a total of eight mix proportions were developed by mainly adjusting both the relative ratios between Portland cement and CSA expansive agent as the binary cement, and the dose of SAP (Table 7-2). The portions of the modified sulfur and sand were fixed at 40 and 35 vol.%, respectively. Thus, the remaining 25 vol.% of the sulfur composites consisted of Portland cement and



CSA expansive agent, which were prepared in four different ratios to render different hydration extent. Finally, SAP was included additionally in a relative 5 wt.% of the modified sulfur or not. In the nomenclature of the mixture, the first character and figure stand for SAP and its volume ratio, respectively. The last figure is the portion of CSA expansive agent, i.e., its subtraction from 25% corresponds to the portion of Portland cement.

**Table 7-2: Mix proportions of tested sulfur polymer composites.**

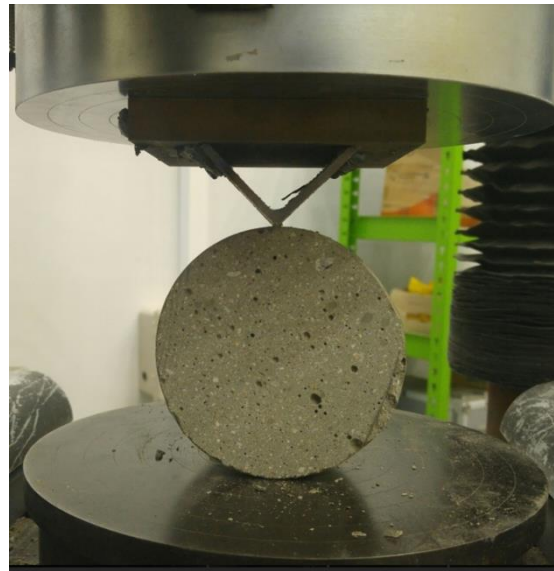
Mixture label	Modified sulfur		Binary cement				Sand		SAP
			Portland cement		CSA expansive agent				
	vol.%	kg/m <sup>3</sup>	vol.%	kg/m <sup>3</sup>	vol.%	kg/m <sup>3</sup>	vol.%	kg/m <sup>3</sup>	
S0-25			-	-	25	713			
S0-15	40	764	10	313	15	428	35	910	-
S0-10			15	470	10	285			
S0-0			25	783	-	-			
S5-25			-	-	25	713			
S5-15	40	764	10	313	15	428	35	910	5 wt.% of modified sulfur
S5-10			15	470	10	285			
S5-0			25	783	-	-			

### 7.2.3. Sample preparation

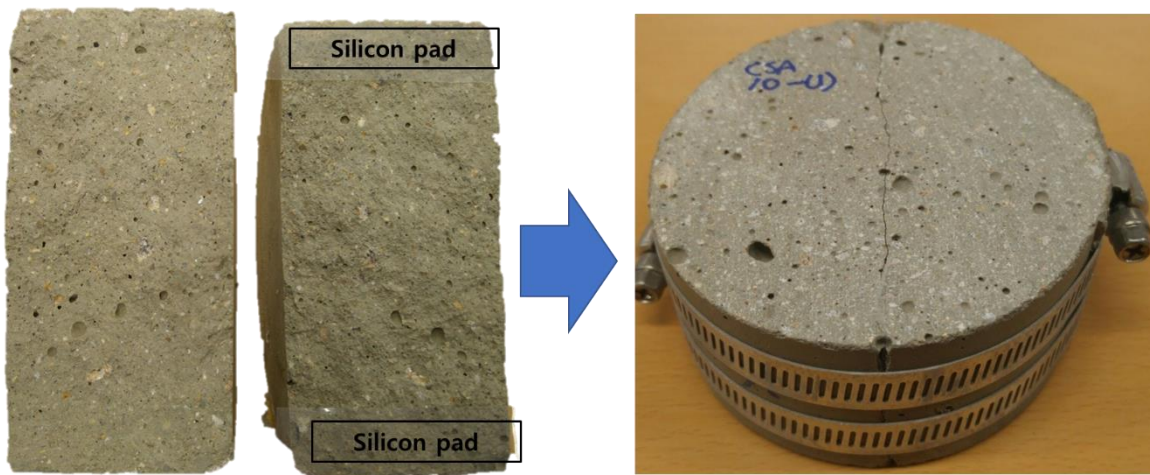
In order to prepare the sulfur mixtures, molten modified sulfur was initially prepared using a controlled mixing bowl at 140°C. Then, both binary cement (blend of Portland cement and CSA expansive agent) and sand, which had been preheated in an oven at 150°C for 6 hours, were poured into plastic modified sulfur and mixing continued for about 5 min. Then, SAP powder was poured into the mixture, which was mixed for 15 min as a whole using a mechanical hand mixer generating 100 rpm. All the instruments, such as steel molds and a mixing paddle, were preheated in the same way as for the binary cement and sand. Finally, the homogenized plastic mixtures with a surface temperature of approximately 140°C were prepared for casting.

Before making the through crack samples, cylindrical specimens with a diameter of 100 mm and a height of 200 mm were prepared, from which three slices of disk sample with a height of 50 mm were taken off. Then, they were split using a universal testing machine at a loading rate of 5 mm/min (Fig. 7-4(a)). As shown in Fig. 7-4(b), certain sheets of silicon pad with a thickness about 0.3 mm were inserted between the split pieces to produce a certain crack width and an effective crack length of 70 mm. Then, they were tightened using steel hose bands.

Two groups of through crack samples were prepared in this study. In the first group, one sheet of silicon pad was inserted at each end of the samples. The samples of the other group had two sheets of silicon pad at each end. Accordingly, the insertion of different sheets of silicon pad formulated distinct crack widths.



(a)



(b)

**Figure 7-4: Through crack sample preparation: (a) split tension test setup, (b) insertion of silicon pad and tightening.**

#### 7.2.4. Test methods

After 28 days of curing, compression tests were performed using the cylinder samples with a diameter of 50 mm and a height of 100 mm. At least three samples were tested for each mixture. The main purpose of the compression test was to investigate the effects of the relative ratios of Portland cement and CSA expansive agent, and the portion of SAP on the strength development of hardened sulfur composites. The detailed test conditions are specified in Section 2.3.1.

For the cracked samples, there were two environments for crack healing in this study. One was the water curing that kept the samples in a water bath at a controlled temperature of  $20 \pm 3^\circ\text{C}$ . The other was the water permeability test that allowed a constant pressure water head at 250 mm. As for the moment of splitting, the disk samples due for water curing with one sheet of silicon pad inserted were split after 20 days of curing, whereas all the others were split after 35 days of curing. Both the water curing and the water permeability test commenced when the disk samples were split.

In the water curing, all the cracked samples were immersed for seven days. Overall, the main objective of water curing was to promote a stable healing environment and to evaluate the self-healing performances of the sulfur composites. At specified curing ages from 12 h to 7 days, the self-healing of each crack sample was monitored using an optical microscope to measure a surface crack area. In addition, elastic wave tests were conducted for the samples which were crack-free, cracked, and crack-healed after 7 days of curing. Meanwhile, a series of cracked samples with one sheet of silicon pad was prepared separately and evaluated only by the CT before and after water curing.

Contrary to the water curing, the water permeability test was dedicated to evaluating the self-healing performance of sulfur composites under an instant water ingress. Only the cracked samples with one sheet of silicon pad were used in the water permeability test. They were tested without water curing. After the cracked samples were mounted at a testing device (Fig. 7-5(a)), the test commenced as soon as the pressure water head reached 250 mm. Instantaneously, the weight of water flow through the crack was measured using a precise balance (Fig. 7-5(b)). The outflow of water through the crack was measured every 15 sec during an initial 5 min and every 1 min afterward. The tests were carried out for 30 min considering that at least 5 min was needed for the SAP powder to achieve its maximum swelling [106]. Both the elastic wave test and surface crack monitoring were conducted before and after the water permeability test.

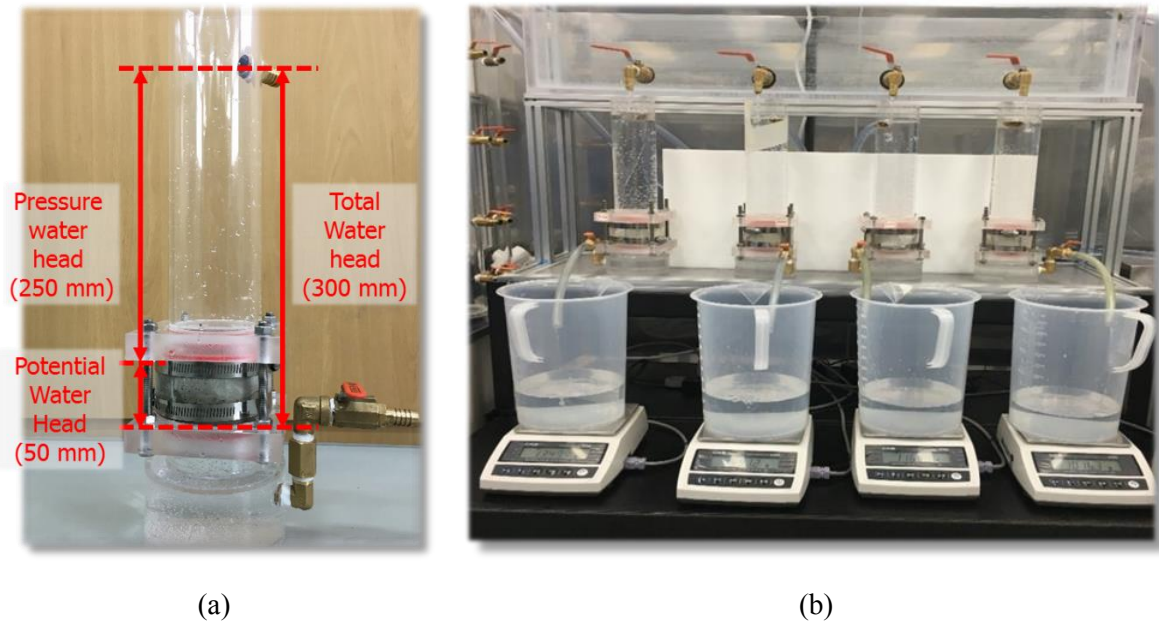


**Figure 7-5: Constant head water permeability test: (a) mounted sample, (b) entire test setup.**

The changes in the surface crack areas of the samples was acquired using a stereo zoom microscope (AxioZoom.V16, Zeiss, Germany) at the specified ages. Because this apparatus can automatically calibrate the z-axis of each tile-image and stitch all of them together, the stitched images cover a large field in focus. At the specified ages, the objective field of the sample was appointed at the strip of entire crack, which was used to measure the area of surface crack at a chosen region. Consequently, an average width of the surface crack was calculated by dividing the measured area by an effective crack length.

As a nondestructive technique, the extent of crack healing was evaluated by measuring the elastic wave signal transmission of the samples that were crack-free, cracked, and healed. A small aluminum cone attached transducer (Proceq P-wave transducer, no. 325 40 131) with a 54 kHz center frequency were attached as a transmitter and a pair of accelerometers (PCB 353 B 15) were attached as a receiver. The pair of receivers were affixed by couplant on the surface of specimen. The spacings between the impact and receiver, and between two receivers were 20 mm (Fig. 7-6). 50 kHz pulse signals were generated through a function generator (Keysight Technologies 33512 B) with 50 Hz repetition rates. Then, the generated signals were amplified using a power amplifier (NF HSA-4014). The transient signals across the receivers were amplified 10 times by a signal conditioner (PCB 482 C 15), and the amplified signals were digitized by a digitizer (Pico Technology Picoscope 4262). The sampling rate of the digitizer was 2.5 MHz and the measured raw data were time-averaged 100 times to improve signal-to-noise ratios. All the locations of the impacts and receivers were marked and kept constant for each test conducted for all the samples. Because the signal consistency of the tests was in the frequency range of 10 to 60 kHz, the signals in this domain were analyzed.

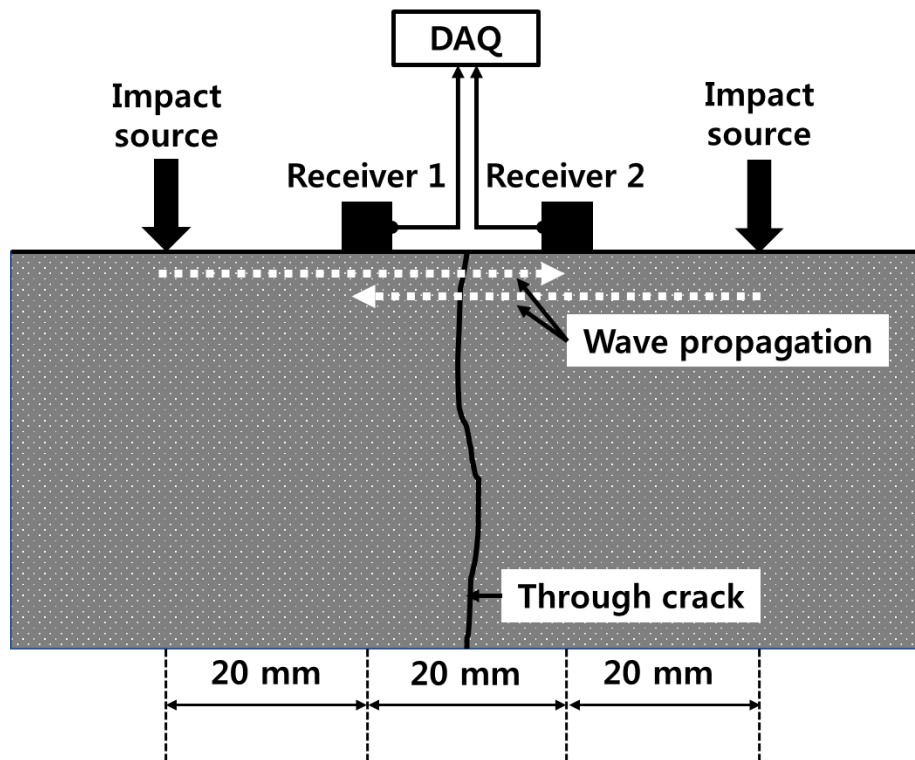


**Figure 7-6: Transmission of elastic wave in a through crack sample.**

Fig. 7-7(b) shows the specimen mounted on a microfocus 3D CT system (XT H 320, Nikon, Japan). It consists of an X-ray source which emits a high voltage range up to 320 kV delivering up to 320 W of power, and a high resolution flat panel which is used to collect high quality images. The X-ray CT tests were performed to visualize any change in cracked volume according to the swelling of the SAP and the setting and hydration of the binary cement resulting from water inflow. Thus, the CT tests were conducted before and after the water curing. After completion of the water curing, all the samples were kept in a dry room at a temperature of  $20 \pm 3^\circ\text{C}$  for 24 h to remove the remaining water in the crack volume. Then, the tests commenced.

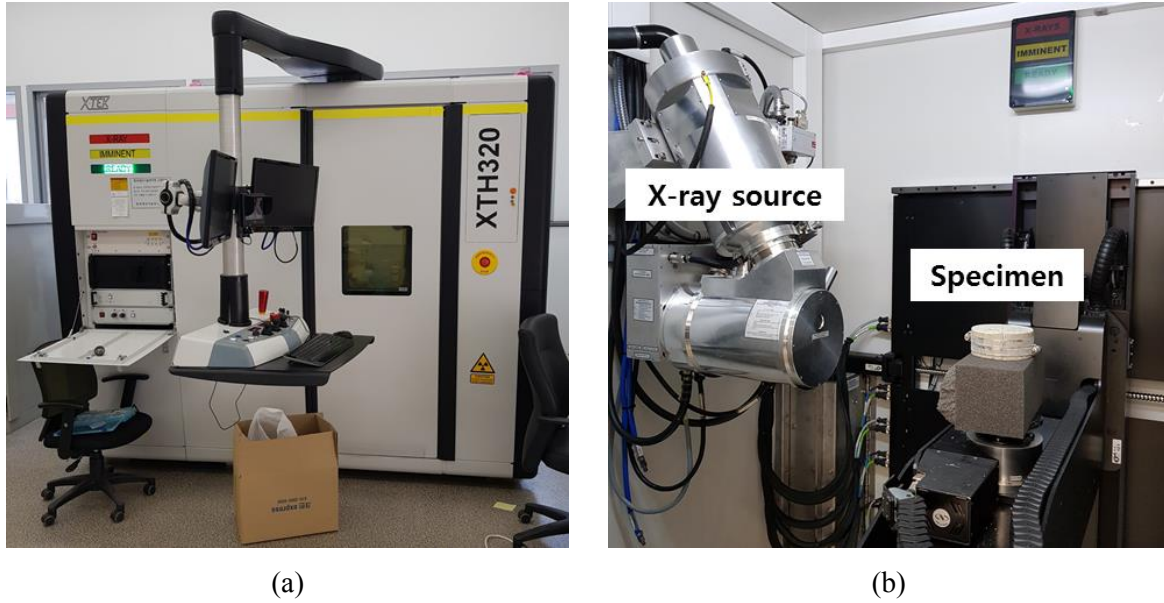


**Figure 7-7: X-ray CT test setup: (a) test device, (b) specimen mounted on CT scanner.**

### 7.3. Results and Discussions

#### 7.3.1. Compressive strength

Overall, the sulfur composites with 5% SAP developed lower compressive strengths than those with no SAP (Table 7-3, Fig. 7-8). This phenomenon was deemed because of the low density of dry SAP powder that likely increased the total porosity of the sulfur composites [107,108]. In both cases of “0% SAP” and “5% SAP”, the compressive strengths of the sulfur composites generally became lower according to a more CSA expansive agent. In other words, a higher dose of Portland cement than CSA expansive agent in the given binary cement caused a higher compressive strength. This phenomenon was deemed attributable to the larger indentation modulus of raw Portland cement than CSA expansive agent [61], as was reflected in the larger density of Portland cement than the CSA expansive agent. In spite of the strength reduction due to 5% SAP, all the samples in this study developed a compressive strength of at least 20 MPa.

**Table 7-3: Compressive strengths of the tested composites.**

Mixture label	Compressive strength (MPa)	
	Average	Standard deviation (CV*)
S0-25	45.3	9.77 (0.22)
S0-15	62.1	1.39 (0.02)
S0-10	64.8	5.81 (0.09)

S0-0	58.3	0.02 (0.00)
S5-25	26.9	2.82 (0.10)
S5-15	20.0	1.32 (0.07)
S5-10	41.1	2.27 (0.06)
S5-0	53.5	0.04 (0.00)

\* CV denotes coefficient of variation.

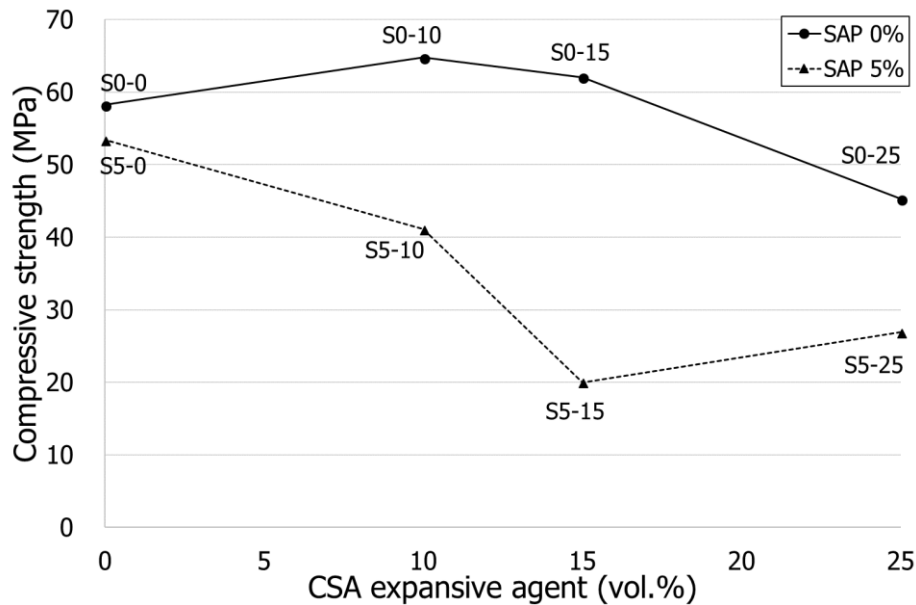


**Figure 7-8: Compressive strengths of tested sulfur composites.**

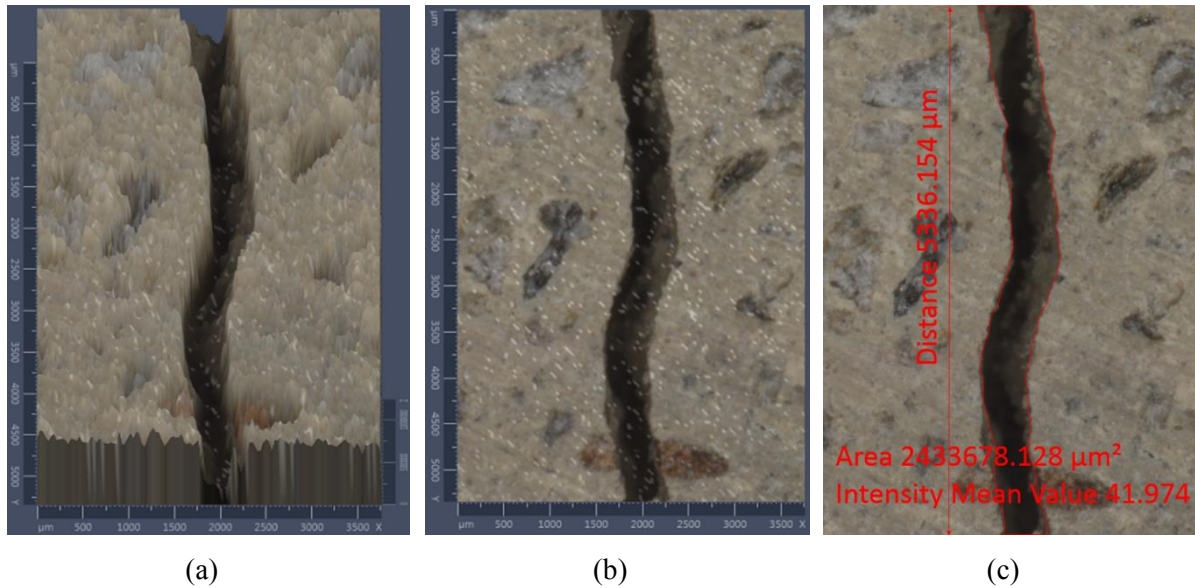
### 7.3.2. Water curing

In order to foster a stable environment for the self-healing of through cracks, two groups of through crack samples were cured in a water bath for 7 days. Initial crack widths of all the samples were effectively formulated by inserting different sheets of silicon pad. The extent of self-healing for all the samples was monitored using a microscope, and was evaluated by an elastic wave transmission. In addition, the through crack samples with one sheet of silicon pad on each edge were cured separately from the foregoing two groups and tested only by the X-ray CT. The detailed test results are discussed as follows.

#### 7.3.2.1. Surface crack monitoring

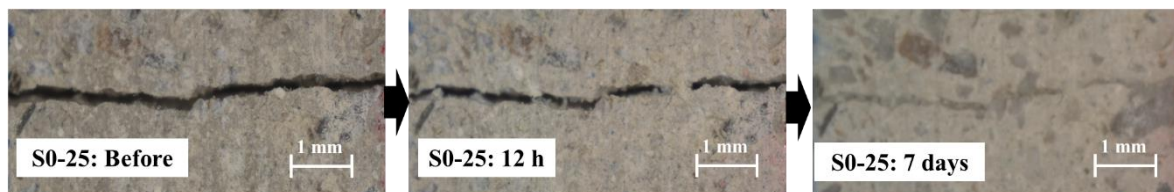
Fig. 7-9 shows an example of measuring a surface crack area. Because the microscope used could calibrate the z-axis of the acquired surface image, it offered 2.5 dimensional images (Fig. 7-9(a)),

which were used to select crack edges distinctly. Thus, average crack width was calculated by dividing the measured surface crack area by an effective crack length in a selected region for analysis (Fig. 7-9(c)). Thus, initial surface crack widths of all the samples were calculated and successively compared with the others at different curing ages. In this study, the calculated crack width was deemed to represent the average crack width of a sample as an alternative to a few measurements of line distance between the crack. At each curing age, the region of analysis was kept the same for each sample.

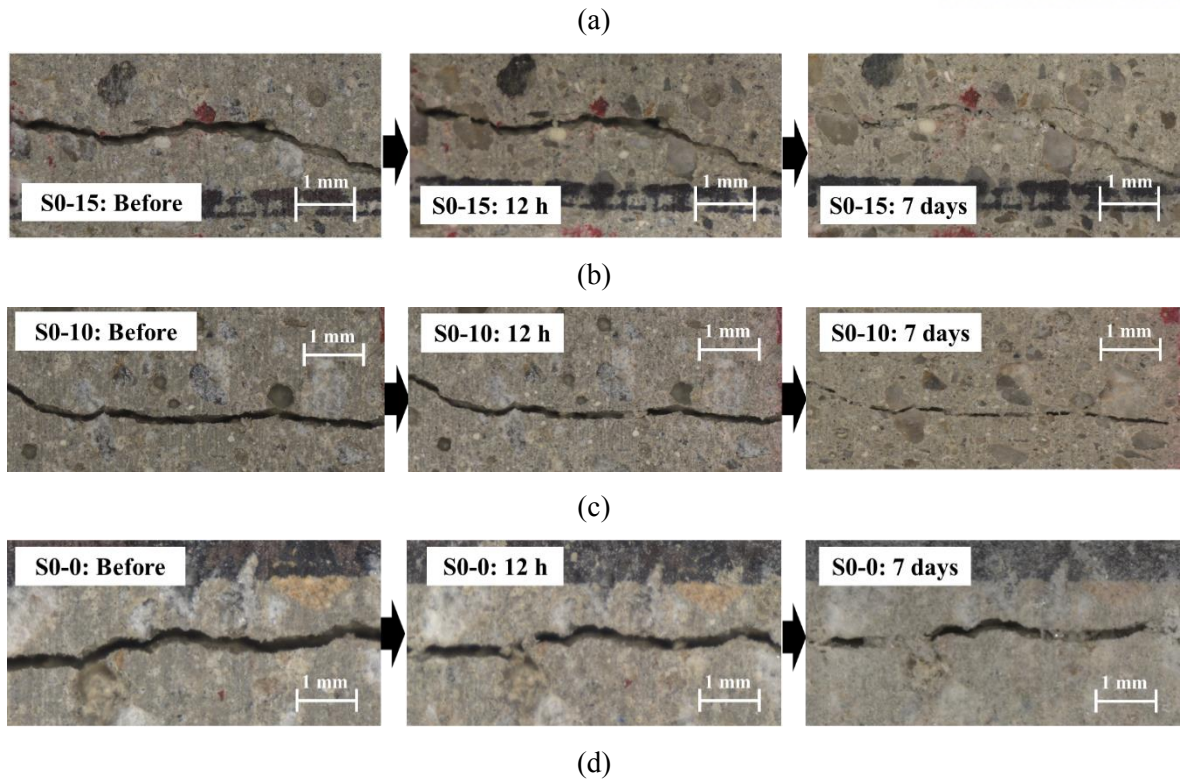


**Figure 7-9: An example of measuring surface crack area: (a) 2.5D image, (b) 2D image, (c) measured crack area.**

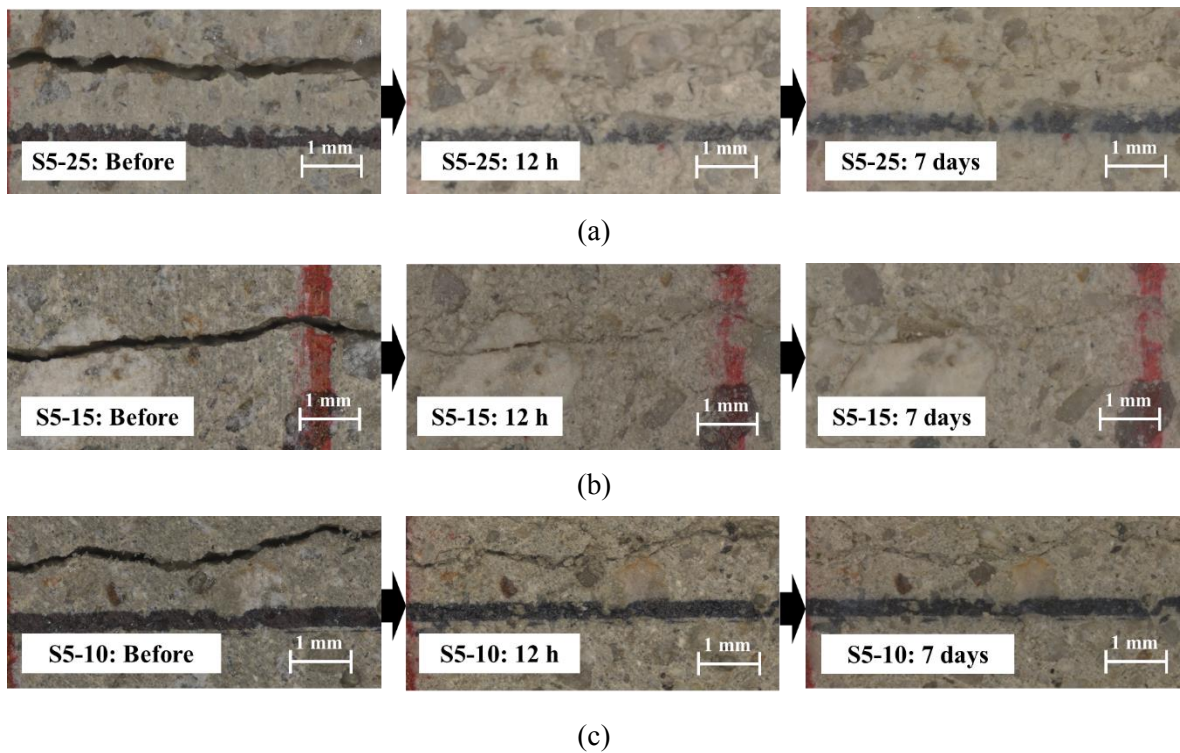
As shown in Table 7-4, initial crack widths of the samples holding one sheet of silicon pad ranged from 168 to 316  $\mu\text{m}$ . The samples without the SAP exhibited a slow closure of crack width until end of the 7-day curing period (Fig. 7-10), whereas the samples with the SAP presented a complete closure of crack width after 12 h of curing (Fig. 7-11). Regarding the samples without the SAP, it was confirmed that a faster self-healing resulted from a higher ratio of CSA expansive agent than Portland cement in the given binary cement. Moreover, the effect of the binary cement composition on the self-healing was cumulative to that of the swelling of SAP, as was revealed by the complete closure of all the samples incorporating the SAP after 12 h of curing (Table 7-3).

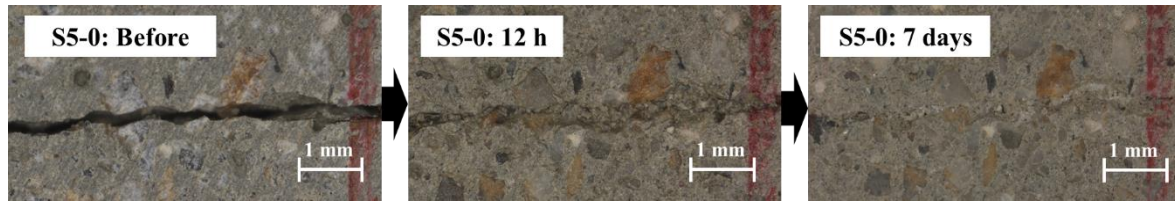






**Figure 7-10: Microscopy images of samples (one sheet of silicon pad) according to water curing: (a) S0-25, (b) S0-15, (c) S0-10, (d) S0-0.**





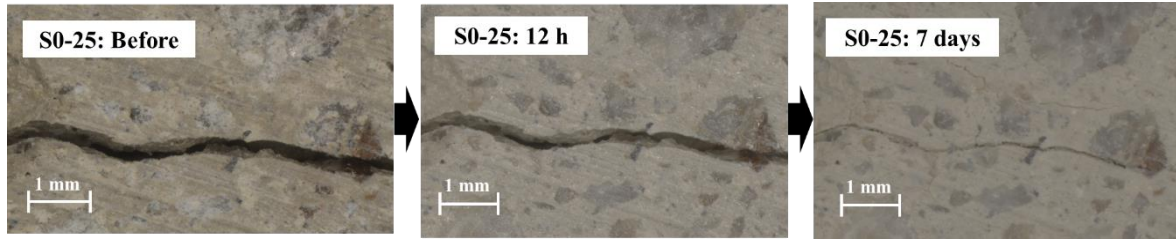
(d)

**Figure 7-11: Microscopy images of samples (one sheet of silicon pad) according to water curing: (a) S5-25, (b) S5-15, (c) S5-10, (d) S5-0.**

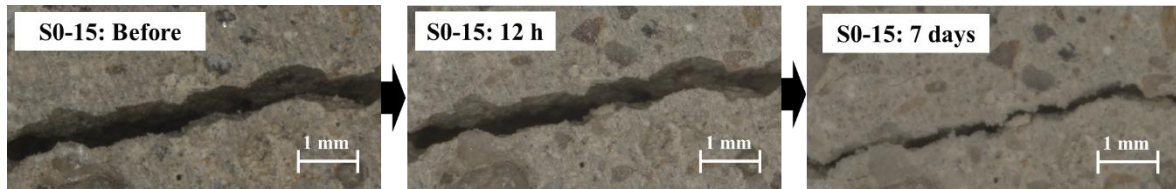
**Table 7-4: Average crack widths of samples (one sheet of silicon pad) at each curing age.**

Mixture label	Average crack width ( $\mu\text{m}$ ), (ratio)			
	Before curing	After 12 h	After 3 days	After 7 days
S0-25	215 (1)	154 (0.72)	46.0 (0.21)	-
S0-15	236 (1)	210 (0.89)	141 (0.60)	33.0 (0.14)
S0-10	168 (1)	145 (0.86)	126 (0.75)	65.0 (0.38)
S0-0	177 (1)	167 (0.94)	131 (0.74)	101 (0.57)
S5-25	275 (1)	-	-	-
S5-15	185 (1)	-	-	-
S5-10	193 (1)	-	-	-
S5-0	316 (1)	-	-	-

As shown in Table 7-5, the insertion of two sheets of silicon pad generated an initial crack width ranging from 368 to 463  $\mu\text{m}$ , of which the average value was larger than that of the samples with one sheet of silicon pad. Thus, regardless of the SAP, a larger initial crack width led to a more delayed closure of the surface crack with respect to the same types of mixtures (Figs. 7-12 and 7-13, Table 7-5). With two silicon pads inserted, however, all the mixtures without SAP were also subjected to the effect of the binary cement composition. Nevertheless, Mixture S0-25 containing the maximum portion of CSA expansive agent did not show a perfect closure of the crack after 7 days of curing (Fig. 7-12). However, all the samples with SAP obtained a substantial closure of crack width after 12 h of curing. Among them, mixtures with a larger portion of CSA expansive agent saw a faster closure of the crack, which was further promoted by the swelling of SAP. For example, Mixture S5-25 gained an approximately 87% recovery of the initial crack width after 12 h of curing. In this regard, it was considered that the mixtures containing SAP could facilitate the complete closure of a crack width of up to about 400  $\mu\text{m}$  after 7 days of curing.



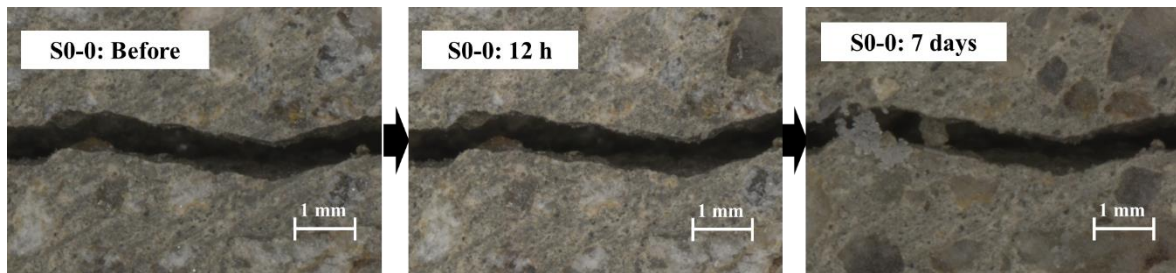
(a)



(b)



(c)



(d)

**Figure 7-12: Microscopy images of samples (two sheets of silicon pad) according to water curing: (a) S0-25, (b) S0-15, (c) S0-10, (d) S0-0.**



(a)

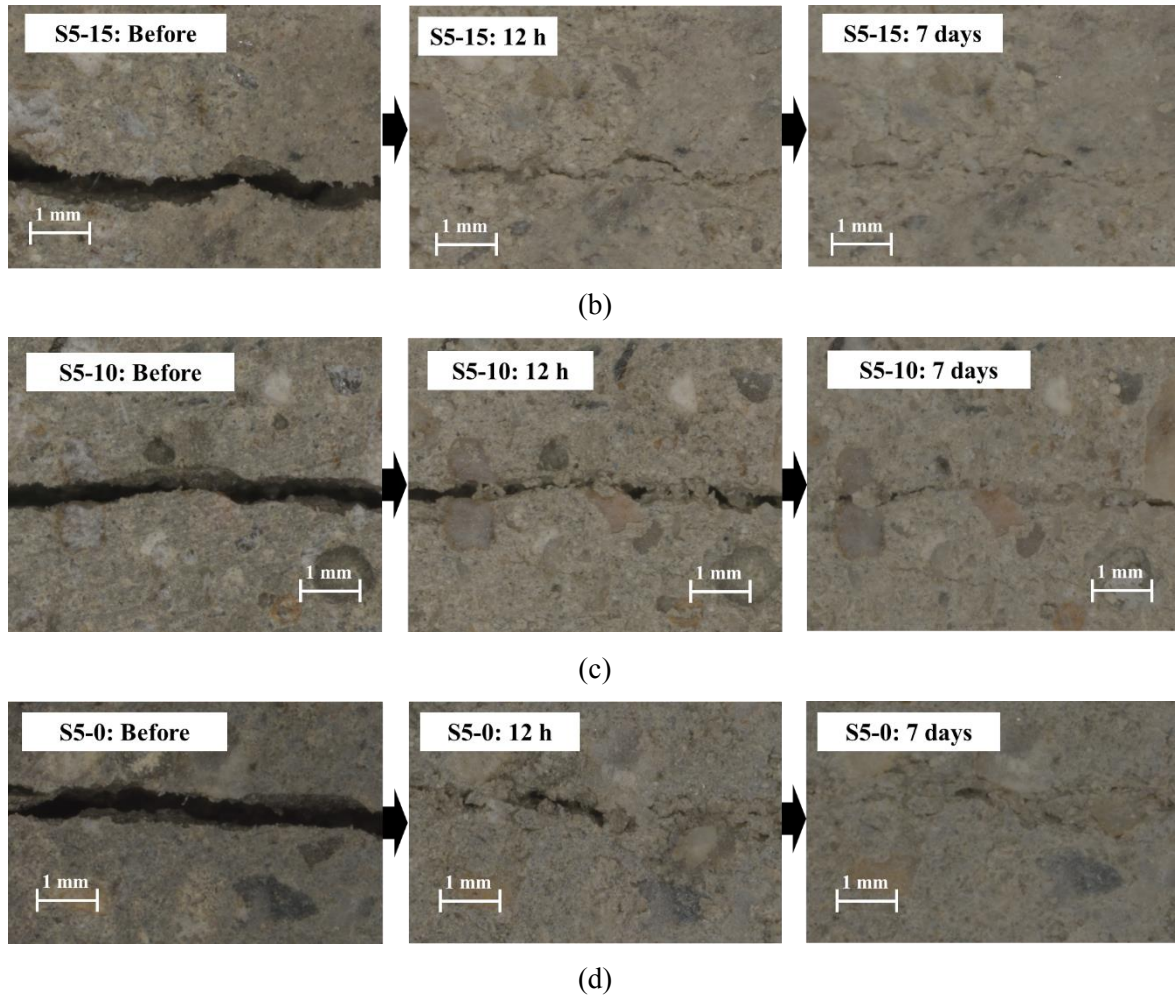


**Figure 7-13: Microscopy images of samples (two sheets of silicon pad) according to water curing: (a) S5-25, (b) S5-15, (c) S5-10, (d) S5-0.**

**Table 7-5: Average crack widths of samples (two sheets of silicon pad) at each curing age.**

Mixture label	Average crack width ( $\mu\text{m}$ ), (ratio)				
	Before curing	After 12 h	After 24 h	After 4 days	After 7 days
S0-25	368 (1)	329 (0.90)	215 (0.58)	21.0 (0.06)	18.0 (0.05)
S0-15	430 (1)	406 (0.95)	369 (0.86)	272 (0.63)	208 (0.48)
S0-10	442 (1)	426 (0.96)	406 (0.92)	355 (0.80)	345 (0.78)
S0-0	463 (1)	458 (0.99)	421 (0.81)	376 (0.81)	357 (0.77)
S5-25	414 (1)	53.0 (0.13)	17.0 (0.04)	-	-
S5-15	383 (1)	-	-	-	-
S5-10	392 (1)	62.0 (0.16)	38.0 (0.10)	-	-
S5-0	404 (1)	93.0 (0.23)	23.0 (0.06)	12.0 (0.03)	-

According to several construction codes [109,110,111], the maximum allowable crack widths were specified to range between 0.1 and 0.4 mm in different exposure conditions. Thus, considering the maximum allowable crack widths, hydraulic cement mortars generally require CSA expansive additive and various crystalline admixtures in the mixture design to achieve the self-healing of cracks [99,112,113]. Many researchers have proposed the maximum cracks widths of up to 300  $\mu\text{m}$  so as for the cracks to obtain a complete self-healing [103,114,115]. They commonly conducted a series of water curings before and after the cracking of the samples, whereas this study did not perform the curing before the cracking of samples. Moreover, all the mixtures in this study excluded water in the mixing process, which resulted in a faster hydration of the binary cement and the swelling of SAP on the crack surfaces only if they were exposed to water. More details about the effect of binary cement and SAP on the self-healing will be discussed in relation to the water permeability test in Section 7.3.3.

#### 7.3.2.2. Self-healing evaluation using elastic wave

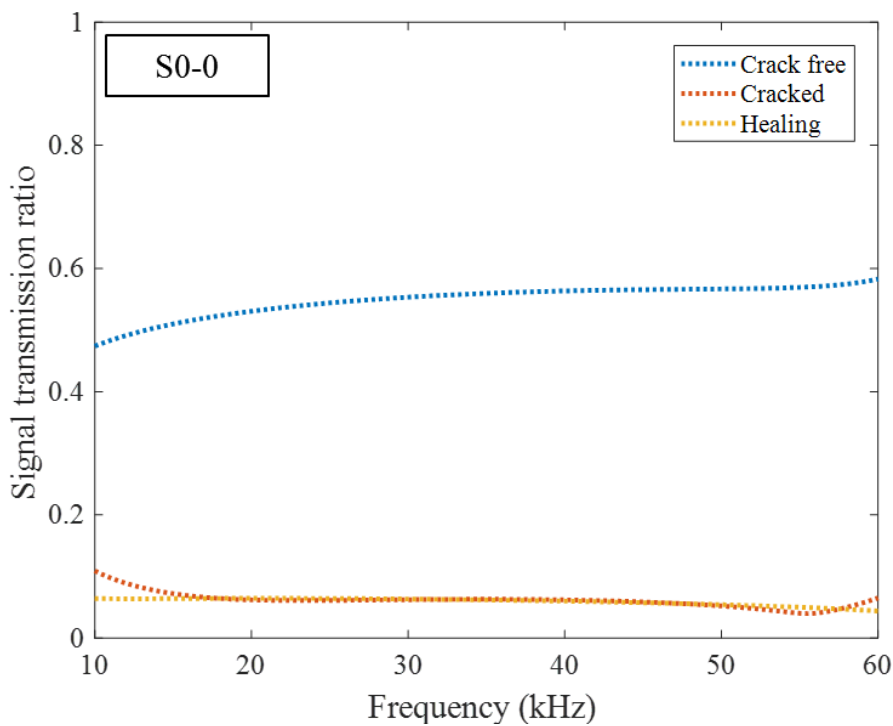
Although the closure of surface cracks was monitored using a microscope, the extent of self-healing inside the crack volume could not be judged. Accordingly, referring to several studies [116,117], elastic wave tests were conducted for all the samples, which were crack-free, cracked, and healed after 7 days of curing. Through the tests, signal transmission ratios of each sample with different crack widths were calculated. For example, Fig. 7-14 illustrates the change of signal transmission ratios of Mixtures S0-0 and S5-25 holding one sheet of silicon pad until cracking. While Mixture S0-0 barely exhibited an increase in signal transmission ratio after 7 days of curing (Fig. 7-14(a)), Mixture S5-25 showed a significant elevation of signal transmission ratio after 7 days of curing (Fig. 7-14(b)). This observation likely suggests comparative analyses of self-healing for each sample. However, because a group of cracked samples had varying initial crack widths despite the insertion of the same sheets of silicon pad, the signal transmission ratio itself could not be used to directly compare the samples. Therefore, the spectral wave-transmission energy, which is the integration of the signal transmission ratios in frequency domain, was calculated for all the samples [117]. Then, the calculated spectral wave-transmission energy was normalized for each sample. Thus, spectral energy transmission ratios were compared.

Overall, regardless of the varying widths and SAP, all the cracked samples exhibited a similar level of spectral energy transmission ratios (Figs. 7-15 and 7-17). After 7 days of curing, the same mixture generally rendered a higher spectral energy transmission ratio to the sample with one sheet of silicon pad than that with two sheets of silicon pad. In this regard, the extent of self-healing likely progressed more in the samples with one sheet of silicon pad.

With one sheet of silicon pad inserted, all the samples with SAP plus Mixture S0-25 containing

only CSA expansive agent showed similar spectral energy transmission ratios of at least 0.6 after 7 days of curing (Fig. 7-15). This phenomenon was also reflected in the microscope image of Mixture S0-25 that hardly displayed a residual crack after 7 days of curing (Fig. 7-10(a)). However, the others without SAP showed a decrease in the spectral energy transmission ratios in relation to the size of the portion of CSA expansive agent, i.e. the smaller the portion, the bigger the decrease. Therefore, the effect of binary cement compositions was deemed cumulative to that of the swelling of SAP.

Similarly, as shown in Fig. 7-14, the signal transmission ratios were calculated for all the samples holding two sheets of silicon pad (Fig. 7-16). Although the extent of self-healing was considered delayed in all the samples with two sheets of silicon pad, they also presented the synergetic effect of both the binary cement compositions and the swelling of SAP in terms of the spectral energy transmission ratios (Fig. 7-17).



(a)

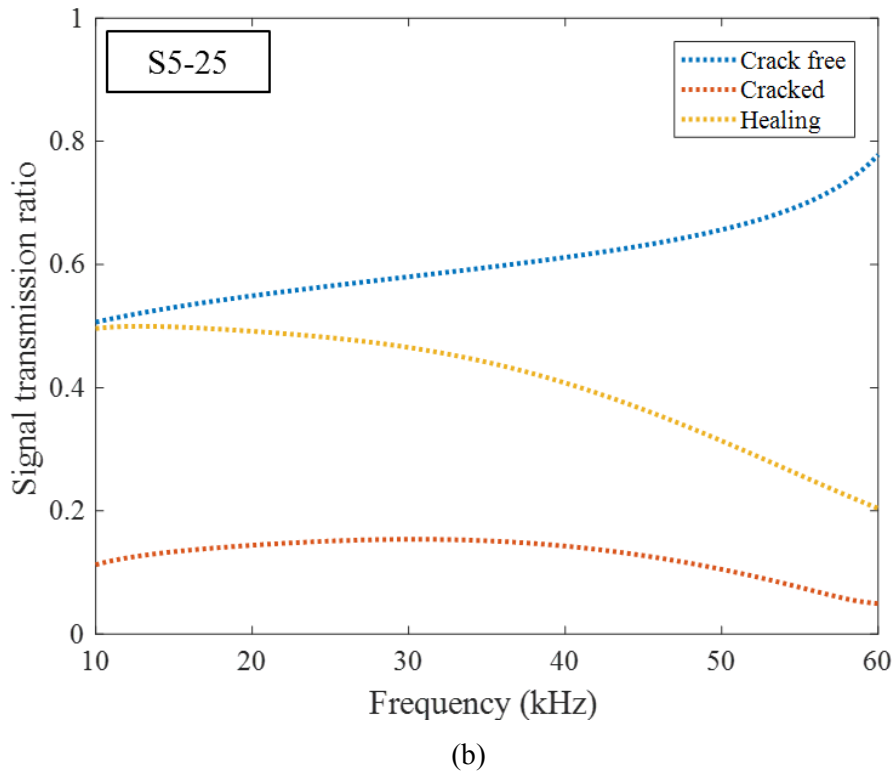


Figure 7-14: Signal transmission ratios of samples (one sheet of silicon pad) according to water curing: (a) Mixture S0-0, (b) Mixture S5-25.

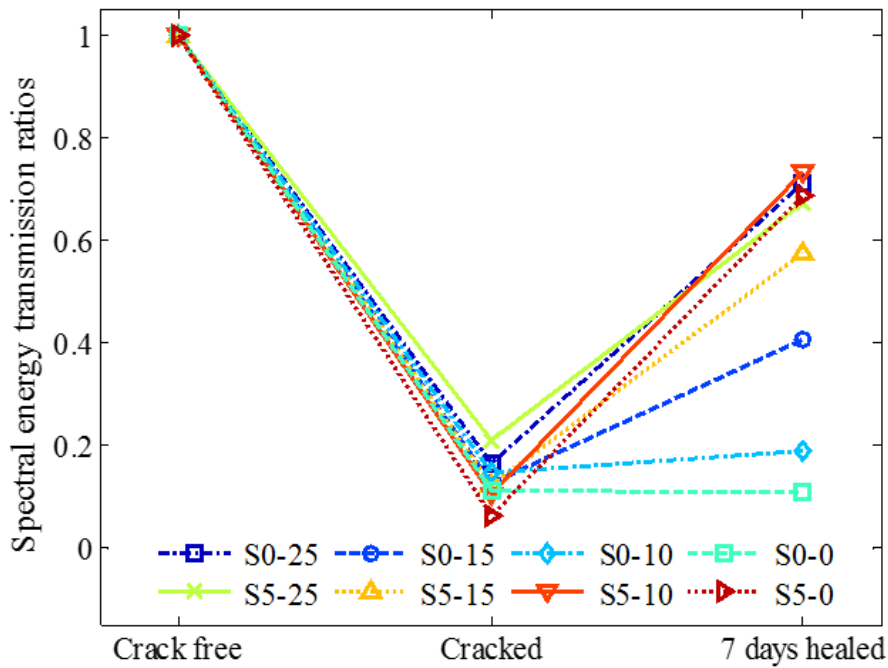
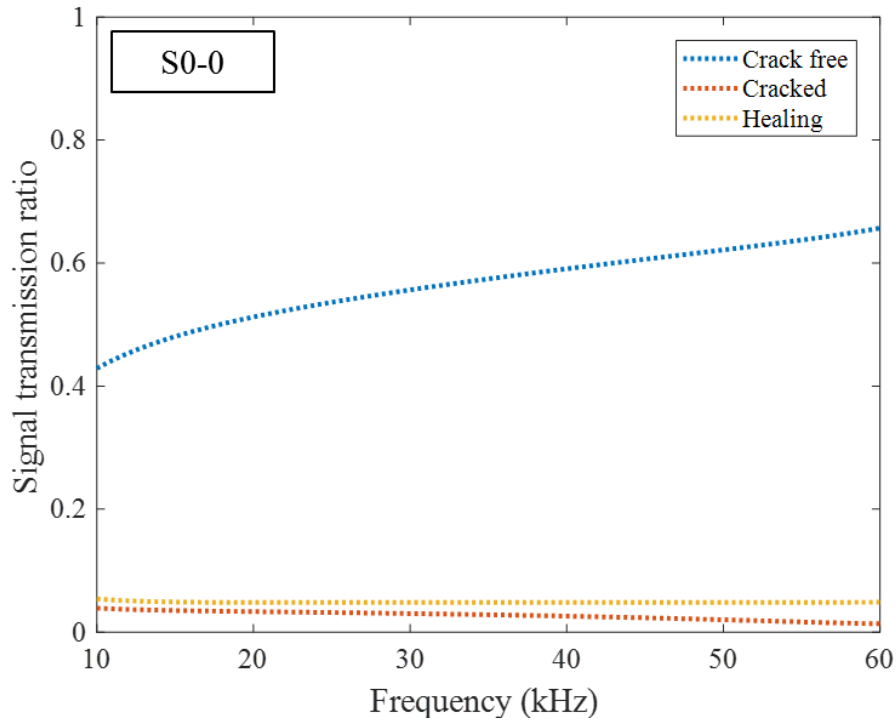
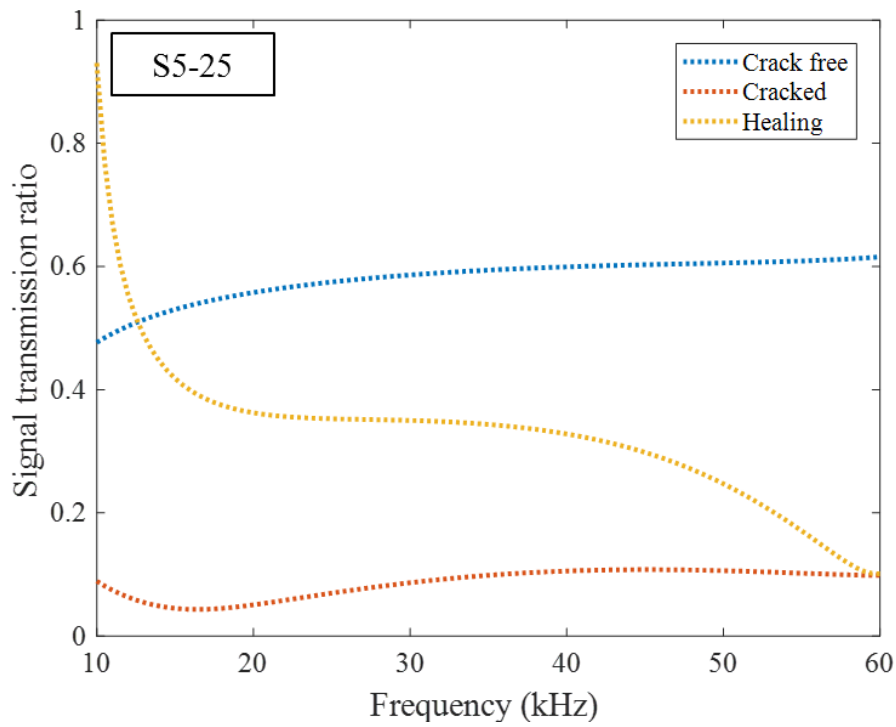


Figure 7-15: Calculated spectral energy transmission ratios of samples (one sheet of silicon pad)

according to water curing.



(a)



(b)

Figure 7-16: Signal transmission ratios of samples (two sheets of silicon pad) according to water



curing: (a) Mixture S0-0, (b) Mixture S5-25.

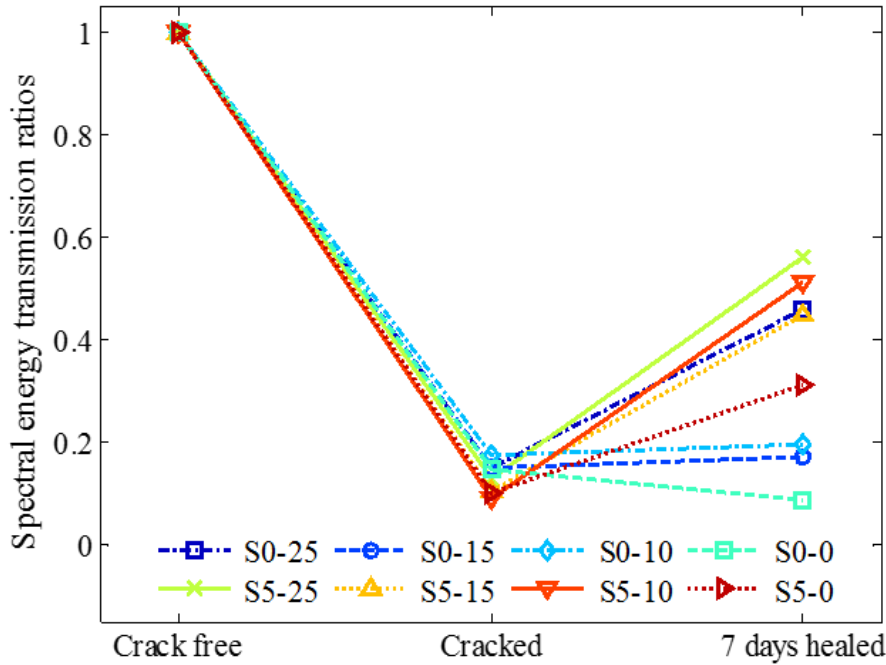


**Figure 7-17: Calculated spectral energy transmission ratios of samples (two sheets of silicon pad) according to water curing.**

### 7.3.2.3. Monitoring of through crack using computed tomography

After the crack samples holding one sheet of silicon pad were cured for 7 days, each sample was scanned to observe the change of internal crack width after water curing. Then, the tomographic (cross-sectional) images of each sample at mid-height before and after the curing were compared. Among eight mixtures, the images from only two samples of Mixtures S0-0 and S5-15 are presented in this section. As shown in Fig. 7-18, Mixture S0-0 scarcely presented the change of internal crack width, whereas Mixture S5-15 displayed the distinct closure of internal crack width after 7 days of curing (Fig. 7-19), as was observed by the decrease of the surface crack width by an optical microscope. Thus, it was reckoned that the change of surface crack width could represent the extent of entire through crack width. In addition, the variation of internal crack width was deemed parallel with the trend of the recovery in the spectral energy transmission ratios (Figs. 7-15 and 7-17).

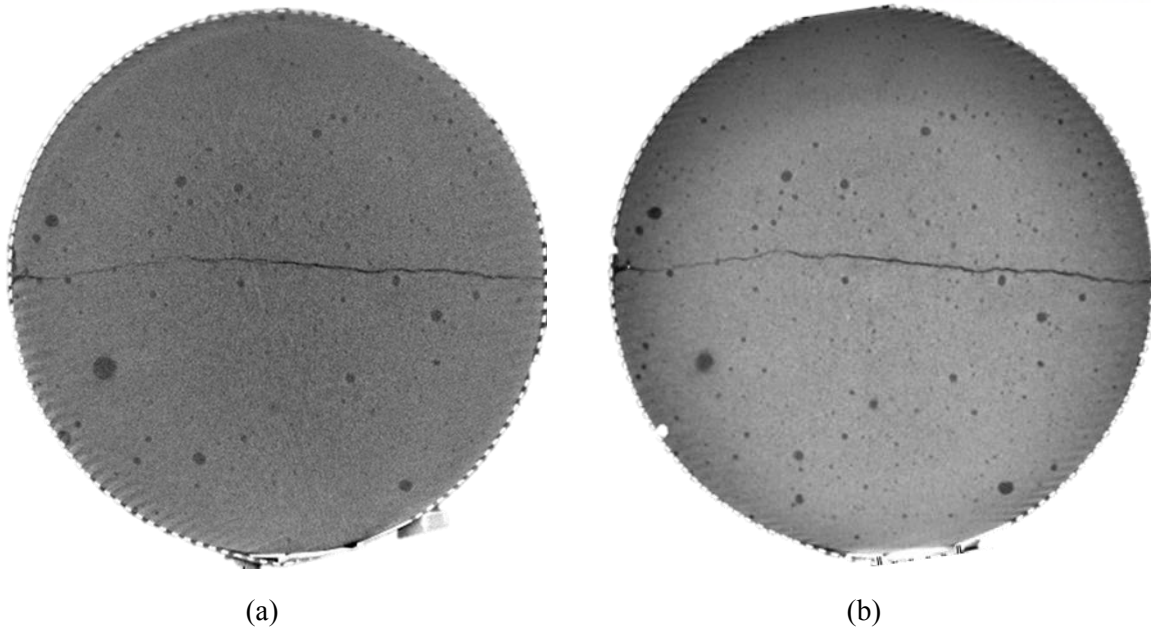


**Figure 7-18: Tomographic images of Mixture S0-0 at mid-height: (a) before curing, (b) after 7 days of water curing.**

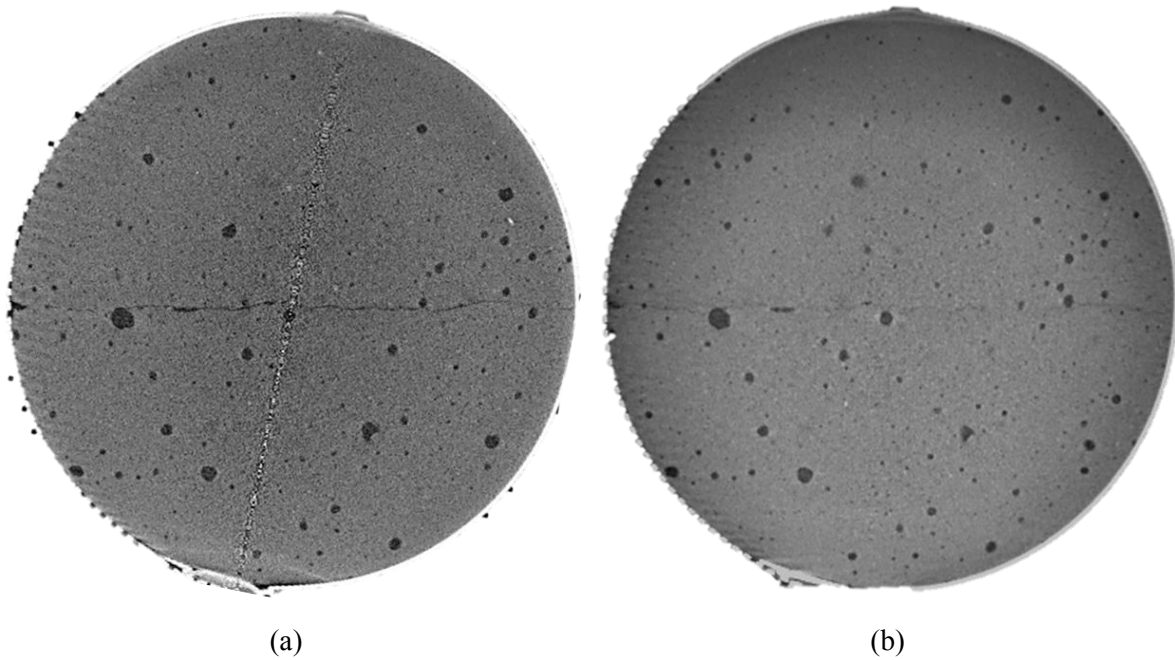


**Figure 7-19: Tomographic images of Mixture S5-10 at mid-height: (a) before curing, (b) after 7 days of water curing.**

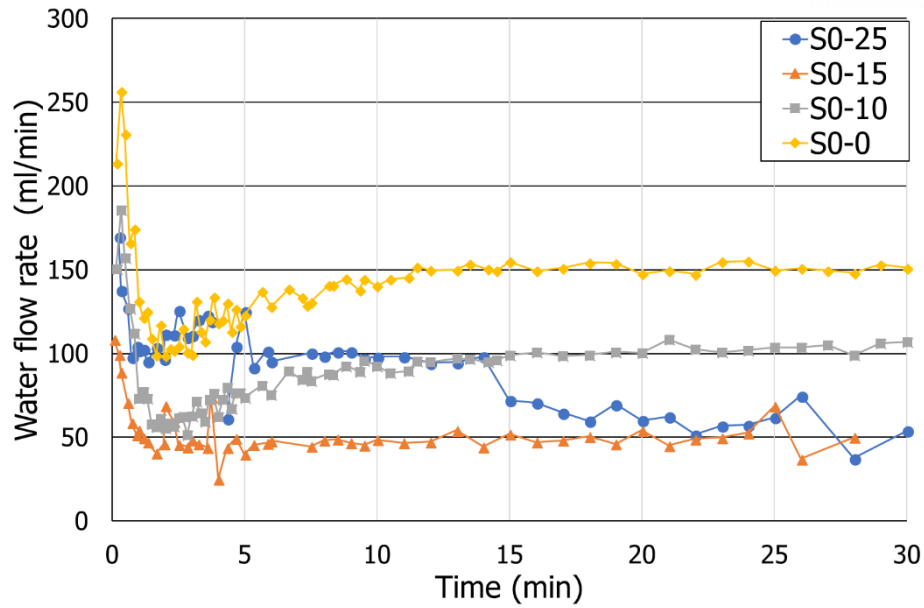
### 7.3.3. Water permeability test

Fig. 7-20 shows the results of the water permeability tests for the samples without and with 5%

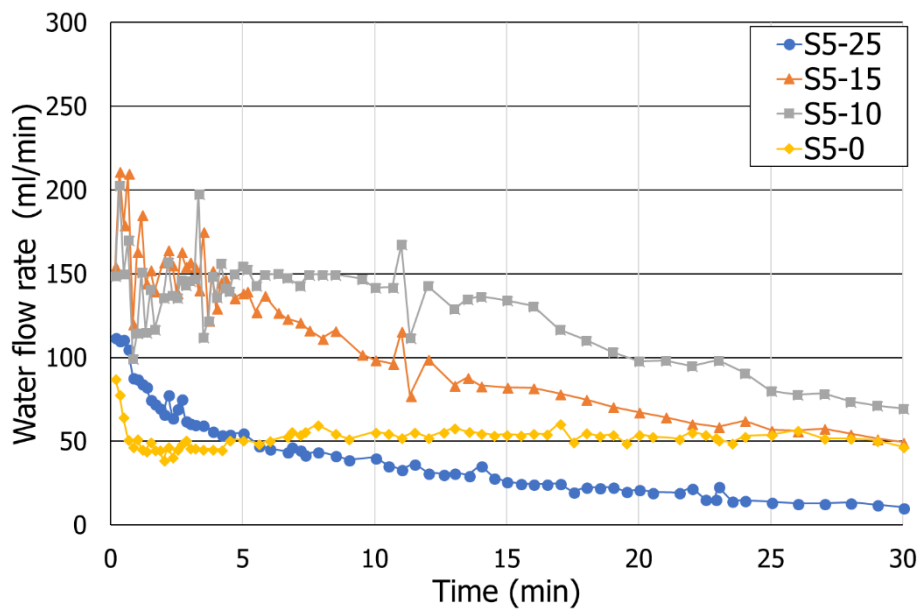
SAP. The outflow of water through the crack was measured as soon as the pressure water head reached 250 mm. Overall, regardless of the SAP, the water flow rate versus the time for all the tested samples presented an unstable variation during an initial 5 min, after which it did not. Thus, only the time interval between 5 and 30 min was chosen for the test analyses. It was noted that the differences of initial water flow rates between the samples resulted from the varied initial crack widths of the samples, which are revealed in Section 7.3.3.1.

As shown in Fig. 7-20(a), only Mixture S0-25 containing 25% CSA expansive agent presented a descending water flow rate, whereas the others showed steady water flow rates over time. This phenomenon suggests that the water flow rate was subjected to the relative ratios between the Portland cement and CSA expansive agent on the crack surfaces, which likely afforded different extents of initial setting time. Thus, it was assumed that a higher ratio of CSA expansive agent than Portland cement shortened the setting time. This assumption is also supported by the fact that the initial setting time of CSA-based cement systems ranged from 5 to 34 min with varying water/cement ratios [118,119,120].

Although the descending behavior of water flow rate was seen by only Mixture S0-25 among the samples without SAP, all the samples containing 5% SAP except Mixture S5-0 exhibited decreasing water flow rates (Fig. 7-20(b)). In this regard, it appears that the SAP particles accelerated the hydration of binary cement by rapidly swelling on the crack surfaces [106], at which the formed hydration products remained stable. Due to the swelling of SAP, it seems that a higher ratio of CSA expansive agent in the binary cement triggered a faster decrease in the water flow rate. Consequently, Mixture S5-25 containing 5% SAP and 25% CSA expansive agent achieved the fastest reduction of water flow rate in this study. However, the water flow rates of Mixture S5-0 without the CSA expansive agent remained steady during test. Thus, it can be concluded that a sudden water penetration through the crack of sulfur composites could be blocked off effectively by adjusting the portions of the CSA expansive agent and SAP in the mixtures.



(a)



(b)

**Figure 7-20: Variation of water flow rate with time for different samples: (a) “S0” series, (b) “S5” series.**

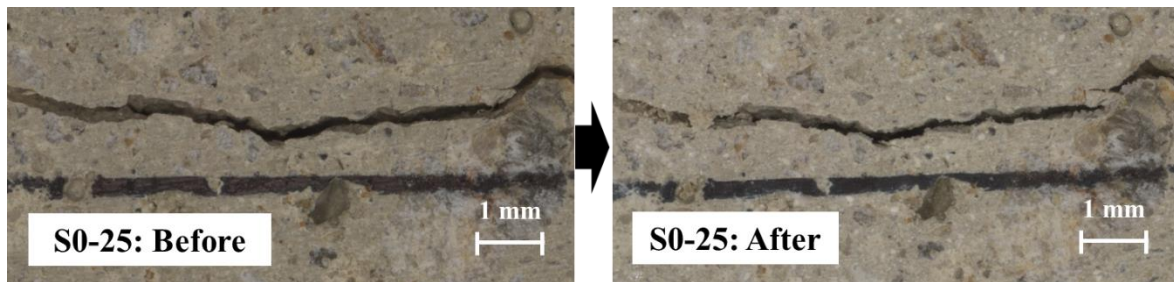
#### 7.3.3.1. Surface crack monitoring

After 30 min of water permeability tests, all the samples were observed using a microscope. The samples without SAP barely presented a recovery of initial crack width (Fig. 7-21), whereas the samples with SAP attained a considerable closure of surface cracks after 30 min (Fig. 7-22).

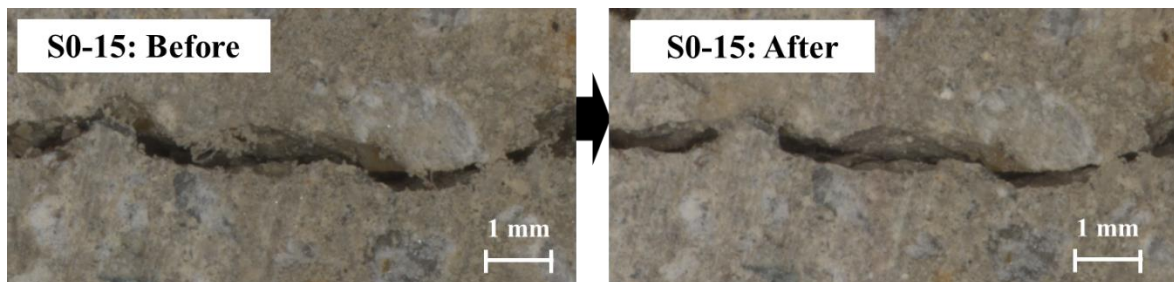
Among the samples without SAP, the mixtures with more CSA expansive agent offered a

higher recovery ratio of a surface crack width to the cracked samples than those with less CSA expansive agent (Table 7-6). Even though Mixtures S0-10 and S0-0 did not recover the surface crack width at all, the others (Mixtures S0-25 and S0-15) showed a slight recovery of surface crack widths, which was deemed due to more rapid initial setting of the binary cements.

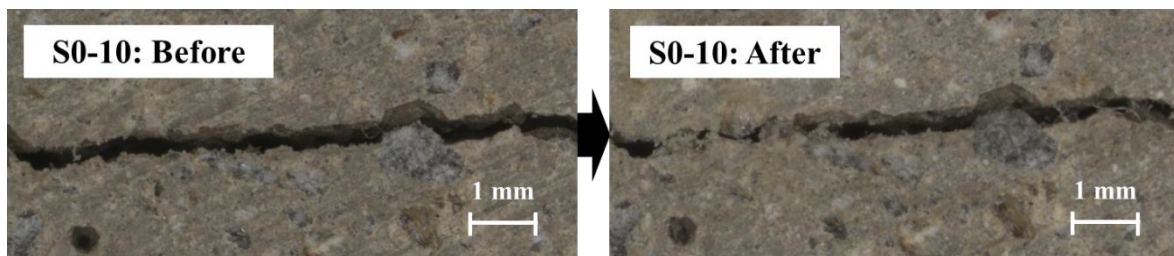
Among the samples with 5% SAP, all the samples except Mixture S5-0 containing only Portland cement attained a nearly complete closure of the surface cracks after 30 min. In this regard, the swelling of SAP was deemed a critical factor in the cutting off of the water leakage within a short time of 30 min. In spite of the assistance from the swollen SAP particles, Mixture S5-0 recovered only about 31.6% of the initial crack width, which can likely be attributed to the absence of the CSA expansive agent. Although the recovery of the surface crack widths was observed using a microscope, it was noted that the recovery of the inner crack width could not be assessed. Thus, the recovery of the inner crack width was confirmed by computed tomography in Section 7.3.2.3.



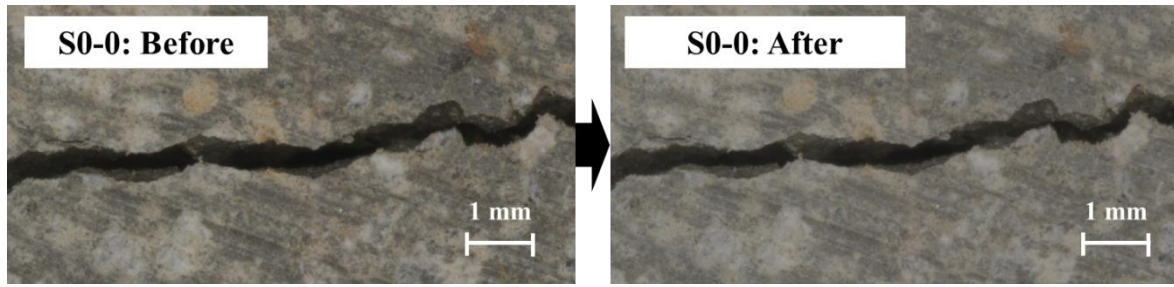
(a)



(b)

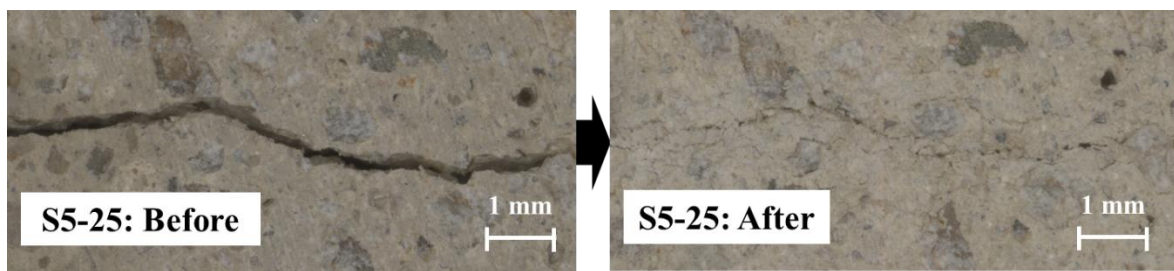


(c)

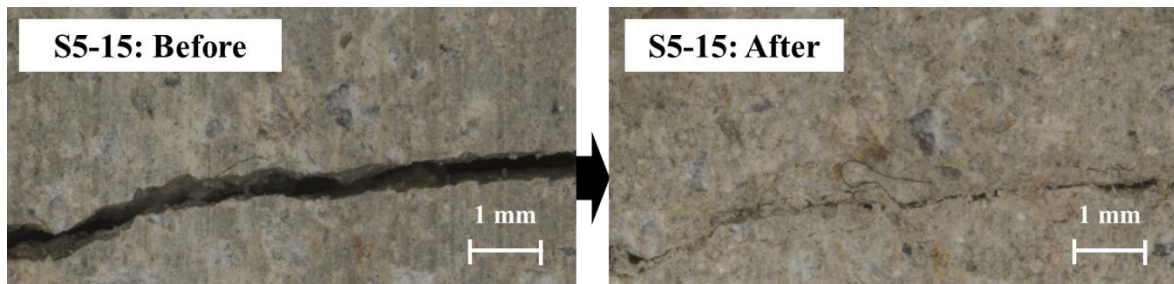


(d)

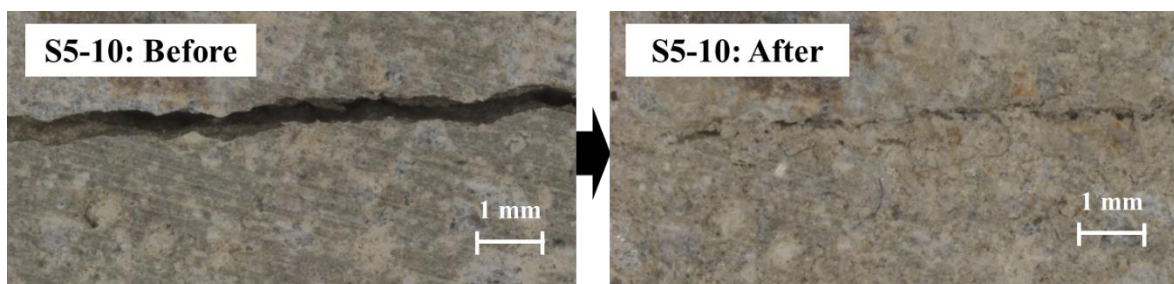
Figure 7-21: Microscopy images of samples (one sheet of silicon pad) according to water permeability test: (a) S0-25, (b) S0-15, (c) S0-10, (d) S0-0.



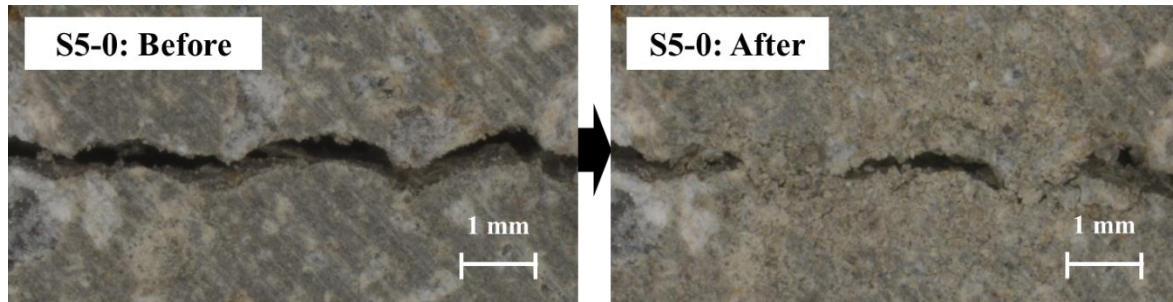
(a)



(b)



(c)



(d)

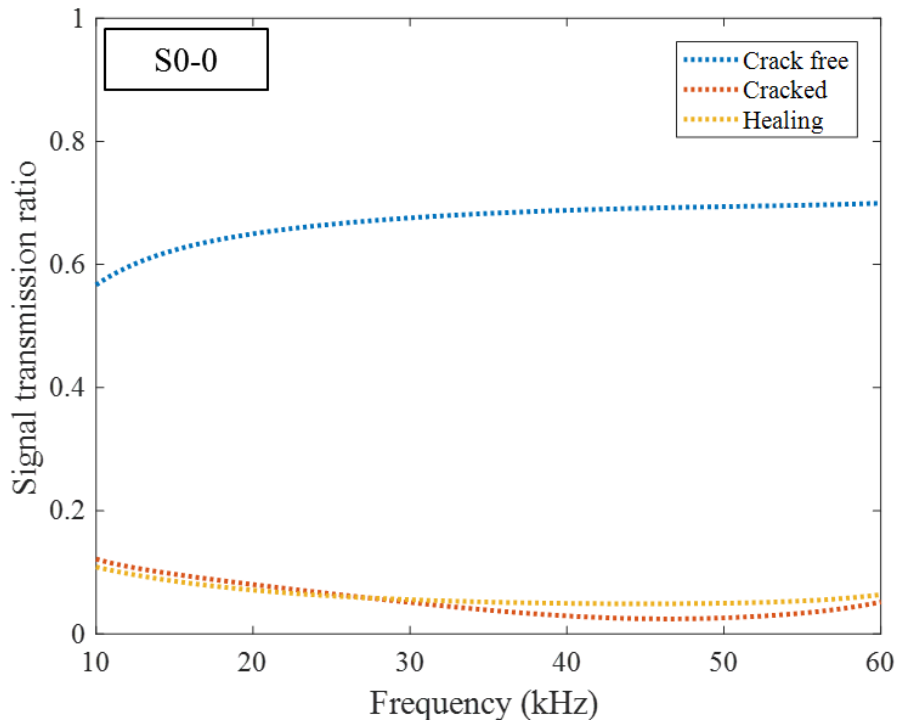
**Figure 7-22: Microscopy images of samples (one sheet of silicon pad) according to water permeability test: (a) S5-25, (b) S5-15, (c) S5-10, (d) S5-0.**

**Table 7-6: Average crack widths of samples (one sheet of silicon pad) according to water permeability test.**

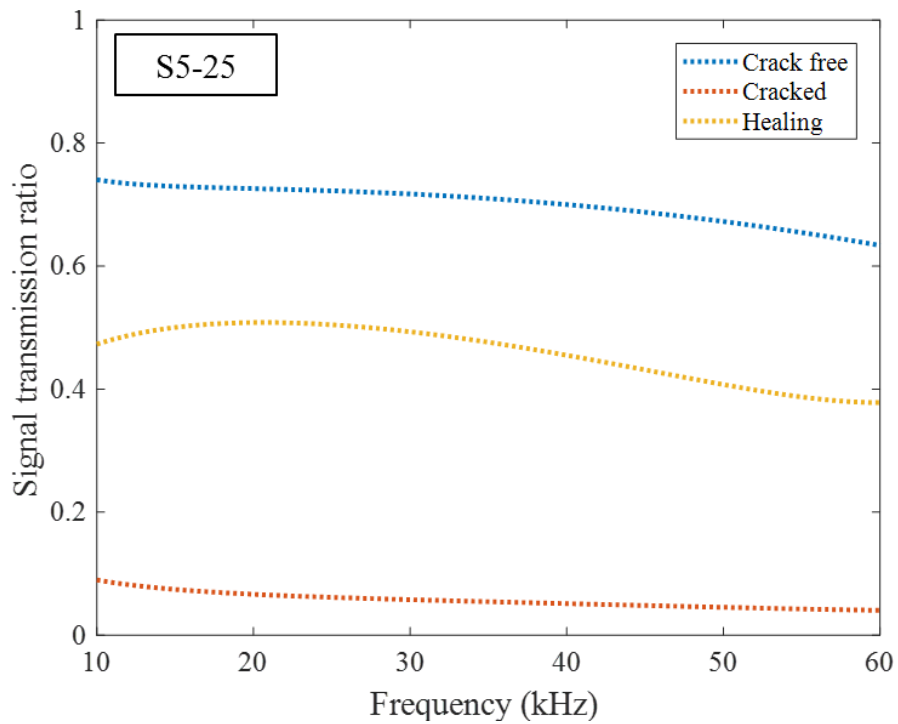
Mixture label	Average crack width ( $\mu\text{m}$ ), (ratio)	
	Before	After
S0-25	336 (1)	250 (0.74)
S0-15	248 (1)	221 (0.89)
S0-10	322 (1)	316 (0.98)
S0-0	354 (1)	351 (0.99)
S5-25	298 (1)	-
S5-15	384 (1)	-
S5-10	366 (1)	11.0 (0.03)
S5-0	305 (1)	208 (0.68)

### 7.3.3.2. Self-healing evaluation using elastic wave

After 24 h of natural drying, the signal transmission ratios of all the tested samples were calculated as shown in Fig. 7-23. In the same manner as for the samples cured in water, the spectral transmission energy ratios were calculated and used to compare the samples which were crack-free, cracked, and healed after 30 min (Fig. 7-24). All the samples with 5% SAP presented ascending spectral energy transmission ratios after the water permeability tests. However, the others without SAP barely showed any elevation of spectral energy transmission ratios after the water permeability tests. Thus, it was deemed that the incorporation of SAP in the mixture design of sulfur composites was essential to achieve a self-healing capacity within a short time. In addition, it was concluded that the swelling of SAP accelerated the effect of binary cement compositions on self-healing.



(a)



(b)

**Figure 7-23: Signal transmission ratios of samples (one sheet of silicon pad) according to water permeability test: (a) Mixture S0-0, (b) Mixture S5-25.**



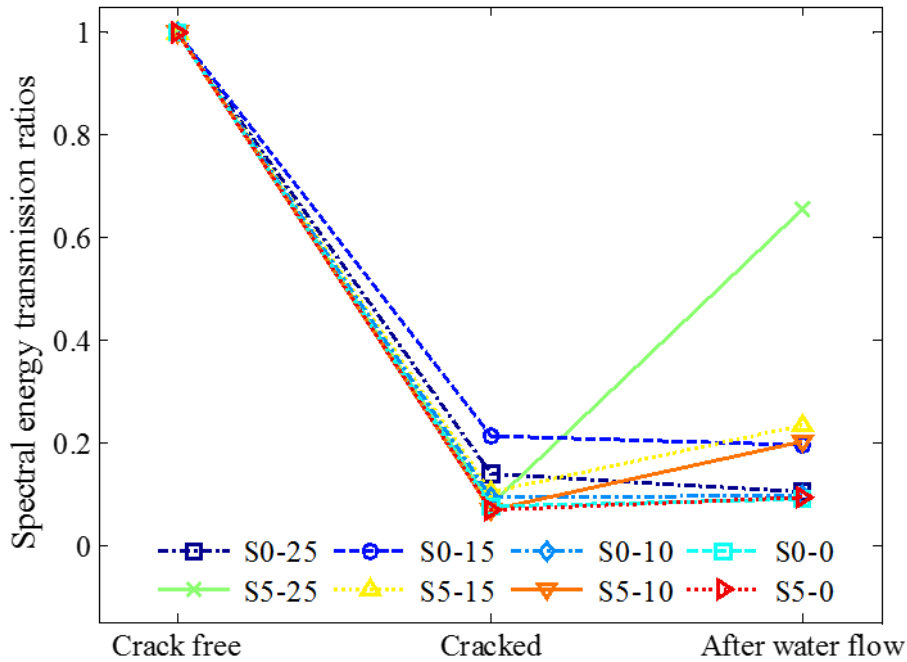


**Figure 7-24: Calculated spectral energy transmission ratios of samples (one sheet of silicon pad) according to water permeability test.**

#### 7.4. Conclusions

This study developed a total of eight self-healing sulfur composites incorporating varying blends of Portland cement and CSA expansive agent as the binary cement, and SAP powder. The initial surface crack widths of all the samples were adjusted by inserting different sheets of silicon pad. Then, the self-healing of the through crack samples was promoted in two different environments. One was water curing, the other was a water permeability test. In each environment, the extent of self-healing of the samples was monitored and evaluated by a stereo zoom microscope and elastic wave transmission test, respectively. Moreover, the self-healing of the inner cracks was confirmed by computed tomography. The summary and conclusions from this study are summarized as follows:

- ✓ Regardless of the use of SAP, a higher relative ratio of Portland cement than CSA expansive agent in the binary cement facilitated a higher compressive strength in the sulfur composites, which likely inherited from the larger indentation modulus of the Portland cement than CSA expansive agent. However, all the samples with 5% SAP showed a relatively low compressive strength due to the increase of porosity from the SAP particles.
- ✓ In the water curing, although two groups of through crack samples were prepared, they commonly

exhibited the synergetic effect of both the binary cement compositions and the swelling of SAP on the self-healing. The samples containing a higher ratio of CSA expansive agent than Portland cement and SAP showed a faster closure of both the surface and inner crack widths, and a larger spectral energy transmission ratio after 7 days of curing. Thus, it was deemed that the initial surface crack width of up to 400  $\mu\text{m}$ , which is the maximum allowable crack width according to construction codes, could be completely recovered by the self-healing of sulfur composites after 7 days of curing.

- ✓ All the samples without SAP except Mixture S0-25 sustained the steady water flow rates during 30 min of water permeability testing, whereas all the samples with SAP except Mixture S5-0 presented a faster decrease of the water flow rates according to a larger ratio of CSA expansive agent than Portland cement. This phenomenon was attributed to a more rapid initial setting of the binary cement stimulated by the swollen SAP particles on the crack surfaces. Considering that only the samples with the SAP exhibited an increased spectral energy transmission ratio after the water permeability test, the swelling of SAP particles was considered critical for cutting off the water penetration and subsequent setting and hydration of the binary cement on the crack surfaces within a short time period of just 30 mins.

## 8. Concluding Remarks

### 8.1. Overall Conclusions

This thesis mainly focused on the development of sustainable sulfur composites using DCPD-modified sulfur polymer, various micro-fillers (e.g., Portland cement, fly ash, and CSA expansive agent), superabsorbent polymer, and micro fibers. The use of both micro-fillers (in sole or binary cement) and rubber powder effectively resulted in the enhanced compressive strength and the reduced unit weight of modified sulfur composites, respectively. The flexural stress-strain responses of the modified sulfur composites were also converted into a ductile behavior with microcracks by adding micro fibers. The rheology test results suggested the optimal temperature range of fresh modified sulfur composites favorable for placement. Based on the integrity of cementitious and SAP particles in the hardened sulfur composites, the self-healing of through crack was obviously acquired through a water curing or water permeability test. This thesis can be summarized as follows.

#### 1) Development of high strength and lightweight sulfur polymer composites using micro-fillers and waster rubber

Generally, the use of micro-fillers (e.g., Portland cement, fly ash) as a replacement of modified sulfur polymer substantially resulted in the enhanced compressive strength of sulfur composites with a converted morphology. In particular, the use of Portland cement aimed at providing the self-healing capacity of the sulfur composites when exposed to wet environments. When the micro-fillers were prepared as the binary cement of Portland cement and fly ash, the binary cement had a greater effect on the compressive strength than sole fly ash. This phenomenon was deemed associated with the larger indentation modulus of Portland cement than fly ash as well as the different particle characteristics (e.g., particle size distribution, particle shape) of the used micro-fillers. Moreover, a decreasing porosity according to a more use of micro-filler and the chemical bond between the modified sulfur polymer and the rubber powder revealed the rationales for the strength development. Besides, the use of rubber powder effectively lowered the unit weight of the modified sulfur composites without a severe strength reduction. The experimental details and results have been described in Chapters 3 and 4.

#### 2) Development of ductile micro fiber-reinforced sulfur polymer composites

Overall, all the micro fiber-reinforced sulfur composites acquired an increased post-peak ductility in flexure, which could not be observed by non-reinforced sulfur composites. In addition, the hybrid use of more steel fiber than glass fiber caused the flexural strain hardening and softening behaviors of specimens that presented an uniform distribution of flexural strain followed by multiple

micro-cracks at midspan. The multiple micro-cracks were monitored using DIC. The modified sulfur composites generally entrained a more cumulative volume of big pores (>50 nm) with a larger total fiber. Although this neglected the general solid-porosity relationship, this was regarded as the unique characteristic of the modified sulfur composites inherited from the modified sulfur. The experimental details and results have been described in Chapter 5.

### 3) Experimental validation of the rheological properties of fresh sulfur polymer composites with respect to temperature and particle characteristics of micro-fillers

Regardless of temperature, an increasing portion of micro-filler with a larger surface area led to a gradual growth of the yield stress as well as the plastic viscosity of fresh modified sulfur mixtures. At 140°C, each fresh mixture presented a higher level of shear stress in the second shearing cycle as compared to the first shearing cycle. This was likely due to the further production of longer amorphous sulfur chains in the fresh modified sulfur. The fresh sulfur mixtures with a surface temperature of about 140°C showed a smaller spreading diameter with a more portion of micro-fillers through the mini slump flow test. This observation was in parallel with the increased yield stress due to a more portion of micro-filler through the rheology test at 140°C. Besides, both the yield stress and the plastic viscosity of fresh sulfur mixtures were higher at 140°C than 120°C. Thus, the optimal mixing temperature favorable for the placement of fresh modified sulfur mixtures is assumed to be 120-135°C. The experimental details and results have been described in Chapter 6.

### 4) Development and evaluation of self-healing sulfur polymer composites containing binary cement and SAP

Although two groups of though crack samples with different crack widths were prepared, they commonly exhibited the synergetic effect of both the binary cement compositions and the swelling of SAP on the self-healing. The samples containing a higher ratio of CSA expansive agent than Portland cement, and SAP showed a faster closure of both surface and inner crack widths, and a larger spectral energy transmission ratio after 7 days of water curing. Thus, it was deemed that the initial surface crack width of up to 400 μm, which was the maximum allowable crack width as per construction codes, could be completely recovered by the self-healing of sulfur composites after 7 days of water curing. Considering that only the samples with the SAP exhibited an increased spectral energy transmission ratio after water permeability test, the swelling of SAP particles was considered critical for cutting off the water penetration and subsequent setting and hydration of the binary cement on the crack surfaces within a short time of 30 min. The experimental details and results have been described in Chapter 7.

## 8.2. Path Forward

### 1) Experimental validation of the setting and hydration of self-healing materials on crack surfaces

Although the self-healing of modified sulfur composites was confirmed by the morphological monitoring of surface and inner cracks, and non-destructive evaluation method, the healing mechanism formed on crack surfaces has not been studied yet. Considering that both CSA expansive agent and Portland cement are hydraulic materials, of which combination has been reported to render different initial setting times, the setting and hydration of binary cement must be identified. Once setting time test is conducted for the various binary cements composed of the CSA expansive agent and the Portland cement, its result will be compared with the water permeability test result that presented the different shutoff times of water outflow. Because this thesis has built two healing environments varying the duration of exposure to water, the hydration products formed in the volume of through crack must be identified over time.

### 2) Assessment of the self-healing properties of fiber-reinforced sulfur composites in direct tension

Considering that the self-healing of modified sulfur composites was facilitated for the crack width of up to approximately 400  $\mu\text{m}$ , future research will assess the self-healing properties of fiber-reinforced modified sulfur composites in the direct tension that can generate numerous microcracks. The microcracks can be formed by incorporating micro fibers in modified sulfur composites, which have been dealt in Chapter 5. Thus, this attribute likely affords structural cracks rather than the artificial crack made by a splitting tension test. Firstly, the fiber-reinforced modified sulfur composites will be subjected to the direct tension in an elastic range to produce the microcracks on samples. Then, the samples will be cured in water during a certain period. Finally, the cured samples will be tested again to check the recovery of tensile stiffness. Through this procedure, the self-healing performance of the modified sulfur composites will be quantitatively assessed in terms of the tensile stiffness.

## REFERENCES

1. TSI 2008, Sulfur outlook. <http://www.sulphurinstitute.org/publications/index.cfm>.
2. Gallagher, K. S., & Oliver, H. H. (2005, July). Providing Low-Sulfur Fuels for Transportation Use: Policy Options and Financing Strategies in the Chinese Context. In *Conference Paper for the Kennedy School of Government, Harvard University*.
3. Mohamed, A. M. O., & El-Gamal, M. (2010). *Sulfur concrete for the construction industry: a sustainable development approach*. J. Ross Publishing.
4. Ober, J. A. (2002). *Materials flow of sulfur* (No. 2002-298).
5. Bacon, R. F., & Davis, H. S. (1921). *Recent advances in the American sulphur industry*.
6. Duecker, W. W. (1934). Admixtures improve properties of sulfur cements. *Chemical and Metallurgical Engineering*, 41(11), 583-586.
7. Gregor, R., & Hackl, A. (1978). A new approach to sulfur concrete. *Advances in Chemistry Series*, 165, 54-78.
8. Lin, S. L., Lai, J. S., & Chian, E. S. (1995). Modifications of sulfur polymer cement (SPC) stabilization and solidification (S/S) process. *Waste management*, 15(5-6), 441-447.
9. McBee, W. C., Sullivan, T. A., & Jong, B. W. (1983). Corrosion-resistant sulfur concretes. *NASA STI/Recon Technical Report N*, 83.
10. McBee, W. C., & Weber, H. H. (1990, August). Sulfur polymer cement concrete. In *Proceedings of the Twelfth Annual Department of Energy Low-level Waste Management Conference CONF-9008119 National Low-Level Waste Management Program, Idaho Natl. Engineering Lab., Idaho Falls, Idaho*.
11. Mohamed, A. M. O., & El Gamal, M. (2009). Hydro-mechanical behavior of a newly developed sulfur polymer concrete. *Cement and Concrete Composites*, 31(3), 186-194.
12. Pickard, S. S. (1981). Sulfur Concrete: Understanding/Application. *Concrete International*, 3(10), 57-67.
13. Pryor, W. A. (1962). *Mechanisms of sulfur reactions*. McGraw-Hill.
14. Rylova, M. V., Samuilov, A. Y., Sharafutdinova, D. R., Khrapkovskii, G. M., & Samuilov Y. D. (2002) Interaction of bicyclopentadiene with elemental sulfur initial stages of the reaction. *Chemistry and Computational Simulation, Butlerov Communications*, 3(9), 29-32.
15. Texas Gulf Sulfur Co. (1961). *Properties of sulfur*.
16. Vroom, A. H. (1998). Sulfur concrete goes global. *Concrete international*, 20(1), 68-71.
17. Gannon, C. R., Wombles, R. H., Hettinger, W. P., & Watkins, W. D. (1983). New concepts and discoveries related to the strength of plasticized sulfur. STP 807, ASTM, Philadelphia, PA, p. 84-101.
18. Blight, L., Currell, B. R., Nash, B. J., Scott, R. A. M., & Stillo, C. (1978). Preparation and properties

- of modified sulfur systems. *Advances in Chemistry Series*, 165, 13-30.
19. Nimer, E. L., & Campbell, R. W. (1983). *U.S. Patent No. 4,376,830*. Washington, DC: U.S. Patent and Trademark Office.
  20. Bahrami Adeh, N., Mohtadi Haghighi, M., & Mohammad Hosseini, N. (2008). Preparation of sulfur mortar from modified sulfur. *Iranian Journal of Chemistry and Chemical Engineering (IJCCE)*, 27(1), 123-127.
  21. Sander, U. H. F., Fischer, H., Rothe, U., & Kola, R. (1984). *Sulphur, sulphur dioxide and sulphuric acid*. British Sulphur Corporation Ltd.
  22. Diehl, L. (1976). New uses for sulfur and pyrites, In *Madrid Symposium : The Sulphur Institute*.
  23. Sullivan, T. A., McBee, W. C., & Blue, D. D. (1975). Sulfur in coatings and structural materials. *Advances in Chemistry Series, No. 140, American Chemical Society*, p. 55-74.
  24. Currell, B., Williams, A. J., Mooney, A. J., & Nash, B. J. (1975). Plasticization of sulfur.
  25. Sliva, P., Peng, Y. B., & Peeler, D. K. (1996). *Sulfur polymer cement as a low-level waste glass matrix encapsulant* (No. PNNL--10947). Pacific Northwest Lab., Richland, WA (United States).
  26. McBee, W. C., & Sullivan, T. A. (1979). *Development of specialized sulfur concretes* (No. BUMINES-RI-8346 Invest Rpt).
  27. Bordoloi, B. K., & Pearce, E. M. (1978). Plastic sulfur stabilization by copolymerization of sulfur with dicyclopentadiene. *Advances in Chemistry Series, No. 165, American Chemical Society*, p. 31-53.
  28. Leutner, B., & Diehl, L. (1977). *U.S. Patent No. 4,025,352*. Washington, DC: U.S. Patent and Trademark Office.
  29. McBee, W. C., & Sullivan, T. A. (1982). *U.S. Patent No. 4,348,313*. Washington, DC: U.S. Patent and Trademark Office.
  30. McBee, W. C., & Sullivan, T. A. (1982). *U.S. Patent No. 4,311,826*. Washington, DC: U.S. Patent and Trademark Office.
  31. American Society for Testing and Materials. Committee C-1 on Cement. (2013). *Standard test method for compressive strength of hydraulic cement mortars (Using 2-in. or [50-mm] cube specimens)*. ASTM International.
  32. Blissett, R. S., & Rowson, N. A. (2012). A review of the multi-component utilisation of coal fly ash. *Fuel*, 97, 1-23.
  33. ETRMA 2011, European tyre & rubber industry statistics.  
<http://www.etrma.org/uploads/Modules/Documentsmanager/20120612-etrma-statistics-2011.pdf>.
  34. Segre, N., & Joeques, I. (2000). Use of tire rubber particles as addition to cement paste. *Cement and concrete research*, 30(9), 1421-1425.
  35. Eldin, N. N., & Senouci, A. B. (1993). Rubber-tire particles as concrete aggregate. *Journal of*

- materials in civil engineering*, 5(4), 478-496.
36. Siddique, R., & Naik, T. R. (2004). Properties of concrete containing scrap-tire rubber—an overview. *Waste management*, 24(6), 563-569.
  37. Lv, J., Zhou, T., Du, Q., & Wu, H. (2015). Effects of rubber particles on mechanical properties of lightweight aggregate concrete. *Construction and Building Materials*, 91, 145-149.
  38. Moustafa, A., & ElGawady, M. A. (2015). Mechanical properties of high strength concrete with scrap tire rubber. *Construction and Building Materials*, 93, 249-256.
  39. Shu, X., & Huang, B. (2014). Recycling of waste tire rubber in asphalt and portland cement concrete: An overview. *Construction and Building Materials*, 67, 217-224.
  40. Coninck, H. D., Loos, M. A., Metz, B., Davidson, O., & Meyer, L. (2005). IPCC special report on carbon dioxide capture and storage. *Intergovernmental Panel on Climate Change*.
  41. Shin, M., Kim, K., Gwon, S. W., & Cha, S. (2014). Durability of sustainable sulfur concrete with fly ash and recycled aggregate against chemical and weathering environments. *Construction and building materials*, 69, 167-176.
  42. Moon, J., Kalb, P. D., Milian, L., & Northrup, P. A. (2016). Characterization of a sustainable sulfur polymer concrete using activated fillers. *Cement and Concrete Composites*, 67, 20-29.
  43. Vroom, A. H. (1981). *U.S. Patent No. 4,293,463*. Washington, DC: U.S. Patent and Trademark Office.
  44. American Society for Testing and Materials. Committee C-9 on Concrete and Concrete Aggregates. (2005). *Standard specification for coal fly ash and raw or calcined natural pozzolan for use in concrete*. ASTM International.
  45. ACI Committee. (1993). Guide for mixing and placing sulfur concrete in construction. *Reported by ACI Committee*, 548.
  46. Simard, G. L., & Warren, B. E. (1936). X-ray study of amorphous rubber. *Rubber Chemistry and Technology*, 9(3), 417-421.
  47. Naskar, A. K., Bhowmick, A. K., & De, S. K. (2001). Thermoplastic elastomeric composition based on ground rubber tire. *Polymer Engineering & Science*, 41(6), 1087-1098.
  48. Maraghechi, H., Ahmadi, I. F., & Motahari, S. (2011). Effect of adding crumb tire rubber particles on the mechanical properties of DCPD-modified sulfur polymer mortars. *Journal of Mechanics of Materials and Structures*, 6(9-10), 1283-1294.
  49. ASTM, C. (2006). 642, Standard test method for density, absorption, and voids in hardened concrete. *Annual book of ASTM standards*, 4, 02.
  50. Chindapasirt, P., Jaturapitakkul, C., & Sinsiri, T. (2007). Effect of fly ash fineness on microstructure of blended cement paste. *Construction and Building Materials*, 21(7), 1534-1541.
  51. Yue, L., Caiyun, J., & Yunping, X. (2006). The properties of sulfur rubber concrete (SRC). *Journal*



- of Wuhan University of Technology-Mater. Sci. Ed.*, 21(1), 129-133.
52. ACI Committee 213. (2014). Guide for Structural Lightweight-aggregate Concrete. American Concrete Institute.
  53. Monteiro, P. (2006). *Concrete: microstructure, properties, and materials*. McGraw-Hill Publishing.
  54. Dalen, A. V., & Rijpkema, J. E. (1989). *Modified sulphur cement: A low porosity encapsulation material for low, medium and alpha waste* (No. EUR--12303). Commission of the European Communities.
  55. Kerr, E. A. (2008). *Damage mechanisms and repairability of high strength concrete exposed to elevated temperatures*. University of Notre Dame.
  56. Poon, C. S., Kou, S. C., & Lam, L. (2006). Compressive strength, chloride diffusivity and pore structure of high performance metakaolin and silica fume concrete. *Construction and building materials*, 20(10), 858-865.
  57. Vlahović, M. M., Jovanić, P. B., Martinović, S. P., Boljanac, T. Đ., & Volkov-Husović, T. D. (2013). Quantitative evaluation of sulfur-polymer matrix composite quality. *Composites Part B: Engineering*, 44(1), 458-466.
  58. Gwon, S., Jeong, Y., Oh, J. E., & Shin, M. (2017). Sustainable sulfur composites with enhanced strength and lightweightness using waste rubber and fly ash. *Construction and Building Materials*, 135, 650-664.
  59. Pane, I., & Hansen, W. (2005). Investigation of blended cement hydration by isothermal calorimetry and thermal analysis. *Cement and concrete research*, 35(6), 1155-1164.
  60. Menéndez, G. V. B. B., Bonavetti, V., & Irassar, E. F. (2003). Strength development of ternary blended cement with limestone filler and blast-furnace slag. *Cement and Concrete Composites*, 25(1), 61-67.
  61. Hu, C. (2014). Microstructure and mechanical properties of fly ash blended cement pastes. *Construction and Building Materials*, 73, 618-625.
  62. Urabe, H., Nomura, Y., Shirai, K., Yoshioka, M., & Shintani, H. (1999). Effect of filler content and size to properties of composite resins on microwave curing. *Journal of Materials Science: Materials in Medicine*, 10(6), 375-378.
  63. Liu, G., Fang, Q., Xu, W., Chen, H., & Wang, C. (2004). Vibration assignment of carbon-sulfur bond in 2-thione-1, 3-dithiole-4, 5-dithiolate derivatives. *Spectrochimica Acta Part A: Molecular and Biomolecular Spectroscopy*, 60(3), 541-550.
  64. Linstrom, P. J., & Mallard, W. G. (2001). NIST Chemistry webbook; NIST standard reference database No. 69.
  65. Yoo, D. Y., Shin, H. O., Yang, J. M., & Yoon, Y. S. (2014). Material and bond properties of ultra high performance fiber reinforced concrete with micro steel fibers. *Composites Part B:*

- Engineering*, 58, 122-133.
66. Kang, S. T., Lee, Y., Park, Y. D., & Kim, J. K. (2010). Tensile fracture properties of an Ultra High Performance Fiber Reinforced Concrete (UHPFRC) with steel fiber. *Composite Structures*, 92(1), 61-71.
  67. Mirza, F. A., & Soroushian, P. (2002). Effects of alkali-resistant glass fiber reinforcement on crack and temperature resistance of lightweight concrete. *Cement and Concrete Composites*, 24(2), 223-227.
  68. Wang, S., & Li, V. C. (2006). High-early-strength engineered cementitious composites. *Materials Journal*, 103(2), 97-105.
  69. He, R., Chen, S. F., Sun, W. J., & Gong, R. (2014). Deformation behavior of high performance fiber reinforced cementitious composite prepared with asphalt emulsion. *Journal of Central South University*, 21(2), 811-816.
  70. Sahmaran, M., & Yaman, I. O. (2007). Hybrid fiber reinforced self-compacting concrete with a high-volume coarse fly ash. *Construction and Building Materials*, 21(1), 150-156.
  71. Atiř, C. D., & Karahan, O. (2009). Properties of steel fiber reinforced fly ash concrete. *Construction and Building Materials*, 23(1), 392-399.
  72. Li, V. C. (2003). On engineered cementitious composites (ECC). *Journal of advanced concrete technology*, 1(3), 215-230.
  73. Li, V. C., & Leung, C. K. (1992). Steady-state and multiple cracking of short random fiber composites. *Journal of Engineering Mechanics*, 118(11), 2246-2264.
  74. Banthia, N., & Sappakittipakorn, M. (2007). Toughness enhancement in steel fiber reinforced concrete through fiber hybridization. *Cement and Concrete Research*, 37(9), 1366-1372.
  75. Bacon, R. F., & Fanelli, R. (1943). The Viscosity of Sulfur. *Journal of the American Chemical Society*, 65(4), 639-648.
  76. Kim, S., Park, H., Kim, J., & Jung, Y. (2016). Characteristics of the warm-mix asphalt mixtures using the modified sulfur binder. *Journal of Korean Recycled Construction Resources Institute*, 4(4), 489-495.
  77. Neville, A. M. (1995). *Properties of concrete* (Vol. 4). London: Longman.
  78. Roberts, F. L., Kandhal, P. S., Brown, E. R., Lee, D. Y., & Kennedy, T. W. (1991). Hot mix asphalt materials, mixture design and construction.
  79. ASTM International. (2013). *ASTM D5/D5M-13 Standard Test Method for Penetration of Bituminous Materials*. Retrieved from [https://doi.org/10.1520/D0005\\_D0005M-13](https://doi.org/10.1520/D0005_D0005M-13)
  80. ASTM International. (2016). *ASTM D6373-16 Standard Specification for Performance Graded Asphalt Binder*. Retrieved from <https://doi.org/10.1520/D6373-16>
  81. Yildirim, Y. (2007). Polymer modified asphalt binders. *Construction and Building Materials*, 21(1),

66-72.

82. Polacco, G., Kříž, P., Filippi, S., Stastna, J., Biondi, D., & Zanzotto, L. (2008). Rheological properties of asphalt/SBS/clay blends. *European Polymer Journal*, 44(11), 3512-3521.
83. Roussel, N., Stefani, C., & Leroy, R. (2005). From mini-cone test to Abrams cone test: measurement of cement-based materials yield stress using slump tests. *Cement and Concrete Research*, 35(5), 817-822.
84. ASTM International. (2017). *ASTM C1749-17a Standard Guide for Measurement of the Rheological Properties of Hydraulic Cementitious Paste Using a Rotational Rheometer*. Retrieved from <https://doi.org/10.1520/C1749-17A>
85. Ferraris, C. F., & de Larrard, F. (1998). *Testing and modelling of fresh concrete rheology*. US Department of Commerce, Technology Administration, National Institute of Standards and Technology.
86. Ferraris, C. F., Obla, K. H., & Hill, R. (2001). The influence of mineral admixtures on the rheology of cement paste and concrete. *Cement and concrete research*, 31(2), 245-255.
87. ASTM International. (2015). *ASTM C1437-15 Standard Test Method for Flow of Hydraulic Cement Mortar*. Retrieved from <https://doi.org/10.1520/C1437-15>
88. ASTM International. (2014). *ASTM C230/C230M-14 Standard Specification for Flow Table for Use in Tests of Hydraulic Cement*. Retrieved from [https://doi.org/10.1520/C0230\\_C0230M-14](https://doi.org/10.1520/C0230_C0230M-14)
89. Macosko, C. W. (1994). *Rheology: principles, measurements, and applications*. Wiley-vch.
90. Larsen, L. H. (1991). *U.S. Patent No. 4,981,740*. Washington, DC: U.S. Patent and Trademark Office.
91. Park, S. B., Kim, S. C., Kim, K. H., & Hong, C. H. (2007). Experimental Study on Development of Artificial Fishing Reefs Using Environment-Friendly Sulfur Concrete. *Journal of ocean engineering and technology*, 21(3), 58-64.
92. Hadjmeliiani, M. (2015). Degradation of sewage pipe caused Sinkhole: A real case study in a main Road. In *M06 Colloque Euro Méditerranée*. AFM, Association Française de Mécanique.
93. Azenha, M., Sena-Cruz, J., Camões, A., & Ferreira, R. M. (2011, July). Numerical simulation of the structural behaviour of concrete tetrapods subject to imposed deformations and applied loads. In *CMNE2011–Congresso de Métodos Numéricos em Engenharia 2011* (pp. 1-16).
94. Van Breugel, K. (2007, April). Is there a market for self-healing cement-based materials. In *Proceedings of the first international conference on self-healing materials* (pp. 1-9).
95. Van Tittelboom, K., De Belie, N., De Muynck, W., & Verstraete, W. (2010). Use of bacteria to repair cracks in concrete. *Cement and Concrete Research*, 40(1), 157-166.
96. Xu, J., & Yao, W. (2014). Multiscale mechanical quantification of self-healing concrete incorporating non-ureolytic bacteria-based healing agent. *Cement and concrete research*, 64, 1-10.

97. Wang, X., Xing, F., Zhang, M., Han, N., & Qian, Z. (2013). Experimental study on cementitious composites embedded with organic microcapsules. *Materials*, 6(9), 4064-4081.
98. Mostavi, E., Asadi, S., Hassan, M. M., & Alansari, M. (2015). Evaluation of self-healing mechanisms in concrete with double-walled sodium silicate microcapsules. *Journal of Materials in civil engineering*, 27(12), 04015035.
99. Ahn, T. H., & Kishi, T. (2010). Crack self-healing behavior of cementitious composites incorporating various mineral admixtures. *Journal of Advanced Concrete Technology*, 8(2), 171-186.
100. Ferrara, L., Krelani, V., & Carsana, M. (2014). A “fracture testing” based approach to assess crack healing of concrete with and without crystalline admixtures. *Construction and Building Materials*, 68, 535-551.
101. Lee, H. X. D., Wong, H. S., & Buenfeld, N. R. (2010). Potential of superabsorbent polymer for self-sealing cracks in concrete. *Advances in Applied Ceramics*, 109(5), 296-302.
102. Snoeck, D., Dewanckele, J., Cnudde, V., & De Belie, N. (2016). X-ray computed microtomography to study autogenous healing of cementitious materials promoted by superabsorbent polymers. *Cement and Concrete Composites*, 65, 83-93.
103. Reinhardt, H. W., & Jooss, M. (2003). Permeability and self-healing of cracked concrete as a function of temperature and crack width. *Cement and Concrete Research*, 33(7), 981-985.
104. Herbert, E. N., & Li, V. C. (2013). Self-healing of microcracks in engineered cementitious composites (ECC) under a natural environment. *Materials*, 6(7), 2831-2845.
105. Nishiwaki, T., Kwon, S., Homma, D., Yamada, M., & Mihashi, H. (2014). Self-healing capability of fiber-reinforced cementitious composites for recovery of watertightness and mechanical properties. *Materials*, 7(3), 2141-2154.
106. Hong, G., & Choi, S. (2017). Rapid self-sealing of cracks in cementitious materials incorporating superabsorbent polymers. *Construction and Building Materials*, 143, 366-375.
107. Hasholt, M. T., Jespersen, M. H. S., & Jensen, O. M. (2010, August). Mechanical properties of concrete with SAP part I: Development of compressive strength. In *International RILEM Conference on Use of Superabsorbent Polymers and Other New Additives in Concrete* (p. 10). RILEM Publications SARL.
108. Laustsen, S., Hasholt, M. T., & Jensen, O. M. (2015). Void structure of concrete with superabsorbent polymers and its relation to frost resistance of concrete. *Materials and Structures*, 48(1-2), 357-368.
109. ACI 224. (2001). 224R–Control of Cracking in Concrete Structures. In *American Concrete Institute*.
110. ACI Committee, American Concrete Institute, & International Organization for

- Standardization. (2014). Building code requirements for structural concrete (ACI 318-14) and commentary. American Concrete Institute.
111. CEN, E. (1992). Eurocode 2: Design of concrete structures. *European Committee for Standardization*.
  112. Sisomphon, K., Copuroglu, O., & Koenders, E. A. B. (2012). Self-healing of surface cracks in mortars with expansive additive and crystalline additive. *Cement and Concrete Composites*, 34(4), 566-574.
  113. Sahmaran, M., Yildirim, G., & Erdem, T. K. (2013). Self-healing capability of cementitious composites incorporating different supplementary cementitious materials. *Cement and Concrete Composites*, 35(1), 89-101.
  114. Jacobsen, S., Marchand, J., & Hornain, H. (1995). SEM observations of the microstructure of frost deteriorated and self-healed concretes. *Cement and Concrete Research*, 25(8), 1781-1790.
  115. Şahmaran, M., & Yaman, İ. Ö. (2008). Influence of transverse crack width on reinforcement corrosion initiation and propagation in mortar beams. *Canadian Journal of Civil Engineering*, 35(3), 236-245.
  116. Aldea, C. M., Song, W. J., Popovics, J. S., & Shah, S. P. (2000). Extent of healing of cracked normal strength concrete. *Journal of materials in civil engineering*, 12(1), 92-96.
  117. Shin, S. W., Zhu, J., Min, J., & Popovics, J. S. (2008). Crack depth estimation in concrete using energy transmission of surface waves. *Materials Journal*, 105(5), 510-516.
  118. Hargis, C. W., Telesca, A., & Monteiro, P. J. (2014). Calcium sulfoaluminate (Ye'elimité) hydration in the presence of gypsum, calcite, and vaterite. *Cement and Concrete Research*, 65, 15-20.
  119. García-Maté, M., Angeles, G., León-Reina, L., Losilla, E. R., Aranda, M. A., & Santacruz, I. (2015). Effect of calcium sulfate source on the hydration of calcium sulfoaluminate eco-cement. *Cement and Concrete Composites*, 55, 53-61.
  120. Hu, Y., Li, W., Ma, S., & Shen, X. (2017). Influence of borax and citric acid on the hydration of calcium sulfoaluminate cement. *Chemical Papers*, 71(10), 1909-1919.

## ACKNOWLEDGEMENT

It's been 10 years since I entered Ulsan National Institute of Science and Technology (UNIST) in 2009 as a freshman. The campus has been built around the Gamak Pond where people were few, but talented professors and students gathered around and committed themselves to research. As a result, UNIST is increasingly considered a renowned university in the world. Most of all, I would like to thank my parents who gave me a healthy body and raised my sound spirit so that I could devote myself to study in such a good environment. I would like to thank my brother, Sungmin, who has always encouraged me. On June 7, 2018, I completed my Ph.D. and left a retrospective and a thank-you note.

From the third year of my undergraduate course at UNIST, I experienced various research themes covering structures and construction materials under the guidance of Professor Myoungsu Shin in the School of Urban and Environmental Engineering. Based on this experience, I have received the Global PhD Fellowship for five years (NRF-2014H1A2A1020435). First of all, I would like to pay homage to Professor Shin for he is an admirable mentor, giving me continuous teaching and advice. In addition, I would like to thank Emeritus Professor Chung-Bang Yun in the School of Urban and Environmental Engineering for his reviewing my research proposal and writing a recommendation letter when I applied for the Global PhD Fellowship. I would also like to thank Professor Jae Eun Oh and Sung-Han Sim in the School of Urban and Environmental Engineering, UNIST, Professor Soowon Cha in the Department of Civil and Environmental Engineering, University of Ulsan, and Professor Young Cheol Choi in the Department of Civil and Environmental Engineering, Gachon University for their serving as thesis committee members giving insightful comments on my research. I would also like to thank all the professors in the School of Urban and Environmental Engineering, UNIST for helping me familiarize myself with the doctoral coursework. I would also like to thank Professor Kwang Myung Lee in the Self-Healing Green Concrete Research Center, Sungkyunkwan University and Professor Seung Yup Jang in the Department of Transportation System Engineering, Korea National University of Transportation for their supporting the study of this thesis and the examination on ultra-rapid hardening cement concrete.

Finally, I would like to express my sincere gratitude to my seniors who graduated from Sustainable Structural Systems and Materials Lab, and all of current lab members, Seungpil Kim, Eunjong Ahn, Chanyoung Kim, Seongho Han and Jin Hyun Lee. I would also like to thank Dr. Yeonung Jeong, a former graduate of Professor Jae Eun Oh's Lab, UNIST, for his giving a lot of advice on my research and graduate life. I would also like to especially thank all members of the Concrete/Structural Lab in the Department of Civil and Environmental Engineering, University of Ulsan, and Dr. Sung Geun Bae

in the National Disaster Management Research Institute.

This study was partially supported by the Ministry of Knowledge Economy, Korea, under the RIS (Regional Innovation System) Support Program, supervised by the Korea Institute for Advancement of Technology. I would also like to thank Mr. Dongoh Lee for his years of providing sulfur polymers and laboratory facilities for this research.